Numerical and Experimental Investigations of Nonlinear Dynamics and Heat Transfer Deterioration in Supercritical Natural Circulation Loop

A thesis submitted
in partial fulfillment of the requirements
for the Degree of

Doctor of Philosophy

by

Tanuj Srivastava

Roll No. 186103035
Under the Supervision of
Dr. Dipankar Narayan Basu

Department of Mechanical Engineering
Indian Institute of Technology Guwahati
Guwahati - 781 039

30 September 2024

Dedicated To

All
Who Made Me
What I Am Today

Acknowledgement

Research is often all about the journey, not the destination. If one had to work single-handedly on the complete journey of doctoral research, he/she/they would have never been able to reach the goal. The thesis work presented herein is built upon many individuals' contributions, both personally and professionally, in the past five years. It is not easy to name each individual and their contributions in a short note, although I am forever indebted to them. However, I will take this opportunity to name a few of my well-wishers who helped me at the forefront during my doctoral research at the Indian Institute of Technology Guwahati.

I am very much thankful to my thesis supervisors, Dr.*Dipankar Narayan Basu*, for his immeasurable guidance, invaluable technical advice, and approaches to critical thinking. Their thought processes and ideas aided in the methods and output of my research work. I was greatly benefited by the independent yet competitive working environment that they created while doing research work. By working with them, I gained experience in academic research and, most importantly, of life.

I would like to thank my doctoral committee chairman, Prof. *Vinayak Kulkarni*, doctoral committee members Prof. *Pranab Kumar Mondal*, and Prof. *Pankaj Kalita* for their constructive criticism and valuable suggestions during my research work.

I am thankful to the Department of Mechanical Engineering, IIT Guwahati for providing me the rquired facilities and an excellent working environment. I am thankful to the faculty

members who taught various couraes during my coursework.

I am very lucky to have friends Mr. Brijesh Kumar Singh, Dr. Santanu Kumar Das, Mr. Chandan Nashine, Mr. Pranab Sutradhar , Mr. Rohit Kumar, Dr. Niraj Kumar Prasad, Mr. Bikramjyoti sahariah, Mr. Rishabh Saxena with me who always supported me during my time in IIT Guwahati. Their friendship and continuous encouragement have made my life colorful and precious.

I would like to thank my seniors and labmates Dr. Milan Krishna Sinha Sarkar, Dr. Kiran Saikia, Dr. Nitesh Kumar, Mr. Ashok Kumar Gond, Mr. Biswajyoti Baishya, Mr. Abhijit Pal, Mr. Deepak Kumar Rathour, Mr. Suman Swaraj Mishra, Mrs. Dhanjita Medhi, Mr. Pijush Kakoty, Mr. Sudhanshu and Mr. Suneet for their valuable suggestions and support during my research.

Words will never be enough to express my gratitude towards Ms. Monika Srivastava, for the never-ending support and motivation. I always had the luxury to take your time in this long process.

My family is the sole reason for my accomplishments; however small it may be. I feel a deep sense of gratitude towards my mother Mrs. Anita Srivastava, father Mr. Dilip Kumar Srivastava and brother Mr.Manuj Srivastava and sister in-law Mrs. Aanchal Srivastava who have been extremely patient, understanding, and supportive throughout this journey and beyond. I sincerely appreciate the sacrifices you have made during this journey for turning my dream into reality.

At last I would like to thank the whole Department of Mechanical Engineering and the institute for their constant supervision, guidance and support.

Tanuj Srivastava

CERTIFICATE

This is to certify that the work presented in this thesis entitled "**Numerical and Experimental Investigations of Nonlinear Dynamics and Heat Transfer Deterioration in Supercritical Natural Circulation Loop**" is carried out by **Tanuj Srivastava** for the award of Doctor of Philosophy in the Department of Mechanical Engineering, Indian Institute of Technology Guwahati. The thesis embodies the results of original work and studies carried out by the student himself under my supervision and has not been submitted elsewhere for a degree.

Dr. Dipankar Narayan Basu
Associate Professor,
Department of Mechanical Engineering,
IIT Guwahati, 781039, Assam.

Date: August, 2023
Place: Guwahati

Declaration

I certify that

1. the work contained in this thesis is original and has been done by myself under the general supervision of my supervisors.
2. the work has not been submitted to any other Institute for degree or diploma.
3. I have followed the Institute norms and guidelines and abide by the regulation as given in the Ethical Code of Conduct of the Institute.
4. whenever I have used materials (data, theory and text) from other sources, I have given due credit to them by citing them in the text of the thesis and giving their details in the reference section.
5. the thesis document has been thoroughly checked to exclude plagiarism.

Signature of the Student

Roll No. _____

Abstract

The natural circulation loop (NCL), despite its complex mathematical complexity, points to an efficient way for energy transfer from a high-temperature source to a low-temperature sink without coming into contact. The primary force behind any natural circulation system is the buoyancy force caused by the density gradient. The operating range of single-phase NCLs is constrained by saturation temperature and low flow rate, whereas two-phase loops are highly concerned about the possibility of dry-out and the emergence of different flow regimes with divergent heat transfer behaviour. Due to its strong capacity for heat transfer and significant volumetric expansion, supercritical fluid unveils a strong alternative by combining the benefits of single- and two-phase versions. In conjunction with this, the idea of a supercritical natural circulation loop (sNCL) has emerged as one of the most important endeavours for generation-IV nuclear reactors in the twenty-first century.

The current thesis presents both numerical and experimental evaluation of sNCL with CO_2 as a working fluid. The steady-state and transient behaviour of sNCL have been thoroughly investigated numerically with. Steady state analysis involved 3D numerical simulation while transient simulations were performed in 2D and 1D numerical framework. The cooler side condition is always set to constant temperature while except a few cases of dynamical response under time varying heating condition, the rest of the cases incorporates the constant heat flux input. Nature of the sNCL is governed by interplay between buoyancy force and friction force.

With the increase in the heating power, the dominance of the buoyancy causes the increment of the mass flow rate and heat transfer coefficient. Reaching the optimum condition of the buoyancy dominance at its peak, the flow rate becomes maximum leading to advent of friction dominance slowly, slow drop in the flow rate was witnessed in the mass flow rate after that. The average loop temperature is this case is slightly higher than T_{pc}. This is followed by sharp drop in the mass flow rate followed by huge bulk temperature and poor thermalhydraulics of the system, signifying the dominance of the friction force and lead. The condition termed as Flow induced heat transfer deterioration (FiHTD). The focus of the entire subject matter will be around this phenomenon with its relation to safer zone of operation and its correlation with the stability of the loop which is still untouched in the literature under the different sets of boundary conditions.

Based on the fluid temperature inside the loop, four different heat transfer zone was identified namely Low power regime ($T_{avg} \leq T_{pc}$), enhanced heat transfer regime ($T_{avg} \sim T_{pc}$), transition regime ($T_{avg} \geq T_{pc}$), and deteriorated heat transfer regime ($T_{avg} \gg T_{pc}$). The phenomenon of FiHTD is unavoidable yet, it can be delayed. With the 3D simulation in the ANSYS Fluent, boundary of safer zone of operation has been earmarked incorporating the Buoyancy parameter and friction factor and interestingly, all the simulated data follows the fitted power law curve with $R^2 = 0.946$. Moreover, along the heater section change of slope of friction factor from negative to positive is also an indication of occurrence of FiHTD.

The dissertation reports the static and dynamic instability using 1D numerical framework. Sharp deterioration in the steady-state circulation rate was observed, consistent to existing multidimensional analyses. Loop exhibits Ledinegg instability for an intermediate range of heater power, characterized by multiple steady-state solutions. Appearance of static instability has been substantiated following the pressure drop versus mass flow rate profiles. Dynamic instability has also been identified by introducing perturbation during transient simulations, and the range of both static and dynamic instabilities conforms well with each

other. Moreover, transient response of the system was analysed on imposing the time varying heat input profile. Under the action of sinusoidal heating profile, chaotic oscillations can be identified for an intermediate band of imposed frequency and amplitude. While for the ramp and step heating profile, former one showed stable transient due to slow generation of buoyancy force. Interestingly, in either of the cases investigated, the resultant dynamics are found to be strongly correlated with the heat transfer regimes.

2D model has also been designed to envisage the instabilities in the start-up transient which is well explored phenomenon in single and two-phase NCL. What makes the sNCL more intricate to understand is the large properties variation around pseudocritical point. Bulk motion initiation is found to be highly affected by the phenomenon like piston effect, Rayleigh-Taylor instability, adiabatic heating. Combination of all causes the formation of hot fluid packet inside the heating section, motion of which governs the transient of the system. Multiple flow reversal or chaotic nature of the system is due to the intermittent generation and disappearance of fluid packet which causes the negative temperature difference of the two vertical arms.

Experiments have been conducted with CO_2 as the working fluid to enlarge the corresponding experimental database for sNCL. The identification of the thermalhydraulic characteristics and stability behaviour of sNCL is the motivating factor behind the current experimental study. The experimental assessment was done into the effects of sink temperature, operating pressure, tilt angle, and input heating power. The mass flow rate rises with power and reaches its maximum before beginning to fall. The highest mass flow rate is seen for the vertical loop, and it decreases with the tilt angle. Instability is not seen for the chosen range of operating conditions. While the temperature levels after the fall did not rapidly surge as was the case with actual FiHTD, the trend of mass flow rate was discovered to be similar to the simulation result.

Contents

List of Figures

List of Tables

Nomenclature

Acronyms

DAS	Data Acquisition System
$FiHTD$	Flow Induced Heat Transfer Deterioration
HTC	Heat transfer coefficient
$NAFA$	Numerical Analysis of Fluid flow in Axi-symmetric geometries
NCL	Natural Circulation Loop
$NIST$	National institute of Standard and Technology
$PISO$	Pressure-Implicit with Splitting of Operators
$PRESTO$	Pressure Staggering Option
RNG	Re-normalization group
NCL	Natural Circulation Loop
$sNCL$	Supercritical Natural Circulation Loop
sCO_2	Supercritical Carbon Dioxide
sH_2O	Supercritical Water
$HHHC$	Horizontal Heater Horizontal Cooler
$HHVC$	Horizontal Heater Vertical Cooler

$VHHC$	Vertical Heater Horizontal Cooler
$VHVC$	Vertical heater Vertical Cooler

Greek symbols

β	Volume expansion coefficient (K^{-1})
θ	Inclination angle (-)
ρ	Density ($kg\,m^{-3}$)
$\Delta\rho$	Density Differnce ($kg\,m^{-3}$)
Δp	Pressure Differnce (N)
τ	Time period (s)
ϵ	Turbulence Dissipation rate ($m^2\,s^{-3}$)
κ	Turbulence Kinetic energy ($m^2\,s^{-2}$)
λ	Thermal conductivity ($W\,m^{-1}\,K$)
μ	Dynamic viscosity ($kg\,m^{-1}\,s^1$)

Roman symbols

A	Cross-sectional area (m^2)
Bu	Buoyancy parameter (-)
c_p	Specific heat ($J\,kg^{-1}\,K^{-1}$)
D	Diameter (m)

f	Friction factor
g	Gravitational acceleration ($\mathrm{m\,s^{-2}}$)
Gr	Grashof number
h	Enthalpy ($\mathrm{J\,kg^{-1}}$)
H	Height (m)
U	Heat transfer coefficient ($\mathrm{W\,m^{-1}\,K^{-1}}$)
I	Current (A)
L	length (m)
$\dot{m}$	Mass flow rate ($\mathrm{kg\,s^{-1}}$)
Nu	Nusselt number (-)
P	Pressure ($\mathrm{N\,m^{-2}}$)
Pr	Prandtl number (-)
$\dot{q}''_w$	Heat flux ($\mathrm{W\,m^{-2}}$)
$\dot{q}$	Heater power (W)
Re_m	Modified Reynolds number (-)
T	Temperature (K)
V	Voltage (volt)
x, y, z	Space coordinate (m)

Subscripts

$*$	Non-dimensional
c	Cooler

cr	Critical
in	Inlet
i	node
out	Outlet
m	Modified
pc	Pseudo-critical
ss	Steady-State

Chapter 1

Introduction

We are living in a world where we are surrounded by nature and its natural process. Left unobserved unintentionally, we can observe many days to day life events of natural processes. Common examples of such phenomenon are energy flow, formation of soil and transport of sediment, natural disturbance like storms, the flow of wind, water cycle, and many more to count. The example shown in Fig. 1.1a is of the water cycle. Natural process forms a complex web which means they can also be interconnected to each other or can influence. For example, Climate change can alter the rate at which bedrock forms, which in turn affects the shape of the landscape and the amount of soil that accumulates or is washed away. In short, we can say that plants, animals, and the environment interact to create natural processes. The environment that we live in is not only formed due to natural process, human has also played a very crucial role in nature, but with the advancement of technologies, in a negative sense. Acid rain, deforestation, water, and air pollution are major among all. The absence of any driving phenomenon and unpredictable behavior makes the natural processes even more complex. We can rather put effort into saving the environment from the adverse effects of human acts because it is human who is creating the imbalance in nature which are causing natural disaster. The phenomenon which is driven by the mean of any external driver is termed a forced phenomenon. A common example in our daily life is the human body, in which blood is forced by the human heart, as shown in Fig. 1.1b. The present study is based on the natural phenomenon of heat transfer; hence the forced phenomenon will hardly be discussed.

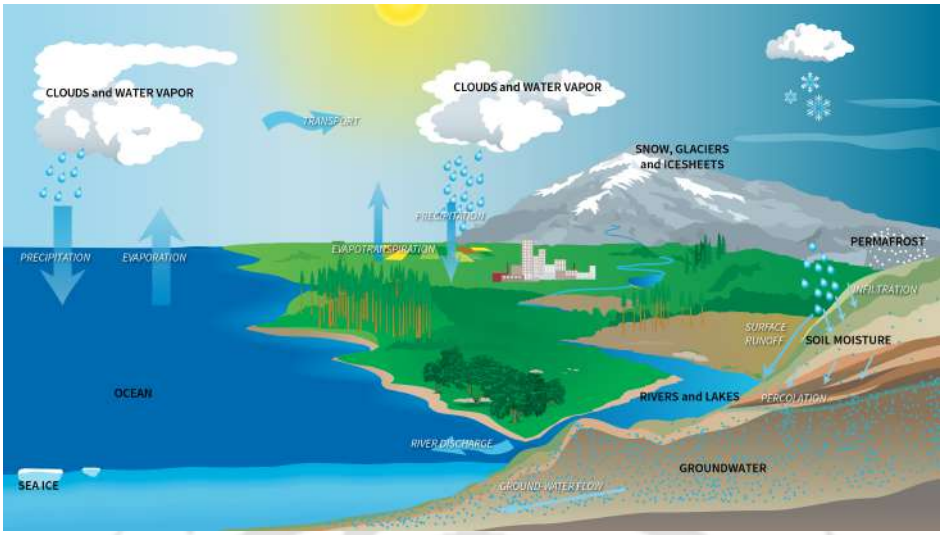

(a)

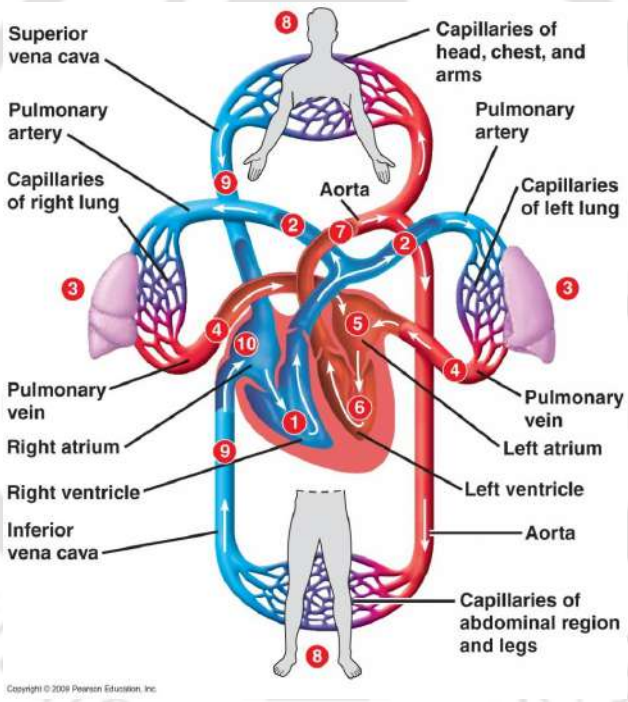

(b)

Fig. 1.1: (a)Water natural circulation cycle (https://bit.ly/2Z05x0c) and (b)Human Blood cycle(https://bit.ly/30GzA9J)

1.1 Basics of Natural Circulation System

From the heat transfer perspective, the natural circulation phenomenon is the mode of heat transfer without external support, and flow appears due to buoyancy generated by the temperature gradient. The system consists of two essential but vital parts, a) heat source (high temperature) and b) heat sink (low temperature). The heat sink is always located above the source. The heat source and heat sink are connected together by pipes to form the natural circulation loop (NCL) or thermosiphon loop system. In the natural circulation loop, the driving force is the gradient of density and available buoyancy, which is induced by heat transport from the source to the sink. Under the influence of the body force field gravity, circulation starts as the heating element is activated, as shown in Fig. 1.2.

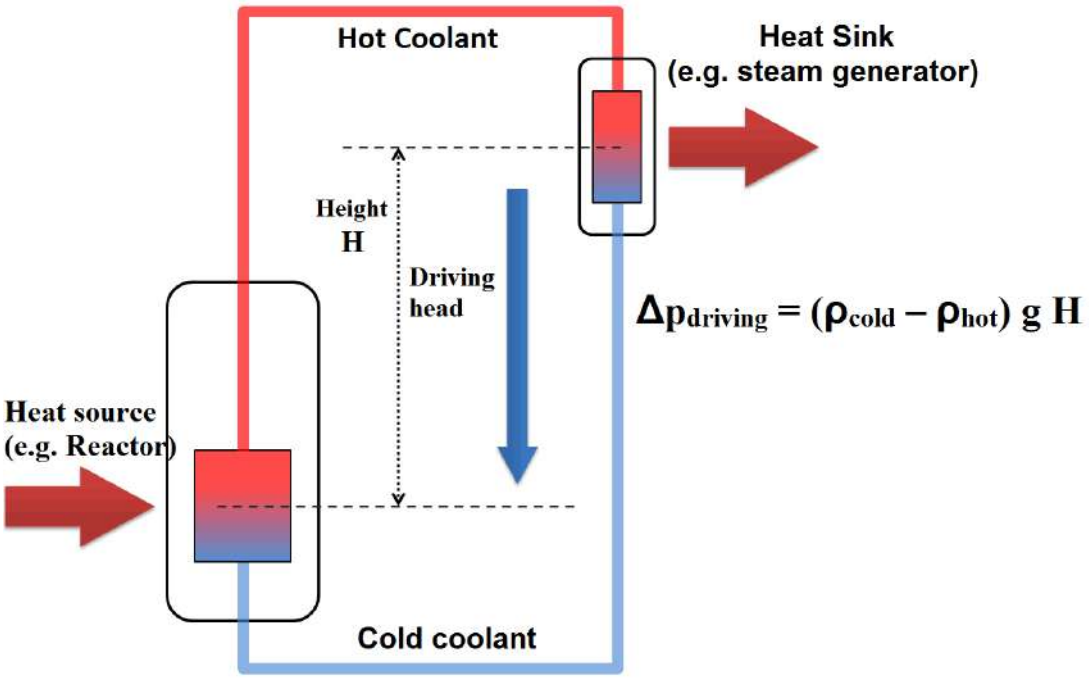

Fig. 1.2: Schematic diagram of natural circulation loop

Under controlled conditions, a steady state is expected to be achieved when heat absorbed at the heater becomes equal to heat rejected at the cooler. Frictional resistance causes hindrance in flow, and when it balances the driving pressure, steady-state reaches. The basis for the calculation of the mass flow rate given by the equation below-

$$(\rho_c - \rho_h)gH = \frac{Rm^2}{2\rho A^2} \tag{1.1}$$

Where R is the hydraulic resistance given by-

$$R = \sum_{i=1}^{N} \frac{f_i L_i}{Di} + K_i \tag{1.2}$$

Rearranging the equation of mass flow using the above equation leads to

$$m = \sqrt{\frac{2\rho A^2(\rho_c - \rho_h)gH}{R}} \tag{1.3}$$

The equation above contains quite significant information as we can observe that the mass flow rate is a strong function of various parameters such as loop height, flow area, the density difference between hot and cold leg as well as the hydraulic resistance. The critical advantage of NCL is that the absence of moving parts causes no or less maintenance and operating cost for the system, making it more reliable from the failure point of view. Due to these advantages, NCL finds numerous engineering applications (Fig. 1.3) in multiple engineering fields, encompassing electronic chip cooling [1], solar heaters [2–5], geothermal systems [6–8] and nuclear reactors [9, 10] just to name a few. Other application includes low-velocity corrosion studies where heat dissipation is done by "liquid fins" [11]. Single-phase system is used in solar heaters, electronic chip cooling, and PWRs, while the two-phase system is used in heat pump, power cycle, etc.

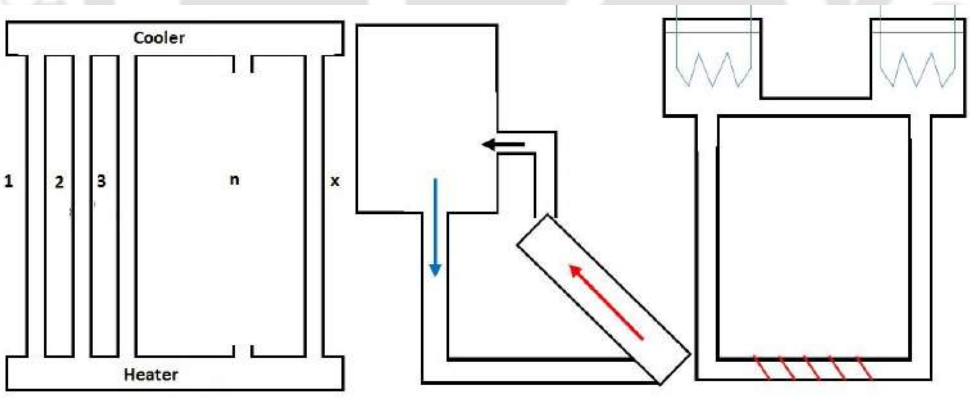

Fig. 1.3: Application of Natural circulation loop

1.2 Advantages of Natural Circulation Loop

- **Simplicity**
  Because of the elimination of the power-consuming equipment, the maintenance and operating cost of the system makes the designer hassle-free about the complicacy of the system design as it only involves simple constructing elements, which can be easily installed.

- **Enhanced Flow Distribution**
  In the case of a forced circulation system, the pressure difference created by an external agent like a pump creates non-uniform pressure distribution causing maldistribution of flow. Whereas in NCL, such a scenario is absent or present in less magnitude.

- **Safety Features**
  For applications like in nuclear reactors, NCL is the better option from safety point of view, or as a backup option for removing the decay heat from the core, as even after the system failure, the NCL provides incessant flow. Though the elimination of external agents makes the system flow rate less, the slow thermal response of the system gives supplementary time to handle the disordered plant.

1.3 Challenges in Natural Circulation Loop

- **Low Driving Force**
  The key disadvantage of NCL is the low driving force which is due to the density difference in both the vertical legs. It can be increased by increasing the height of the loop. But increasing height will increase the plant cost and space issues.

- **Low Mass Flux**
  Low driving force leads to low mass flux, which directly affects the heat transfer characteristics. Due to this larger core volume will be required compared to forced circulation flow.

- **Instability Effects**
  NCL is less stable, and its stabilizing effect is limited compared to forced circulation flow due to its nonlinear phenomenon. The flow is very much dependent on the operating parameters, which can lead to fluctuation in the driving force, and that may cause unwanted fluctuations in the system.

- **Specification of Startup and Operating Procedure**
  During the initiation, NCL is more likely to pass through the unstable zone, which has to be avoided to dodge the occurrence of critical heat flux (which tend to be significantly lower compared to a forced circulation system). Hence startup pressure and temperature conditions should be taken care of properly.

1.4 Classification of Natural Circulation Loop

Classification can be based depending upon the system requirement in real-life implementation. NCL can be classified as the point heat source and sink, rectangular, toroidal, as shown in Fig. 1.4.

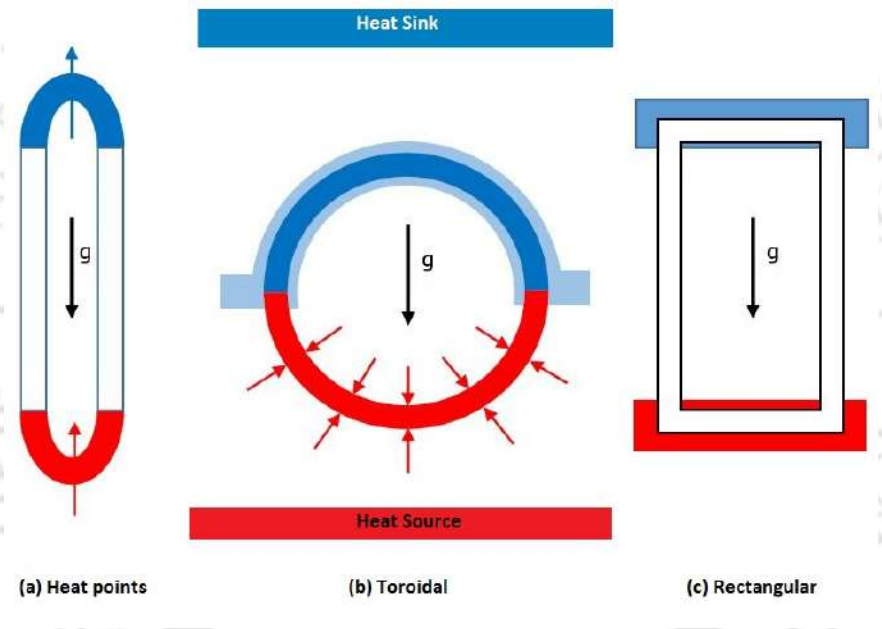

Fig. 1.4: Various types of NCL

In brief, the general classification of NCL can be represented as shown in Fig. 1.5. Moreover, the NCL can be of open-loop or closed-loop type. The difference in both configurations is that one end of the former one is connected to a reservoir while both ends of the latter one are connected together to make the system closed.

Intricacy involves the natural circulation loop due to the nonlinear nature of the phenomenon. Unpredictable thermalhydraulic behavior and the absence of predefined motion make the system difficult to understand. Such a phenomenon is discovered to happen in non-uniform temperature fields when gravity is present. Rayleigh-Benard convection, where

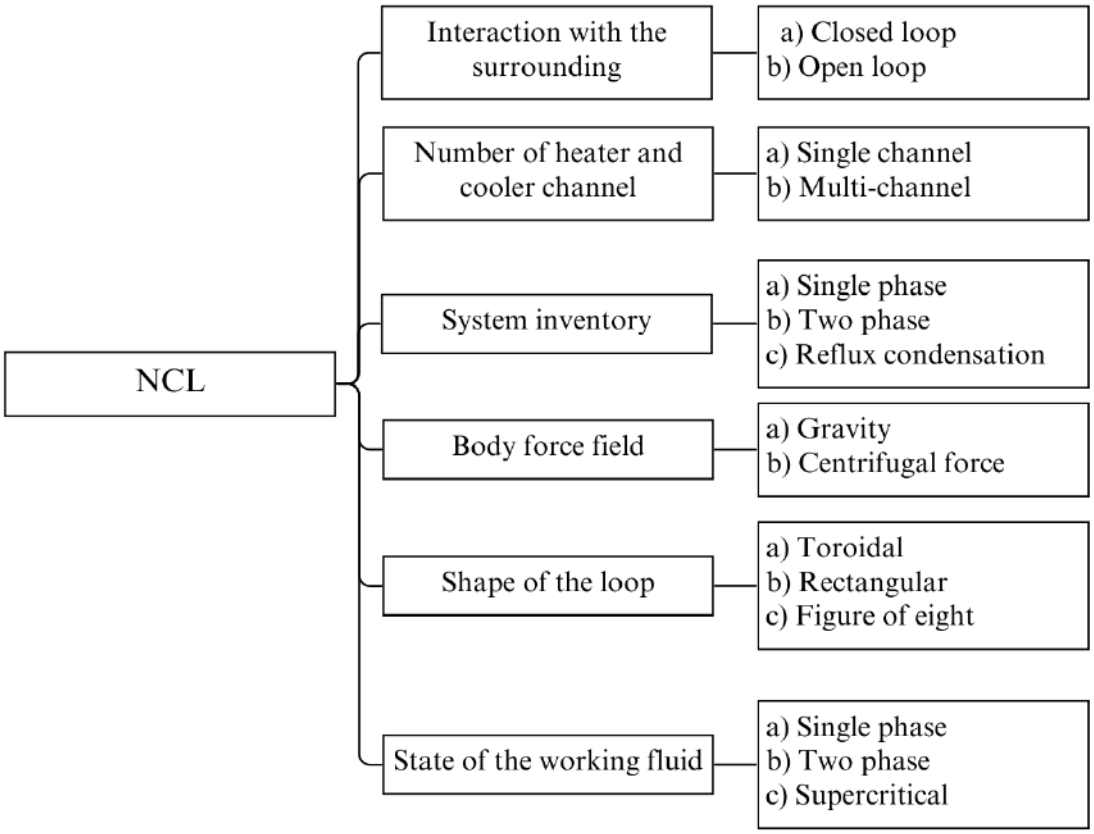

Fig. 1.5: Classification of Natural circulation loop

the fluid forms a regular pattern of Benard cells, is a classic example of a buoyancy-driven phenomenon. Because of the interaction with the nearby wall or the intricate geometry, buoyancy-driven phenomena in closed or narrow cavities (natural circulation loop) are more complex than free-surface convection (flow over the heated plate). The two most important dimensionless numbers that are universally used to study natural circulation are the Rayleigh number and the Grashof number. Rayleigh number (Ra) comes into play in the absence of an external driving agent, like a pump, when the temperature gradient is applied in the system. Such temperature differences by the heat source and sink in NCL. The Rayleigh number is a dimensionless number that is linked to buoyancy-driven flow and can be used as a gauge of the forces that drive natural convection or depicts the dominated mode of heat transfer.

$$Ra = \frac{g\beta\Delta T L^3}{\nu\alpha} \tag{1.4}$$

Different types of flow have their own threshold Rayleigh number. The mode of heat transfer

is through conduction if it is below the critical value, while convection dominates when it surpasses the threshold. For the infinite parallel plate, Jeffreys [12] defined the critical Rayleigh number to be 1708, the system is in steady-state, while for Ra above this value, the instability arises and convection current starts moving in the domain. Similar observations are also witnessed in the theoretical study of Zivrin [13] where $Ra_c > 6$ was the condition for the flow. Grashof number is the ratio of buoyant force and viscous force and has a similar function as that of Reynolds number in fluid flow. The complexity of the fluid nature of the natural circulation loop makes it unstable under various operating conditions.

1.5 Classification of Instability

It is critical to first define flow instability before classifying the type of flow instability that can occur in thermo-hydraulic systems. When a key parameter, such as mass flow rate, returns to its initial state following either internal or external perturbations (such as changes in mass flow rate, inlet temperature, heat input, etc.), the system is said to be stable (flow pattern transitions). If the system stabilizes to a new steady state (static instability) or oscillates with increasing amplitude, it is assumed to be unstable (dynamic instability). If the system parameters oscillate within a certain range, it is said to be in a neutrally stable state. The thermo-hydraulic instabilities are primarily divided into static and dynamic instabilities based on the analysis method. There may be more than one steady-state solution for a system's static instability. Multiple regenerative feedbacks between the flow rate, pressure drop, void fraction, etc., are involved in dynamic instability. Fully transient governing equations are needed to explain the phenomenon and predict the threshold because the dynamic behavior is time dependent [14]. The classification of two-phase flow thermo-hydraulic instabilities discussed by Boure et al. [14] and Fukuda et al. [15] is summarised in Fig. 1.6. The most frequently seen and researched thermo-hydraulic flow instabilities of boiling systems are the Ledinegg static instability and density wave oscillations, and hence, only these two have been explained briefly below.

1.5.1 Ledinegg instability

Flow excursion is another name for Ledinnegg static instability. In an excursive manner, the flow will experience a sudden, large amplitude drift from its initial state before stabilizing at a value lower or higher than the initial value without going back to the initial state. This happens when the channel demand pressure drop - flow rate curve (internal characteristic) is

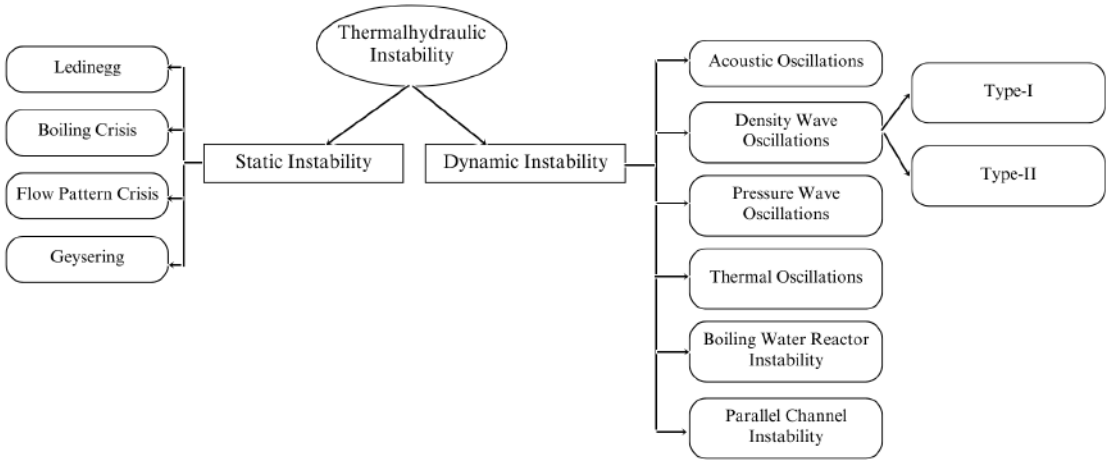

Fig. 1.6: Generalized classification of instabilities in thermalhydraulic systems

smaller than the loop supply pressure drop - flow rate curve (external characteristic). This kind of instability is not observed in a single-phase system.

$$\frac{\partial \Delta P_{sys}}{\partial \dot{m}} < \frac{\partial \Delta P_{ext}}{\partial \dot{m}} \tag{1.5}$$

The characteristics of a channel's pressure drop, nucleation characteristics, and flow regime transition are crucial in figuring out static instability.

1.5.2 Density wave oscillation

This type of instability is the most common and predominant in all types NCLs, irrespective of phase. Three main issues can emerge from flow oscillations in two-phase systems: first, they affect the local heat transfer characteristics and may result in burnout; second, sustained flow oscillations may arise in component mechanical vibration; and third, they affect system control. DWO analysis can be done using linear and nonlinear analysis. The drawback of linear analysis is that it can predict the stability threshold but holds back in elaborating the unstable behavior. On the other hand, the nonlinear analysis gives an insight into the estimation of the oscillation's amplitude as well as the limit cycle. Density wave oscillations were divided into two categories by Fukuda and Kobori [15], type I and type II. Type I instability manifests at low vapor quality and is controlled by gravitational head, whereas type II instability manifests at high quality and is controlled by friction. Frequency domain linear stability analysis is the conventional approach to studying DWO. All steady-state parameters are given a small perturbation, and the resulting equations are linearized to find

the perturbation equations. A detailed, comprehensive review of both instabilities has been done by various research groups [14, 16–18].

1.6 Brief History of Development of Single and Two-phase Natural Circulation Loop

The version of NCL without change of phase, i.e., without significant change in the density, is studied under single-phase NCL. Single-phase system is characterized by its regularized heat transfer characteristics due to large thermal conductivity but provides a low flow rate. A brief application of single-phase NCL has been documented by Basu et al. [19]. Numerical [20] and experimental [21] studies confirm the stable operation of the solar heater in a wide range of operating parameters. The saturation-point criterion for the relevant fluid, however, always places a limit on single-phase loops. Phase change in the system can be begun by increasing the source's power or by appropriately changing the geometric structure. Following that, circulating fluid typically experiences condensation or phase separation at one section of the loop and boiling or flashing at another. Stronger buoyancy can be produced by a two-phase mixture with a much larger density difference from a single-phase liquid, which leads to increased circulation, improved system performance, and compact design. Although the advantages of two-phase natural circulation loops (NCLs) over their single-phase counterparts promise widespread applications in a variety of technological fields, they also present a number of technical difficulties. The design is challenging due to the complexity of boiling, condensation, and two-phase flow, particularly through a natural circulation system.The instabilities in two-phase NCLs are numerous and have more severe characteristics. Schmidt [5] first demonstrated the potential of two-phase thermosiphons for cooling gas turbine rotor blades a very long time ago. In their review of various approaches to cooling gas turbine blades, Cohen and Bayley [22] concluded that the thermosiphon was the most alluring choice. A wide range of energy could be transferred from the hot to the cold end of the loop without bothering about the quantity of coolant. In a two-phase NCL, unstable oscillations have been observed for intermediate power ranges and near the water boiling point [23]. And thus, the development of physics-based modeling methods and the characterization and quantification of two-phase instabilities were the primary priorities of all initial research. With the improvement in computational resources, very accurate prediction of two-phase phenomena is now possible. According to Zvirin [13], the flow in NCL is always induced by the onset of global flow because of heating which is of a second kind among all

kinds of instabilities. Without concerning the system dynamics, it was earlier assumed that the instabilities in NCL are due to properties variation near the critical point of the fluid [24]. As per the theoretical claim by Keller [25], inertia does not play any role in oscillatory behavior; rather, it is due to the interplay between buoyancy and friction force. Welander [26] first introduced the theory of instability using hot and cold pockets, which later came to be noticed by Creveling [24] with water at normal temperature. Sen and Trevino [27] demonstrated that, depending on the case, the loop could have both forward and reverse flow, with the steady-state flow direction being derived by the initial conditions. The experimental and numerical investigation using CFD code by Pilkhwal et al. [28] reveals the oscillatory nature of system parameters. HHHC configuration was found unstable at low power. Observation of flow oscillation in single-phase NCL has been documented by Misale [29]. Experimental investigation on simple configuration for unstable behavior prediction was done at BARC, which is used as a source for further processing of scaling laws and to predict the capability of system code [30–32]. Their work also contributed to envisaging the thermalhydraulics of NCL of the different in-house developed program and system codes based on different numerical schemes [33–35]. Moreover, a single-phase natural circulation loop's thermohydraulic behavior depends on a number of factors, including:

- Thermal conductivity effect of wall [36]
- Inclination of loop, heater power [37] and geometrical dimension [38]
- Orientation of heater and cooler [39]
- Loop stabilization via regional pressure drops[40]

A number of fluids have been investigated in the previous century to investigate the two-phase natural circulation system. Ethylene glycol, water, acetone, R-11, R-12, R-134, etc., are among the famous names. Lee and Mital [41] found that the quality of working fluid does not have much effect on the heat transfer coefficient; rather, the system pressure is found to have a huge impact on it. At a low charge level, there is a high possibility of dry-out at higher fluid temperature [42]. A review of available data of PWR showed that the flow rate is not a strong function of heater power, but rather is more dependent on the system void [43]. Various research groups have used different methods and commercial codes to predict the steady-state characteristics of NCL accurately. Some of them are REPAS (Reliability Evaluation of Passive Safety Systems) [44], APSRA (Assessment of Passive System Reliability) [45], RELAP5 (Reactor Excursion and Leak Analysis Program) [46], ANSYS Fluent

[47] etc. As per the experimental observation of flow excursion at low pressure and low flow rates from an R-113 loop by Babelli et al. [48], the demand curve for any system should be plotted to confirm the existence of a local minimum. Furthermore, they proved that, in parallel downward flow systems, flow excursion predominates over density-wave oscillation, which wasn't anticipated to have much of an influence. Jiang et al. [49] explained that the flow excursion is a long-term process. Fluid temperature changes at the heated section exit will result from variation of heat transfer in the sub-cooler caused by a reduction in flow rate. The fluid enthalpy at the exit and the internal subcooled boiling condition will both fall, as a result, further lowering the mass flow rate. This continuing cyclic process leads to flow excursion. Yang et al. [50] used a four-equation drift flux model with subcooled boiling and condensation models to establish the respective conceptual background. There has been a lot of interest in the research of Ledinegg instability in microchannel flow [51–55]. The experimental study of Garrity et al. [64] showed that the height of the condenser and stochastic flow rate variation both affect static instability. Clausse and Lahey [56], using the 1D model, proposed a pioneering nonlinear diabatic boiling flow model. The system parameter showed limit cycle behavior as well as chaotic nature similar to experimental data. Lin and Pan [57] looked into the nonlinear dynamics of a two-phase NCL in order to find the characteristics of limit cycle oscillations and transient response to step-change in power supply. Multiple other endeavors [58, 59] have assessed nonlinear dynamics using a similar methodology.

In the present era, efforts are being made to operate the reactor at high temperatures so as to get higher thermal efficiency. To fulfill the need for high temperatures (which single and two-phase cannot meet due to saturation temperature criterion), advancement in materials sectors led to the development of supercritical water reactors (SCWR). SCWR work above the critical point of water (373.946 ^{o}C, 22.064 MPa) which enhances thermal efficiency to be over 45%, noteworthy escalation compared to Generation III and III+ water-cooled reactors with the elimination of CHF and phase change phenomenon. The design of SCWR matches the working condition of the supercritical water turbine and can be utilized directly. Before getting further, let us have a brief look at the supercritical fluids.

1.7 Supercritical Fluids (SCF)

It is an appealing aspect for the researcher to broaden its exploration to enhance its energy efficiency and seek an eco-friendly energy source because of environmental pollution as a

result of energy needs. In the past century, the average temperature of the earth has increased between 0.4 to 0.8 °C and as per the report of the Intergovernmental Panel on Climate Change (IPCC), due to global warming effect on the ecosystem, by the end of the 21^{st} century, this rise will go to 1.4 to 5.8 °C [60]. According to scientific research, the reason for this drastic adverse alteration of the atmosphere could be the melting of glaciers (causing the rise in acidification), drought, wildfire, greenhouse gases (GHG), and increasing carbon dioxide (CO_2) level in the atmosphere. In the preceding era, the excessive practice of fossil fuels has a significant contribution (78%) to GHG emissions. The fluid which works above the critical point (maximum pressure and temperature above which liquid and vapor state cannot exist together) are called SCF (Fig. 1.7).

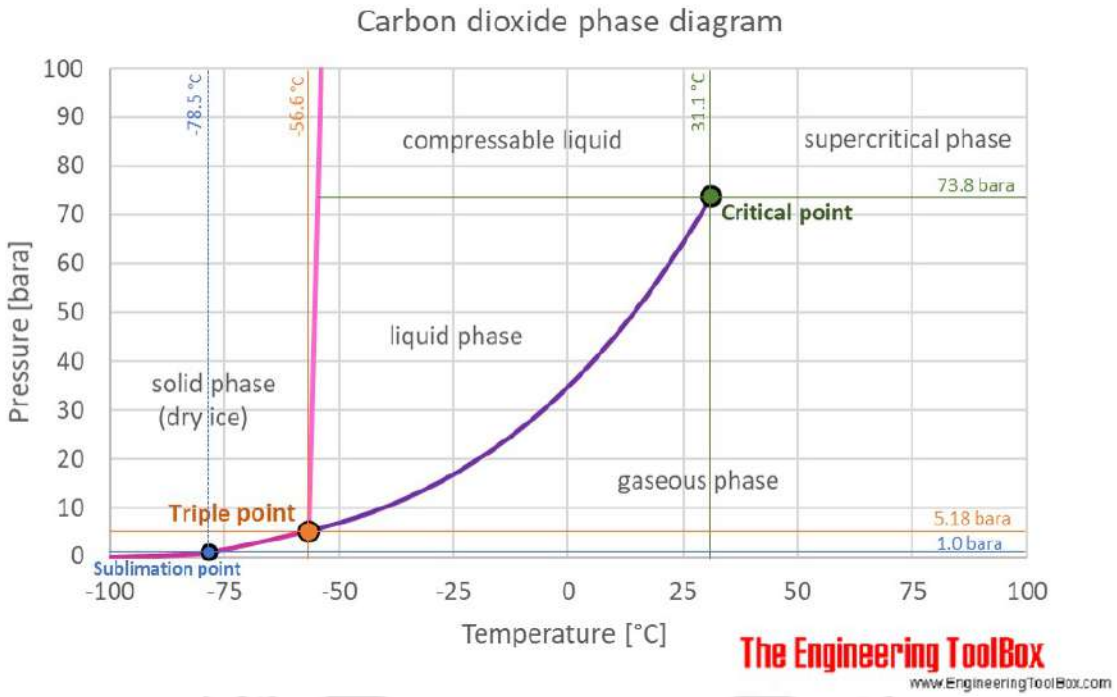

Fig. 1.7: Phase diagram of CO_2 (source: https://bit.ly/2LuMeRW)

The most commonly used supercritical fluids are carbon dioxide (Tc=304.1 K and Pc=7.38 MPa) and water (Tc=647.096 K and Pc=22.064 MPa). The attractive features of SCF are its properties at a supercritical state, especially around the "pseudocritical" point where fluid can have properties of single and two phase. Pseudo-critical temperature is nearly around 36∘C, along which large properties variation are observed as shown in Fig. 1.8(a) for CO_2 for 8.6 MPa. Researchers have also discovered R134a recently, which has low critical pressure (Pcr = 4.059 MPa and Tcr = 374.2 K). But at elevated temperatures, their compatibility

with material still remains the challenging part to deal with. Pseudo-critical temperature may vary depending upon the pressure, as shown in Fig. 1.8(b) for density variation of water at different pressure.

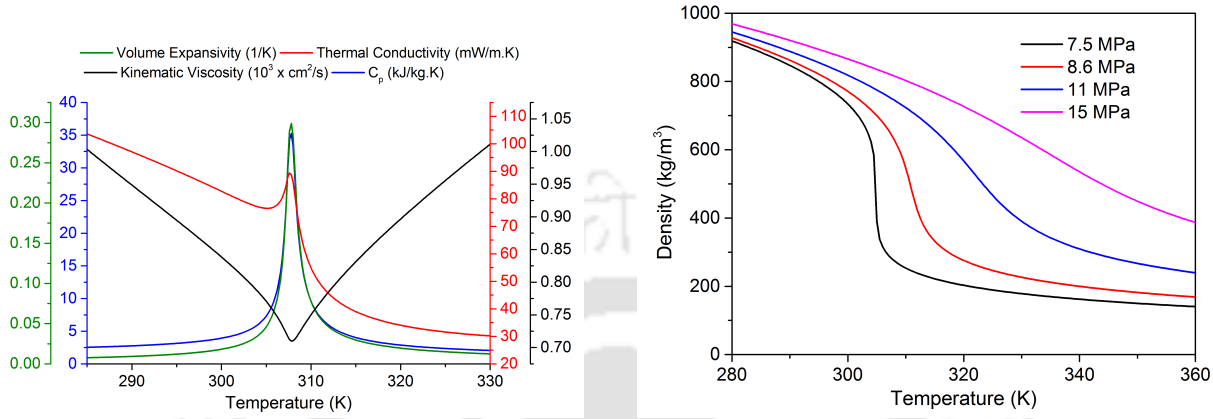

Fig. 1.8: (a)CO_2 properties variation with the temperature at 8.6 MPa and (b)Density plot of CO_2 with the temperature at various pressure

The significant change diminishes as the temperature increases, and at high temperatures, fluid starts to behave like a gas. Hence it is essential to note that to harness the maximum potential, it is crucial to recognize the working regime. Many gases at high pressures are considered as supercritical fluids, which also causes an increase in density, but they will not liquefy until their temperature is decreased below critical point temperature. Recently, the interest in supercritical fluid increased due to its heat transfer capability and higher flow rate. Steady-state characteristics of sNCL are similar to two-phase, while stability response is similar to single-phase. Despite the similar properties variation, CO_2 is preferable compared to water due to its lower critical point and tremendous advantages like a) Non-toxic, b) Non-flammable, c) Eco-friendly, d) low critical and triple point, e) high refrigeration volumetric capacity, f) high heat transfer capacity, g) inexpensive, h) Natural and readily available, i) no harm to ozone layer depletion, j) high volumetric efficiency. Because of these, it is possible to design a cost-effective and compact design. All these traits, in turn, lead to the application of CO_2 in preparation of material and deposition processes [61], refrigeration [62], heat pump [63], chemical extraction [64] and nuclear reactor application [65].

1.8 Supercritical Natural Circulation Loop

The significant advantage of operating NCL with the supercritical fluid condition is that, near pseudo-critical temperature, considerable variation in the properties can create the driving forces compared to the two-phase system and hence more competent than conventional LWRs. Apart from these, heat transfer characteristics are excellent, and as the system is operated in single-phase, limitations associated with critical heat flux are avoided along with it dryers and separators are eliminated. Due to these, it has grasped the attention of designers of nuclear reactor B-500 SKDI [66] and CANDU-X [67] and fossil-fuelled (first plant was based on SC water in the UK since 1999) plants. As it comprises the advantages of both single and two-phase systems and due to its compact design (elimination of bulky accessories) and high projected efficiency, in the current era, it is considered as a significant initiative under generation IV nuclear reactors. Hence it has attracted the attention of researchers across the globe; in fact, over the last decade, pioneering work has been done already, and the focus is now a day is in advancement in the field. The technology is apparently new and requires loads of attention due to the fact of high sensitivity of properties variation near critical point with temperature. Due to such variation, special care is needed while investigating the whole phenomenon. At the pseudo-critical point, volumetric expansion is the highest aides generating ample buoyancy compared to two-phase NCLs. Property enhancement at supercritical state imposes significant advantages compared to single and two-phase while carrying a few similarities as well like density variation is similar to liquid to vapor phase change. Prandtl number exhibits high values, which aids in achieving excellent heat transfer characteristics. Single-phase system is characterized by its regularized heat transfer characteristics due to large thermal conductivity but provides a low flow rate. While on the other hand two-phase system provides a large flow rate but is highly susceptible to instabilities and unstable fluctuations. Instead of the compelling advantages, sNCL has some challenges in implementations like at high pressure and temperatures, system stability, material selection is crucial, and laboratory equipment are more expensive than the single and two-phase systems.

The most attractive fluid in a supercritical state is carbon-di-oxide CO_2, and Water H_2O due to heat transfer characteristics and properties near critical point very similar to each other for both. At the same time, inventory requirement is marginally less for CO_2 as compared to H_2O [68]. Due to the relatively new field, the process of thorough research is still going on with pioneering work started in the late 20^{th} century. Related works are mostly theoretical and numerical, while experimental knowledge/validation reported are less.

Some studies have also reported the use of commercial software. Most analytical studies based on steady-state or transient are either 1D or 2D. 1D developed codes are FIASCO, NOLSTA, SPORTS, RELAP5, and SUCLIN, while the 2D code is NAFA-Loop. 1D code is comparatively simple to put constraints in execution because, in 1D code, it is assumed that flow is fully developed; hence marginal deviations are found compared to the actual scenario. At the same time, 2D code can capture developing as well as the developed region. Thermal hydraulic aspects have been explored in detail in steady-state and transient with various geometric parameters like loop diameters, loop height, inclination angle, heater, cooler length, etc. NCL being very attractive in terms of longer response time, enhanced reliability, and increased passive safety, do have some barriers in the form of low hydraulic head and instabilities, which are essential to investigate while designing such a critical system. Because of its tremendous potential, the sNCL system is considered the future of nuclear reactor core cooling. Cooling of the reactor through NCL is a relatively new technology that enhances the thermohydraulic performance of the reactor because of the simplicity of the design. Carbon dioxide is considered the best suitable substitution for supercritical water as the property variation of water and CO_2 are parallel at supercritical conditions. Notable examples of sNCL are S5G and S8G US naval reactors (https://bit.ly/2Z05x0c). A subcritical study done by [38, 69–71] was not found suitable for the supercritical state because of different behavior. Hence independent study needs to be carried out.

For better performance of the system, it is the prime duty of the design engineer to investigate different aspects for a better understanding of the system under different conditions like different loop diameters, loop heights, pressure, etc. The following section will deal with the parametric study of the system considering steady-state flow characteristics and heat transport. The key advantage of using sNCL is an extreme variation of properties near the pseudo-critical point. The small temperature difference between the heater and cooler can cause a large Reynolds number [72–76]. But, it can cause deterioration in heat transfer as investigated by [77], causing poor heat transfer characteristics. Better heat transfer characteristics are obtained when operating in the supercritical region compared to the subcritical region, especially when the operating point is near the pseudo point [78, 79]. Capturing the proper behavior and, subsequently, essential modification in the system design is the motto of science.

Due to the absence of forced convection or an external flow device, the mechanism of flow takes place because of natural convection. In natural convection, the thermalhydraulic role is played by buoyancy and gravity. When fluid is heated, then due to temperature increase,

it becomes lighter and lifts up, displacing fluid in its way, and fluid above it, due to its relatively dense nature, comes down. A simple, practical example is heating water or milk in a pan. The unsymmetrical nature of temperature and velocity exists in the cross-section of the heater and cooler due to cross-sectional temperature gradient or local buoyancy effect [68, 80–82]. The direction of motion depends upon the temperature of the wall and fluid, as shown in Fig. 1.9.

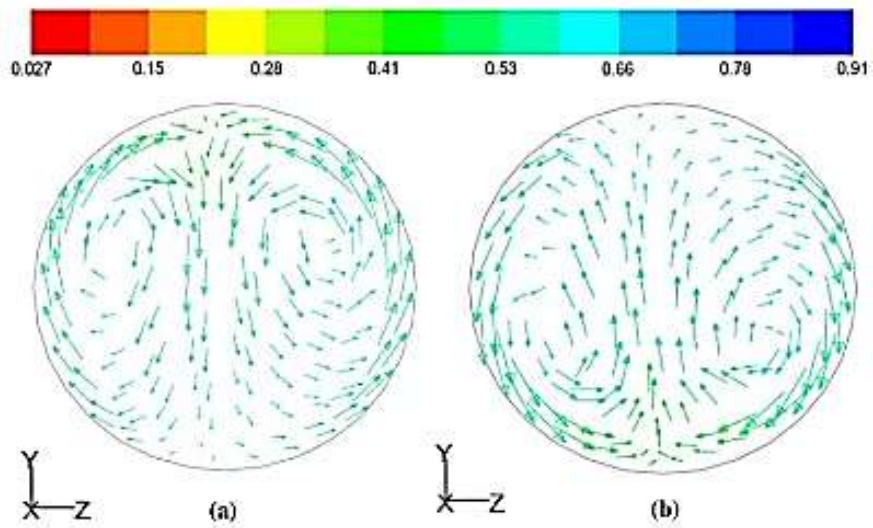

Fig. 1.9: velocity vector plot for HHX water inlet at 343 K at the center of (a) HHX and (b) CHX [80][1]

Hence it is essential to summarise the comprehensive history of behavior sNCL under different circumstances to date before moving into more insights into this system. This chapter summarises all those aspects which give an insight into sNCL and the contribution of various researchers in this field. With the advancement in the system, some benchmarks and efforts have been made to provide guidelines and research gaps so as to fulfill the void of knowledge.

In the field of thermalhydraulic performance, such as steady-state characteristics and stability of sNCL was studied in the early 21^{st} century by [83]. He developed an analytical model for investigation of the open-loop in HHHC configuration with water as working fluid at 25 MPa and 350 °C and solved the corresponding equations by some modification in

[1] "Reprinted from International Journal of Advances in Engineering Sciences and Applied Mathematics , 4, Ajay Kumar Yadav, M. Ram Gopal, Souvik Bhattacharyya, Computational fluid dynamic analysis of a supercritical CO_2 based natural circulation loop with end heat exchangers, 119-126., 2012, with permission from Springer."

SPORTS (Special Prediction of Reactor Transients and Stability) code [84] which had been used earlier for stability analysis at low pressure due to subcooled boiling. For properties calculation, the STEAM [85] package was used. In the investigation, it was observed that with the increase in power, the steady-state flow rate increases and reaches the maxima, and starts decreasing, which was the profound outcome from his analysis for the criterion for stability boundary (equation 1.6) as shown in Fig. 1.10.

$$\frac{\partial G}{\partial Q} = 0 \tag{1.6}$$

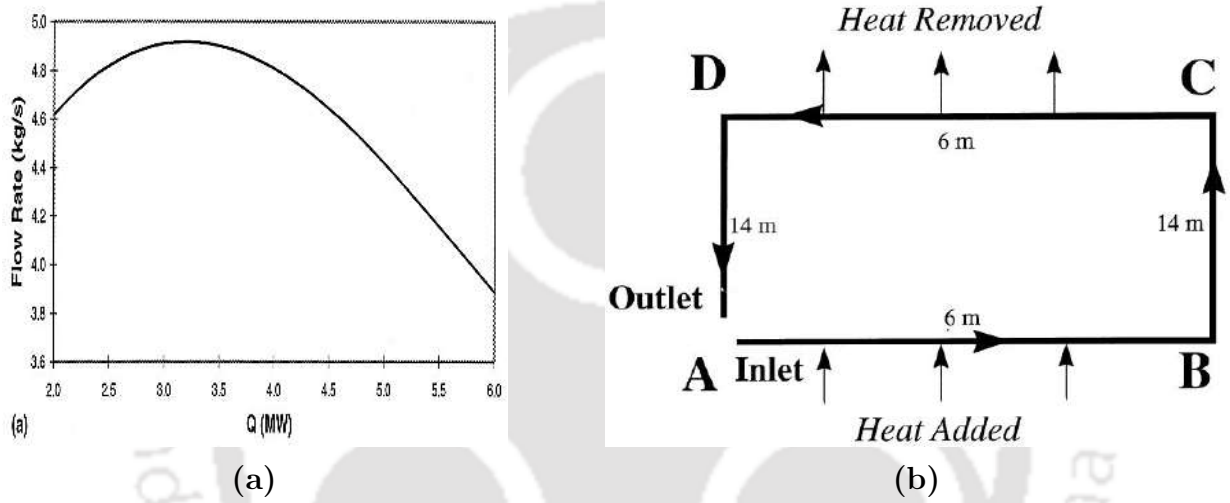

Fig. 1.10: (a) Steady-state solution with point heat source and sink and (b) Schematic diagram of the loop by [83][2]

Integrating the equation for mass flow, momentum, and energy, the corresponding expression for steady-state mass flow rate

$$G^2 = \frac{2Dgh_t(\rho_1 - \rho_2)}{\left(\frac{f_1 z_1 + f_3 z_3}{\rho_1}\right) + \frac{f_2 z_2}{\rho_2}} \tag{1.7}$$

Using the criterion as per the equation 1.6, the expression for bounding power and the maximum mass flow rate was

$$Q_b^* = \frac{Q_b}{AG_m h_1} \tag{1.8}$$

[2] "Reprinted from International Journal of Heat and Mass Transfer, 44, Vijay Chatoorgoon, Stability of supercritical fluid flow in a single-channel natural-convection loop, 1963-1972, 2001, with permission from Elsevier."

$$G_m = \rho_{b2}\xi \tag{1.9}$$

The bounding power got affected when friction and inlet temperature was changed.

Vijayan and Austregesilo [86] derived the correlations which are considered as the benchmark for any NCL. Theoretical studies suggest that the important parameters are modified Grashof number, modified Reynolds number, and modified Stanton number for steady, transient as well as stability behavior.

$$Gr_m = \frac{g\beta D^3 \rho^2 \dot{Q} H}{A\mu^3 C_p} \tag{1.10}$$

$$Re_{ss} = \frac{D\dot{m}_{ss}}{A\mu} \tag{1.11}$$

The theoretical study showed that for simulation of steady-state behavior, the plot of steady-state mass flow rate and modified Grashof number on log-log graph results in a straight line as shown in Fig. 1.11a which was supported by experiments on three loops and confirmed importance of parameter $Gr_m \frac{D}{L_{tot}}$ for steady-state behavior while for transient behavior parameter $\left(Gr_m \frac{D}{L_{tot}}\right)^{\frac{b}{3-b}}$ is important.

This was later on extended by [87] for non-uniform diameter as well with good agreement. Though mostly investigations are for uniform diameter loops, e.g., rectangular loop [88, 89], toroidal loop [24], open-loop [90]. The obtained relation was of the below-mentioned form-

$$Re_{ss} = C\left(Gr_m \frac{D}{L_{tot}}\right)^r \tag{1.12}$$

where, $b = 3 - \frac{1}{r}$ and $p = \frac{2}{3-b}$

The limitation of the correlation mentioned above is that when the contribution of friction flow is more, then the equation will not hold its validity.

The analysis was done for various loop configurations like HHHC, HHVC, VHHC, and VHVC. Because the nature of the supercritical fluid is very different depending on the temperature and pressure, sigmoidal relation was used to divide the zone into three parts. The correlations were found to be applicable for CO_2, H_2O, and other fluids.

The following bullet points will be discussed as part of the brief history of the sNCL-

- Steady-state characteristics
- Stability characteristics

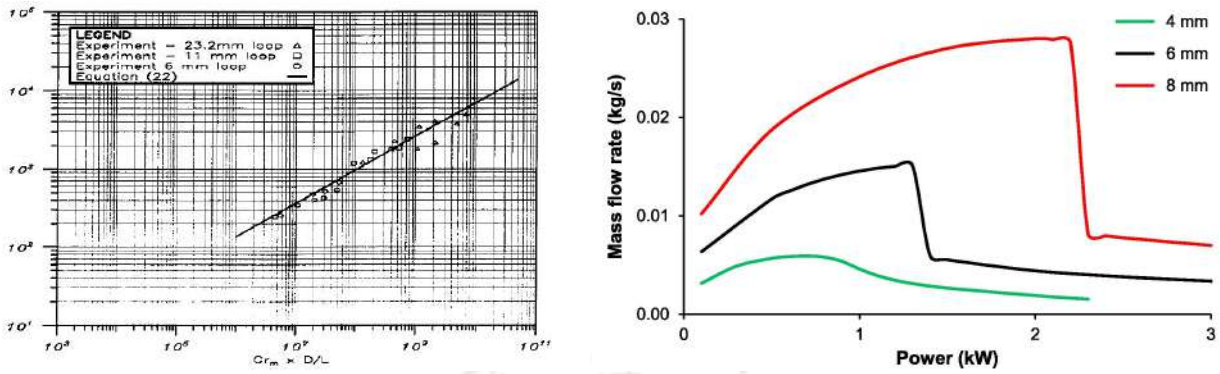

(a) (b)

Fig. 1.11: (a) Steady-state non-dimensional data for various diameter loop [86] [3]and (b)effect of loop diameter on mass flow rate for HHHC configuration at 8 MPa [77][4]

1.9 Steady-State Characteristics

Steady-state characteristics are those which are independent of the variation of time. The occurrence of a steady state depends upon the balance between friction and buoyancy force. The steady-state investigation is vital from the point of view of flow as well as heat transport aspects of NCL. Extensive study has been done in the last decade, mostly numerical investigation with less experimental support. Hence comprehensive knowledge is necessary before further proceeding. The section will summarise the experimental as well as analytical study, which was done by many investigators in parametric form.

• **Effect of diameter**

Tube diameter is one of the key factors from the heat transfer and flow characteristic point of view. Changing the diameter changes its circumferential area as $A_c = \pi D$. Due to the increase in surface area, to obtain the same level of temperature, higher power will be required. Moreover, a larger diameter imposes manufacturing costs and space issues. Increasing the pipe diameter increases the mass flow rate because of the increase in gravity dominant region, which causes enhanced buoyancy region over the friction region. Moreover, for a small diameter loop, the viscosity becomes less, leading to chances of flow reversal, while such possibility is less for a higher diameter due to high flow velocity. But after a threshold power mass flow rate starts decreasing due to increased friction. [91] considered

[4] "Reprinted from Nuclear Engineering and Design, 152, P.K Vijayan,H Austregesilo, Scaling laws for single-phase natural circulation loops, 331-347, 1994, with permission from Elsevier."

[4] "Reprinted from Nuclear Engineering and Design, 324, Milan K.S. Sarkar,Dipankar N. Basu, Influence of geometric parameters on thermalhydraulic characteristics of supercritical CO2 in natural circulation loop, 402-415, 2017, with permission from Elsevier."

four different diameter loops (7 mm, 14 mm, 20.7 mm, and 28 mm) in their analytical study using SUCLIN code for water (at 25 MPa and heater inlet temperature of 370 °C) and found that as the slope in mass flow and power changes sign from positive to negative, heater outlet temperature starts increasing. [92] used nonlinear code NOLSTA code and considered CO_2. For different diameters (7 mm, 13.88 mm, 20.7 mm, and 28 mm) and for loop pressure of 9 MPa and at a heater inlet temperature of 30 °C found the similar nature as earlier as shown in Fig. 1.11b. A similar phenomenon was observed by [93]. The substantial decrease in mass flow rate was termed FiHTD by Sarkar and Basu[77].

A numerical study performed by Chen et al. [74] for 6 and 15 mm diameter (operating condition 9 MPa, cooler temperature 298K, and heater temperature 323 K, 523 K, 823 K, 1023 K). A larger diameter enhances heat transfer performance even at high-temperature conditions, the advantage of which can be in the field where high heat transfer removal is required, like reactor core cooling. Moreover, at low heating temperatures, the Nusselt number is more for the heater and vice versa for the cooler at higher heating temperatures.

• **Temperature differential between source and sink**

The loop mass flow rate is affected when temperature ranges near the pseudo-critical point. If the temperature reaches near the pseudo-critical point in the cooler, then the effect of buoyancy overcomes the viscous effect causing an increment in mass flow. A similar phenomenon occurred for high temperatures. 2D model of sCO_2 was investigated by Cao and Zhang[94], and it was found that for sink temperature 310 K, if the temperature difference between source and is increased from 10 K to 40 K, there is the rise in mass flow rate (0.0014 kg/sec to 0.0025 kg/sec) and Nusselt number as well. The results were consistent with the experimental study of sCO_2 based solar collector [95]. Qualitatively, results were also similar to experimentally similar to that of water [96]. The authors also validated the consistency of the present study by using the Lattice-Boltzmann Method (LBM). With the further increment in temperature difference, thermalhydraulic properties started degrading as temperature crossed T_{pc}. Mass flow keeps on decreasing beyond the pseudocritial point because, at high temperatures, the viscosity of the fluid begins increasing (termed as "second pseudo critical" by Chen et al.[97] and Reynolds number showed the same nature. The degraded mass flow rate was also reported in 3D simulation with an end heat exchanger (CHX inlet temperature = 305 K and HHX inlet temperature = 313 K to 353 K at 8 MPa operating pressure) with an increase in temperature differential [78, 80]. Keeping the heater temperature and increasing cooler temperature also decreases the mass flow rate [98].

On the other hand, an experimental study of Chen et al. [99] showed that with the

variation in bulk temperature, the heat transfer coefficient in the cooler remains more or less the same due to stable temperature, while the same for heater decreases due to the low value of thermal conductivity near pseudo-critical point. The extent of the heat transfer coefficient is way better than the single-phase loop. Heat transfer coefficient increases as the pressure increases due to the fact that the pseudo critical point also shifts to higher temperature [78, 100].

• **Effect of loop height**

Adequate buoyancy generated is dependent on loop height also. The larger the height, the larger will be the pressure difference created between vertical legs. Loop height can be small for chip cooling applications and can be large for nuclear reactor cooling applications. Due to experimental intricacy, the effect of height has been investigated numerically or analytically. With the increase in height, the pressure difference between the two legs increases, causing an increase in mass flow rate. With the increase in height, friction also increases, but the buoyancy-driven region dominates over the friction region, causing an increment in mass flow. But as the friction force becomes significant, the mass flow rate starts decreasing. An increase in mass flow in a taller loop causes a lesser cooler temperature, which causes a lower loop average temperature [93]. In the case of CO_2 as a supercritical fluid, increasing height also delays the heat transfer deterioration due to lesser loop average temperature [77]. But beyond the height of 2.12 m, the effect of height is insignificant as HTD occurs after almost at the same power due to chemical properties of CO_2. The analytical study with water using SUCLIN code [91] observed the same phenomenon for scH_2O for loop heights of 4.4 and 11.1 m.

But due to the faster rate of change of internal volume, mass flow increment is more pronounced in the case of diameter compared to height variation. Hence increase in diameter is considered a better option for mass flow increment.

• **Effect of pressure**

The pseudo-critical point depends upon the pressure. Pseudo critical point shifts to a higher temperature with an increase in pressure. An analytical study done by Sharma et al. [92], using Nonlinear stability analysis (NOLSTA) code for open as well as closed-loop showed that due to shifting of the pseudo critical point, peak mass flow rate moves right even for a higher power. Archana et al. [82] used 2D axis-symmetric NAFA-LOOP (heater power varied from 200 W to 3000 W) for 8.5, 9, 9.5 MPa pressure, respectively. The mass flow rate increased till loop the pseudo-critical temperature reached. The behavior was similar to a two-phase natural circulation loop. A similar phenomenon was observed by Sarkar and

Basu[101] in their numerical study for the pressure of 6, 8, and 10 MPa. As the 6 MPa is sub-critical (saturation temperature 295.13 K), the mass flow rate drop phenomenon was not observed (Fig. 1.12)

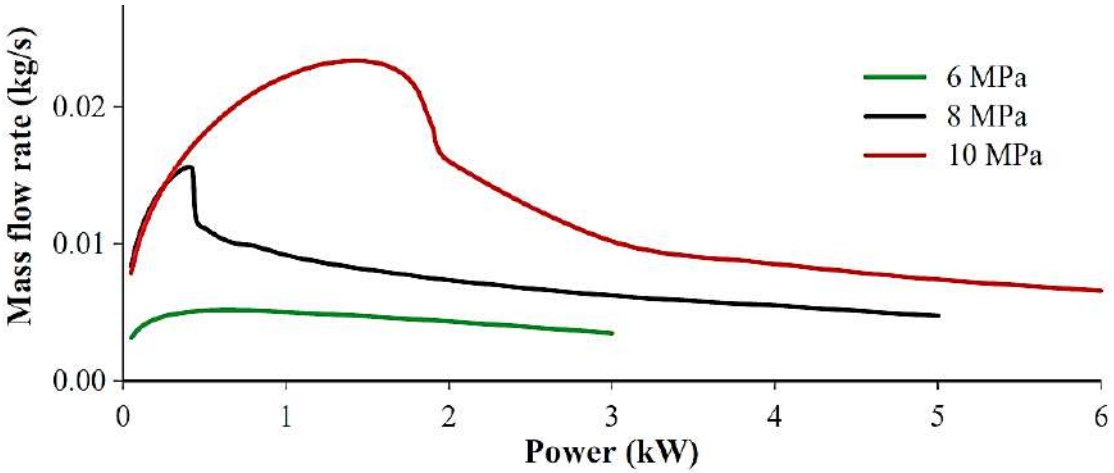

Fig. 1.12: Variation of mass flow rate at different pressure with power [101][5]

In the experimental study of Liu et al.[76], it was observed that if, for a closed-loop system, the heater inlet temperature is controlled by varying coolant temperature (though it is a complex task) and maintained at 22°C. It was observed that the dominant buoyancy region could be extended beyond pseudo-critical temperature. Density difference beyond pseudo-critical increases slowly while the inverse of density, which represents the frictional resistance, increases at a faster rate. The results were contradictory to the [92] because, in their study, heater inlet temperature was not kept constant as it varied as the heater power was increased. For lower pressure (7.45 MPa), friction dominated soon as compared to high pressure (8.90 MPa). It was also observed that if inlet temperature was maintained near pseudo-critical temperature, then the peak of mass flow rate touched shortly.

Despite the higher mass flow rate at 10 MPa in the study of [101], it was observed that at 8 MPa peak, the heat transfer coefficient is more than that of 10 MPa. This is because, at 8 MPa, the property variation is expressively higher than other supercritical pressures, as shown in Fig. 1.13. The study of Yadav et al.[78] and Archana et al. [82] (2D axisymmetric NAFA-LOOP) supports this result using and beyond the peak of Nusselt number is more for higher pressure loop as shown in figure 1.13. The trend was similar for the cooler section

[5] "Reprinted from Nuclear Engineering and Design, 293, Milan K.S. Sarkar,Dipankar N. Basu,Working regime identification for natural circulation loops by comparative thermalhydraulic analyses with three fluids under identical operating conditions, 187-195, 2015, with permission from Elsevier."

Nusselt number. The reason for this is the change in the Prandtl number trend, as the

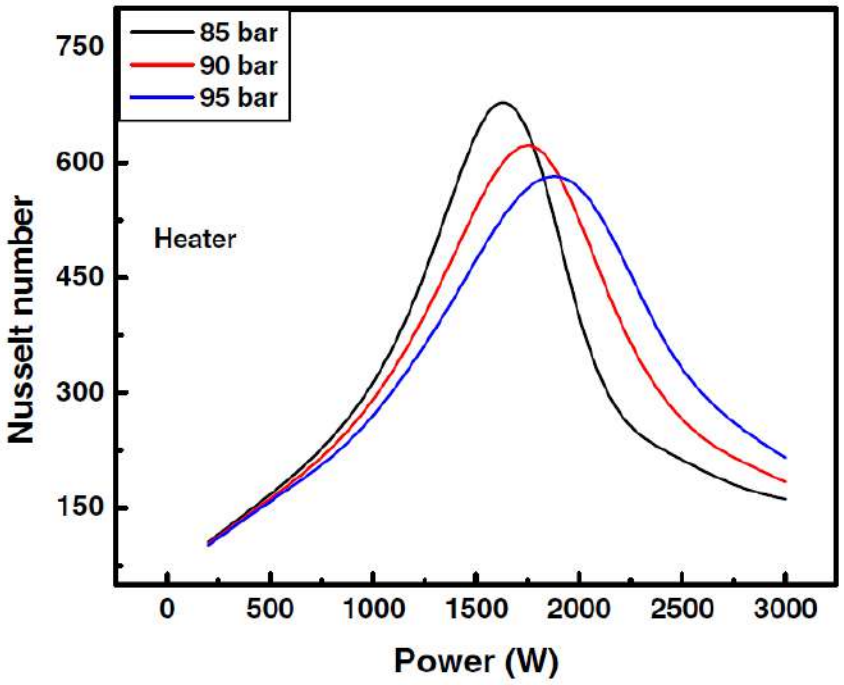

Fig. 1.13: Nusselt number at a heater for different pressure [82]

Nusselt number is the function of the Reynolds number and Prandtl number.

• **Loop orientation**

It can be studied in three separate sections-

(a) **Effect of inclination angle**

Tilting the loop in any direction causes the reduction in gravity by cos θ and will be considered as a reduced gravity scenario. Due to the inclination of cos θ, buoyancy also decreases by θ angle. Chen et al.[102] in their experimental study considered 0° to be a horizontal loop, and as the loop inclination was increased, the loop mass flow started increasing as expected, as shown in Fig. 1.14b. As the loop tends to get vertical, the effect of the inclination effect showed little impact on the flow rate as the gravity component changed a little. A similar result was reported by different groups [77, 78, 103]. It was interesting to see that the power level corresponding to FiHTD was quite similar for different inclination angles.

The heat transfer performance was found to degrade with the inclination angle as the

[6] "Reprinted from Nuclear Engineering and Design, 265, Lin Chen,Xin-Rong Zhang,Bi-Li Deng,Bin Jiang, Scaling laws for single-phase natural circulation loops, 895-908, 2013, with permission from Elsevier."

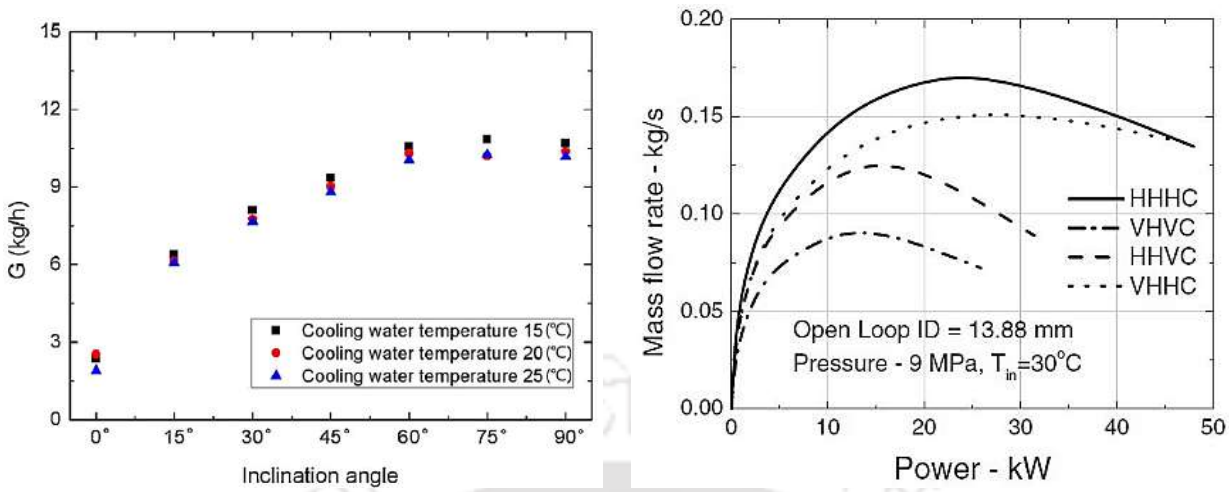

(a) **(b)**

Fig. 1.14: (a) Evolution of mass flow rate for different inclination angle [102][6]and (b) Mass flow rate variation for different loop configuration [92]

Reynolds number decreases [94]. Inferior performance due to inclination can be enhanced to some extent at higher heat flux as depicted by Chen et al. [102] for heat flux conditions of 600, 6000, 60000 W/m^2. For 600 W/m^2, the Nusselt number showed a poor value of 14.7, while for 60000 W/m^2, a promising value of Nusselt number (2085.0) was obtained for 45° inclination. The parameter "thermal resistance" is defined as

$$TR = \frac{\Delta T}{G\Delta h} \tag{1.13}$$

was used to compare performance at different inclination angles. It was observed that at 0° inclination, thermal resistance is more, causing poor heat transfer performance as the thermal resistance is higher for 0°. Moreover, Yadav et al. [103] compared the effect of inclination for supercritical with subcritical vapor and liquid. The results were evident that in a supercritical state, the heat transfer rate is far better.

(b) **Effect of the heater and cooler orientation**

The paramount driving potential of the loop fluid comes from the optimization of the heater and cooler location, length, and applied conditions, as the density is directly affected by the condition applied, which causes an alteration in mass flow.

(c) **Heater length**

This controlling parameter is important from the point of view of material issues. Loop

effectiveness is defined as

$$\varepsilon_{NCL} = \frac{\dot{q}_c}{\dot{q}_h} \tag{1.14}$$

Considering the same operating conditions, power input causes an increase in heat flux due to less heat transfer area

$$\dot{q}''_w = \frac{\dot{q}}{A} \tag{1.15}$$

Due to this, the heater outlet temperature increases, causing a less effective loop. A numerical study by Sadhu et al. [93] showed that the increment in temperature did not show a prominent effect, but the effectiveness increment is promising. As the same conditions are applied over the loop, the same temperature profiles (or slight variations) are obtained, due to which the loop experiences identical friction and buoyancy. A numerical study of Sarkar and Basu [77] showed the same mass flow and heat transfer behavior with the same power level of FiHTD. Hence there was no significant issue found with heater length, though this can be further investigated based on thermal stresses on the material.

(d) **Cooler length**

Reduction in cooler length (keeping all parameters the same) causes less heat transfer to the secondary side (generally water), hence high temperature at the cooler exit, which will create a hindrance for fluid to accept heat from the heater section. For smaller cooler lengths, FiHTD occurs soon [77]. Moreover, loop effectiveness will also degrade. The effect of cooler length on effectiveness is more prominent compared to heater length. Hence for better heat transfer longer heater and cooler length is recommended [93].

(e) **Heater and cooler configuration**

Experiments were conducted by Swapnalee et al. [104] to investigate the effect of the heater and cooler in both horizontal and vertical positions. The possible configurations are HHHC, HHVC, VHHC, and VHVC. For the configuration HHHC, the value of Re and Gr is high as compared to other configurations, which causes the highest mass flow rate in the HHHC case and lowest for VHVC case, as confirmed by investigation of Sharma et al. [92]). For the same elevation difference, VHHC gives a better flow rate than HHVC. It was found that for all vertical heater configurations or asymmetric configurations, there are no chances of flow reversal due to predefined flow direction, while for other combinations (symmetric configurations), flow reversal may take may depending upon the conditions applied [105]. It is clearly evident that loop configuration has a noticeable effect on flow rate than the heat transfer characteristics.

• **Effect of corner bend**

The loop is connected by bends to complete the closed loop. With the increase of the bend radius, centrifugal action is imparted, which causes asymmetry in the fluid stream, though asymmetry is inherently there due to local buoyancy, mainly when the temperature is near the pseudo-critical temperature. A study for two different bend radii of 5 mm and 15 mm at 2 kW showed that due to centrifugal action, only asymmetry is imparted, causing a high-velocity zone dominated at the bottom. No effect on FiHTD was observed with power when the bend radius was altered [77].

To prevent the heat from the pipe wall to the surroundings, a sufficient thickness of insulation is 50 mm. After that, the effect becomes insignificant [93]. Noticeable HTD was witnessed by Liu et al. [106] in an experimental study. The characteristics of HTD were found to be similar to that found in the forced flow case, i.e., local rise in wall temperature inside the test section. With the increment of heater power, the point of HTD shifts towards the heater inlet. The flow and heat transfer characteristics were found to be a huge function of buoyancy parameter and flow acceleration. No HTD was observed for the value of Bu less than 2 x 10^{-5}. There are several criteria available for force convection that are not applicable to natural convection. Intense experimentation of Yuanlu et al. [107] came up with a new dimensionless parameter SBO for capturing the HTD phenomenon. The new correlation introducing a parameter significantly improves, capturing 96.31% of the data with a 30% accuracy.

1.10 Stability Behavior of sNCL

One of the basic necessities for understanding the stability behavior of NCLs is the availability of generalized dimensionless groups (or scaling parameters) which are not loop-specific. Such dimensionless groups are useful in comparing the performances of different loops and extending data from small-scale loops to the prototype. Investigations, both analytically and experimentally, for different loop configurations (rectangular loop [26], Toroidal [24]) have been made by many researchers. However, the facts have gained momentum in the recent decade only. Most of the results may be observed analytically but are skipped out while observing experimentally. Boundary conditions and structure of loop have an effect on stability behavior [108]. Due to dependencies on the Equation of States (EOS) of the properties and transient nature, stability is instead a complex phenomenon.

Research codes like SPORTS [83], SUCLIN [91], RELAP5 [109], FIASCO [110], NOLSTA [111], NAFA-LOOP [72] were proposed to steady-state and stability analysis, but 3D code is still not developed due to nonlinear nature of the system. Commercial software fluent has been used by various research groups [100, 103]. The point hydraulics model (PHM) was developed theoretically to predict the self-sustaining flow oscillations which are applicable to the system which is cooled by supercritical water.

Two approaches are used to understand the stability phenomenon-

- **Frequency domain approach**
  In the Frequency domain or linear approach, it is assumed that perturbation is infinitesimally small and perturbation is imposed over the steady-state operating point in time-dependent conservation equations, and the nature of corresponding equations is found out based on the nature of Eigenvalues. The system will be stable and unstable for the negative and positive real parts, respectively, whereas, for the neutrally stable system, the system will have purely imaginary values.

- **Time-domain approach**
  In a nonlinear or time-domain approach, small perturbation is given in the steady-state solution, and equations acquired are solved. If oscillations decay with time, then it is stable, or if it grows, then it is unstable. Whereas if oscillations happen with constant amplitude, then it is neutrally stable.

1.10.1 Theoretical and numerical studies

Welander [26] has predicted that flow oscillations in a single-phase NCL occur in small amplitudes, which later on increase until the flow is completely reversed from the original direction. Chen [112] investigated that in a single-phase rectangular loop, the aspect ratio (width/height) of the rectangular loop affects the modified Grashof number (associated with Buoyancy), which in turn affects the stability of the loop. The loop is only stable if the Grashof no. is above a critical value. Cammarata et al. [113] showed that a single-phase NCL flowing in the square loop is the least stable, while slender loops are the most durable. Slender loops are not only stable but are also less sensitive to modifications or perturbations in operating conditions. This fact was considered in many investigations for supercritical NCL done by Chen and Zhang [74] with CO_2 as the operating fluid.

Pioneering work for the stability analysis of supercritical fluid was done by Chatoorgoon [83] using the SPORTS code. SPORTS was found suitable in those regions where liquid-

to-vapor variation takes place. STEAM property package was used for the calculation of properties. It was found that the positive slope of flow-power characteristics defines stable operating regions. After this, instability starts amplifying, which was captured roughly by the SPORTS code, as can be seen in Fig. 1.15; the reason for divergence was approximations considered while solving.

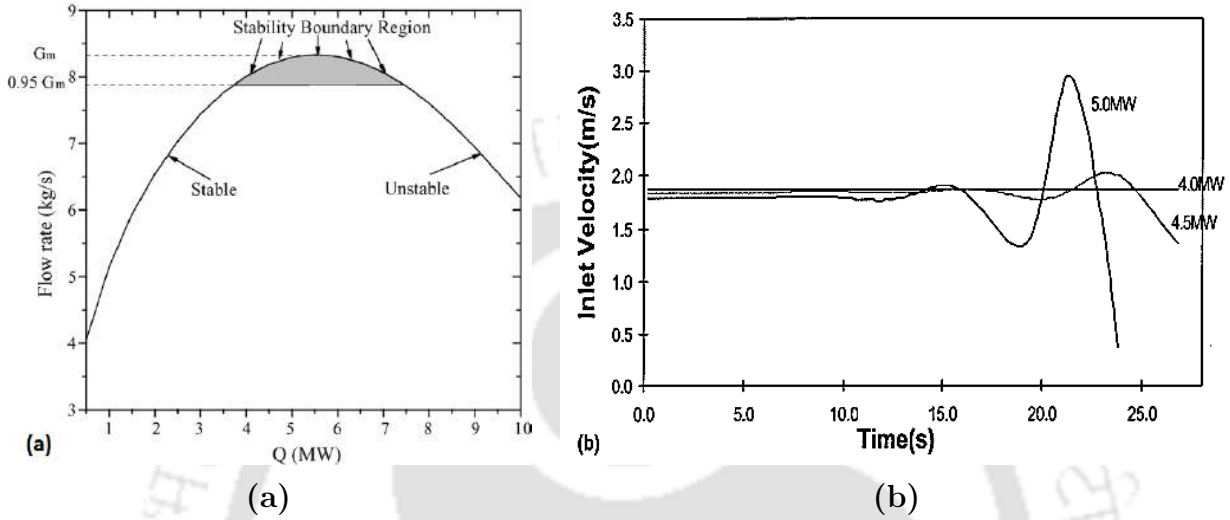

(a) **(b)**

Fig. 1.15: (a) Steady-state profile of flow rate, demonstrating stable and unstable regimes [114][7], and (b) the stability boundary region [83][8]

To verify the authenticity of the code, a theoretical model was also developed. To make the code simpler, point source and sink were considered instead of taking uniform heat flux so that equations become linear and relatively easier to solve, skipping the complications arising from the nonlinear nature of temperature and density neat critical points. The results obtained from the above conditions were in good agreement with SPORTS. Similar to two-phase flow, an approximate stability boundary criterion was developed, and that was a major breakthrough at that time.

Non-dimensional group for uniform diameter proposed by Vijayan and Austregesilo [86] was used by Vijayan [87] for a linear stability model in non-uniform diameter loop. In their study, nonlinear conservation equations were linearized. The system was considered to be unstable if there existed any real root of the equation. To envisage the instability, there is

[8] "Reprinted from Nuclear Engineering and Design, 235, V. Chatoorgoon,A. Voodi,D. Fraser, The stability boundary for supercritical flow in natural convection loops Part I: H_2O studies, 2570-2580, 1994, with permission from Elsevier."

[8] "Reprinted from International Journal of Heat and Mass Transfer, 44, Vijay Chatoorgoon, Stability of supercritical fluid flow in a single-channel natural-convection loop, 1963-1972, 2001, with permission from Elsevier."

vital role of the modified Grashof number and modified Stanton number. Parametric studies were done with three different diameter loops (6, 11, and 23.2 mm). It was observed that, at the particular Stanton number, as the fraction of L_t/D increases, the unstable zone shifts up, as shown in Fig. 1.16. A similar phenomenon was observed by Sharma et al.[91] and found that the unstable zone domain diminished with less diameter. The key conclusion considering the real-life situation, the ratio of L_t/D is quite high for the nuclear reactors, so no stability of this kind was found to be detected. Considering the same loop configuration when $St_m > 9.7$, no instability was observed. But it is important to note that special care for the calculation of St_m should be given, as it changes with loop diameter. So it is recommended to increase L_t/D or St_m to suppress the instability.

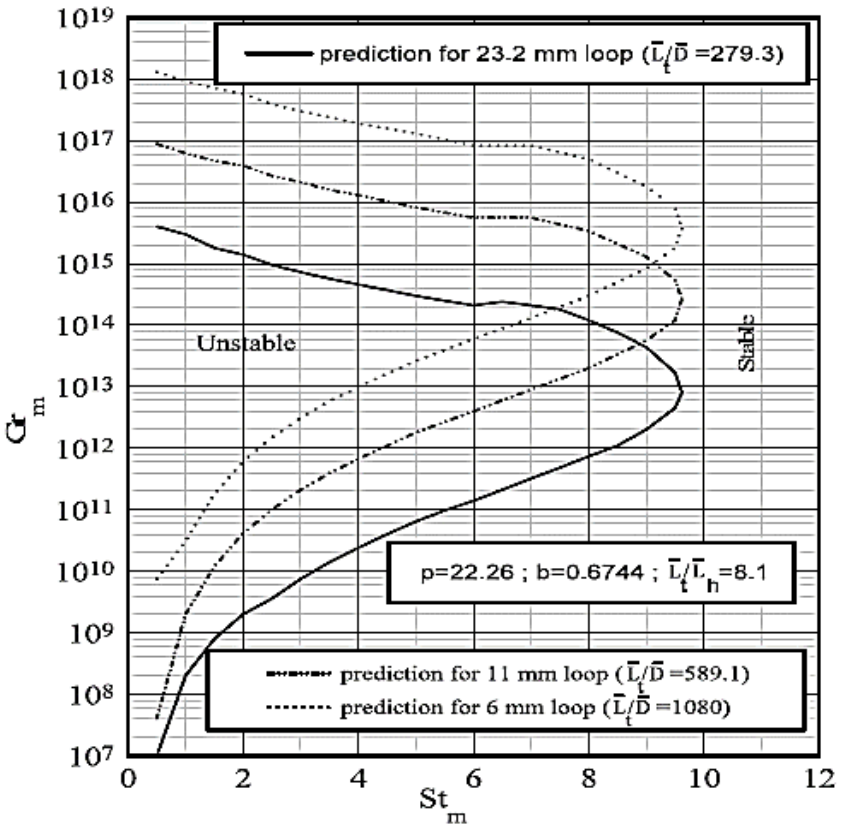

Fig. 1.16: Stability map evaluation for three rectangular loops [87][9]

Earlier proposed non-dimensional numbers for supercritical flow in NCL were examined by Chatoorgoon et al. [114, 115] in a large number of simulations for H_2O (PART-I) and CO_2

[9] "Reprinted from Nuclear Engineering and Design, 215, P.K. Vijayan, Experimental observations on the general trends of the steady state and stability behaviour of single-phase natural circulation loops, 139-152, 2002, with permission from Elsevier."

and H_2 (PART-II) using SPORTS code. Dimensionless numbers nicely predict the stability boundary within 95% of maximum mass flux in dimensionless form.

Zhao et al. [116] attempted to improvise the correlations used in boiling channels for the supercritical fluid case. Earlier, there were phase change numbers and sub-cooling numbers for boiling channels. Their study was taken further by Ambrosini and Sharabi [117] and proposed apparent trans-pseudo critical number N'_{TPC} and the sub-pseudo-critical number N_{SUBPC} for supercritical pressure.

$$N'_{TPC} = \frac{q'_0 \Pi_h L}{\rho_{pc} w_0 A} \frac{\beta_{pc}}{c_{p,pc}} \tag{1.16}$$

$$N_{SUBPC} = \frac{\beta_{pc}}{c_{p,pc}} (h_{pc} - h_{in}) \tag{1.17}$$

The present work was favored by Ambrosini and Ferreri [118] and was made a convenient tool for linear and nonlinear stability analysis. Stability prediction was made with the help of RELAP5/MOD3.3, which shows confidence in the applicability of the proposed model for supercritical fluids. However, the prime drawback of the study was the inconsideration of problems in supercritical fluids like momentum transfer across the pseudo-critical point.

Jain and Rizwan [110] developed a computer code FIASCO (Flow Instability Analysis Under Supercritical Operating Conditions) in FORTRAN90 to analyze the transient stability of supercritical water and CO_2 in NCL. The equations were solved by the implicit finite difference method. Supercritical properties were determined using NIST/STEAM 2.21 [85] and NIST/REFPROP7 [119] respectively for water and CO_2. Results obtained in this investigation always predict the stability threshold to be in the positive slope region of the (steady-state) flow-power curve. Using time step 0.02 s and grid size 0.1 m leads to a stability zone quite early. But results proposed that the stability threshold of a natural circulation loop with supercritical fluid is not confined to the near-peak region of the (steady-state) flow-power curve, which contradicts the threshold stability result of Chatoorgoon et al.[115]. The possible reasons that were diagnosed were the selection of proper time step size. Simulation results undoubtedly showed the significance of the time step used. Consideration of larger time steps and implicit scheme leads to more dissipative nature leading to stability. Reducing the time step to half and quarter from 0.0875 s leads to sustaining and growing oscillations at 1 MW power, while grid size has an insignificant effect. Increasing the pressure stretches the threshold of stability towards a higher flow rate. For small sub-cooling, the stable zone diminishes, but for higher sub-cooling, it enlarges again. The results clearly

remark that the stability threshold does not always stick near the peak value of mass flow, which manifests the prediction of Jain and Corradini [120].

Linear stability code named SUCLIN was developed by Sharma et al. [91] for sH_2O. Assuming initial mass flow and heat rejected to be equal to the heat added, a small disturbance in flow rate, specific enthalpy, and pressure was given. Required properties of water were calculated using the International Association for the Properties of Steam (IAPS) formulation 1984. SUCLIN was found suitable for analysis after successful validation from previous literature [83], which showed that using SPORTS code for the inlet temperature of 350 °C and 25 MPa, the loop was stable for 4 MW but unstable for 4.5 MW, while the SUCLIN code, predicts the threshold to be 4.2 MPa. This difference has been attributed to the stability assessments made with different techniques and assumptions. The trend of results, however, remains similar in both investigations. With the increase of heater inlet temperature above 300 °C, the lower threshold power of instability increases mildly, but the upper threshold of power reduces expressively.

The results were compared by the NOLSTA code, which showed the role of assumptions while developing the code. The unstable zone predicted by NOLSTA is much greater than SUCLIN. The reason being is that all properties were perturbed in the NOLSTA code, while in the SUCLIN code, only enthalpy and specific volume were perturbed [121].

The parametric study was done for various loop diameters (7, 14, 20.7 and 28 mm) at 25 MPa with varying heater inlet temperatures. Stability maps obtained from the investigation show that the instability zone increases with the increase in diameter. However, there exists a specific heater inlet temperature beyond which no instability is observed, and the value of that particular temperature decreases with the increase in loop diameter. Moreover, when the inlet temperature increases beyond the pseudo-critical temperature, the mass flow rate drops significantly, but that could be avoided by increasing the system pressure, but system may still show unstable nature. The loop height, if increased, the instability in the sNCL also increases [91]. These results could be of great importance in designing aspects of the NCL.

Chen et al. [97] performed numerical simulations for sCO_2 where they used the simplified model from solar collector system [122]. It was seen that for high-temperature system oscillation started to die down at temperature 523 K. Simulation results reveal that as per the previous studies [113, 123] suggested that, heat input increment or high temperature imposes system instability. For the CO_2 case, it is not only defined by heat input. Hence a new stability criterion was defined. When the average loop temperature crossed 375 K,

property variations were again observed especially thermal conductivity, which was found to be stabilizing factor. This point is termed as the "second pseudo-critical" temperature. Due to the increase in viscosity, chances for flow reversal also decrease, as observed for high temperatures, as shown in Fig. 1.17. Due to less pressure and friction drop in the loop at high heat temperature, a higher flow rate could be achieved, which could lead to getting higher efficiency.

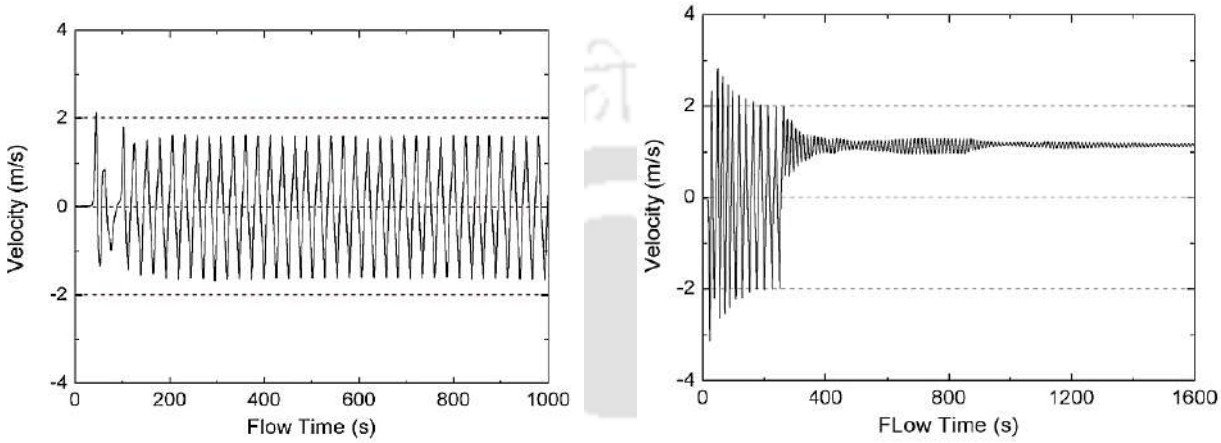

Fig. 1.17: Flow velocity fluctuations for heater temperature (a) 343 K and (b) 523 K [97][10]

The effect of heater orientation was studied numerically by Chen et al. [108] for the following four orientations, a) down the middle, b) down left, c) left down, and d) left middle. Keeping the coolant side at fixed operating condition and pressure at 9 MPa, heating flux was varied from 600 W/m^2 to 60000 W/m^2, continuous fluctuations were observed for conditions a) and b) while in c) and d) cases, steady-state reaches soon indicating stable system because of the stable buoyancy across NCL. A similar pattern was observed when temperature difference was taken as a measuring parameter.

Debrah et al. [109] was the first one to analyze the role of heating structure. Normalization of the CIAE (China Institute of Atomic Energy) VHHC loop was done and solved using RELAP5. When heating structures were considered, it was found that instability in a water-based loop arises at much higher power as compared to earlier studies. When cooler heating structures are considered, the threshold comes early. So in order to understand the phenomenon better non-dimensional numbers proposed by [117] were compared between

[10] "Reprinted from International Journal of Heat and Mass Transfer, 53, Lin Chen,Xin-Rong Zhang,Hiroshi Yamaguchi,Zhong-Sheng (Simon) Liu, Effect of heat transfer on the instabilities and transitions of supercritical CO2 flow in a natural circulation loop, 4101-4111, 2010, with permission from Elsevier."

RELAP5 results and in-house code (without heating structure) for stability response. For in-house code, two different numbers of nodes, namely 168 and 336, were selected, and it was seen that the courser mesh predicts a comparatively large stable zone. RELAP5 approves the predictions made earlier. RELAP5 also precisely predicts the effect of surface roughness and fouling factors. But, compared with the real-life situation, code results with heating structure over envisaged stable behavior. This can be attributed to the reason for having different geometry and boundary conditions.

In a computation study of Ledinegg and density wave oscillations of water Rai et al. [124] found that under the operating condition of 25 MPa and 300 kJ/kg inlet enthalpy, there was no sign of Ledinegg instability for a power range up to 230 kW. In the operating range of density wave oscillations at 58.11 kW power, the system reaches the verge of instability for an inlet enthalpy of 1623.89 kJ/kg. With increasing diameter, the stability boundary shifts towards higher power attributed to higher mass flow. Increasing pressure decreases the stability boundary, and with an increase in loss coefficient, there is a small drop instability boundary, but later on, a drastic drop was seen.

Archana et al. [72] modified a 2D axis-symmetric code NAFA-loop (Numerical Analysis of Flows in Axis-symmetric geometries) considering CO_2 as working fluid and other parameters such as pressure, inlet coolant temperature, and the coolant flow rate was kept constant at 80.4 bar, 8 °C and 56 LPM. A heat transfer deterioration is predicted at around 1300 W, owing to the fact that the inlet and outlet temperature of the heated section is above pseudo-critical temperature, which agrees with the results of Sharma et al. [111]. The code also predicts that the wall temperature increases more sharply than the bulk flow temperature.

The results of Tilak and Basu [125] for the stability dependence of sH_2O NCL on time step and grid size were in agreement with Chatoorngoon et al. [115] and Sharma et al. [111]. In the investigation, Step, ramp, exponential and sinusoidal excitations were imposed on the system, where Step rise in heater power introduced instability into the system and had the most destabilizing influence. The system takes a long time to regain a steady state if the final power is within the stability boundary. Ramp and exponential profiles were found to provide a favorable response during both the power upsurge and the down-surge; however, the exponential transition is preferable from stability's perspective. A longer period of transition allows the system to suppress unstable fluctuations in a better way. Application of sinusoidal transition results in a distorted periodic response while attempting to follow the imposed signal only after sufficient time since the application shows a periodic signal. Repetition of flow reversal is a common phenomenon with supercritical CO_2 based loop due to properties

variation and the transition of various input control such as heater power. A numerical study by Deng et al. [126] depicted that for actual system operations, it is discovered that the rapid or gradual changes in heat influx conditions are crucial. Additionally, each transitional period's Re number reveals some very intriguing changes: Due to significant changes in fluid density in the critical region, abrupt drops and increases can be seen in the transition region, along with repeated flow reversal. 3D simulation in Fluent by Wahidi et al. [127] the flow behavior can switch from bi-directional to unidirectional when the heater power crosses a certain threshold. Repeated continuous fluctuation of flow is due to the intermittent creation of hot pockets at high temperatures and the heat transfer capability if sNCL is more at low operating pressure. By placing a Tesla-type valve in the loop, the directional instability of natural circulation loops can be totally eradicated. Surprisingly, unidirectional flow can be achieved at all heat input levels at the source and even with different loop fluid operating pressures. The temperature level throughout the loop also reduces, consequently leading to steady-state [128]. In order to capture the Ledinegg instability (static) for CO_2, an analytical method was adopted [104], and equation capturing different losses were derived, and no sign of multiple steady-states was found as shown in Fig. 1.18a. In the case of water, it was observed that for high power, excursive instability was observed at high sub-pseudo critical number N_{SUBPC} [129], and the unstable zone gets narrower with the rise in pressure as shown in Fig. 1.18b.

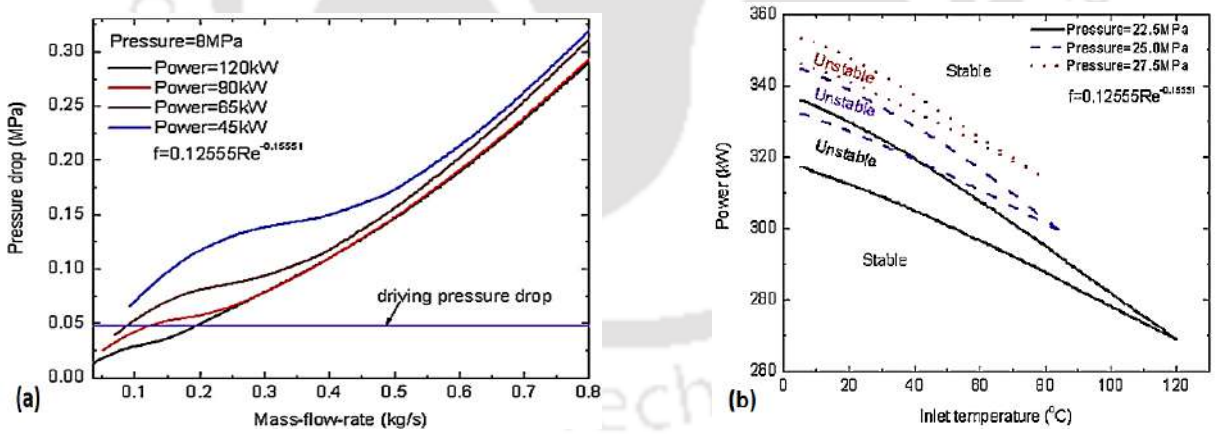

(a) **(b)**

Fig. 1.18: (a)Identification of instability with mass flow vs. pressure drop and (b) stability map with respect to power variation [104][11]

[11] "Reprinted from Nuclear Engineering and Design, 252, B.T. Swapnalee,P.K. Vijayan,M. Sharma,D.S. Pilkhwal, Steady state flow and static instability of supercritical natural circulation loops, 99-112, 2012, with

1.10.2 Experimental investigation

Due to the constraint of high pressure of supercritical fluids, less experimental support is available to validate the analytical results concerning the laboratory environment. Most studies are done by scaling analysis to identify the dimensions of the setup. Various authors have done fluid-to-fluid scaling by making use of dimensionless density and enthalpy.

Lomperski et al.[130], in their experiment, studied the two types of configurations, one with the base case and the other with an orifice in the hot leg. Orifice creates flow disturbances, the effect of which is evident in the heater outlet temperature compared to the base arrangement, and correspondingly mass flow rate peak occurs early. The possible reason could be the dominance of friction losses over the driving head. Experimentally no signs of instabilities were seen. As far as the stability is concerned, the parameter $\frac{\partial m}{\partial \rho}$ showed great significance, as Chatoorgoon V.[83] mentioned about the peak power for instability. When the slope of $\frac{\partial m}{\partial \rho}$ is negative, the disturbance gets neutralized by the rise in mass flow. When the slope is positive, the outlet temperature increases and amplifies the disturbance. Operating the loop for inlet/outlet temperature 20-30 °C/40-85 °C and pressure 75-95 bar, the system was found to be stable in both the regions of power, which was completely contrary to the numerical analysis. Numerical analysis showed that beyond a certain power level, the system did not stabilize. This discrepancy was suggested to be analyzed through further experimentation.

Jain and Corradini [120] found divergences between the results of instability for sCO_2 in an experimental study (stable) at Argonne National Laboratory (ANL) and 1D transient analysis using FORTRAN code (unstable) at the University of Wisconsin, Madison. The stability of the water loop depends upon the accuracy of EOS. EOS2 captures the maximum temperature (821 K) within its specified range (655 K to 850 K), while EOS1 has a range (630K to 820K) below the maximum temperature range. Thus EOS2 yields more accurate results, which are consensus with the experimental results.

In the case of sCO_2, results from experimental analysis depict stable behavior, while linearized transient analysis depicts unstable behavior. The main reason for these discrepancies could be either due to the uncertain nature of the distribution of friction factor along the flow path or improper application of constant heat flux or both. Following modifications were suggested to void these discrepancies-

- Using closed-loop geometry which actually resembles the experimental facility. Open-loop was made in order to validate the linearized code with previous works.

permission from Elsevier."

- Applying more practical boundary conditions like constant flow rate and inlet temperature on secondary side fluid.

Experimental investigation of Chen et al. [99] showed the importance of the initial pressure of the system at a constant cooling water temperature of 15 °C, and at power 182 W. it was found that at an initial pressure of 6.3 MPa, if system pressure reaches critical, then fluctuation died down soon (for all other configuration of supercritical state, the system was stable) and unidirectional flow was observed while, if pressure is below critical then system kept on fluctuating. A similar phenomenon was observed by Chen et al. [98] as well. Control of heating influx and cooler temperature also play a crucial role in the stability aspects of sNCL. Deng et al. [126] revealed that If the cooler temperature falls below the critical point region, the flow will quickly become unstable regardless of how the heater temperature changes. The feature of the heater transition control is its relatively slow response to a decrease in heat influx compared to its extremely quick response to an increase.

Moreover, the series of experiments done by a group of Lin Chen did not provide the facility to maintain constant pressure by using an expansion tank or pressurizer. The aim associated with it was to raise the pressure as well as temperature with the application of heat to investigate a solar heating system model similar to Chen and Zhang[131].

Yu et al. [132] conducted stability analysis experiments in supercritical water. The results were verified with the numerical code, emphasizing the Ledinegg-type instability. Analytical code was run over a wide range of powers. For a particular inlet temperature, till the mass flow reaches 0.066 kg/s, the system is stable. As the condition for Ledinegg instability does not hold true, instability arises. In the range of experiments conducted, no Ledinegg instability was found. To operate the system at a higher mass flow rate without the occurrence of instability, the author recommended using the system at a low inlet temperature because operating at a low inlet temperature leads the system to a higher flow rate, thus causing a delay in instability.

Yu et al. [132] have confirmed oscillations similar to pressure drop oscillations. The effect of inlet temperature also shows that when the pressure increases, the density variation slope is less steep, showing better stability. It also approves that the wall temperature increases more sharply than the bulk temperature [72]. When the low-temperature fluid particle contacts the hot wall, it significantly expands owing to the temperature sensitivity of density near the pseudo-critical point and then moves away from the hot wall. Finally, it would contract in the bulk flow. The obvious variation of the volume of the fluid particle leads to pressure fluctuation in the loop. The experiments also affirm that increasing the

system pressure has a stabilizing effect on the NCL, which is in agreement with [91]. It is also to be noted that when the local resistance of the heat sink section is increased, the loop stabilizes, but at the same time, if the local resistance increases for the heat source section, then the loop becomes susceptible to instability. In the subsequent experimental study of Liu et al. [76] with vertical heating and horizontal cooling with CO_2, the effect of system pressure and intel temperature was seen to have no effect on stable behavior, while inlet temperature does have an effect on mass flow rate and effect becomes noteworthy when it is in the range of pseudo-critical limit. Sharma et al. [111] also experimentally investigated a rectangular sCO_2 NCL for HHHC, HHVC, VHVC, and VHHC configuration. HHHC was found to be the least stable. The instability in the loop was observed in the pseudo-critical temperature range of operation, where the volumetric expansion coefficient of the fluid was the highest. Experiments also affirm the decrease in mass flow rate predicted by NOLSTA. Stability was found to be dependent on the secondary side flow rate. The instability map was made for the pressure of 8.1 MPa and 9.1 MPa for the HHHC combination. It was found that at the higher flow rates, instability disappears, while for lower flow rates, the upper and lower stable zone is found as shown in Fig. 1.19.

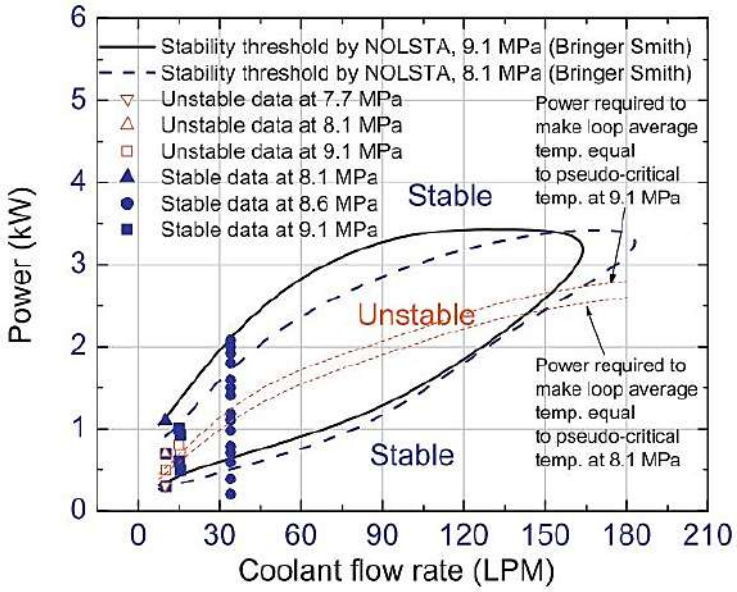

Fig. 1.19: Stability map for different pressure for varying flow rates [111][12]

[12] "Reprinted from Nuclear Engineering and Design, 265, Manish Sharma,P.K. Vijayan,D.S. Pilkhwal,Yutaka Asako, Steady state and stability characteristics of natural circulation loops operating with carbon dioxide at supercritical pressures for open and closed loop boundary conditions, 737-754, 2013, with permission from Elsevier."

1.11 Summary of Literature Review

From the literature survey, it is clear that the investigation in the field of sNCL is a relatively new and hot topic due to its enormous benefits in the wide range of scientific applications. The majority of the works which have been reported are theoretical in nature and range from simple 1D simulations to sophisticated software applications. There aren't many experimental studies in the open literature, and the corresponding database is not yet complete. Numerous codes, including SPORTS, FIASCO, NOLSTA, and SUCLIN, have been developed through numerical work, mostly for the stability characterization of sNCLs. In recent years, there have also been sporadic uses of commercial software like ANSYS-FLUENT and RELAP5. The steady-state mass flow rate increases with the power supply until it reaches a maximum and then decreases, according to theoretical and experimental observations. Properties variation of CO_2 is similar to that of water, and literature revealed that CO_2 is a better option for analysis since the the experiments involving supercritical water are expensive as it involves very high pressure and high temperature equipment. Loop diameter, height, operating pressure, and sink temperature significantly affect the loop performance. With the change of these parameters, buoyancy force and friction force change, and their balance and imbalance cause stable steady-state and unstable fluctuation of system parameters.

Stability analysis has been predicted numerically by time-domain and frequency-domain approaches with a substantially good match in the predicted threshold. Increasing diameter and height widens the instability zone. It was found that a power step-up stabilizes the loop more than a power step-down does. That according to RELAP5 simulations, a gradual rise in the input heat flux can induce less flow instability than a quick one. Such dynamics stability analysis has been extensively done for supercritical water-based NCL, while the same is not explored for sCO_2 and hence an open topic.

While operating the system at higher heating power may cause the temperature throughout the loop to be higher than the pseudocritical temperature. Since the properties variation around this range is quite drastic and hence the system may operate at degraded conditions, termed HTD. The effect can be observed till this point in time and maybe local (experimental study of Liu et al. [76]) or can be global (Numerical study of Sarkar and Basu [133]). Sarkar and Basu modified the term HTD to FiHTD since the phenomenon is observed due to the sharp drop in flow rate and higher bulk temperature in the natural circulation system. The FiHTD phenomenon is relatively new and needs attention from safety concerns rather than thermalhydraulic behavior. Such phenomenon has been found in 3D numerical simulations and does not have proper support of less dimensional model and experimental analysis. It

was found that the phenomenon can not be avoided, yet attempts can be made to delay the same by altering the boundary conditions and loop geometry.

1.12 Research Objective

From the discussion above, it can be seen that for optimum thermalhydraulic behavior with the safer operation, FiHTD is indeed a topic to explore. Hence, the following is a description of the current dissertation's scope.

1. Numerical identification of the regimes of heat transfer in sNCL under steady-state
2. Characterization of the static and dynamic instabilities in sNCL using 1D numerical model
3. Nonlinear dynamics of sNCL under the influence of various types of time-dependent profiles of input power
4. Comprehensive appraisal of the startup transients and thermalhydraulics of flow initiation in sNCL using 2D computational model
5. Design and development of the experimental facility, and detailed characterization through systematic experiments

1.13 Outline of the Thesis

1. **Chapter 1:** This chapter deals with the historical background of the natural processes and practical applications of the natural circulation loop. Moreover, the advantage of supercritical fluids in NCL over conventional single and two-phase NCL has been discussed. A detailed literature review reveals the literature gap to find out the objective of the present thesis.
2. **Chapter 2:** This chapter deals with the thermalhydraulics of the loop under inclined conditions and its effect on FiHTD. The onset of FiHTD was visualized using the threshold Buoyancy parameter (Bu) value and change of trend of friction factor (f). These help in designing a safer operational zone of the loop.
3. **Chapter 3:** This chapter deals with the identification of static and dynamic instabilities of HHHC-oriented sNCL following a 1D numerical framework. A zone of stable as

well as safer operation (from the point of view of FiHTD) was marked in conjunction with the non-dimensional numbers.

4. **Chapter 4:** This chapter is the continuation of chapter 3, where the dynamic response of the same model was analyzed under the periodic and non-periodic input heating power profile. The heat trnasfer regime found to enttertain a pivot role under every type of heating profile. Chaos was found under certain cases and slight delay in FiHTD is also witnessed under sinusoidal profile.

5. **Chapter 5:** In this chapter of 2D simulation, The thermal and hydrodynamic fields was monitored starting from the quiescent condition, and the underlying physics, specifically pertinent to the supercritical fluid, was unearthed.

6. **Chapter 6:** This chapter focus on the experimental investigation of sNCL. Effect of pressure and sink temperature was analysed to envisage the FiHTD phenomenon.

7. **Chapter 7:** This chapter summarises the conclusion and future recommendations.

Chapter 2

Numerical Characterization of Heat Transfer Deterioration

2.1 Preamble

The basic operation of NCL involves an interplay between buoyancy force and friction force. The dominance of one defines the nature of the system. Imposed boundary condition of both the Dirichlet and Neumann type has previously been explored by various research groups along with basic thermalhydraulic behavior. The transport of heat transfer is a major function of system configuration and imposed boundary conditions. In all the cases, the common aspect is the nature around pseudocritical temperature. Drastic properties variation leads to the unpredictable nature of the system. The average loop temperature increases with the increase in the heater power. Once it crosses the pseudocritlcal limit, loop characteristics sharply drop, termed FiHTD [134], leading to higher bulk temperature. This particular term was coined by them to differentiate with the well-known HTD, which is relevant to the forced-flow channels. The loop diameter was identified to have a pivotal influence, with early initiation of FiHTD in small-diameter systems, while an optimum level of height was suggested. The relative orientation of the heating and cooling segments can also have a substantial influence, as that can directly modulate the developed buoyancy field. It is the prime duty of the design engineer to have all round focus on safety; hence design optimization and boundary conditions are vital. In forced flow cases, HTD is quite common, and various correlations are available in the literature of its prediction and characterization for supercritical water [135, 136] as well as for supercritical CO_2 [137, 138]. This is where the natural circulation phenomenon in the supercritical loop lacks behind, where property

variation is the major driving force. No explicit universally accepted correlation is available. Direct experimental validation for local heat transport characteristics is not feasible, primarily owing to the limitations of available instruments at higher pressures and temperatures. Consequently, the experimental studies on sNCL are mostly restricted to the appraisal of gross thermalhydraulics and correlation development. A recent experimental investigation by Yuanlu et al. [107] developed a new correlation based on the Supercritical Boiling number (SBO), which accurately predicts the heat transfer behavior of sNCL. Though the obtained HTD was local in behavior, unlike Sarkar and Basu numerical study [133], where overall loop performance degrades, leading to higher bulk temperature throughout. The accurate prediction of FiHTD is crucial, and in the thorough literature, no such criterion has been provided due to the lack of focused research on the topic FiHTD of sNCL. Modulation in the effective buoyancy force with any alteration in the geometry adds another level of intricacy for NCLs. Accordingly, both the local and global heat transport characteristics of the sNCL, and hence FiHTD, are expected to be dominated by choice of system pressure and effective temperature range, along with the geometrical features. That broaches a major challenge in defining any quantifiable criterion to delineate FiHTD in sNCL and also prepares the backdrop for the present study, which focuses on characterizing FiHTD in terms of the buoyancy parameter, with emphasis on envisaging the the role played by inclination. A computational model has been developed, as detailed in Section 2.2, and the role of relevant control variables, such as system pressure, heat flux, sink temperature, and inclination angle, has been methodically analyzed to acquire a comprehensive understanding of the phenomenon.

2.2 Computational Model Development

A rectangular loop in HHHC orientation is considered as the domain of interest in this study, a schematic representation of which is shown in Fig. 2.1 along with the dimensions. The loop is made of SS316 with 1 mm wall thickness ($\lambda_w = 16.3$ W/mK) and the corner bends are set to have a radius of 5 mm. The heater is subjected to a constant wall heat flux and the surface temperature of the cooling section is maintained unchanged, while the remainder of the system wall is perfectly insulated. The loop can be rotated in the $X - Y$ plane, thereby deviating from the HHHC configuration, with the constraint of retaining the cooler-center at a higher elevation than the heater-center to yield favorable density gradient.

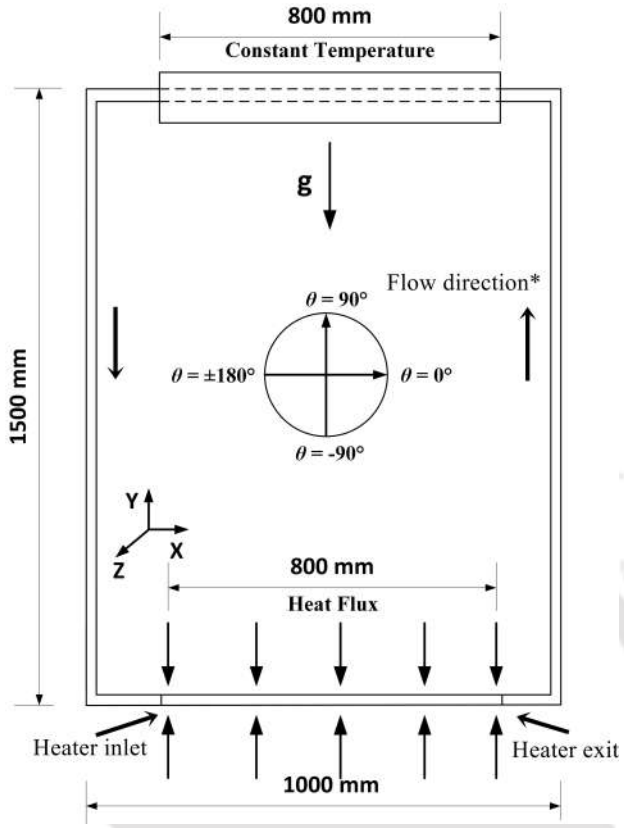

Fig. 2.1: Schematic of the computational domain under consideration (* flow direction can be clockwise or anticlockwise and accordingly heater inlet and outlet will interchange)

2.2.1 Governing equations

A 3D Cartesian coordinate system is adopted in the present study. The steady-state versions of the mass, momentum and energy conservation equations are summarized below

$$\frac{\partial}{\partial x_j}\left(\rho u_j\right) = 0 \tag{2.1a}$$

$$\frac{\partial}{\partial x_j}\left(\rho u_j u_i\right) = \frac{\partial p\prime}{\partial x_j} + \frac{\partial \tau_{ji}}{\partial x_j} + \rho g_i \tag{2.1b}$$

$$\frac{\partial}{\partial x_j}\left(\rho u_j h\right) = \frac{\partial}{\partial x_j}\left(\lambda_{eff}\frac{\partial T}{\partial x_j} + u_j \tau_{ji}\right) + S_E \tag{2.1c}$$

Here the modified pressure and viscous stress are respectively defined as,

$$p\prime = p + \frac{2}{3}\rho\kappa + \frac{2}{3}\mu_t \frac{\partial u_k}{\partial x_k} \tag{2.2}$$

$$\tau_{ji} = \mu_{eff}\left(\frac{\partial u_i}{\partial x_j} + \frac{\partial u_j}{\partial x_i} - \frac{2}{3}\delta_{ij}\frac{\partial u_k}{\partial x_k}\right) \tag{2.3}$$

where the effective viscosity, $\mu_{eff} = \mu + \mu_t = \mu + C_\mu \rho \kappa^2/\epsilon$. The source term ($S_E$) appearing in Eq. (2.1c) accounts for the energy addition and rejection at the heating and cooling section respectively. The order of the Reynolds number (Re) typically being 10^6, the flow is essentially turbulent. RNG $\kappa - \epsilon$ turbulence model is a popular choice in literature [78, 101], and the same is adopted here with standard values of the coefficients. Axial conduction of heat through the solid layer is also considered.

2.2.2 Numerical scheme

The conservation equations need to be discretized to facilitate numerical solution, and the finite-volume framework of ANSYS-Fluent is used for that purpose in the present work. The implicit second-order upwind scheme is followed to discretize both the convective and diffusive terms of the governing equations. Remaining consistent with the relevant literature, PRESTO scheme is embraced to discretize the pressure terms, while selecting the PISO algorithm to resolve the pressure-velocity coupling [126–128]. No-slip boundary condition is imposed at the walls, with standard wall functions for precise profiling of parameters interior to the boundary layer. A convergence criterion of 10^{-6} is selected for the residual of the energy equation and 10^{-3} for all the other quantities.

2.2.3 Thermophysical property estimation

The phenomenon of natural circulation is governed by an interplay between buoyancy and frictional forces, and hence precise estimation of the relevant thermophysical properties are of utmost importance here. Besides, the supercritical fluid demonstrates drastic changes in the magnitudes of most of the thermodynamic and transport properties from a *liquid-like* level to a *vapor-like* level around T_{pc}, making the property evaluation an arduous task. The gradient of properties with the temperature at T_{pc} can be very steep, unlike in regimes away from it. The NIST standard reference database [119] can be activated within the Fluent environment by evoking the real gas model, and the same is followed here, as the common property database of Fluent is incapable of handling supercritical fluids. The adopted database employs the thermodynamic formulation of Span and Wagner [139], along with additional resources for the estimation of certain transport properties [140, 141], with reported uncertainty levels of ±0.05%, ±1.19% and ±0.3% respectively in density, thermal conductivity and viscosity predictions.

2.2.4 Grid generation and sensitivity analysis

Correctness of the solution of the discrete set of equations is dependent on the adopted grid structure. A careful mesh sensitivity analysis has therefore been performed with sequential increase in the number of nodes in each of the coordinate directions, and comparing the magnitudes of the resultant output variables of significance. Finer meshes have been considered near the walls for accurate resolution of the boundary layer. The observations with different mesh systems are summarized in table 2.1. Here all the simulations have been performed at operating pressure of 8 MPa, and source and sink temperatures of 331 and 305 K respectively. It is clearly noticeable that raising the number of elements from mesh 3 to mesh 4 induces merely about 0.3% change in average velocity and mass flow rate, and 0.03% change in the bulk fluid temperature, with all values corresponding to the central cross-sectional plane of the heater. The concerned change in pressure drop across the heater is also just about 0.6 Pa, which is negligibly small. The model 3, therefore, is continued with for the remainder of the present study, cross-sectional view of which is shown in Fig. 2.2. Corresponding values for mesh skewness and orthogonality are 0.114 and 0.981 respectively, both of which are within acceptable limits.

Table 2.1: Details of mesh sensitivity test for the computational domain

	Grid 1	**Grid 2**	**Grid 3**	**Grid 4**
Number of nodes	182512	295568	331240	432490
Average velocity (m/s)	0.72732	0.70606	0.70928	0.71142
Mass flow rate (kg/s)	0.008994	0.008792	0.008847	0.008885
Bulk temperature (K)	316.911	317.373	317.270	317.195
Pressure drop across heater (Pa)	157.070	156.039	156.889	156.295

2.2.5 Model validation

In order to test the precision of the developed numerical framework, it is imperative to compare with reliable dataset or relation from literature. The steady-state relation proposed by Swapnalee et al. [104] is selected here, as it has found sufficient cognizance from the sNCL community. Simulations have been performed over a wide range of control parameters, namely, pressure (p) of 8 to 10 MPa, sink temperature (T_c) of 285 to 295 K and heater power ($\dot{Q}$) of 10 to 2500 W. Following two dimensionless groups, respectively the Reynolds

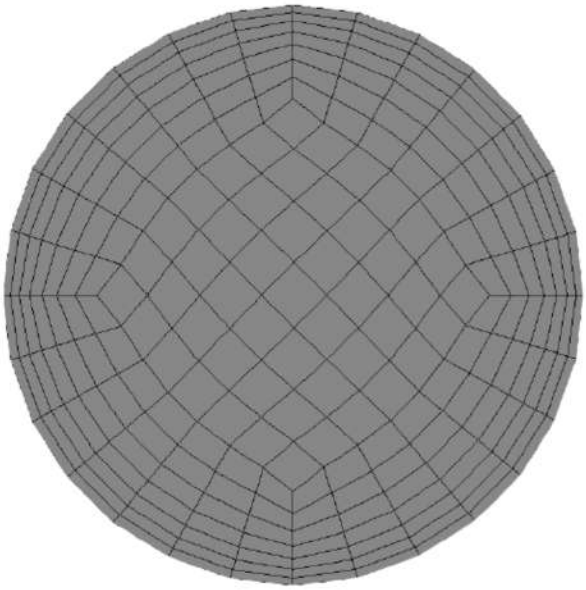

Fig. 2.2: Cross-sectional view of the selected mesh structure at the heater center

number and the modified Grashof number, need to be defined to facilitate comparison in a dimensionless plane.

$$Re = \frac{4\dot{m}}{\pi D\mu} \qquad Gr_m = \frac{g\beta D^3\rho^2\dot{Q}H}{A\mu^3 c_p} \tag{2.4}$$

Excellent degree of conformity can be observed between the simulated predictions and correlation from Sharma et al. [104] over the entire parameter range considered, as is illustrated in Fig. 2.3(a). Predicted results are also put in context to two different theoretical works from literature, and are found to adhere much better to the experimental relation of Sharma et al. [104] compared to both Chen and Zhang [74] and Wahidi et al.[127]. Present data can be correlated as,

$$Re_{ss} = 4.15\left(\frac{Gr_m D}{L}\right)^{0.3641} \tag{2.5}$$

Here the obtained exponent is practically the same reported by Swapnalee *et al.*[104], which endorses the correctness of the present results. Variation in friction factor with Re is also compared in Fig. 2.3(b) with the seminal work of Filonenko [142].

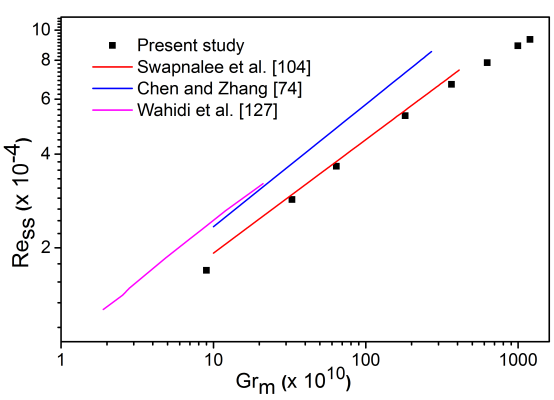

(a) Re vs. Gr_m

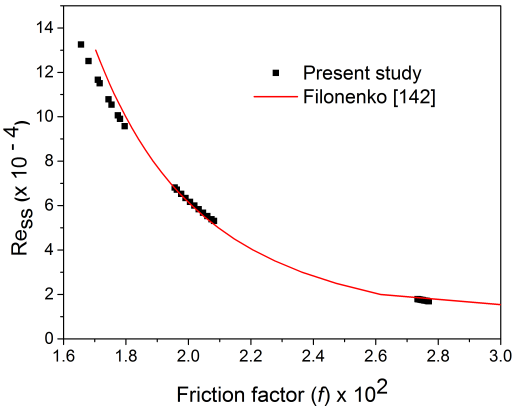

(b) Friction factor

Fig. 2.3: Comparison of present predictions with (a) the experimental relation of Swapnalee *et al.*[104], and theoretical predictions of Chen and Zhang[74] and Wahidi *et al.*[127], and (b) the friction factor data of Filonenko[142]

2.3 Results and Discussion

2.3.1 General thermalhydraulic characteristics

The phenomenon of natural circulation is governed by the driving influence of buoyancy and restraining impact of friction. While the local value of the latter is determined by the viscosity of the fluid layer in contact with the wall, the former is proportional to the density differential ($\Delta\rho$) between the fluid columns in the two parallel vertical arms and the height of the loop. In single-phase NCLs, $\Delta\rho$ is quite small, as the fluid continues with the same phase, commonly liquid, resulting in reasonably low flow rate. On the contrary, boiling NCLs generally have a saturated liquid-vapor mixture in one arm and subcooled liquid in the other, yielding substantially larger buoyancy and hence circulation. A supercritical loop can uniquely exhibit both depending on the prevailing temperature level of the fluid. Two different cases are demonstrated in Fig. 2.4 corresponding to two different power levels, while maintaining identical values for the other parameters, by plotting density contours along the central $x - y$ plane. For $\dot{Q} = 1000$ W, average density differential between the riser and downcomer is hovering over 200 kg/m^3, whereas the same drops close to 50 kg/m^3 for $\dot{Q} = 1750$ W, producing considerable difference in the concerned buoyancy force. Here in the first case, fluid temperature level in the downcomer is lower than T_{pc}, giving it a liquid-like appearance, whereas the fluid is more gas-like during upflow in the riser, the concerned temperature being above T_{pc}. However, for $\dot{Q} = 1750$ W, fluid temperature level throughout

the loop is greater than T_{pc}, culminating mostly into a single-phase-type behavior.

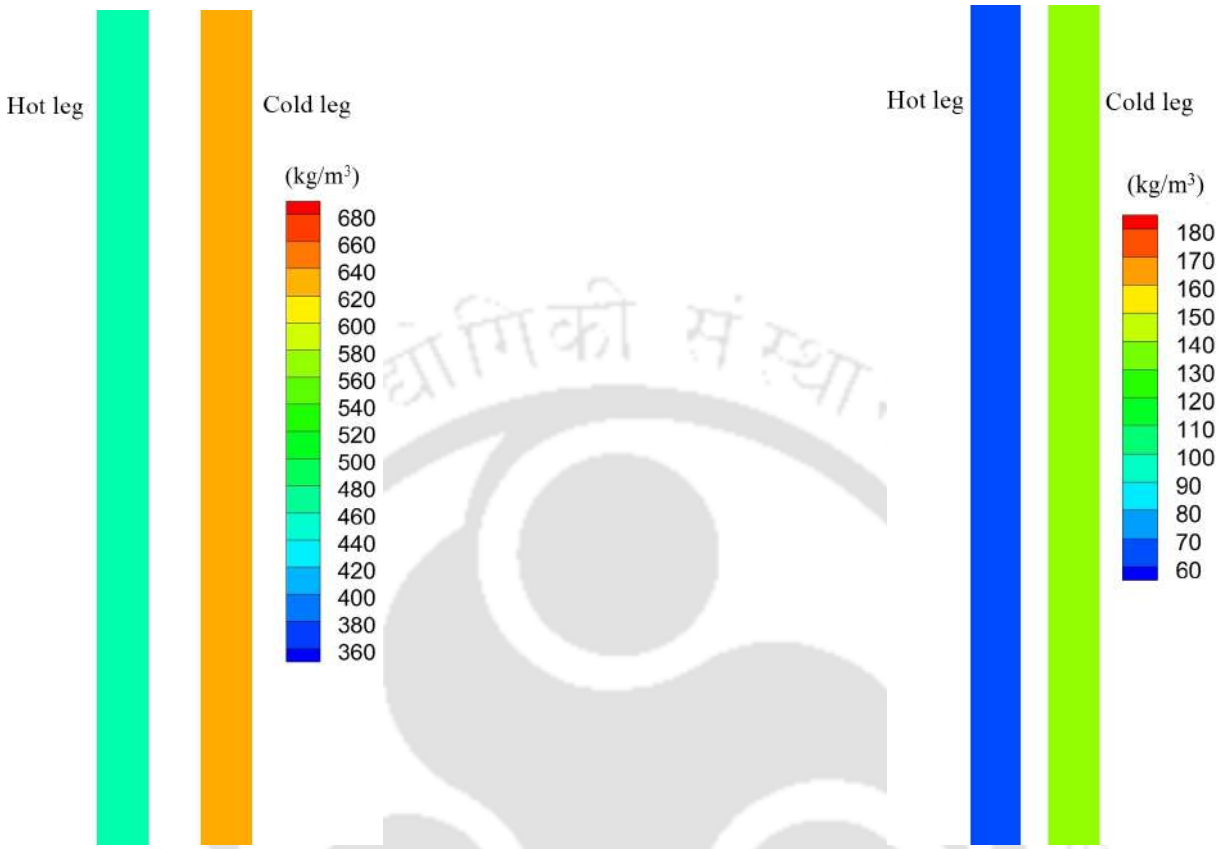

(a) $\dot{Q} = 1000$ W **(b)** $\dot{Q} = 1750$ W

Fig. 2.4: Density contours of the loop fluid in the two vertical arms along the central $x - y$ plane at two different power levels with $p = 8$ MPa and $T_c = 295$ K

The change in viscosity of sCO_2 across T_{pc} is less substantial compared to density, which regulates the wall shear stress profile, and hence the overall frictional characteristics. The variations in average wall shear stress in the flow direction over the entire loop are shown in Fig. 2.5 for the same two power levels. Here the average value at any particular cross-section has been calculated by numerically integrating over the concerned periphery and data from twelve azimuthal locations have been used for the same. Increase in temperature along the heater leads to a reduction in viscosity of the fluid layer in contact with the wall and subsequently a decrement in the shear stress, while the reverse is true for the cooler. Both the profiles are quite similar in appearance, albeit with a noticeable difference in the concerned magnitudes. Both high- and low-viscosity zones exist for $\dot{Q} = 1000$ W, owing to the considerable variation in the nature of fluid during its passage through heater and

cooler. For $\dot{Q} = 1750$ W, though, viscosity level is consistently low, resulting in low frictional resistance. The extent of decrease in friction with increase in power, however, is relatively less significant compared to the same in buoyancy, eventuating a lower circulation rate at $\dot{Q}$ = 1750 W than 1000 W, as is substantiated by the drop in Re_{ss} from 96644 to 32478. A direct consequence of the weakened flow rate at higher power is an appreciable surge in the fluid temperature level, as is demonstrated in Fig. 2.6. The temperature rise of sCO_2 across the heater is restricted to less than 3 K for $\dot{Q} = 1000$ W, whereas the same is in excess of 250 K at $\dot{Q} = 1750$ W, with the peak value raising over 600 K.

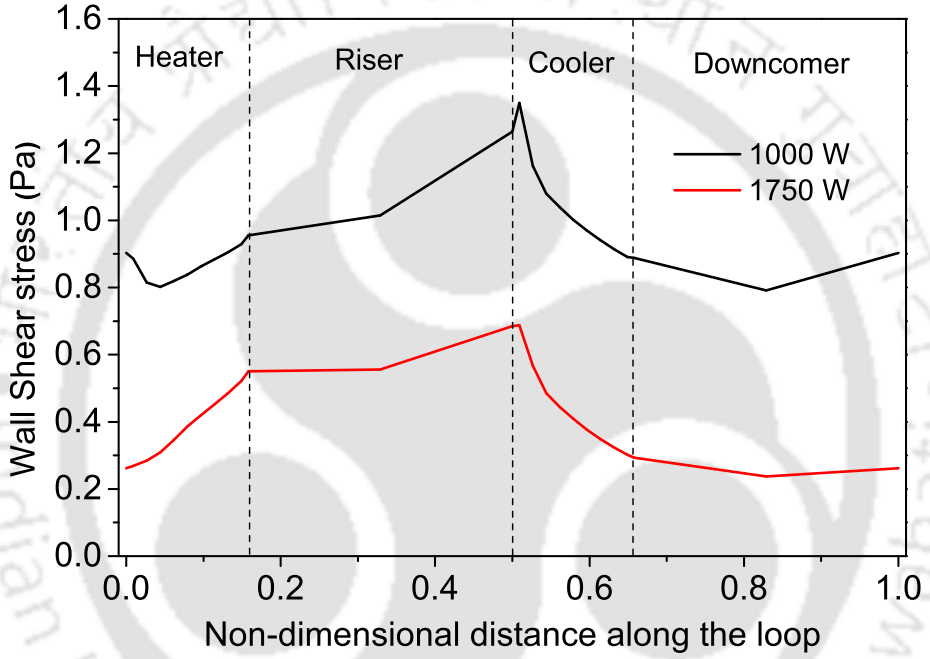

Fig. 2.5: Variation in average wall shear stress along the length of the loop at two different power levels with $p = 8$ MPa and $T_c = 295$ K

Consequently, two distinct regimes of operation can be identified for the sNCL, primarily based on the fluid temperature levels in the vertical arms, and the same is earmarked in Fig. 2.7(a). With increase in the heater power, circulation rate increases sharply, owing to the rise in $\Delta\rho$. When the fluid crosses T_{pc} within the heat-exchanging sections, considerably larger buoyancy force is generated, leading to large mass flow rate. The effect is particularly prominent when the temperature in the riser is in the vicinity of T_{pc}, owing to the large magnitude of $\left(\frac{\partial\rho}{\partial T}\right)_p$ and consequent peak in the volumetric expansion coefficient. That particular domain is identified as the *enhanced heat transfer regime* and the operation with

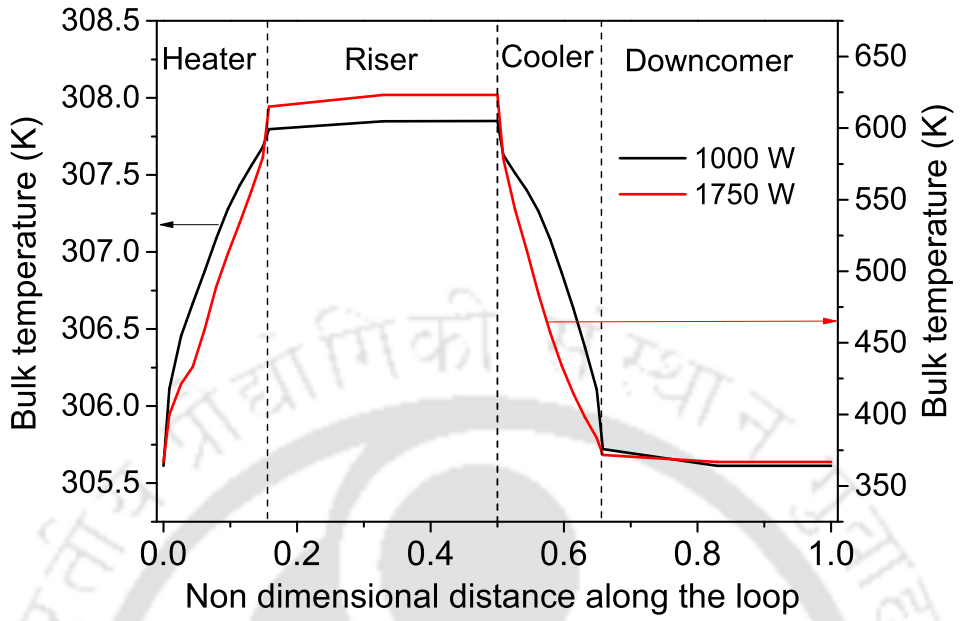

Fig. 2.6: Variation in bulk fluid temperature along the length of the loop at two different power levels with $p = 8$ MPa and $T_c = 295$ K

$\dot{Q} = 1000$ W conforms to this one, as is marked in Fig. 2.7(a). As explained by Kiss *et al.*[143], loop characteristics within this regime is dominated by the driving buoyancy head. On the contrary, $\dot{Q} = 1750$ W corresponds to the *deteriorated heat transfer regime*, where loop fluid maintains temperature higher than T_{pc} throughout the flow path, which is possible at reasonably higher power levels. The effect of friction can be envisaged to be more authoritative in this regime. It is, in fact, possible to have a third regime of operation during the low-power modes, where the heater power is not sufficient to raise the fluid temperature beyond T_{pc} within the heater, the fluid thereby retaining the liquid-like appearance over the entire loop. The circulation rate during this *low-power regime* can be comparable to the same in the deteriorated heat transfer regime. However, the flow rate increases almost linearly with heater power here, contrary to the persistence with near-identical magnitude in the other zone.

The region sandwiched between the enhanced and deteriorated heat transfer regimes experiences a steep decline in the circulation rate, which has been identified as FiHTD in literature[77, 134]. As detailed by Sarkar and Basu[134], the sink-side HTC closely mimics the profile of the circulation rate variation with power, exhibiting a maxima nearly at the

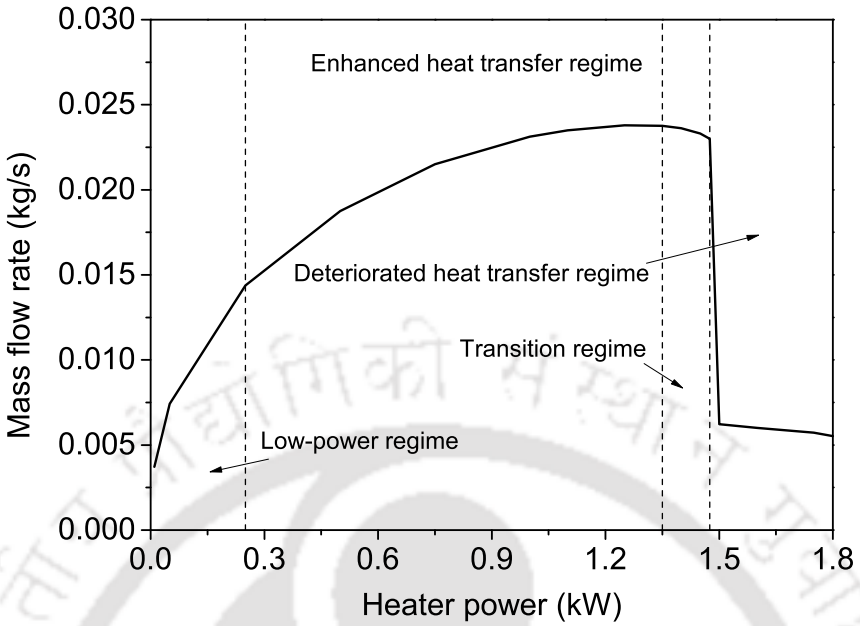

(a) Mass flow rate variation with power

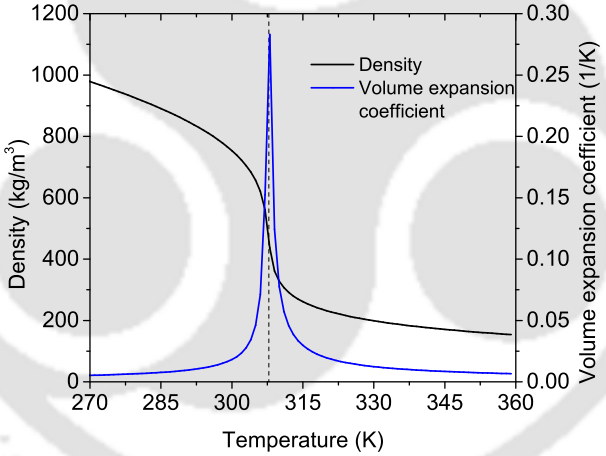

(b) Density variation with temperature

Fig. 2.7: (a) Variation in the loop circulation rate with power at $p = 8$ MPa and $T_c = 295$ K, where all the regimes of heat transfer are clearly identified; (b) Variation in density (ρ) and volumetric expansion coefficient (β) of sCO_2 with temperature at $p = 8$ MPa, where the pseudocritical temperature (T_{pc}) is shown by the dashed vertical line

same power level and a sharp deterioration thereafter. The loop fluid temperature level can also rise substantially following this *transition regime*, as has already been seen earlier in Fig. 2.6. As can be from Fig. 2.7(a), the flow rate starts to diminish gradually after attaining

the apex around 1350 W, which also marks the culmination of the enhanced heat transfer regime, owing to the growing dominance of frictional effects, and suffers the FiHTD around 1475 W. The appearance of all the regimes can comprehensively be correlated using the property variations represented in Fig. 2.7(b). Here the vertical dashed line corresponds to T_{pc}, and hence to the associated maxima in β and reduction in density around it. If the entire operation is restricted to the left of this line, the low-power regime is encountered, while the deteriorated heat transfer regime appears for systems limited completely to the right of it. Enhanced heat transfer regime is possible only for power levels encroaching into both sides of this line of segregation.

2.3.2 Effect of inclination

The inclination of the loop directly alters the effective buoyancy force. A brief attempt was made by Sarkar and Basu[77] to inspect the same, without reaching any proper conclusion. To properly reconnoitre the impact of inclination on FiHTD in sCO_2-driven sNCL, systematic parametric investigation has been performed over a reasonably wide range of control variables and inclination of 0° to 60° conceived by the adiabatic arms with the vertical axis in $y-z$ plane, as shown in Fig. 2.8. Corresponding variations in the circulation rate with power for four different inclination angles are illustrated in Fig. 2.9(a), with 0° referring to the standard vertical loop. As the loop is gradually inclined, the vertical distance covered by the warmer, and hence lighter, fluid exiting the heater continually decreases. The same is pertinent to the cooler heavier fluid in the downcomer as well, emanating lower buoyancy head. The total length of the frictional path, however, remains unchanged, obliging the system toward the friction-dominated operation. The repercussion of imposing inclination, therefore, is a reduction in the loop flow rate, despite maintaining identical level for other control variables, and that can vividly be observed from Fig. 2.9(a). Both the maximum circulation rate, as well as mass flow rate corresponding to any particular heater power, are considerably lower at greater levels of titling. Change in inclination (ψ) from vertical to 30° lessens the peak flow rate by about 6%, while the same drops by about 15% for 45° tilt angle.

Reduction in flow rate is always accompanied by a surge in fluid temperature level, which can be confirmed following the average loop temperature (T_{av}) for different inclinations. The same can be estimated by integrating the bulk temperature along the length of the loop as,

$$T_{av} = \int_{L_{tot}} T_b \, dl = \int_{L_{tot}} \frac{\int_A \rho c_p T \mathbf{V}_n \, dA}{\int_A \rho c_p \mathbf{V}_n \, dA} \, dl \tag{2.6}$$

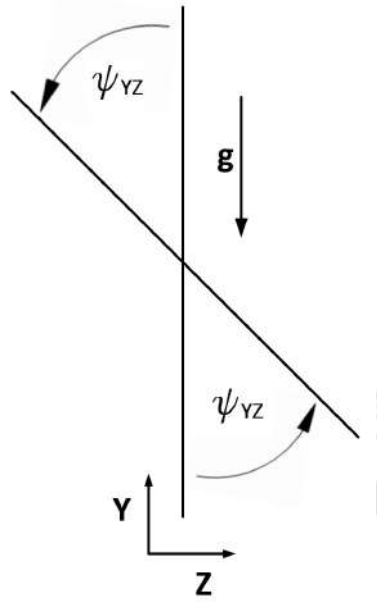

Fig. 2.8: Demonstration of the inclination provided to the loop in the $y - z$ plane

$\mathbf{V}_n$ refers to the velocity vector normal to a particular cross-section, dl is the coordinate along the flow path and L_{tot} is the total length of the loop. Here T_{av} has numerically been calculated considering the bulk temperature (T_b) values at 24 cross-sectional planes distributed throughout the loop and plotted in Fig. 2.9(b), exhibiting consistent rise. For all the selected cases, T_{av} remains below T_{pc}, indicating the operation in enhanced heat transfer regime, which is also consistent with Fig. 2.9(a). While the change in T_{av} with ψ may seem quite small, associated rise in peak fluid temperature is more substantial, as it can increase from 307.55 K for a vertical loop to 309.19 K for the 60° tilted one, ensuring the presence of increasingly-lighter CO_2 in the riser with greater inclination. Such ascension in temperature throughout the loop enforces an early-appearance of FiHTD for the inclined systems. For the vertical loop, peak flow rate approximately corresponds to a power of 1350 W, whereas the same slumps to about 1100 W for $\psi = 45°$, substantiating progressively greater dominance of friction over buoyancy. Quite interestingly, the approximate magnitude of T_{av} corresponding to 1350 W for the vertical loop is 307.83 K, which is extremely close to T_{pc} at this pressure. The same has been observed for all the other angles explored as a part of the present appraisal. It can, therefore, be concluded here that the sNCL attains the highest circulation rate precisely when the loop-averaged temperature equates pseudocritical value. T_{av} consistently remains greater than T_{pc} for the transition and deteriorated heat transfer

regimes.

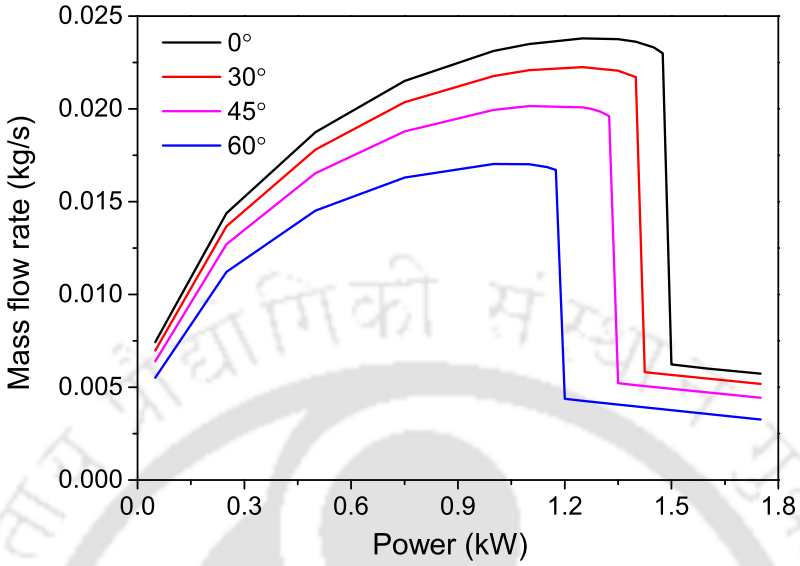

(a) Mass flow rate variation with power for different inclination angles

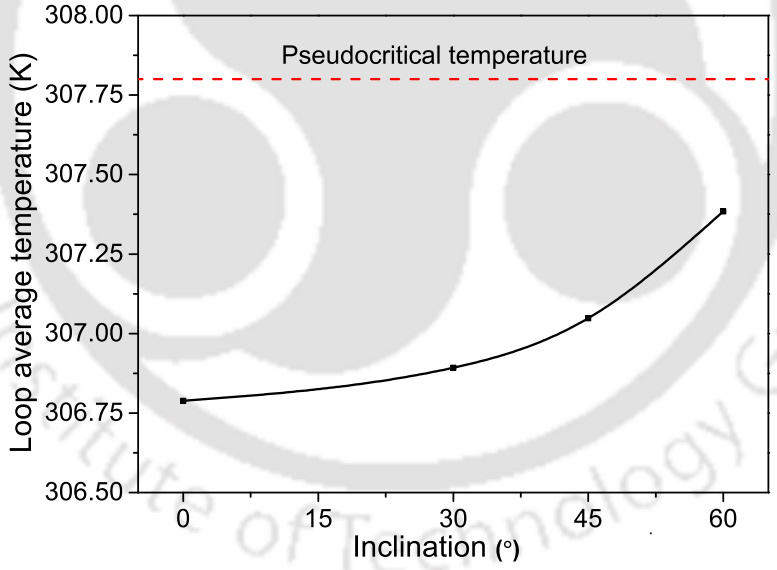

(b) Variation on loop average temperature (T_{av}) with the inclination angle at $\dot{Q} = 1000$ W

Fig. 2.9: Effect of inclination angles on (a) the loop circulation rate and (b) the loop average temperature at $p = 8$ MPa and $T_c = 295$ K

The intensification in frictional effects with inclination can also be illustrated tracking

the associated growth in friction factor. The following correlation is adopted here adhering to the relevant literature[91, 92, 144], with Re_{loc} being the local Reynolds number calculated using bulk properties.

$$f = 0.316 Re_{loc}^{-0.25} \tag{2.7}$$

The variation in f along the length of heater is presented in Fig. 2.10. The largest value is observed for 60° tilt angle, with consistent reduction in the flow direction, owing to the lowering of viscosity with rise in fluid temperature. There is, however, no drastic alteration in the magnitude of f, despite the appearance of FiHTD, for each of the considered cases.

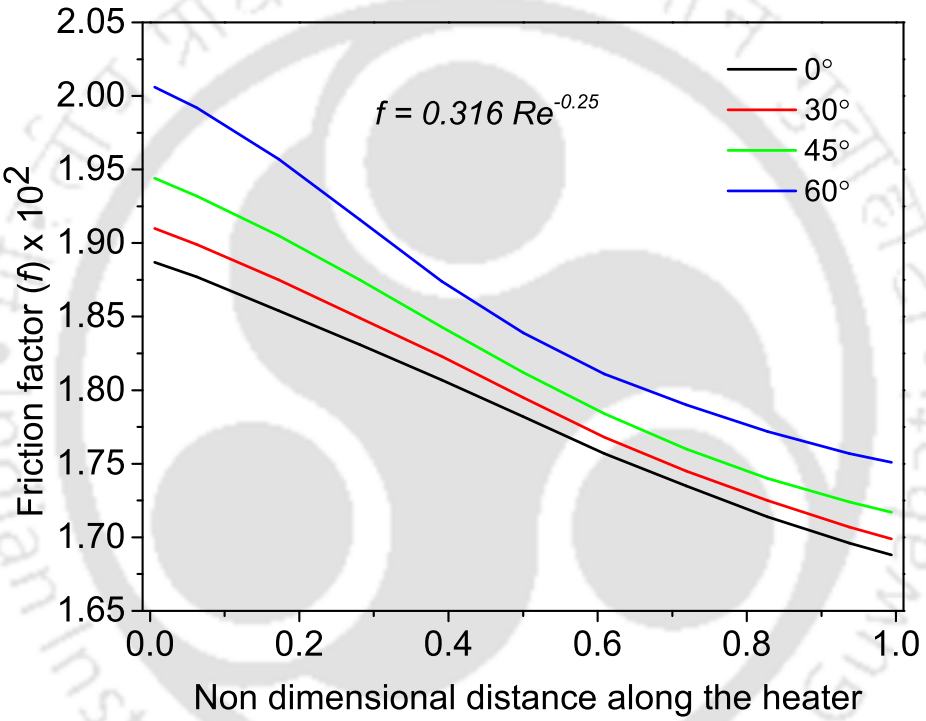

Fig. 2.10: Variation in local friction factor (f) along the length of the heater for different inclination angles with $p = 8$ MPa, $\dot{Q} = 1000$ W and $T_c = 295$ K

2.3.3 Presence of thermal asymmetry

One of the most prominent impact of the substantial property variation of sCO_2 with temperature is the appearance of thermal asymmetry in the heat-exchanging sections of sNCL. As the fluid crosses T_{pc} inside both heater and cooler during operation within the enhanced heat transfer regime, considerable disparity in density can be observed along heater/cooler.

Besides, the fluid particles in contact with the wall of the heater can directly absorb the energy, which makes it warmer, and hence lighter, than the bulk. Consequently, upward motion of the fluid along the wall of the heater can be envisaged, with the reverse being true for the cooler section, which leads to strong density stratification and local recirculation inside the horizontal sections of the vertical loop. This conjecture can be affirmed from Fig. 2.11, where the gradual stratification is clearly evident, with the lighter density fluid being clustered towards the upper part of the channel. Two distinct recirculation zones are also visible at the downstream locations, emphasizing the presence of local buoyancy effects. The same is pertinent for the cooler section as well, with the heavier fluid flowing downward along the cold wall, and the warmer fluid rising along the center.

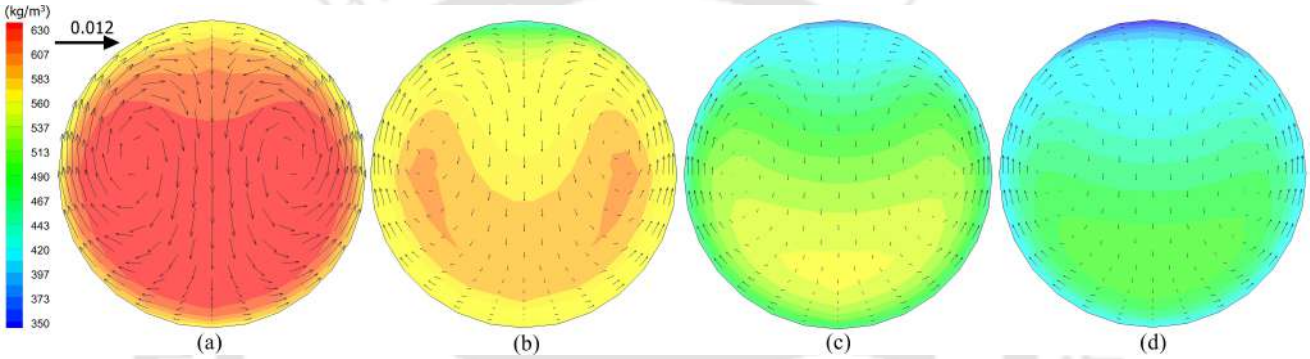

Fig. 2.11: Density contours and velocity vectors at 4 different locations of the heater of the vertical loop ($\psi = 0°$) with $p = 8$ MPa, $\dot{Q} = 1000$ W and $T_c = 295$ K, illustrating the presence of density stratification and local recirculation; here locations marked as (a), (b), (c) and (d) are 0.04, 0.22, 0.58 and 0.76 m downstream of the heater inlet

Immediate effect of such asymmetry is on the peripheral variation in the nature of thermal communication between the wall and adjoining fluid layer. Top half of any horizontal section is occupied mostly by higher-temperature fluid, which has lower viscosity, resulting in reduced magnitude of local Reynolds number. The local Prandtl number, however, is expected to be higher, particularly when the temperature is around T_{pc}. The combined effect of both is a thinner thermal boundary layer and greater magnitude of the local heat transfer coefficient (HTC) along the top surface, which is defined as,

$$U = \frac{\dot{q}''_w}{T_w - T_b} = \frac{\dot{q}''_w}{\Delta T} \tag{2.8}$$

with $\dot{q}''_w$ being the local wall heat flux, which is calculated by dividing the heater power by the surface area of the heater. Variation in U, as well as ΔT, averaged over the bottom and

top half surfaces, along the length of the cooler are presented in Fig. 2.12. Here bottom half surface refers to the azimuthal position of $\theta = 0°$ to $(-180°)$ (Fig. 2.1), whereas the top half surface corresponds to the rest. A total of 12 azimuthal locations have been considered in each cross-sectional planes to perform numerical integration while estimating the area averages. Noticeable difference in U in both the surfaces are observed. While the wall temperature is expected to vary in the flow direction interior to the heater, the ΔT-profiles smoothly complement U. The peak of HTC corresponds to the minima in ΔT, which appears around the location the bulk temperature cross T_{pc}.

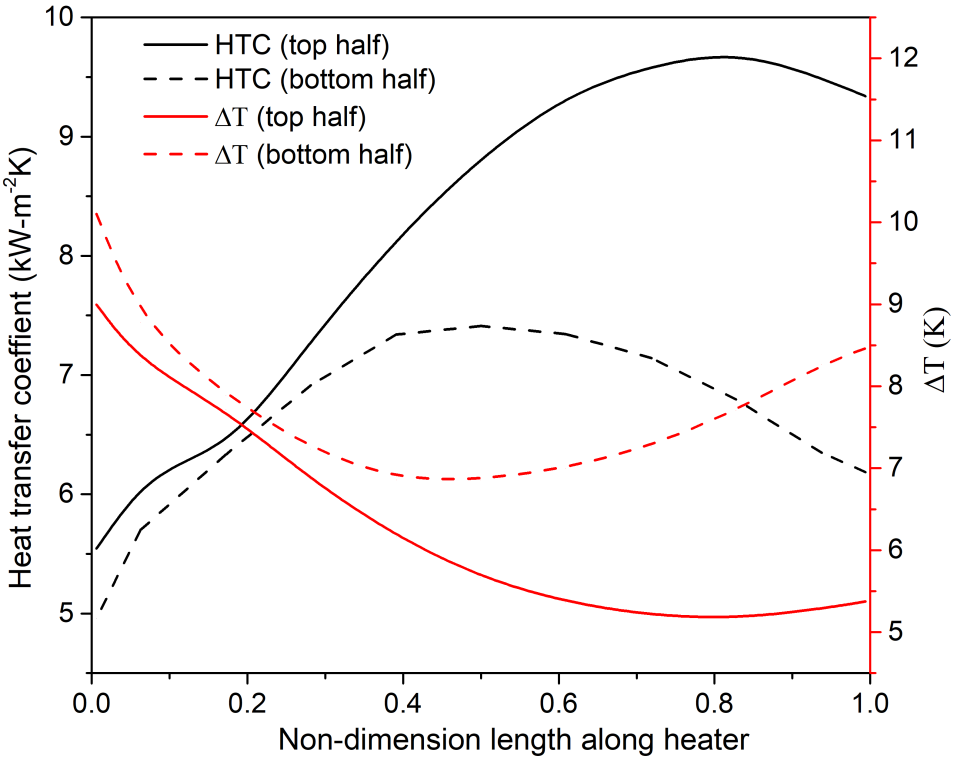

Fig. 2.12: Variation in area-averaged heat transfer coefficient (U) and wall-to-bulk temperature differential (ΔT) over bottom and top half surfaces along the heater of the vertical loop ($\psi = 0°$) with $p = 8$ MPa, $\dot{Q} = 1000$ W and $T_c = 295$ K

The role of the inclination angle on such azimuthal variation can be envisaged by following the peripheral profile of U at the particular location, and the same is presented in Fig. 2.13 for the cooler center. Substantial disparity in the top and bottom surfaces can be observed, with the peak HTC corresponding to the tip of the channel ($\theta = 90°$). It is quite obvious, as the local recirculation is always attempting to drive the warmer fluid towards that point. On the contrary, the lowest level appears around $\theta = -90°$. Imposing inclination to the

loop is not found to have any significant impact of the azimuthal variation, apart from the obvious lowering in the overall level of HTC. The profiles of wall heat flux ($\dot{q}''_w$) meticulously emulate the same for U, which is also expected considering the enforced boundary condition of constant outer wall temperature for the cooler. For each of the considered cases, T_b at heater exit is slightly above T_{pc}, with $\psi = 60°$ registering the highest value. The temperature, however, drops slightly owing to axial conduction during the passage of fluid through the riser, which forces T_b at the cooler inlet to be lesser than T_{pc} for all the cases, except the loop inclined with $\psi = 60°$. Consequently, an increase in HTC immediately on entering the cooler can be found for that particular loop, with fluid temperature remaining close to the pseudocritical one. However, the corresponding heat flux consistently remains lower that the same for all the other considered cases throughout the cooler, because of the low circulation rate. At higher power levels, fluid enters the cooler warmer than T_{pc} for all the loops, yielding profiles similar to the ones presented in Fig. 2.12, with the peak of HTC progressively getting shifted towards the cooler exit with rise in $\dot{Q}$. Accordingly, the cooler-side overall HTC (U_c), defined as

$$U_c = \int_{L_c} \int_{A} U \, dA \, dl \tag{2.9}$$

increases almost linearly with heater power ($\dot{Q}$) over the entire enhanced heat transfer regime, before suffering a radical plunge on encountering FiHTD (Fig. 2.14). It is only logical that the profiles of U_c for each of the considered inclination angles show perfect coherence to the mass flow rate profiles of Fig. 2.9(a). In the deteriorated heat transfer regime, HTC-level is very low because of both the low mass flow rate and inferior thermal conductivity of the *gas-like* sCO_2 throughout the system. The impact of inclination on FiHTD is quite noticeable, as the peak HTC reduces approximately by 6%, 14% and 26% for $\psi = 30°$, 45° and 60° respectively from the vertical loop. The heater power corresponding to FiHTD also declines by about 20% for $\psi = 60°$, which is an appreciable change as well.

2.3.4 Identification of FiHTD

It is pretty evident from the above discussion that the thermalhydraulic characteristics of any sNCL differ sufficiently on either side of the realization of FiHTD. The prodigious levitation in the temperature level of sCO_2 in the deteriorated heat transfer regime can be a cause of concern in real-life appliances, earmarking FiHTD as a possible limit of operation. That necessitates the identification of some criterion for categorically quantifying the point of appearance of FiHTD, which is one of the primary objectives of the present study, and

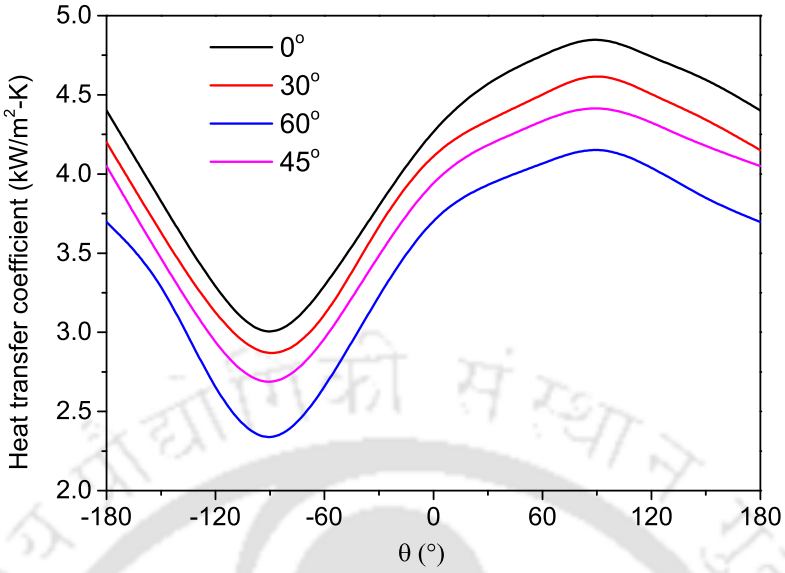

(a) Local heat transfer coefficient (U)

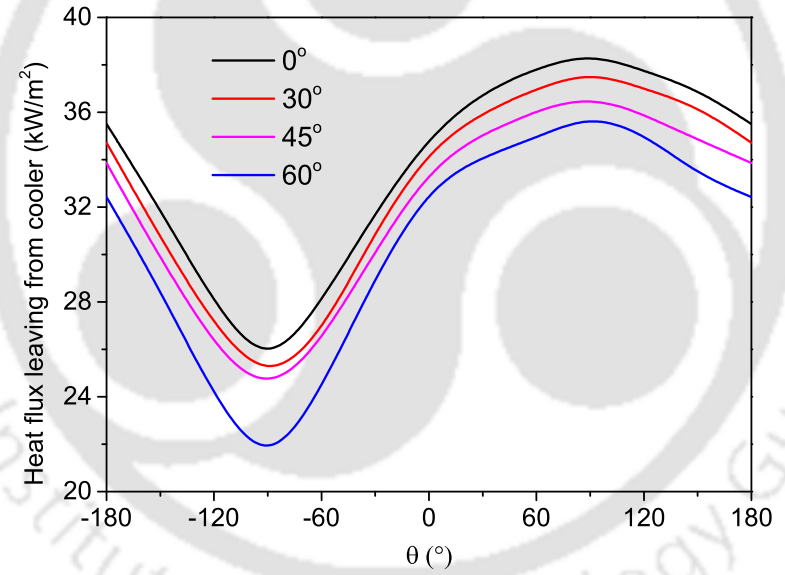

(b) Local wall heat flux ($\dot{q}''_w$)

Fig. 2.13: Effect of inclination angles on (a) the local heat transfer coefficient (U) and (b) the wall heat flux ($\dot{q}''_w$) at the cooler center at $p = 8$ MPa, $\dot{Q} = 1000$ W and $T_c = 295$ K

hence several such attempts are presented below to ascertain the most-acceptable one.

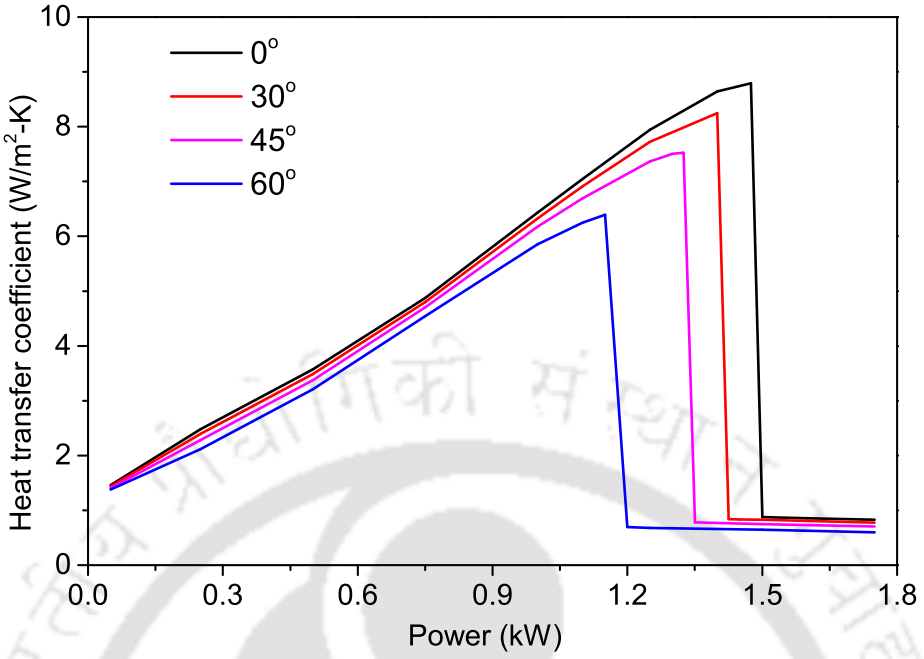

Fig. 2.14: Variation in cooler-side overall heat transfer coefficient (U_c) with heater power ($\dot{Q}$) for different inclination angles at $p = 8$ MPa and $T_c = 295$ K

2.3.4.1 Driving density differential

The driving potential in any NCL is primarily generated by the average difference in density of the fluid flowing through the two adiabatic arms ($\Delta\rho$). The heat-exchanging sections, of course, do participate in modulating the net buoyancy force in the inclined loops. $\Delta\rho$ can still be viewed as a logical representative of the main stimulation towards circulation and its variation with power for different tilt angles is presented in Fig. 2.15(a). It is intriguing to note that the peak of $\Delta\rho$ for each of the cases perfectly dovetails with the same for mass flow rate, before suffering a sharp decline. In the post-FiHTD zone, fluid temperature remains greater than T_{pc} throughout the flow path, which explains the low value of density differential. It is, however, interesting to note that the magnitude of $\Delta\rho$ increases with ψ for identical power levels in both enhanced and deteriorated heat transfer regimes, as a consequence of lower flow rate, and even the maxima is also markedly higher. Therefore, a higher level of density difference not necessarily suggests a greater flow rate. The same can further be demonstrated following Fig. 2.15(b), where two vertical loops with different heights have been compared. The taller loop consistently exhibits lower $\Delta\rho$, despite being capable of producing larger circulation[93]. Hence, it is not prudent to earmark $\Delta\rho$ as an

option for quantifying FiHTD, as it fails to provide logical comparison between multiple sNCLs.

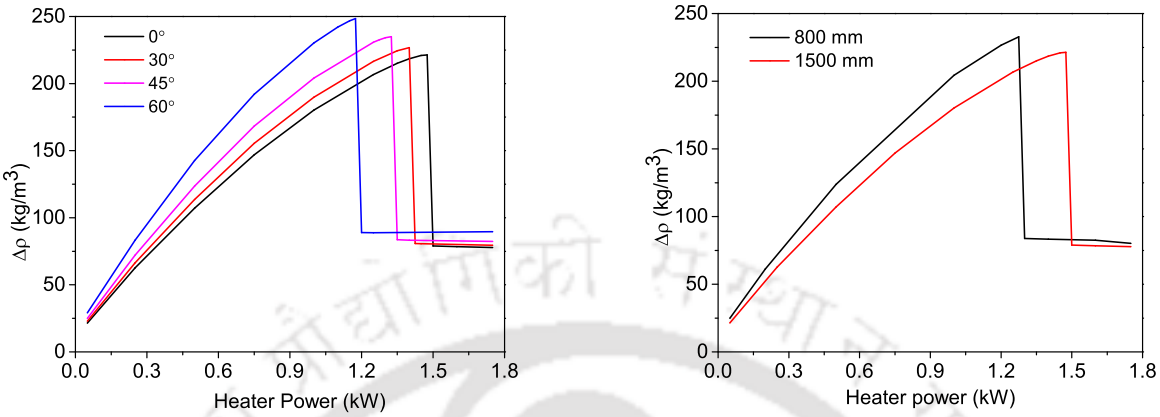

(a) Effect on inclination angle **(b)** Effect of loop height for vertical loop

Fig. 2.15: Variation in the average density difference of the fluid between the two adiabatic arms ($\Delta\rho$) with heater power ($\dot{Q}$) at $p = 8$ MPa and $T_c = 295$ K

2.3.4.2 Profiles of friction factor

The circulation is sNCL is regulated by the contrasting roles of buoyancy and friction, and hence the frictional characteristics can also offer crucial insight. As has been discussed above in conjunction with Fig. 2.10, local friction factor reduces along the heater, because of the continuous increase in Re_{loc} as a combined response to enhanced velocity and lowered viscosity. That trend, however, is specific to the pre-FiHTD domain and can be associated to the enhanced heat transfer regime. It has already been observed that the temperature level is very high in the post-FiHTD region (Fig. 2.6), well beyond the so-called second pseudo-critical point[97], where the dynamic viscosity actually increases with rise in temperature, a behavior consistent to the *gas-like* representation of sCO_2. Consequently, the friction factor is expected to increase along the heater, and that is indeed the case, as can be confirmed from Fig. 2.16. While the spatial gradient of f is negative for any inclination angle prior to the appearance of FiHTD, that turns out to be positive beyond it. Such perceptible change in the slope strongly indicates the transition from enhanced to deteriorated heat transfer. Despite viscosity being a moderate function of pressure, the profiles of f are found to be reasonably apart for a vertical loop, where the deviation in flow rate has a more pivotal role. For identical geometric configuration and boundary conditions, $\Delta\rho$ varies only by 0.2% with

a change in pressure from 8 to 9 MPa within the enhanced heat transfer regime, yielding similar mass flow rates. That disparity, however, swells to about 10% after deterioration, which forces the profiles to veer away further from each other.

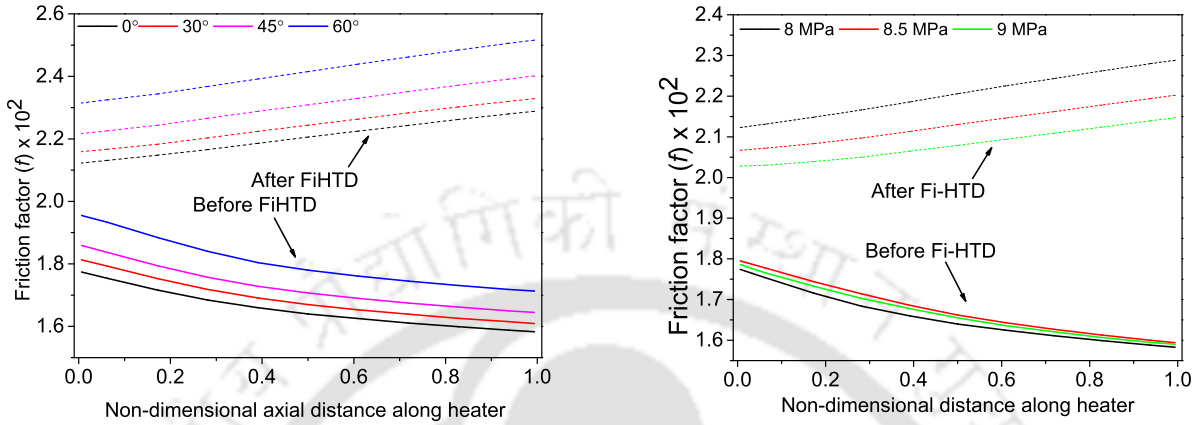

(a) Effect on inclination angle at $p = 8$ MPa **(b)** Effect of pressure for vertical loop

Fig. 2.16: Effect of (a) inclination angle and (b) pressure on the variation in the friction factor (f) along the length of the heater at two different power levels at $T_c = 295$ K; the continuous and dashed lines respectively refer to power level before the appearance of FiHTD and after FiHTD

2.3.4.3 Buoyancy parameter

While each of the above options can provide a qualitative estimate about the nature of heat transfer (enhanced or deteriorated), it is not possible to have any quantifiable estimate, as that obligates a combination of both buoyancy and friction. The concept of the buoyancy parameters was used earlier for configurations involving mixed-type flow[106]. The same is used here for pure natural convective motion by defining as the ratio of the two involved forces as,

$$Bu = \frac{Gr_m}{Re_{ss}^2} \tag{2.10}$$

Here both Gr_m and Re_{ss} have been estimated as averaged over the heater. Natural convection effects dominates over forced convection for $Bu \gg 1$, and any modification hampering the buoyancy field is expected to lower Bu. Consequently, an increase in system pressure or decrease in sink temperature for a given geometry enhanced Bu and also delays the appearance of FiHTD[76, 77]. The buoyancy field being weaker in an inclined loop, lower value of Bu can be noted, alongside early FiHTD. The variation in Bu, therefore, is consistent with

the direction of change in FiHTD, and it can be a viable option for quantification. Moreover, the parameter also exhibits a maxima with change in heater power at the point of initiation of FiHTD, advocating towards the largest buoyancy field, as can be seen from Fig. 2.17(a). More interesting trend can be observed following Fig. 2.17(b). There is a complete reversal in the $Bu - U_c$ profile on appearance of FiHTD. Hence, it is logical to recommend the use of Bu for characterizing FiHTD, with its peak for a given geometry earmarking the critical power limit. It is, in fact, possible to make use of Eq. 2.5 to establish an approximate correlation of the form $Bu = Bu\left(\dot{Q}\right)$, simply with the knowledge of geometry and operating conditions, and get a rough estimate about the power limit of safe operation. In must also be marked that the magnitude of Bu, even after the decline, remains considerably higher than one, signifying pure natural circulation. The variations in the maxima in Bu (Bu_{max}) with different operating and geometric variables are presented in Fig. 2.18, which provides a quite comprehensive coverage about the allowable zone of operation for sCO_2-driven NCLs.

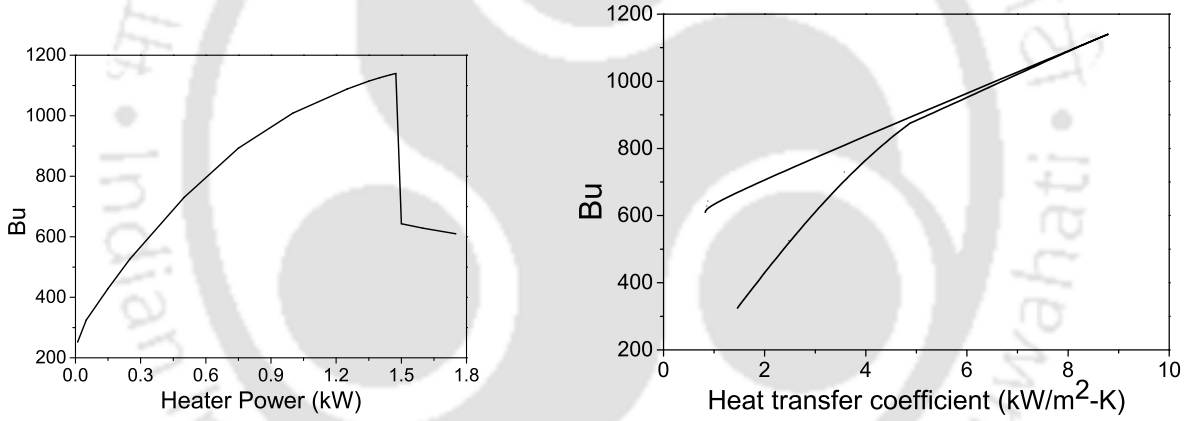

(a) Variation with heater power **(b)** Variation with mass flow rate

Fig. 2.17: Variation in the buoyancy parameter (Bu) with (a) heater power ($\dot{Q}$) and (b) cooler-side overall heat transfer coefficient (α_c) at $p = 8$ MPa and $T_c = 295$ K; the arrows in (b) indicate the direction of increase in the heater power

A final attempt is made to commingle all the cases contemplated within the scope of the present study by correlating the peak of the buoyancy parameter (Bu_{max}) with the friction factor (f_{av}), averaged along the heater. The developed dataset is presented in a scatter plot in Fig. 2.19 to represent the limiting conditions for safe operation over a reasonably-wide range of pressure, sink temperature, inclination angle and loop height. Corresponding power-law-fit can be viewed as the representative of the threshold heater power ($\dot{Q}$) ensuring

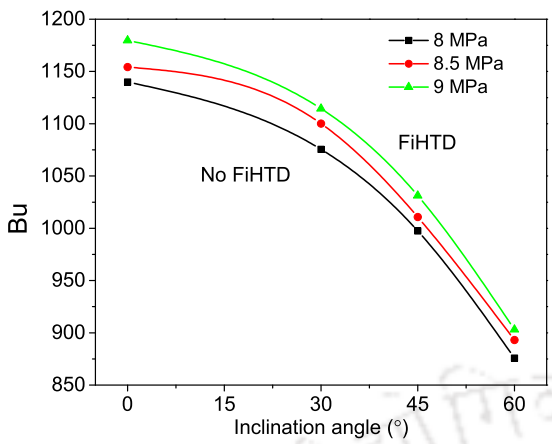

(a) Effect of system pressure

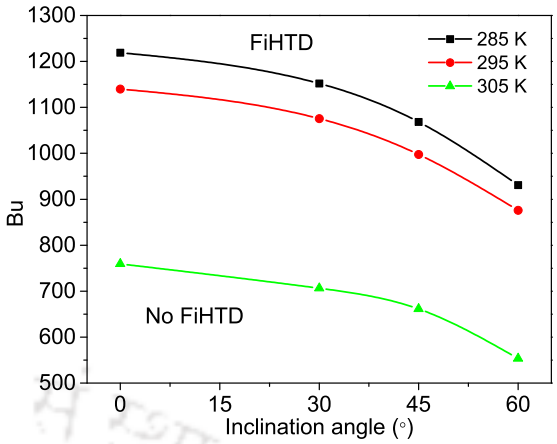

(b) Effect of sink temperature

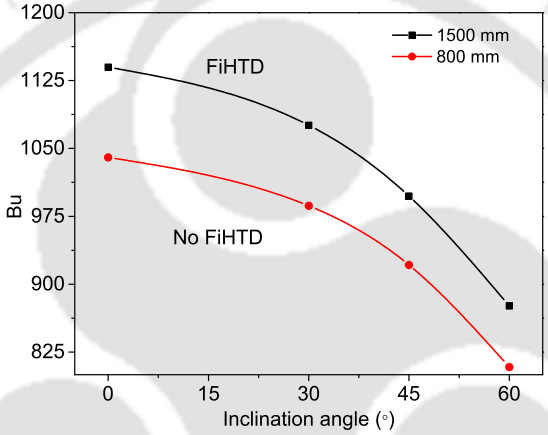

(c) Effect of loop height

Fig. 2.18: The variation in the maximum value of the buoyancy parameter (Bu_{max}) with inclination angle and different operating and geometric variables

operation with enhanced heat transfer and avoiding FiHTD, which can be imposed on any rectangular sNCL operating with similar boundary conditions.

2.4 Summary

The phenomenon of FiHTD is always a matter of concern in sNCL, as it is preferable not to operate in the deteriorated heat transfer regime, in order to avoid high fluid temperatures and steep thermal gradients. While quite a few recent studies have looked into the influence of certain geometric and operating parameters on the appearance of FiHTD, the role of inclination has not been explored much. The cognizance of FiHTD itself remains an open topic

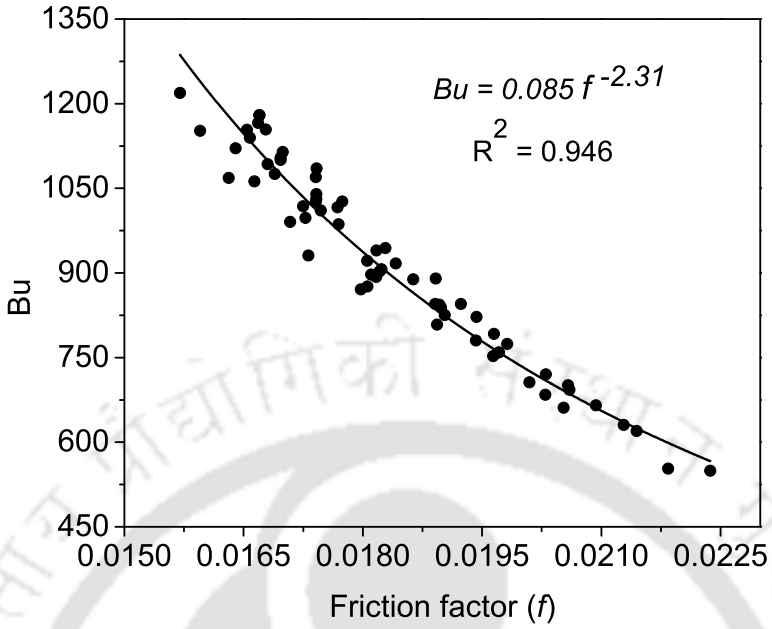

Fig. 2.19: Variation in the peak of the buoyancy parameter (Bu_{max}) with heater-side average friction factor (f_{av}) for all the cases considered

of research. Present study aims on identifying a generalized criterion for prior identification of FiHTD in sCO_2-driven rectangular NCL, with particular emphasis on the inclination to vertical. A 3D computational model has been developed, remaining consistent to the relevant literature, and that shows amicable agreement with relevant literature. Followings are some of the major conclusions from the detailed appraisal of the considered configuration.

- Operating regime of sNCL can differ substantially with change in heater power. Four different regimes have been earmarked, primarily based on the temperature levels in the adiabatic arms. It is preferable to operate within the enhanced heat transfer regime, as it offers high HTC, with reduced temperature levels and large rate of circulation. Average temperature level can jump by several hundred degrees on the inception of the deteriorated heat transfer regime.

- Both the circulation rate and HTC noticeably reduces for the tilted loop, owing to the diminishing effective height, without any change in the length of the frictional path. The level of friction factor also enhances with inclination, confirming the increased dominance of friction over buoyancy. Height of the loop is found to have stronger influence in modulating the driving potential over the density differential between the

hot and cold fluid.

- Largest circulation rate corresponds to the heater power, which yields $T_{av} \approx T_{pc}$ for any inclination angle, thereby providing a theoretical option of identifying FiHTD.

- Presence of thermal asymmetry in the horizontal sections of the loop emanates considerable azimuthal variation in the thermal communication between fluid and wall, and also strong local recirculation. HTC along the top half surface remains appreciably higher than the same along the bottom half surface, which is also complemented by the peripheral variation in the wall heat flux interior to the cooler.

- Qualitative recognition of FiHTD is possible following the nature of asymmetry in temperature and density contours at certain cross-sections, variation in the radial velocity profiles along heater/cooler and the slope of the variation in friction factor along heater.

- A comprehensive identification of FiHTD is possible using the concept of Bu, a non-dimensional quantity relating the natural and forced convective forces, which follows similar nature of dependence of the heater power corresponding to FiHTD on all relevant geometric and operating variables. At a given condition, FiHTD corresponds to the maxima in Bu, which can be related to the average friction factor for distinct identification of the critical power level prior to operation.

Chapter 3

Numerical Evaluation of Static and Dynamic Stability Characteristics

3.1 Preamble

Stability appraisal of the buoyancy-driven systems has fascinated researchers over several decades, primarily because of the intricate local-level physics and also as a classical mathematical exercise. Starting from the seminal works of Batchelor [145] on free convection inside closed cavity and Gallagher and Mercer [146] on mixed convective motion, numerous attempts can be found in the open literature, practicing a wide range of analytical and numerical approaches, and evaluating a variety of buoyancy-dominated flows. The first plausible theoretical model for a thermosyphon and rationale behind the emergence of instability in such devices can be credited to Welander [26], whereas Creveling et al. [24] were the first to experimentally demonstrate oscillatory motion. Several research groups subsequently explored the nature of instability in NCLs, considering its pivotal role during any operation. In fact, as explained by Zvirin [13], the initiation of motion in a closed loop itself is associated with an instability. While the static instability is the most prevalent one with single-phase loops, both Ledinegg instability and density-wave oscillations are significant in boiling loops, as has been comprehensively reviewed by several research groups [14, 16, 17].

The drastic variation in the thermophysical properties of SCF along an isobar, especially around the pseudocritical temperature (T_{pc}), adds another dimension to modulate the thermalhydraulic characteristics. The order of change in properties for two common SCFs is demonstrated in Fig. 3.1. Despite the absence of explicit phase change, thereby avoiding interfacial instabilities, the possibility of substantial density variation over a short flow path

actuates the so-called *feedback effect* on flow rate, analogous to multiphase loops. Consequently, a sNCL can also suffer various kinds of instabilities, instigating a handful of research endeavors over the last couple of decades.

First experimental recognition of oscillations can be credited to Harden and Boggs [147] with the bulk temperature approaching T_{pc}, as they explored Freon in the near-critical region. Similar observations were reported by Adelt and Mikielewicz [148] with supercritical CO_2 (sCO_2). They, however, did not explore much of the stability behavior, as their focus was on heat transfer. Pioneering analytical work on steady-state and stability aspects of sNCL is attributed to Chatoorgoon [83]. He analyzed an open loop with both point and distributed heat source and sink using the 1D nonlinear code SPORTS. The steady-state flow rate was reported to exhibit a maxima with heater power, which was postulated to correspond to the stability threshold. The follow-up studies [114, 115] supported the same for multiple fluids with about 95% adherence. Jain and Rizwan-uddin[110], however, strongly contradicted Chatoorgoon[83], suggesting the stability threshold to lie on the positive slope of the flow-power curve, and not around the peak. Another 1D code was developed by Sharma et al.[111], and the concerned outcomes were compared with their indigenous experimental data. A shallow, unstable zone was predicted in their subsequent work [149] with supercritical water. The need of incorporating precise equation-of-state was also emphasized by Jain and Corradini [120]. Accurate evaluation of thermophysical properties is of critical importance for the appraisal of sNCL. The complete transformation from the unstable flow with repetitive flow reversals to stable unidirectional motion is also possible under certain operating conditions, as was observed by Chen et al. [97]. No instability, however, was observed by Yu et al. [132] through both experiments and 1D simulations, as they restricted the highest temperature well below T_c even at supercritical pressures. Sharma et al.[111] deliberated about the role of orientation of heater and cooler of sNCL on the stability response and earmarked HHHC configuration as the most unstable one, whereas the relative influences of several geometric and operating parameters were contemplated by the same group in a different work [91] using another 1D code NOLSTA.

Most of the studies referred above are limited to the open loops, which allow direct control of the fluid temperature and pressure at the heater inlet by incorporating a reservoir, thereby making it easier to impose the boundary conditions numerically. The closed loop, however, is more practicable. A decent model of closed sNCL was recently proposed by Archana et al.[72], with the primary focus being on heat transfer characteristics and also to assess the gain possible with a 2D-axisymmetric model over the 1D approach. [111, 149] did explore the

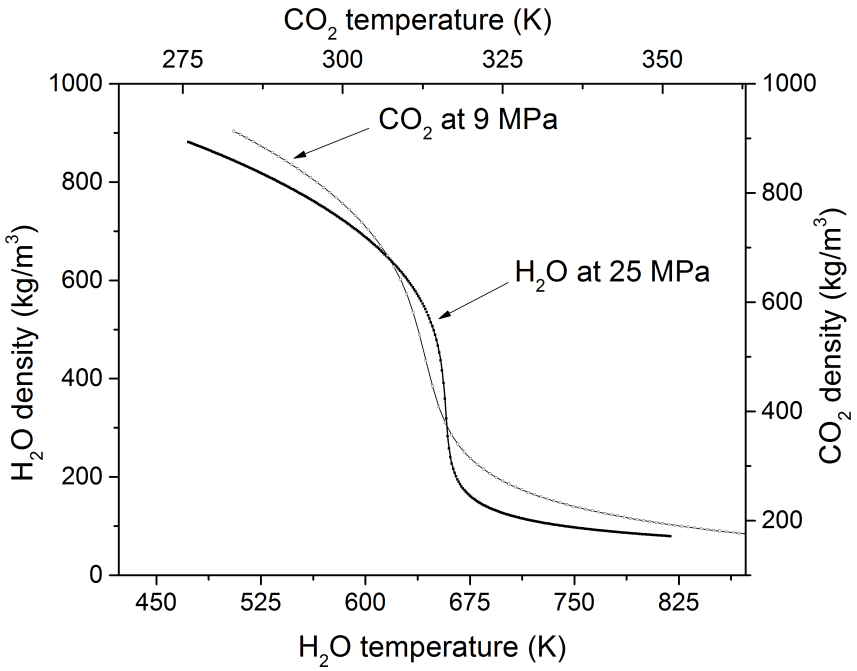

(a) Density (ρ)

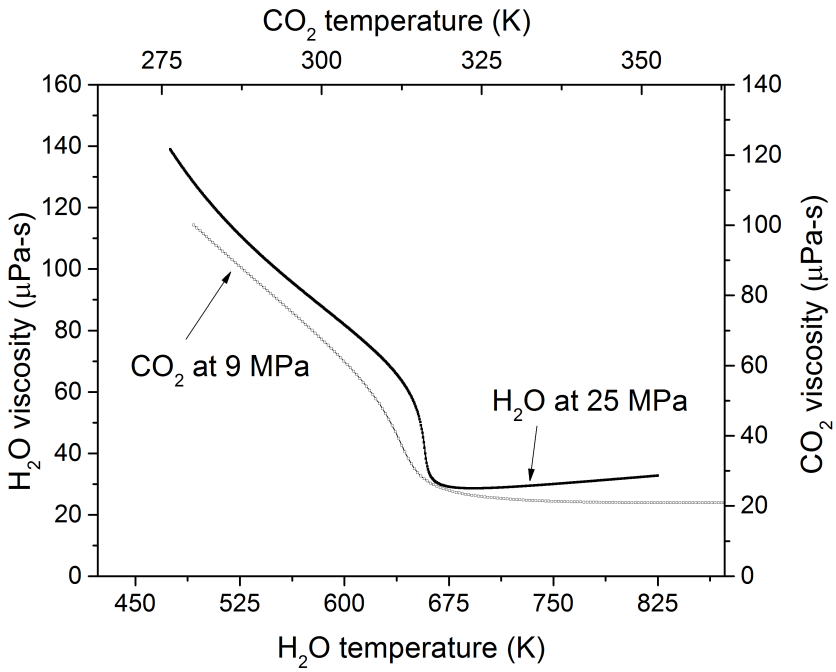

(b) Dynamic viscosity (μ)

Fig. 3.1: Variations in properties of sH2O at 25 MPa and CO2 at 9 MPa withtemperature obtained using NIST RefProp[119]

stability characteristics using a 1D numerical structure, and reported oscillations over a wide range of heater power for the closed loop. They suggested the use of appropriate model for wall thermal capacitance or adoption of 3D codes for more realistic predictions. Swapnalee et al. [104] attempted linear stability analysis of a closed sNCL assuming simplistic relation between density and enthalpy, such as sigmoidal or linear functional forms, but failed to observe any for CO_2-driven system.

That culminates in a very thin knowledge base regarding the stability aspects of closed sNCL and provides the necessary impetus for the present study. Here the focus is on the nonlinear stability analysis of a closed rectangular sNCL in HHHC orientation, which has been identified as the most unstable one earlier in literature. Many of the previous researches concern supercritical water, primarily because of its relevance with supercritical water reactor (SCWR). Supercritical CO_2, though, has recently found very encouraging applications in small-to-large heat transport devices and is being projected as one of the coolants for future. As reported by Swapnalee et al.[104], because of the differences in the properties in supercritical region of sH_2O and CO_2, it is expected that for CO_2, the stability response may be different. Therefore, the present study contemplates sCO_2 as the working fluid and incorporates comprehensive property relations in a 1D numerical framework, more details on which are available below. Both the static and dynamic stability characteristics, identified through the appearance of multiple steady-states and diverging flow oscillations respectively, have been analyzed in sufficient detail. The relative effects of the relevant geometric and operating variables have also been systematically explored on the nonlinear response and stability maps, allowing a comprehensive appraisal of the preferable regime of operation for sCO_2-driven NCL.

3.2 Computational Model Development

3.2.1 Governing equations

As mentioned above, a rectangular sNCL in HHHC orientation is considered for the present appraisal, schematic representation of which is shown in Fig. 2.1. Flow is assumed to be one-dimensional, thereby neglecting any changes in the radial or azimuthal direction, and s is employed as the sole spatial coordinate of importance, which runs along the loop. The Fig. **??** shows the distribution of nodes along with different section of the loop. Since the loop is closed, the 1st node of the heater coincides with the last node of the cold leg. Effects of viscous dissipation and changes in potential and kinetic energies have been assumed to

be inconsequential. Accordingly, the applicable set of conservation equations for a loop with uniform diameter (d) is the following one.

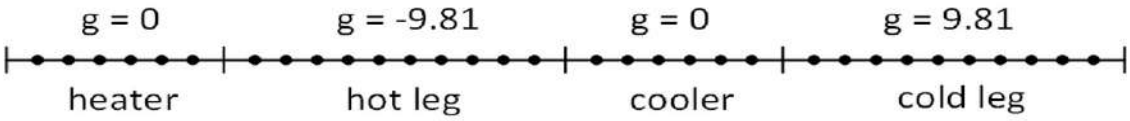

Fig. 3.2: Representation of the node distribution in rectangular sNCL under consideration in 1-D

$$\frac{\partial \rho}{\partial t} + \frac{\partial G}{\partial s} = 0 \tag{3.1a}$$

$$\frac{\partial G}{\partial t} + \frac{\partial}{\partial s}\left(\frac{G^2}{\rho}\right) = -\frac{\partial p}{\partial s} - \rho \bar{g} - \left(\frac{f_d}{d} + K_L\right)\left(\frac{G^2}{\rho}\right) \tag{3.1b}$$

$$\frac{\partial}{\partial t}(\rho h) + \frac{\partial}{\partial s}(Gh) = \frac{4\dot{q}''_w}{d} - \frac{4U}{d}(T - T_\infty) \tag{3.1c}$$

Here K_L is used to replicate the combined pressure drop incurred in the four elbows of the rectangular frame. A decent estimate for it can be found following the empirical relation proposed by Vijayan et al.[111] for a particular experimental facility, which was later adopted in the model of [72] and is also incorporated in the present work.

$$K_L = 0.55 + 2.23 \exp\left(-\frac{Re}{7959.5}\right) \tag{3.2}$$

$\bar{g}$ appearing in the momentum conservation equation provides the effective magnitude of gravitational acceleration in any particular location of the loop, depending on the direction of motion. The right hand side of the Eq. 3.1(c) is applicable as it is for heater section with non-zero heat flux, whereas for the cooler side only last term containing U is applicable. Use of the Blasius relation is quite common for realistic estimation of the friction factor (f_d) [72, 110, 125] and is continued here as well. There is no such consensus for the computation of the local value of the heat transfer coefficient (U) for supercritical fluids, with most of the available models suffering from large inaccuracy around T_{pc}. The same was highlighted by Sharma et al.[111] as well. It is a common observation that turbulence is initiated in NCLs at lower Re values compared to the forced-flow channels as a possible consequence of the enhanced role of buoyancy. That has motivated some research groups to explore with forced-flow correlations in NCLs or propose system-specific modifications to that [150]. A few such

relations have been considered as a part of the present model as well, without observing any substantial difference in local or overall predictions. Therefore, the present model adopts the Dittus-Boelter relation, mostly to suit the associated range of Re (typically of the order of 10^4) and also considering its reasonable performance over a large temperature range.

3.2.2 Discretization of the governing equations

The nonlinear partial differential equations governing the conservation of variables are converted to a set of coupled algebraic equations following the approaches of Sharma et al.[111] and Tilak and Basu[125]. The researchers who nurtured the idea of using the code in a simple manner is should be given to [110] but, the methodology has some differences beacuse they have used the code considering the open loop, while the present system is the closed system. FTFS (Forward in Time and Forward in Space) scheme is employed for discretization in both time and space domain, resulting in a time-explicit form of the final expressions. The physical domain is described by a set of discrete computational nodes, placed along the s-direction, with the last node coinciding with the first one to provide a closed loop. Accordingly, the discretized versions of the conservation equations at the i^{th}-node in the n^{th}-time instant embrace the following forms.

$$G_{i+1}^{n+1} = G_i^{n+1} - C^n \left(\rho_{i+1}^{n+1} + \rho_i^{n+1} - \rho_{i+1}^n - \rho_i^n\right) \tag{3.3a}$$

$$p_{i+1}^{n+1} = p_i^{n+1} - \left[1 + \frac{\Delta s}{2}\left(\frac{f_d}{d} + K_L\right)_{i+1}^n\right]\left(\frac{G^2}{\rho}\right)_{i+1}^n + \left[1 - \frac{\Delta s}{2}\left(\frac{f_d}{2d} + K_L\right)_i^n\right]\left(\frac{G^2}{\rho}\right)_i^n - \Delta s\left(\frac{\rho_{i+1}^n + \rho_i^n}{2}\right)\bar{g} - C^n\left(G_{i+1}^{n+1} + G_i^{n+1} - G_{i+1}^n - G_i^n\right) \tag{3.3b}$$

$$h_{i+1}^{n+1} = \frac{\frac{4\dot{q}\Delta s}{d} - \frac{4U\Delta s}{d}\left(T_{i+1}^{n+1} - T_\infty\right) + G_i^{n+1}h_i^{n+1} - C^n\left((\rho h)_i^{n+1} - (\rho h)_{i+1}^n - (\rho h)_i^n\right)}{G_{i+1}^{n+1} + C^n\rho_{i+1}^{n+1}} \tag{3.3c}$$

where, $C^n = \frac{\Delta s}{2\Delta t^n}$ is a combination of inter-nodal distance and instantaneous time step.

Precise estimation of local instantaneous thermophysical properties is very crucial for accurate appraisal of any supercritical flow systems, as even a small change in temperature around T_{pc} can conjure substantial alteration in several properties. All the relevant thermodynamic and transport properties have been estimated here using the CoolProp module (https://bit.ly/3FW6HfF) of Python[151]. It is a C++ library, which permits complete communication with NIST RefProp library and facilitate highly accurate property estima-

tion by tabular interpolation in a computationally efficient manner. Comparisons between the predicted values of density and specific heat of sCO_2 at a pressure level of 8 MPa from the present 1D code and the same from NIST database are presented in Fig. 3.3. Amicable agreement is palpable over the entire temperature range illustrated here, demonstrating the adequacy of the incorporated property module.

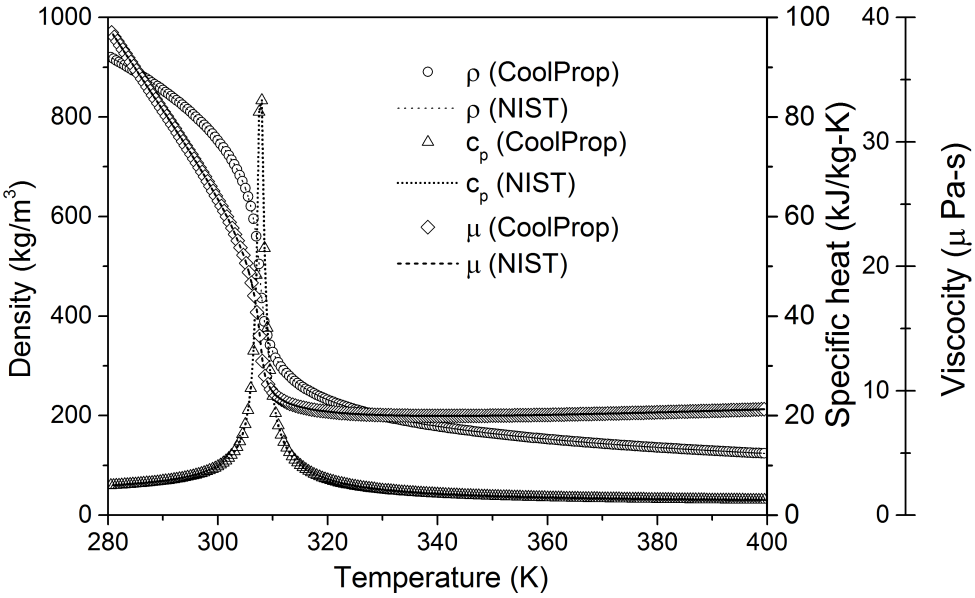

Fig. 3.3: Comparisons of property values predicted by present code and obtained from NIST RefProp for sCO_2 at 8 MPa

3.2.3 Selection of grid spacing and time step

Appropriate selections of node-to-node distance (Δs) and time step (Δt) are essential during both steady and transient simulations, to eliminate the possible influence of artificial diffusion on the predictions. Accordingly, a wide range of grid sizes have been explored in the present study, systematically refining it from coarser (0.1 m) to finer (0.01 m) values. The transient profiles of non-dimensional mass flow rate have been shown in Fig. 3.4 for four such choices. Hardly any distinguishable change can be observed for a change in Δs = 0.025 m to 0.01 m, and hence, 0.025 m is continued with for the remainder of the present study. The time step, however, is a variable, in an effort to maintain the Courant number ($= V_{max}\Delta s/\Delta t^n$) around one throughout the loop at every time instant [152]. Here V_{max} is the maximum fluid velocity within the loop, which can change with time, accordingly modulating Δt.

The steady-state versions of the discretized equations 3.3(a-c) are solved initially after

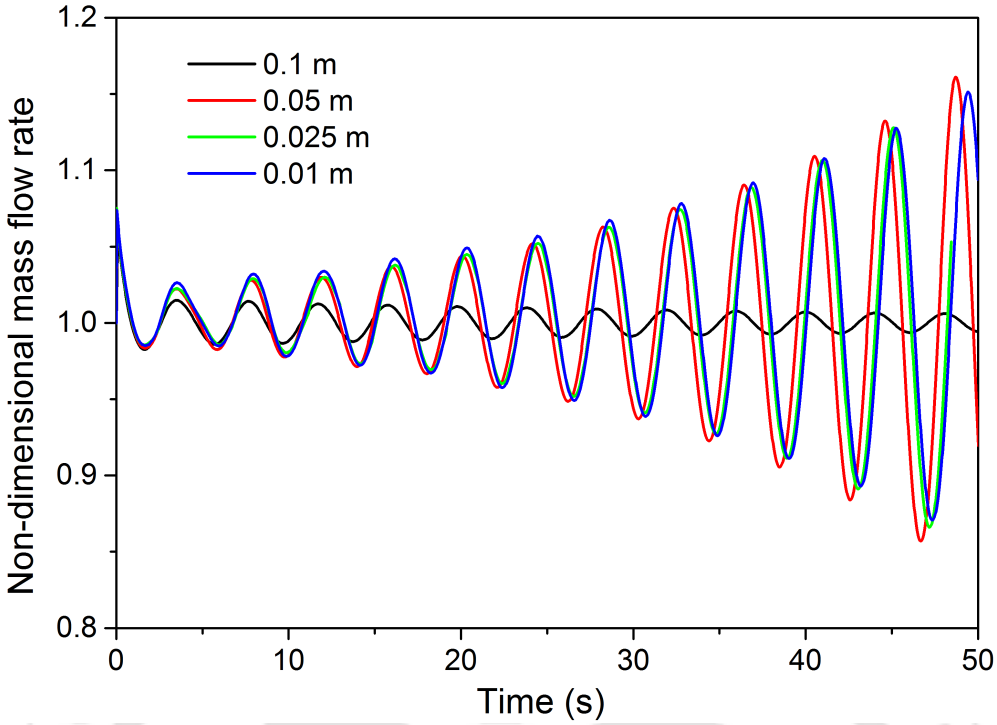

Fig. 3.4: Effect of grid spacing on the temporal variation in non-dimensional mass flow rate at $p = 8$ MPa, $T_\infty = 295$ K and $\dot{q} = 1600$ W

imposing the desirable set of boundary conditions, in terms of the heater power ($\dot{q}$), temperature of the cooling fluid (T_∞) and system pressure (p). The last parameter is required primarily for the estimation of local properties, as the pressure drop around the loop must always be zero. The *method of bisection* is used with two initial guesses for the steady-state mass flux and the final solution is achieved through an iterative procedure, with a density convergence of 0.05 kg/m^3 at every node during the inner iterations, and temperature and pressure convergences of 0.05 K and 1 Pa respectively during the outer iterations. Transient simulations are instigated after imposing 5% perturbation on the steady-state mass flow rate and temporal variations in important system variables have been followed over a sufficiently long period to ascertain the nature of system response. A detailed representation of the solution algorithm is presented in Fig. 3.5.

3.2.4 Validation of the numerical framework

It is imperative to compare the predictions from any numerical setup with appropriate experimental data, in order to gain confidence about the capability of the developed solver. It is, however, illogical to compare with the dimensional information obtained from a different

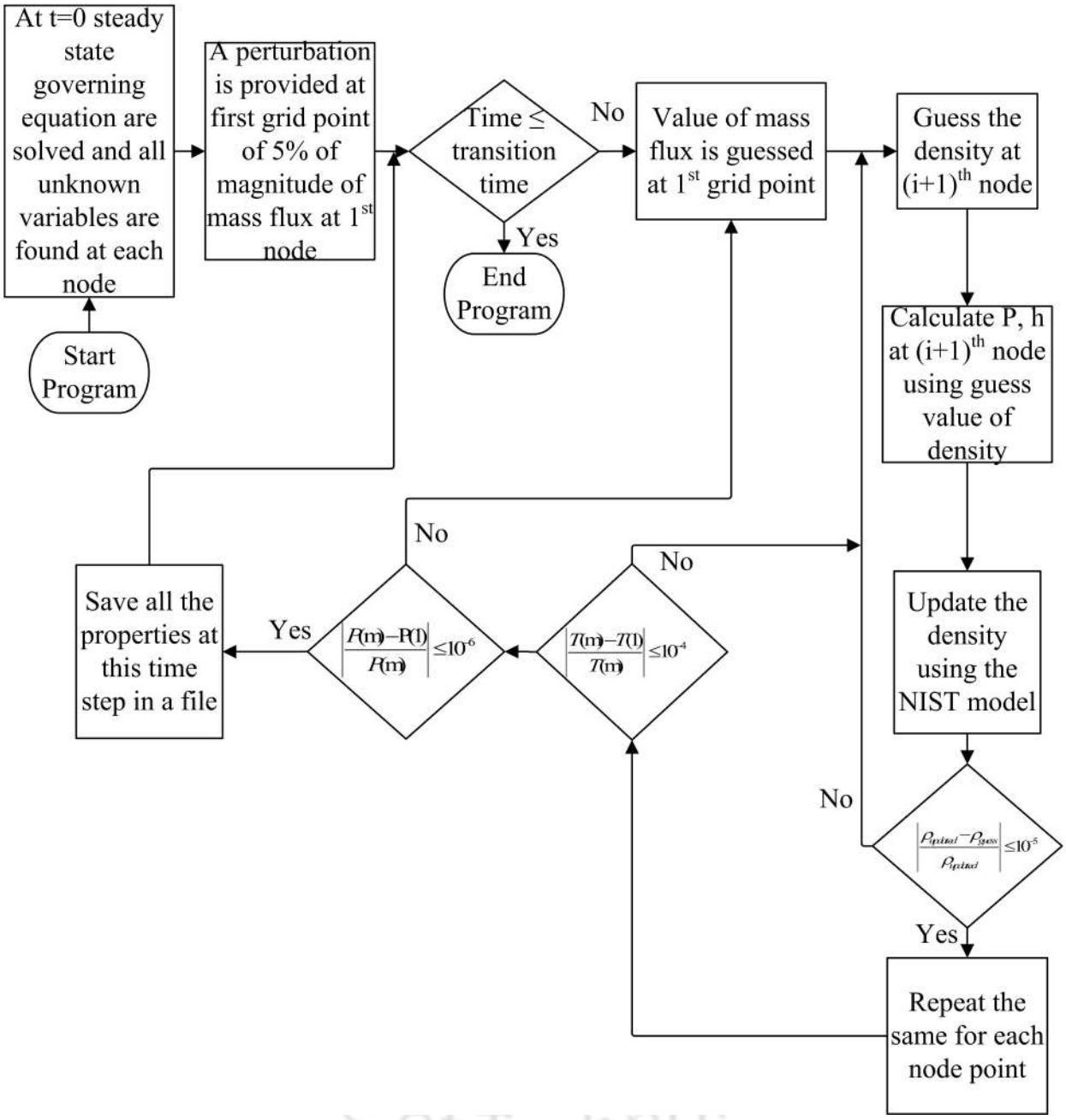

Fig. 3.5: Flow chart for the solutions of time-dependent conservation equations

experimental facility, particularly taking the dearth of test data on closed sNCL into consideration. Therefore, the predicted steady-state values are compared with the experimental correlation proposed by Swapnalee et al.[104] and the same is graphically presented on a $Re_{ss} - Gr_m$ plane in Fig. 3.6(a) for $p = 8$ to 9 MPa, $T_\infty = 285$ to 295 K and $\dot{q} = 50$ to 2000

W. Here the characterizing dimensionless groups are defined as,

$$Re_{ss} = \frac{G_{ss} d}{\mu} \qquad Gr_m = \frac{g\beta d^3 \rho^2 \dot{q} H}{A\mu^3 c_p} \tag{3.4}$$

with all the relevant thermophysical properties being calculated using pressure and temperature at the heater center. Excellent degree of conformity can be observed over the entire parametric range explored here, securing confidence about the 1D framework. This particular correlation was developed for a closed sNCL with both supercritical water and sCO_2 as the working fluids, and was also tested for each of the four possible combinations of heater-cooler orientation. It was also able to replicate the observations from several other facilities reported in literature, encompassing sCO_2 and two synthetic refrigerants, thereby substantiating its capability. It has found successful applications in literature in the recent years, thereby further endorsing the claim of it being a generalized flow correlation for any sNCL, and hence has been adopted in the present study.

Similar kind of direct comparison, however, cannot be facilitated with the transient predictions. The trend of temporal evaluation depends on the adopted time step, as well as the associated truncation error and level of numerical diffusion involved, making it unfeasible to have any one-to-one correspondence. Hence, an attempt is made here by drawing qualitative analogy with the results reported by Sharma et al.[111] in Fig. 3.6(b) at $p = 9.1$ MPa and $\dot{q} = 800$ W. A separate computational domain has been created for that purpose, adhering to the dimensions of the concerned facility and identical set of boundary conditions. While there is notable differences in the mass flow rate and time required for flow reversal, similarity is associated dynamics is quite palpable. The difference in the incorporated model for predicting local friction can possibly be a prime reason behind the quantitative disparity. Present model estimates slightly lower value of f_d, resulting in about 25% higher G_{ss} and a delayed flow reversal. The relations used for estimating local values of dynamic viscosity and thermal conductivity also influence the magnitudes quite significantly. Still, present code is able to correctly reproduce the unstable nature of the concerned system, along with near-identical temperature levels throughout. The periods of oscillations are also remarkably similar, having magnitudes of about 17.35 s from literature and 16.75 s in the present work, which can definitely be treated as an indirect testimony regarding the ability of the present framework in reproducing dynamics of sNCL.

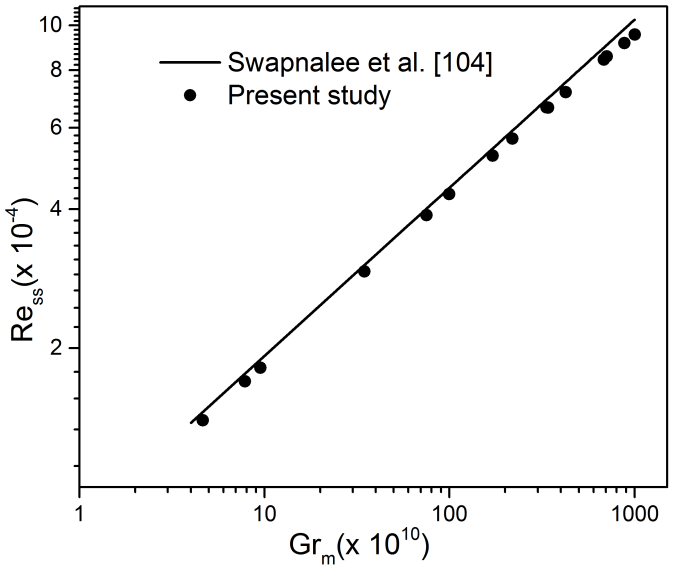

(a) Steady-state comparison with the experimental correlation of Swapnalee et al.[104]

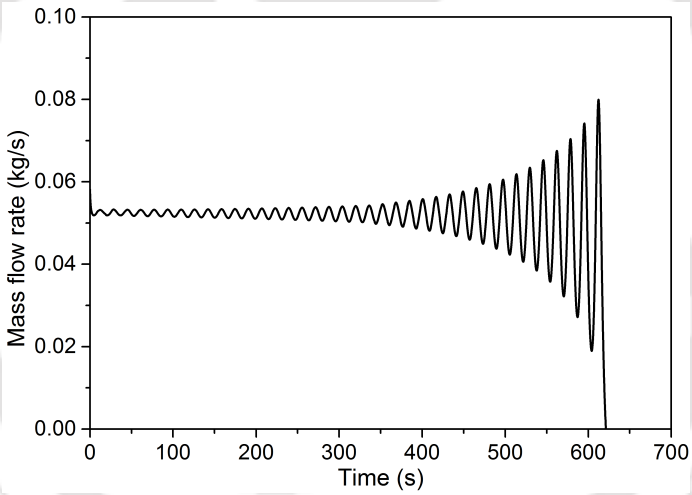

(b) Temporal evolution of the mass flow rate with the geometry of Sharma et al.[111] at $\dot{q}$ = 800 W

Fig. 3.6: Comparison of the steady-state and transient predictions with literature

3.3 Review of the Steady-State Behavior

The operation of any NCL under steady-state is governed by the interaction between buoyancy and friction, as can be substantiated from Eq. 3.1(b). On integration over the entire flow path, after eliminating the time derivative, it leads to a simple balance involving these two forces only. Therefore, any geometric or operating parameter capable of manipulating

either or both of these two forces can influence the steady-state characteristics. As deliberated in detail by Srivastava et al.[153] through their 3D computational model, it is possible to identify four distinct regimes of operation of sNCL, following the variation in mass flux (G) with change in heater power ($\dot{q}$). The regime of enhanced heat transfer is separated from the deteriorated heat transfer regime by a shallow transition zone. As per their inference, the appearance of any specific regime is reliant on the temperature level of the loop fluid. If sCO_2 is allowed to cross T_{pc} within the heater/cooler, strong buoyancy field is developed, allowing large flow rate and enhanced heat transfer. The deteriorated heat transfer regime, on the contrary, appears when the fluid temperature is greater than T_{pc} throughout the flow path. The same observation is possible with the present 1D numerical framework as well, as is illustrated in Fig. 3.7. Consistent rise in the flow rate can be observed over both the low-power regime and enhanced heat transfer regime. This is in accordance to the near-linear profile of density differential ($\Delta\rho$) between the to vertical arms, which is a direct representative of the driving buoyancy force. Moderate reduction in the flow rate with change in $\dot{q}$ can be observed over the transition regime, as the highest fluid temperature hovers around T_{pc}. It is interesting to note that the initiation of the deterioration in mass flow rate coincides with the maxima in $\Delta\rho$. Sarkar and Basu[134] coined the term *Flow-induced heat transfer deterioration* (FiHTD) to distinguish this phenomenon from its forced-flow counterpart and also to emphasize on the correspondence between flow rate and heat transfer coefficient in sNCL. FiHTD appears around $\dot{q}$ = 2900 W for the selected conditions of p = 8 MPa and T_{∞} = 285 K. The rapid decline in both $\dot{m}$ and $\Delta\rho$ during FiHTD is followed by the so-called *gas-like* operation in the deteriorated heat transfer regime, which is also characterized by high temperature levels of sCO_2. No effort can be found in literature to relate the appearance of FiHTD with stability response and that contrives one of the major focus of the present study.

It, however, needs to be noted here that the predictions from a 1D code can have some quantitative bias, with a possible tendency of over-predicting limiting power values. Presence of substantial radial asymmetry in sNCL has been reported in literature through multidimensional modeling [134, 153], which can contribute toward local recirculation and crosswise heat transfer, subsequently affecting the overall thermalhydraulics. The qualitative nature of the phenomenon, however, essentially remains the same, thereby allowing stability appraisal with confidence in the predicted trends.

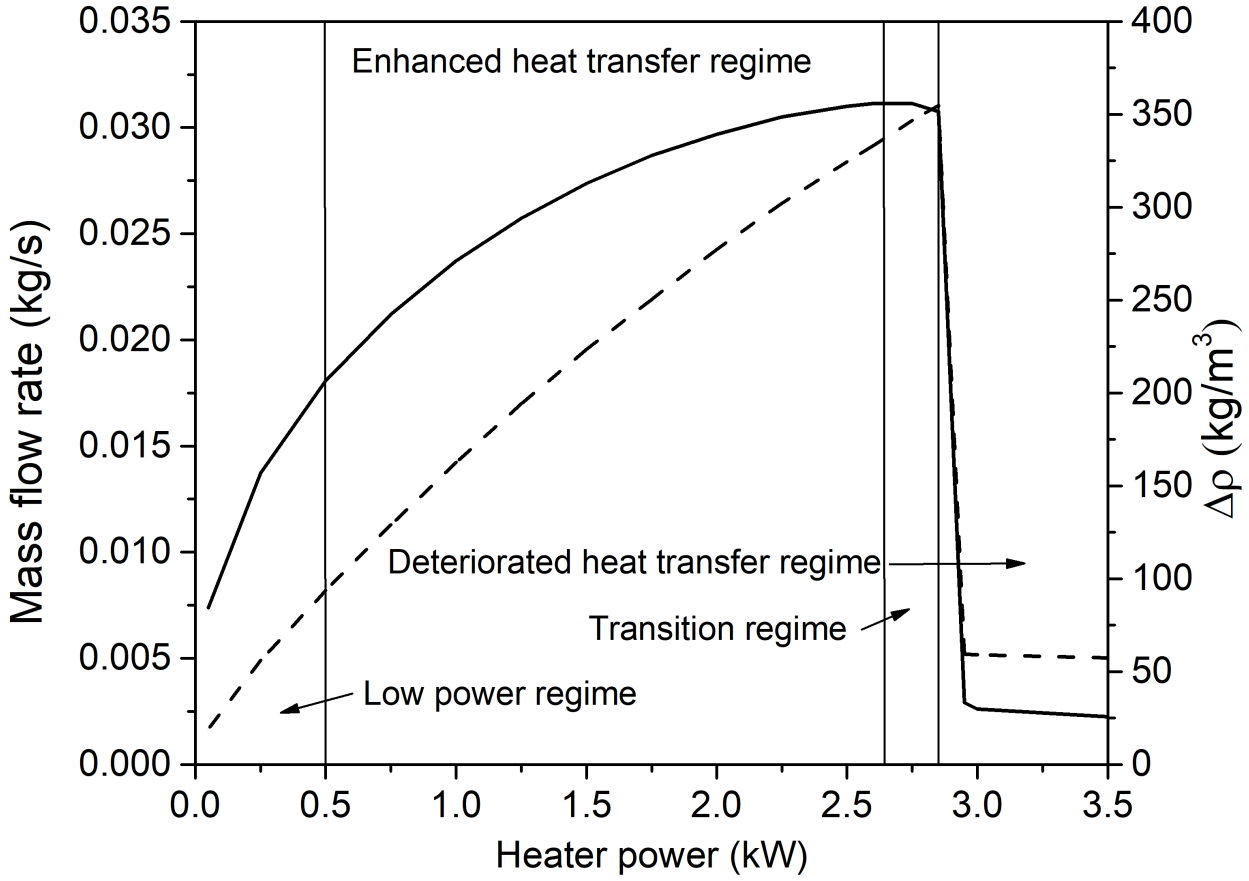

Fig. 3.7: Variation in steady-state mass flow rate ($\dot{m}$) (continuous line) and density differential ($\Delta\rho$) between the vertical arms (dashed line) with heater power ($\dot{q}$) at $p = 8$ MPa and $T_\infty = 285$ K, demonstrating the appearance of different regimes of heat transfer

3.4 Appearance of Static Instability

The steady-state profile of mass flow rate presented in Fig. 3.7 is not an unique one. As mentioned earlier in section 3.2.3, an iterative procedure is necessary to arrive at the steady-state solution, owing to the strong coupling between the momentum and thermal fields. Depending on the choice of the initial guess, it is occasionally possible to have multiple solutions of the associated system of equations (Eq. 3.1(a-c)). With any specific set of boundary conditions, a lower presumption about G_{ss} will induce a larger change in fluid enthalpy across the heater, which is likely to yield high temperature of sCO_2 at heater outlet. The thermal conductivity of any supercritical fluid being considerably low beyond T_{pc}, the resultant heat transfer coefficient on the cooler-side (U) is also expected to be low. Therefore, the external coolant stream may not always be able to extract the entire of the

imparted heater power from the fluid stream, owing to its weakened thermal communication with the circulating fluid, leading to an elevated temperature level at heater inlet. That can cause further rise in the temperature of sCO_2 in riser, culminating in higher overall temperature level of the fluid at the eventual steady-state and appearance of FiHTD-type scenario at noticeably low power levels. A higher guess of G_{ss}, on the contrary, compensates for the reduction in thermal conductivity with enhanced level of Re during the estimation of U, thereby ensuring sufficient rate of energy removal by the coolant. As a result, sCO_2 can maintain a reasonably low level of temperature during its approach to the heater and continue to operate within the enhanced heat transfer regime till substantially high $\dot{q}$, similar to the trend observed in Fig. 3.7. Accordingly, a sNCL can conceive multiple steady-state solutions and the same is illustrated in Fig. 3.8 for the loop under consideration. Subjected to the selection of the initial guess, FiHTD can theoretically be realized either around $\dot{q} =$ 870 W or 2900 W, and the system can produce either of the two possible steady-states over a large range of heater power. A demonstration is provided in table 3.1 for $\dot{q} = 1750$ W. Large disparity in both mass flow rate ($\dot{m}$) and density differential between the vertical arms ($\Delta\rho$) can be noted. The loop with the higher circulation rate operates within the enhanced heat transfer regime, substantiated by the magnitudes of the maximum and minimum fluid temperatures, with the greater one lying very close to T_{pc} and the other well below. The lowest fluid temperature in the other loop, however, is well above T_{pc}, compelling it to function in the regime of deteriorated heat transfer. Here, the average heat transfer coefficient within the cooler (U_{av}) has been estimated by integrating over the entire length of the same and substantial disagreement between them is again palpable.

Table 3.1: Multiple steady-state solutions at $\dot{q} = 1750$ W, $p = 8$ MPa and $T_\infty = 285$ K

$\dot{\mathbf{m}}$ (kg/s)	$\mathbf{T_{max}}$ (K)	$\mathbf{T_{min}}$ (K)	$\boldsymbol{\Delta\rho}$ (kg/m^3)	$\mathbf{U_{av}}$ (W/m^{2}K)
0.00442	741.58	402.83	65.60	355.94
0.02868	307.61	300.79	253.24	4344.93

The above discussion, however, is valid only for the intermediate power levels. For $\dot{q} <$ 870 W with $T_\infty = 285$ K, the energy acquired by the fluid stream within the heater is not sufficient enough to raise the minimum temperature past T_{pc}, regardless of the guessed G_{ss} during iterations. Accordingly, only a single steady-state solution is possible. Such scenario is associated with the low-power regime and also with the early parts of the enhanced heat transfer regime. At very high power levels ($\dot{q} > 2875$ W), again a single solution can be

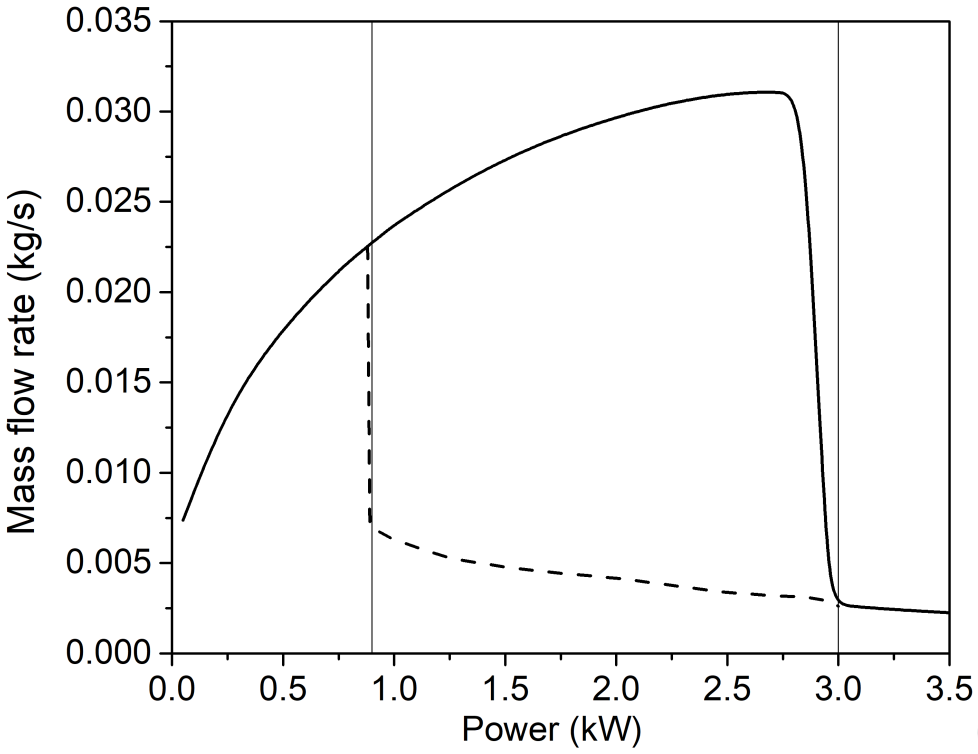

Fig. 3.8: Multiple profiles of steady-state mass flow rate ($\dot{m}$) with heater power ($\dot{q}$) at p = 8 MPa and T_∞ = 285 K, demonstrating the appearance of static instability

obtained, allowing operation only with deteriorated heat transfer rate. Any change in sink temperature can noticeably modify the span of $\dot{q}$ corresponding to such multiple solutions. As explained by Sarkar and Basu[134], rise in sink temperature lowers the power level allied with FiHTD, because of the augmentation in overall temperature level within the loop. sCO_2 is more prone to retain a temperature greater than the pseudocritical value, enforcing an early switch to the deteriorated heat transfer regime at considerably lower $\dot{q}$. That, however, also lessens the mathematical probability of yielding multiple solutions, as can be substantiated following Fig. 3.9 for T_∞ = 295 K and 305 K. Power levels pertaining to both the deterioration reduce quite radically, while the spans of multiple solutions also get drastically constricted. At T_∞ = 305 K, multiple steady-states are possible only over about 100 W expanse of $\dot{q}$. When the coolant temperature is increased beyond T_{pc}, consistently a single steady-state can be realized, albeit at the cost of low circulation rate and inferior heat transfer performance.

Following the systematic classification of thermalhydraulic instabilities in NCLs by Boure et al.[14], the appearance of multiple steady-states within an intermediate band of heater

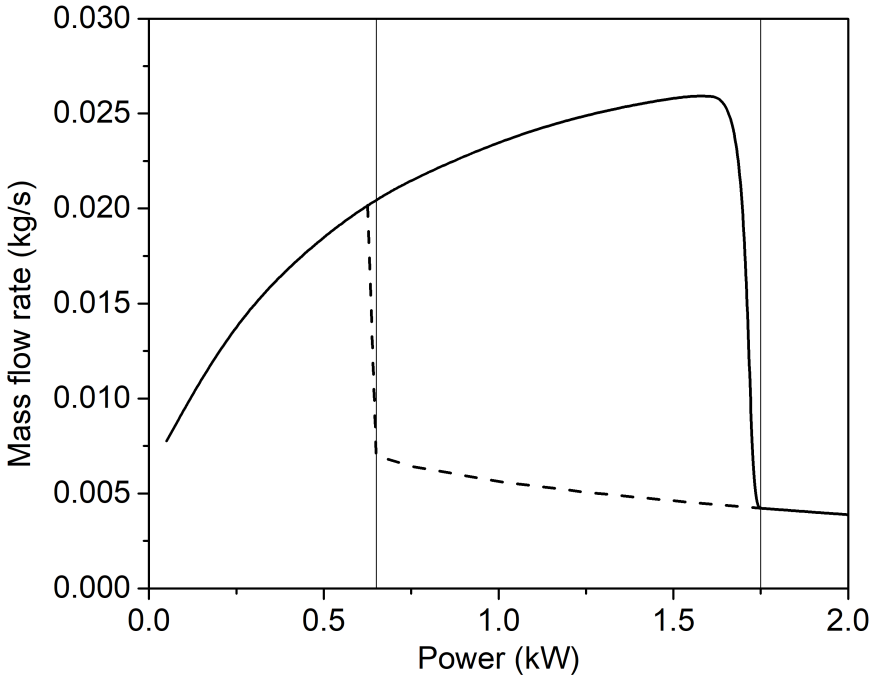

(a) $T_\infty = 295$ K

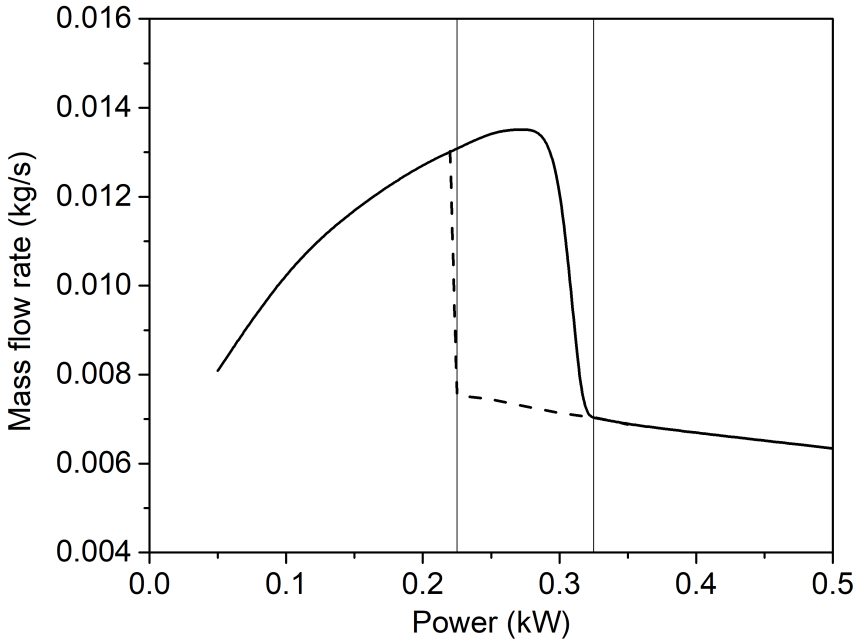

(b) $T_\infty = 305$ K

Fig. 3.9: Multiple steady-state profiles for mass flow rate ($\dot{m}$) with heater power ($\dot{q}$) at p = 8 MPa and two different coolant temperatures

power can be designated as the well-known Ledinegg instability [154]. It is a type of fundamental static instability, which theoretically is feasible when the internal characteristic curve has a negative slope and is also steeper than the external one. In regard to the present system, possibility of Ledinegg instability appears within the domain of operation for which $\frac{\partial \Delta p}{\partial \dot{m}} < 0$, which is very much feasible in an sNCL owing to the rapid decline in density and viscosity around T_{pc}. The variations in total pressure drop over the rectangular flow path with the guessed mass flow rates are presented in Fig. 3.10 for three different power levels. It is clearly evident that only a solitary solution is possible with both $\dot{q} = 750$ W and 3000 W, as the pressure drop around a closed path must be equal to zero. That, however, is not applicable for $\dot{q} = 1750$ W, which can mathematically conceive three different steady-states. The intermediate one, though, is in unstable equilibrium, owing to the negative slope. Any minor change in the operating condition will drive the system to either of the other two solutions, both of which are in stable static equilibrium because of the positive slope of the characteristic curve in their respective neighborhood. Relating this observation with Fig. 3.8, it can be noted that $\dot{q} = 1750$ W is appertained with the *so-called* intermediate power range, experiencing static instability, whereas the other two choices are outside that zone. Any attempt of solving the steady-state equations at $\dot{q} = 1750$ W with some guessed mass flow rate can converge toward either of the two stable equilibrium, depending on the associated direction of propagation of the numerical errors. The same is pertinent for any $\dot{q}$ over the entire zone of static instability.

Ledinegg instability is a common occurrence in boiling NCLs and is, therefore, a well-explored topic [16, 155]. There is, however, very little discussion about the same in relation with sNCLs and closed loop in particular. First numerical attempt to find Ledinegg instability in sNCL can be credited to Yu et al.[132], who, however, failed to observe any. Ledinegg instability was recently identified for an open loop by Rai et al.[156], using an approach similar to the present work, facilitating a comparison between the pressure drop across the cold leg and in the remainder of the loop.

Only similar effort for closed sNCL can be credited to [104], who failed to identify multiple steady-states in sCO_2-driven sNCL despite covering a wide range of pressures, possibly as a consequence of the simplistic property relations employed in their model. This emphasizes the novelty of the present study, which successfully envisages static instability in a closed sNCL with sCO_2 as the working medium.

The zone of the Ledinegg instability observed here is bounded within the two power levels corresponding to FiHTD, and is associated mostly with the enhanced heat transfer regime.

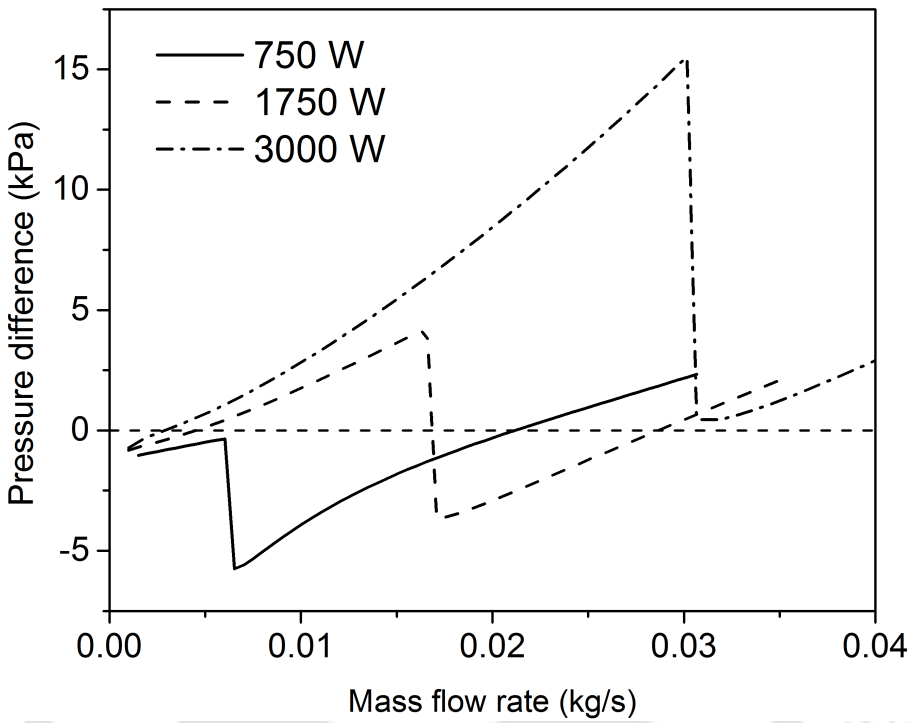

Fig. 3.10: Variation in pressure drop (Δp) over the entire flow path with imposed mass flow rate ($\dot{m}$) for three different power levels, with $p = 8$ MPa and $T_\infty = 285$ K; multiple solution is possible for $\dot{q} = 1750$ W

An increase in the sink temperature (T_∞) considerably narrows the embedded region, albeit with the increased probability of encountering FiHTD at lower power levels. In order to aid generalization, a non-dimensional perspective can be devised by defining the following two dimensionless groups.

$$N_{TPC} = \frac{\dot{q}}{\dot{m}} \frac{\beta_{pc}}{c_{p,pc}} \qquad N_{SPC} = -\left(h_{in} - h_{pc}\right) \frac{\beta_{pc}}{c_{p,pc}} \tag{3.5}$$

Here, h_{in} is the fluid enthalpy at the inlet plane of the heater and all the other thermodynamic properties refer to the pseudocritical point at the operating pressure. The trans-pseudocritical number (N_{TPC}) quantifies the power-to-flow-ratio, whereas the sub-pseudocritical number (N_{SPC}) is a representative of the lowest fluid enthalpy. After encountering FiHTD, the diminished circulation rate generally results in fluid temperature level well above T_{pc} throughout the circuit, yielding negative value of N_{SPC}. Therefore, over the entire zone of static instability, the obtained stable solutions lie on either side of the N_{SPC} spectrum, with one positive and the other negative. Corresponding N_{TPC} values are also

substantially different, owing to the considerable difference in their respective flow rates. The heater power level associated with the threshold of the Ledinegg instability can be identified to form the marginal stability boundary (MSB) and two such points can be obtained for every T_∞. All such MSBs can be joined to form a map of static instability and two such plots are presented in Fig. 3.11. It is clearly evident that any reduction in T_∞ promotes the Ledinegg instability, with enhanced probability of obtaining multiple steady-states. It is possible to generalize such a map by considering variation in geometry and other operating parameters. But that is beyond the scope of the present study and hence is not persuaded with.

3.5 Appearance of Dynamic Instability

Dynamic instability is associated with the feedback effect originating within the system because of the dynamic interactions among the flow variables over time. Any disturbance created at some location of a sNCL is expected to affect all the relevant forces, namely, inertia, friction and buoyancy, thereby upsetting the static balance within the loop. Subsequent changes in the circulation rate and temperature profile over the entire flow domain can affect the very source of the disturbance itself, albeit with a temporal delay corresponding to the time required for the information about the disturbance to travel the loop. The dynamic instability emanates from such delayed feedback effect, with the nature of system response depending on the transient evolution of the initial disturbance. It can computationally be recognized only from the time-dependent simulations. Therefore, as mentioned earlier, simulations have been performed over sufficiently long duration after perturbing the steady-state flow rate by 5%, without any alteration in the boundary conditions, and conclusions have been drawn from the consequent data analyses.

Variations in the normalized mass flow rate ($\overline{m}$) at three different power levels are presented in Fig. 3.12. Here the instantaneous flow rate is normalized by dividing that with the corresponding steady-state value ($\overline{m}\,(t) = \dot{m}\,(t)\,/\dot{m}_{ss}$). The immediate effect of introducing the perturbation in flow rate is a reduction in the enthalpy gained by the fluid within the heater. The highest fluid temperature will, subsequently, be slightly lower during the next run, marginally increasing both the lowest density and viscosity level. Consequently, the buoyancy and frictional fields will be simultaneously revised, affecting the balance established during the steady-state, and the system will experience flow oscillations in an effort to regain the equilibrium. The nature of stability response will be governed by the dominat-

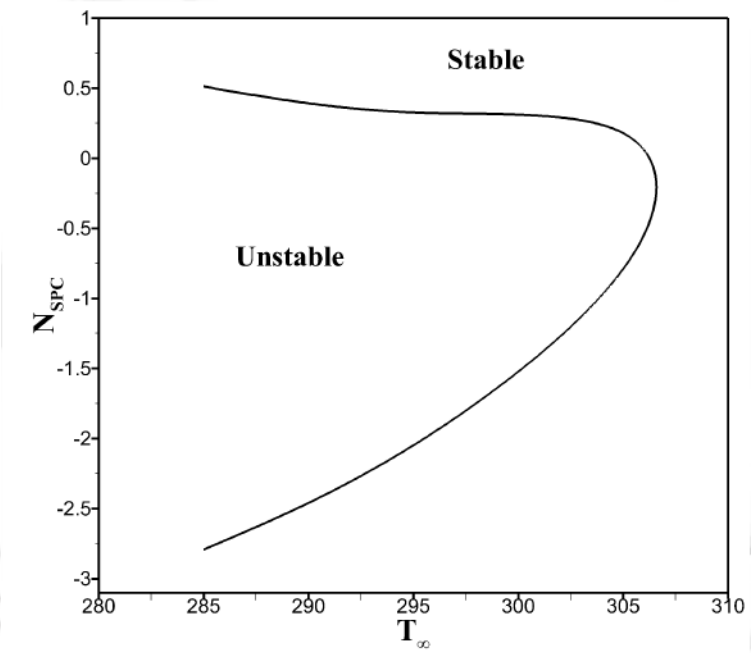

(a) $N_{SPC} - T_\infty$ plane

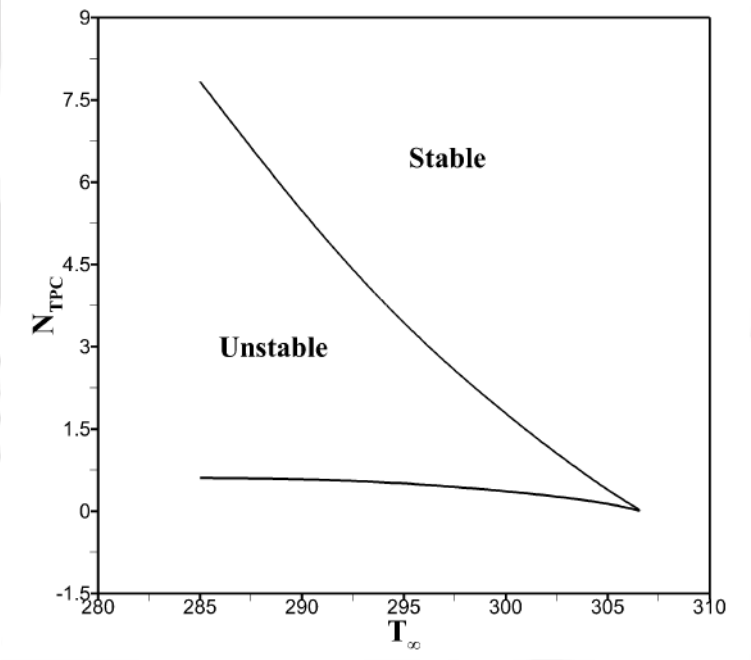

(b) $N_{TPC} - T_\infty$ plane

Fig. 3.11: Locus of MSBs corresponding to the Ledinegg instability on two different planes, clearly demonstrating the unstable zone embedded within the stable zones

ing one. Friction being the restraining influence, it will attempt to subside the fluctuations, whereas buoyancy is the driving force and reinforces the vacillation, thereby promoting instability. Therefore, the overall response will be stable if the introductory perturbation causes greater enhancement in friction compared to buoyancy, and unstable otherwise. As can be seen here, for $\dot{q}$ = 2240 W or lower, after a period of initial development, the oscillations in $\overline{m}$ gradually diminishes with time, implying a stable loop. On the contrary, $\dot{q}$ = 2325 W or higher instill continuous growth in the flow fluctuation, which is the characteristic of an unstable system. The same inferences can also be drawn following the adjacent phase portraits. The attractor intends to converge to a single point with time for $\dot{q}$ = 2240 W, as is illustrated by the trajectory adhering to a series of circles with steadily diminishing diameters, which is the characteristic of a stable system [157]. The trajectory for $\dot{q}$ = 2325 W, however, follows a diverging trend, demonstrated by the continuous gain in the diameter of the successive circles. The temporal evolution in the corresponding buoyancy fields can be estimated following the changes in $\Delta\rho$ with time from Fig. 3.13. While the density differential gradually reduces for $\dot{q}$ = 2240 W, it continually rises for the other case, substantiating the consistent rise in the dominance of buoyancy. A closed orbit is produced at $\dot{q}$ = 2300 W, signifying a neutrally stable system, which can be viewed as the point of transition toward instability with rise in heater power. Changes in the buoyancy and frictional forces are of the same order here, with each dominating periodically, leading to a sustained oscillation, and that is clearly visible from Fig. 3.12(b).

Once the heater power crosses the FiHTD-limit, the dynamics of the loop is dominated primarily by the frictional force. The viscosity of the fluid is low throughout the flow path, as the temperature is greater than T_{pc}, lowering the net magnitude of the flow resistance. The density differential ($\Delta\rho$), however, is also very low due to the *gas-like* nature of sCO_2 throughout. Hence, the resultant buoyancy force is very weak, resembling more like single-phase liquid loops. The domination of friction is expected to stabilize the system beyond FiHTD and the same can be established from Fig. 3.14. The loop exhibits unstable fluctuations till a power level of 2875 W and reverts back to the stable condition with only minor rise in the heater power at $\dot{q}$ = 2900 W. Further rise in the power input results in prompt suppression of any disturbances, accordingly maintaining the stable nature of concerned sNCL. In fact, hardly any oscillations can be observed for $\dot{q}$ = 2900 W or beyond, emphasizing strong dominance of friction. Therefore, the zone of dynamic instability, quite similar to its static counterpart, is limited to an intermediate band of heater power for T_∞ = 285 K. The limiting magnitudes, though, are noticeably different and a comparison on

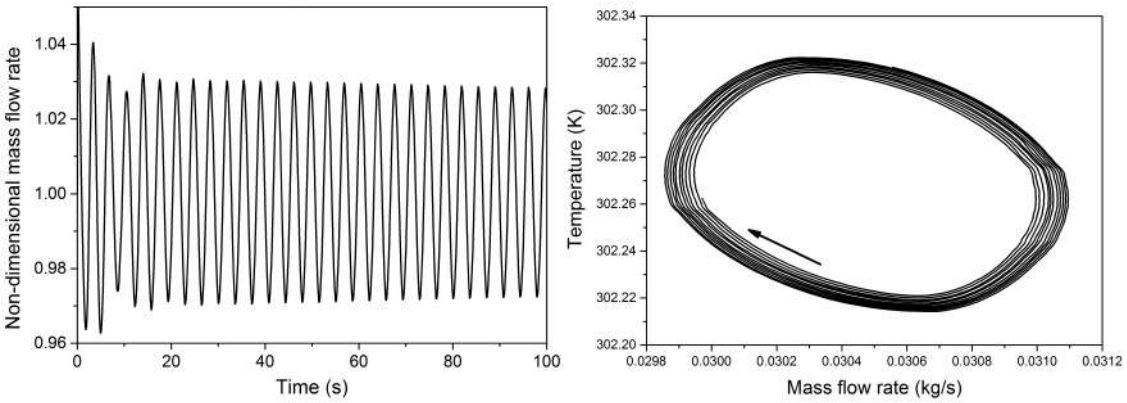

(a) $\dot{q} = 2240$ W (stable)

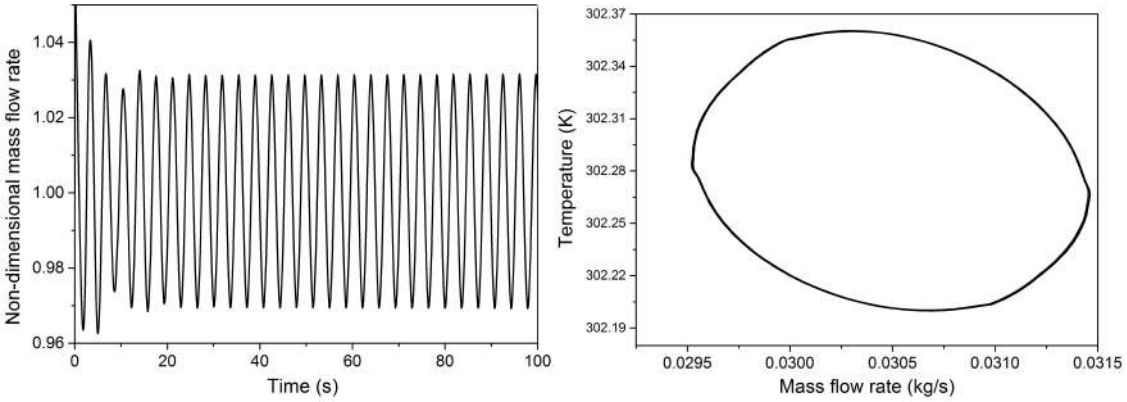

(b) $\dot{q} = 2300$ W (neutrally stable)

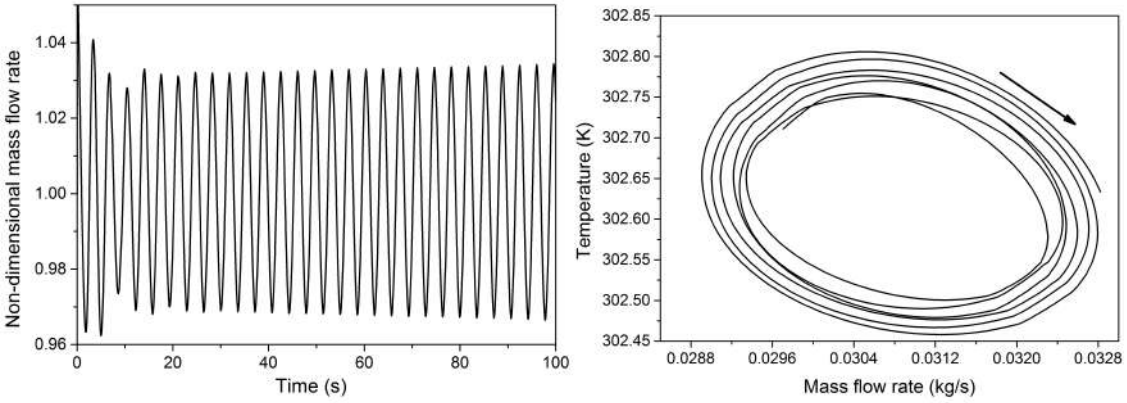

(c) $\dot{q} = 2325$ W (unstable)

Fig. 3.12: Temporal variations in normalized flow rate ($\overline{m}$) (left) and corresponding phase portraits (right) at three different powers with $p = 8$ MPa and $T_\infty = 285$ K, demonstrating different stability responses of sNCL

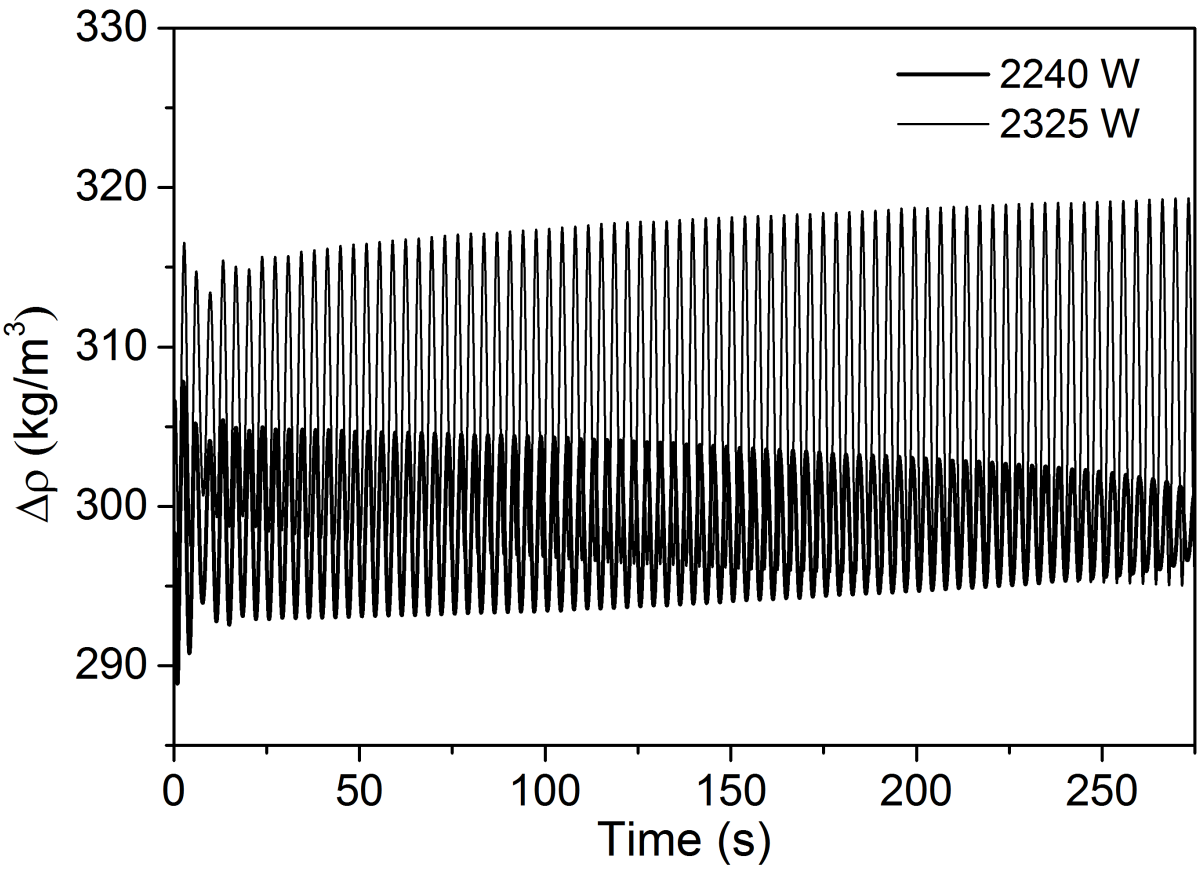

Fig. 3.13: Temporal variations in density differential ($\Delta\rho$) between the vertical arms for two different power levels, with $p = 8$ MPa and $T_\infty = 285$ K

that is facilitated below.

The amplitude of the unstable oscillations can be quite substantial for power values bounded by these two limits, and can even lead to occasional reversal in the flow direction. Sustained growth in fluctuations in the circulation rate also induce oscillations in the magnitudes of the maximum and minimum fluid temperatures within the loop at any instant of time. If the lowest temperature level is able to momentarily cross T_{pc}, that inflicts a considerable change in the driving potential, and the loop is subjected to enhanced degree of fluctuations. Present geometric configuration being symmetric (Fig. 2.1), circulation is equally probable to happen in either direction. Therefore, such instantaneous decline in buoyancy hinders the movement of the fluid in the original direction and incites motion in the opposite direction, which can be explained following the well-celebrated theory of [26] about the emergence of instabilities. The system can experience rapid upsurge in the tem-

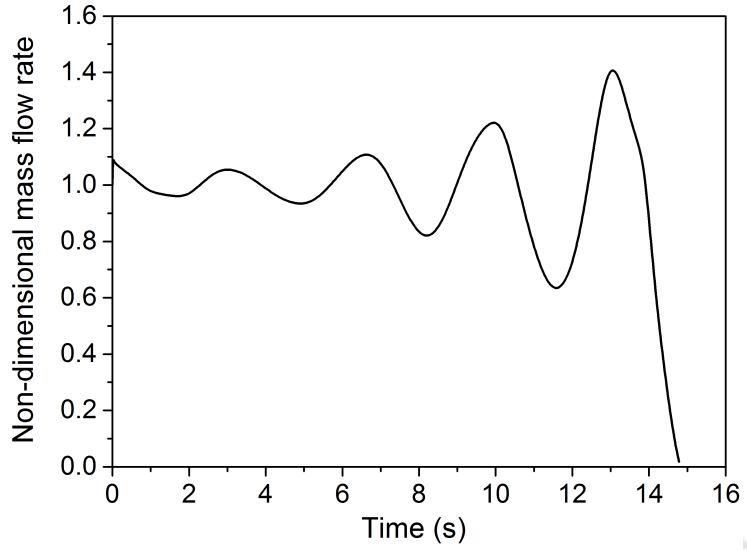

(a) $\dot{q}$ = 2875 W (unstable)

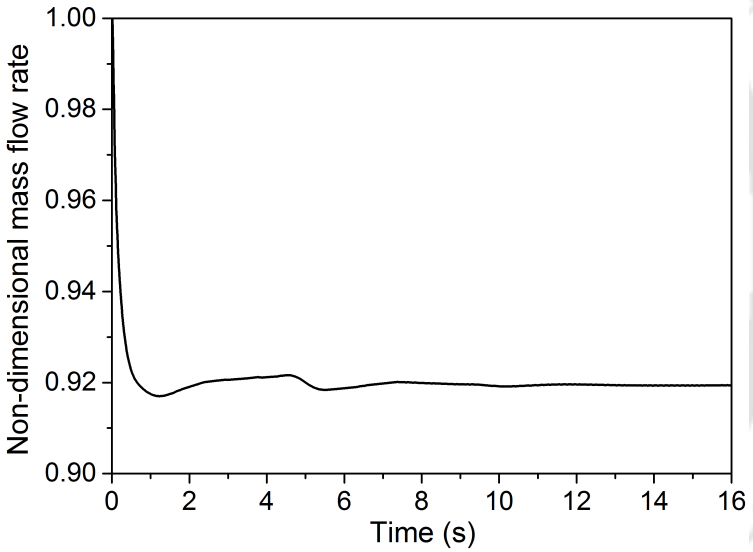

(b) $\dot{q}$ = 2900 W (stable)

Fig. 3.14: Temporal variations in normalized flow rate ($\overline{m}$) at two different power levels with p = 8 MPa and T_∞ = 285 K, demonstrating unstable-to-stable transition at higher powers

perature at heater outlet, as can be seen from Fig. 3.15, suggesting immediate degradation to low flow rates. It is, in fact, possible to attain flow reversal with any power level within the unstable zone, but with difference in the amount of time required to arrive there. The dynamics subsequent to the flow reversal is beyond the scope of the present study and hence is not explored further.

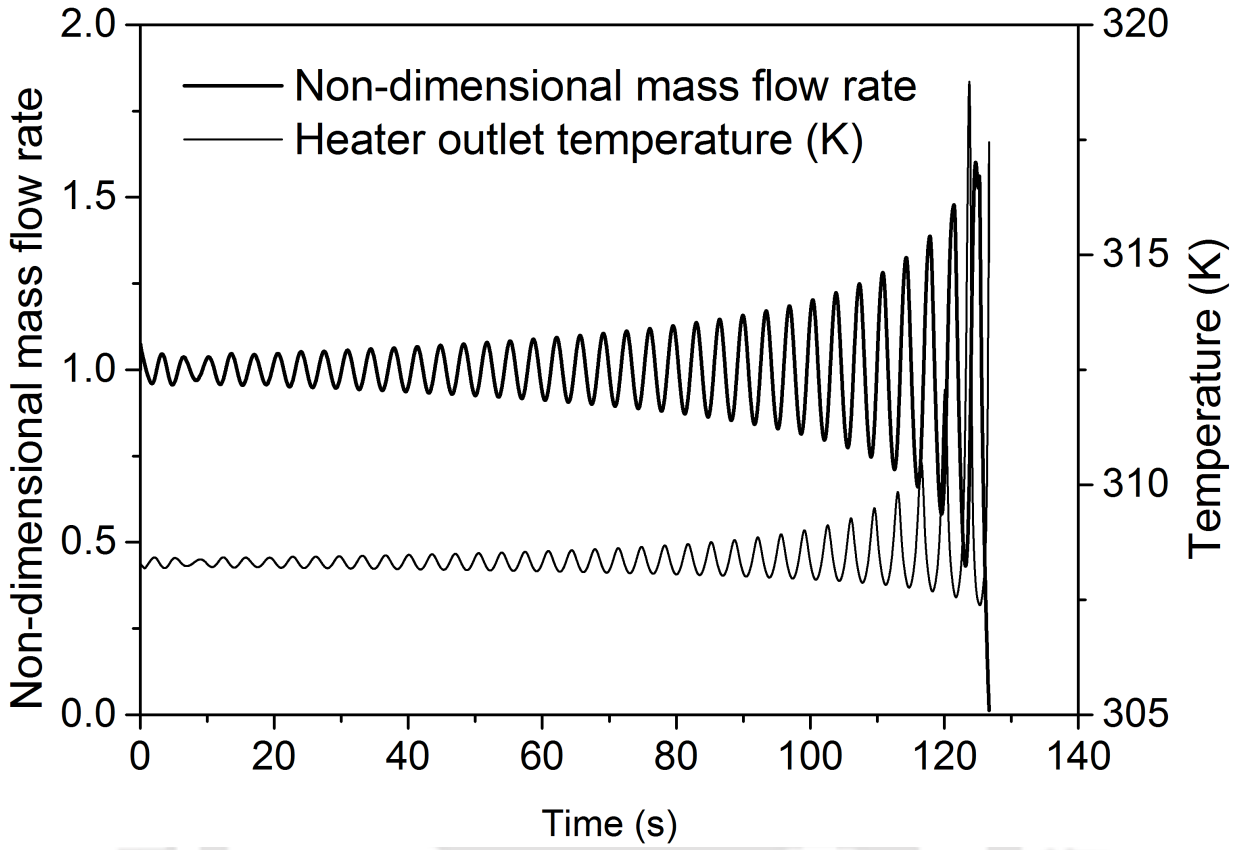

Fig. 3.15: Demonstration of reversal in flow direction at $\dot{q} = 2400$ W, accompanied by sharp increase in the fluid temperature

It is pertinent here to expedite a comparison between the maps of static and dynamic stability on the relevant dimensionless planes and the same can be found in Fig. 3.16. Despite appreciable difference in the associated dimensional values of the limiting powers, the maps exhibit amicable coherence in both the planes, particularly regarding the upper threshold. Such stability maps can, therefore, really help in adjudicating the safe region of stable operation, while also drawing a relation with FiHTD under steady-state.

It needs to be noted here that the perturbation has been imposed on the stead-state solution corresponding to the higher flow rate for each of the above cases, as the concerned power values fall within the zone of static instability. Steady-states characterized by the lower circulation rates are invariably stable, owing to the stronger frictional influence and noticeably weak density differential, which promptly suppresses any oscillations. Any geometric and operating variable capable of modulating either or both of these two forces can affect the stability response. The respective impacts of the operating pressure (p), sink temperature

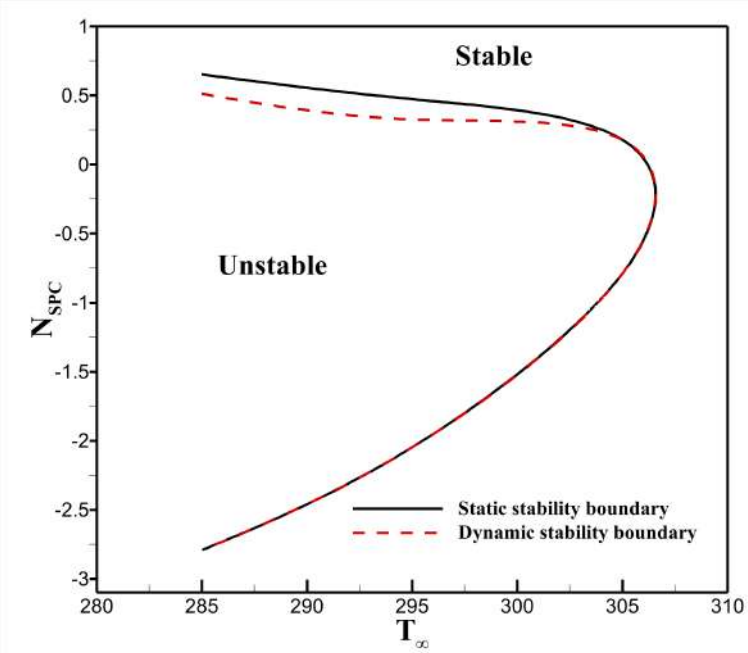

(a) $N_{SPC} - T_\infty$ plane

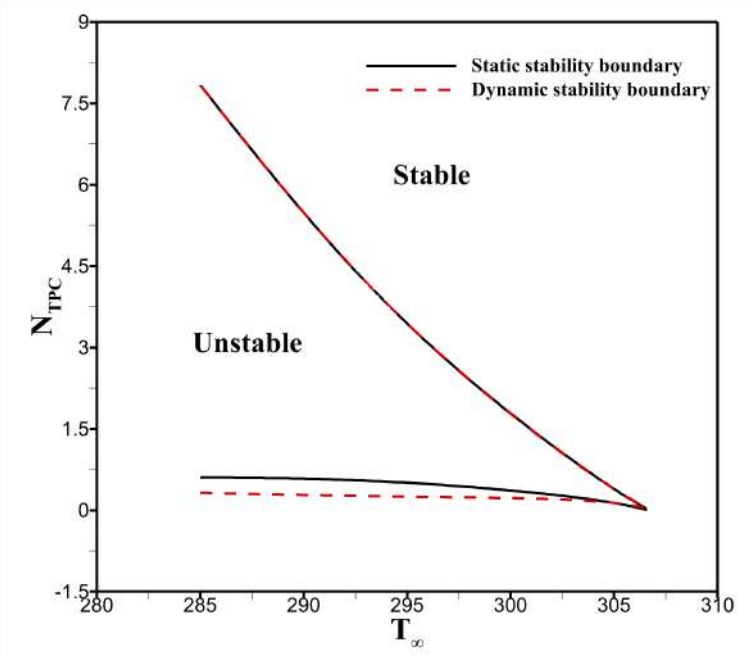

(b) $N_{TPC} - T_\infty$ plane

Fig. 3.16: Comparisons of the maps of static and dynamic stability on two different planes

(T_∞), loop height (H) and pipe diameter (d) are systematically explored in the subsequent sections, to envisage their individual contribution on the dynamic stability response.

3.5.1 Effect of operating pressure (p) and sink temperature (T_∞)

Drastic variation in the thermophysical properties of any supercritical fluid is most prominent around p_c and is increasingly less pronounced with rise in the pressure level. Accordingly, the order of $\Delta\rho$ even within the enhanced heat transfer regime is noticeably low at higher system pressures, consequently weakening the buoyancy force. Increase in the system pressure, therefore, raises the power level corresponding to FiHTD for any specific sink temperature [134], accompanied by subsequent shifting in the upper limit of the stability threshold. The loci of the stability threshold at three different pressure levels and over a reasonably wide range of sink temperature are presented in Fig. 3.17, with $\dot{q}$ as the primary control variable. At any specific pressure level, the lower and upper points of neutral stability are separated by a bigger difference at lower T_∞. As already discussed, rise in T_∞ enhances the overall temperature level of sCO_2 within the loop. The lowest temperature is more likely to be closer to T_{pc} in the pre-FiHTD region, weakening buoyancy and favoring friction-dominated operation. Therefore, both the stability thresholds converge toward each other with increase in T_∞ and no instability can be observed with $T_\infty > T_{pc}$.

At higher coolant temperatures, immediate effect of enhancement in system pressure is to suppress the domination of buoyancy, thereby shifting the unstable zone of operation to higher powers. Minor widening of the sandwiched unstable zone can also be observed, which can be attributed to the change in the level of dynamic viscosity with pressure. T_{pc} being a sole function of pressure, the highest level of T_∞ corresponding to unstable oscillations also drifts upward concurrent to pressure itself.

3.5.2 Effect of loop height (H)

Buoyancy is the sole driving force in any NCL and it is a direct function of the vertical distance associated with the density differential $\Delta\rho$. Increase in the height of the loop, therefore, augments the buoyancy field. That, however, also extends the total flow path available to the circulating fluid, leading to greater frictional losses. Hence, the impact of loop height on system stability will depend on the intensification in the net propelling force and can be ascertained from Fig. 3.18. Greater level of friction lowers the circulation rate, accordingly increasing the overall level of fluid temperature and lessening the power level corresponding to FiHTD. Reduction in height to 800 mm seems to encourage friction-dominated operation, as is demonstrated by the appearance of the both the stability thresholds at relatively lesser $\dot{q}$. The span of power associated with instability is also sufficiently wider with $H = 800$ mm, particularly apparent at the lower levels of T_∞, which can be viewed as a consequence of

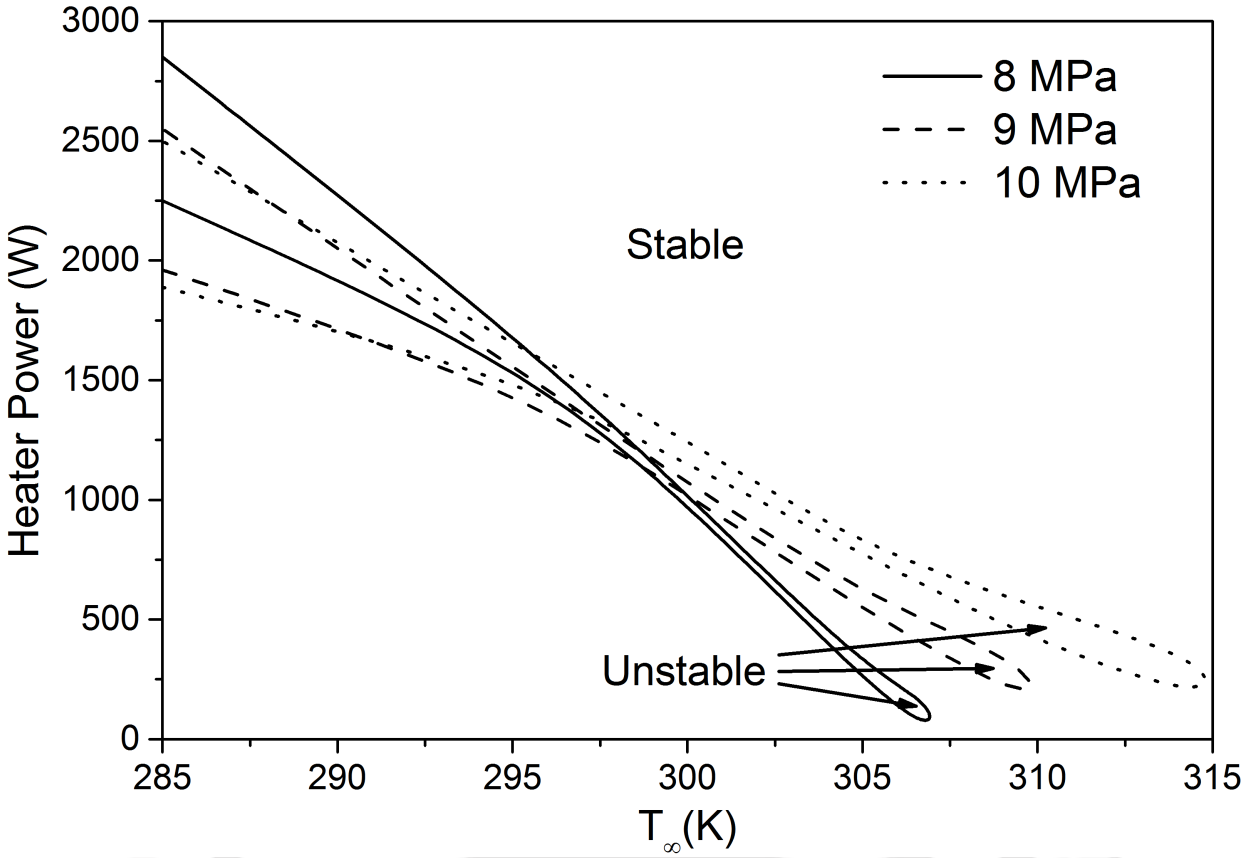

Fig. 3.17: Combined effect of pressure (p) and sink temperature (T_∞) on the map of dynamic stability

elevated friction.

3.5.3 Effect of pipe diameter (d)

The pipe diameter directly affects the friction, offering elevated flow resistance in small-diameter loops, without having any direct influence on the buoyancy field. Therefore, increase in the diameter enhances the circulation rate and delays the appearance of FiHTD [77]. Consequently, the stability thresholds also relocate to higher powers, as shown in Fig. 3.19(a), illustrating the leading role of buoyancy. The difference between the two limiting levels steadily increases with d, as the crosswise fluctuations are allowed to grow. The system continues to exhibit instability till a higher T_∞ as well, which can primarily be attributed to the reduced temperature level in larger-diameter channels for any specific $\dot{q}$. The unstable zone, of course, shrinks noticeably with rise in T_∞, similar to the earlier maps, and completely disappears beyond a certain limit.

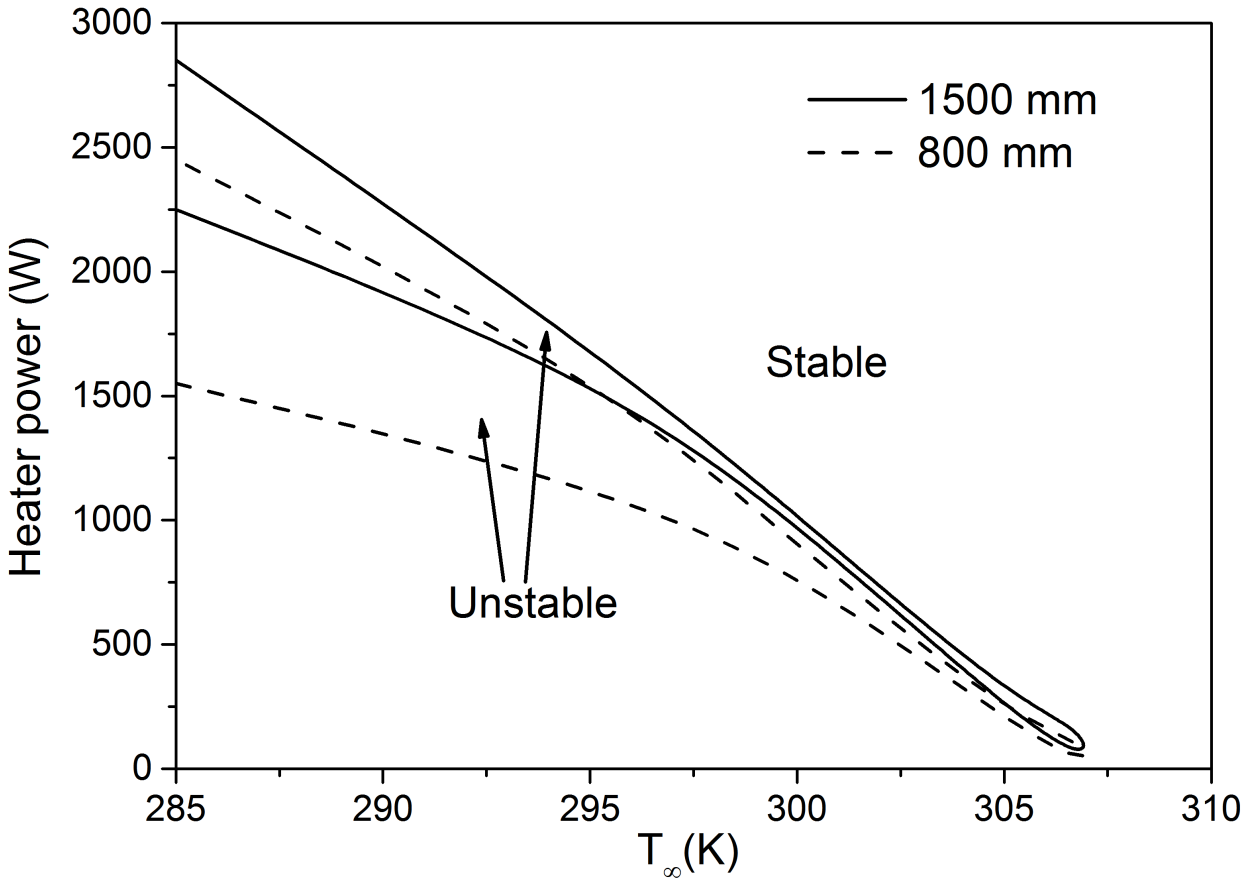

Fig. 3.18: Effect of loop height (H) on the map of dynamic stability at $p = 8$ MPa

It is interesting to observe that loops with larger diameter persuade unstable operation even when $T_\infty > T_{pc}$, albeit for a slender range of heater power, which is in contrary to the observation from the earlier cases. The system experiences growth of disturbances only for low $\dot{q}$-values with higher sink temperatures. When the sink temperature is close to the pseudocritical value, the stability map assumes a near-symmetric shape with respect to T_{pc}, as is evident from Fig. 3.19(b) for very low power levels. Loops characterized by $d = 7$ mm or lesser are always stable regardless of the imposed $\dot{q}$ or T_∞. The width of the unstable zone keeps on increasing with rise in diameter owing to the gradual diminishing in the role of friction. It must be noted here that the loop can be stabilized by raising the power. That, however, will drive the sNCL to the regime of deteriorated heat transfer, typified by low circulation and high temperature levels, and hence is suggested to be avoided. Operation within the enhanced heat transfer regime is possible only at lower powers for T_∞ values marginally below T_{pc}. But that can lead to dynamic instability, as can be observed here,

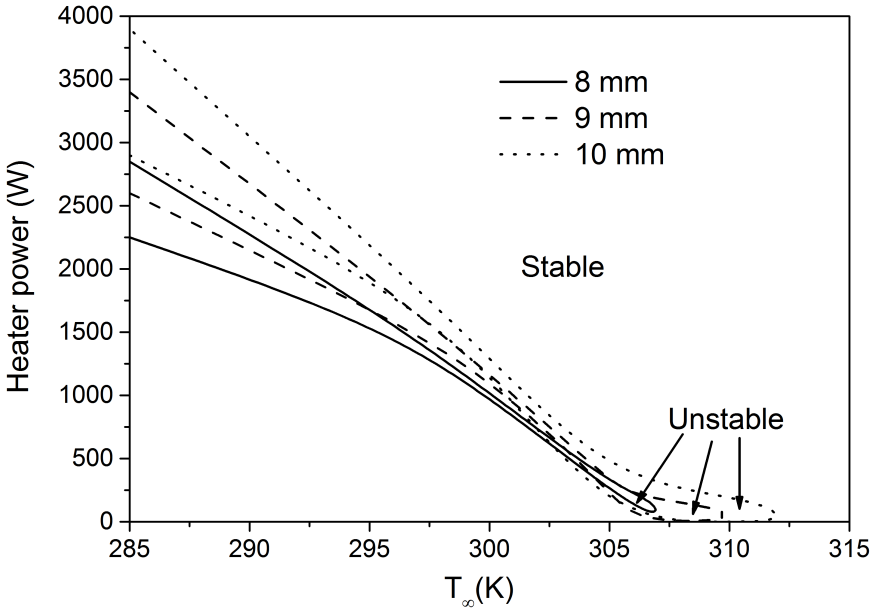

(a)

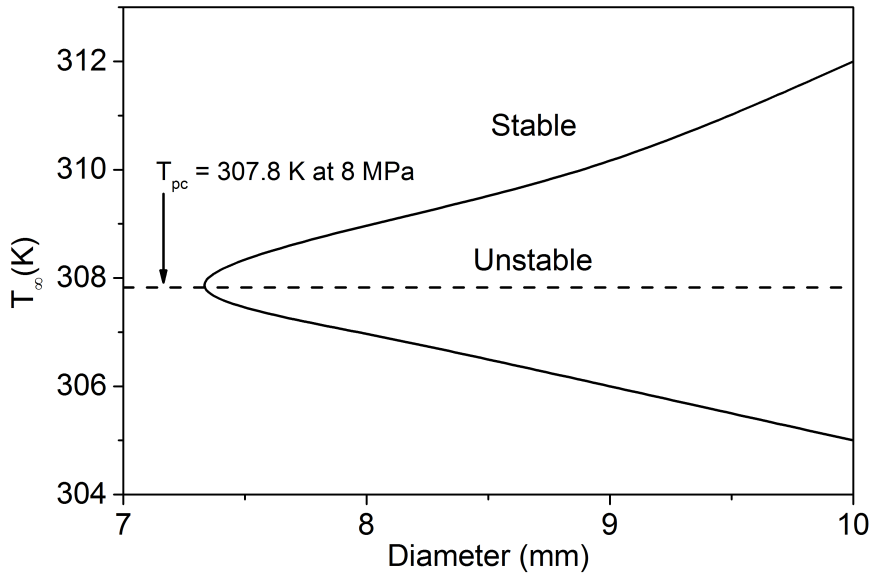

(b)

Fig. 3.19: Effect of pipe diameter (d) on the dynamic stability at $p = 8$ MPa: (a) Stability maps for three different diameters; (b) Limiting values of sink temperature facilitating unstable operation for $\dot{q} \leq 25$ W

and should, therefore, be practiced judicially.

3.6 An Alternative Perspective

An alternative method of envisaging the threshold of dynamic instability can be devised through the statistical analyses of the time-series data generated during the numerical simulations performed over sufficiently-long time span. Both the nature and amplitude of the oscillations can vary significantly based on the boundary conditions, and fast Fourier transform (FFT) can provide important insight about the periodicity present within individual dataset. As a part of the present study, the dominant frequency has been identified from each of the available discrete dataset using FFT, and the summary of the concerned observations is presented in Fig. 3.20. Here the reported frequency values have been classified in three distinct groups based on the stability assessment. It is interesting to note that all the points associated with the stability threshold can be fitted in a power-law profile with a reasonable R^2-value of 0.951. The major utility of this trendline is with all the frequency values characterizing stable states lying below this one, while the unstable ones are generally above. The fitted relation can, therefore, provide an approximate estimate about the location of the stability boundary. It, however, requires more comprehensive exploration, before considering it as a dependable one.

3.7 Summary

The stability characteristics of any sNCL is always an intriguing topic of research, because of the mathematical complexity involved in a simple geometric configuration and also the unique nature of variation in the thermophysical properties. Characterization of a closed loop is even more intricate because of the absence of any explicit boundary condition and, hence, has hardly been explored, providing the necessary motivation for the present study. A supercritical CO_2-driven rectangular loop in HHHC orientation has been explored numerically here, following a 1D framework. Some of the most important conclusions are summarized below.

- The steady-state thermalhydraulics follows the established behavior, observed earlier during multidimensional assessment, albeit with some quantitative over-prediction.
- Over an intermediate range of heater power, the system exhibits Ledinegg instability, demonstrated by the appearance of multiple steady-state solutions and negative slope of the pressure drop profile.

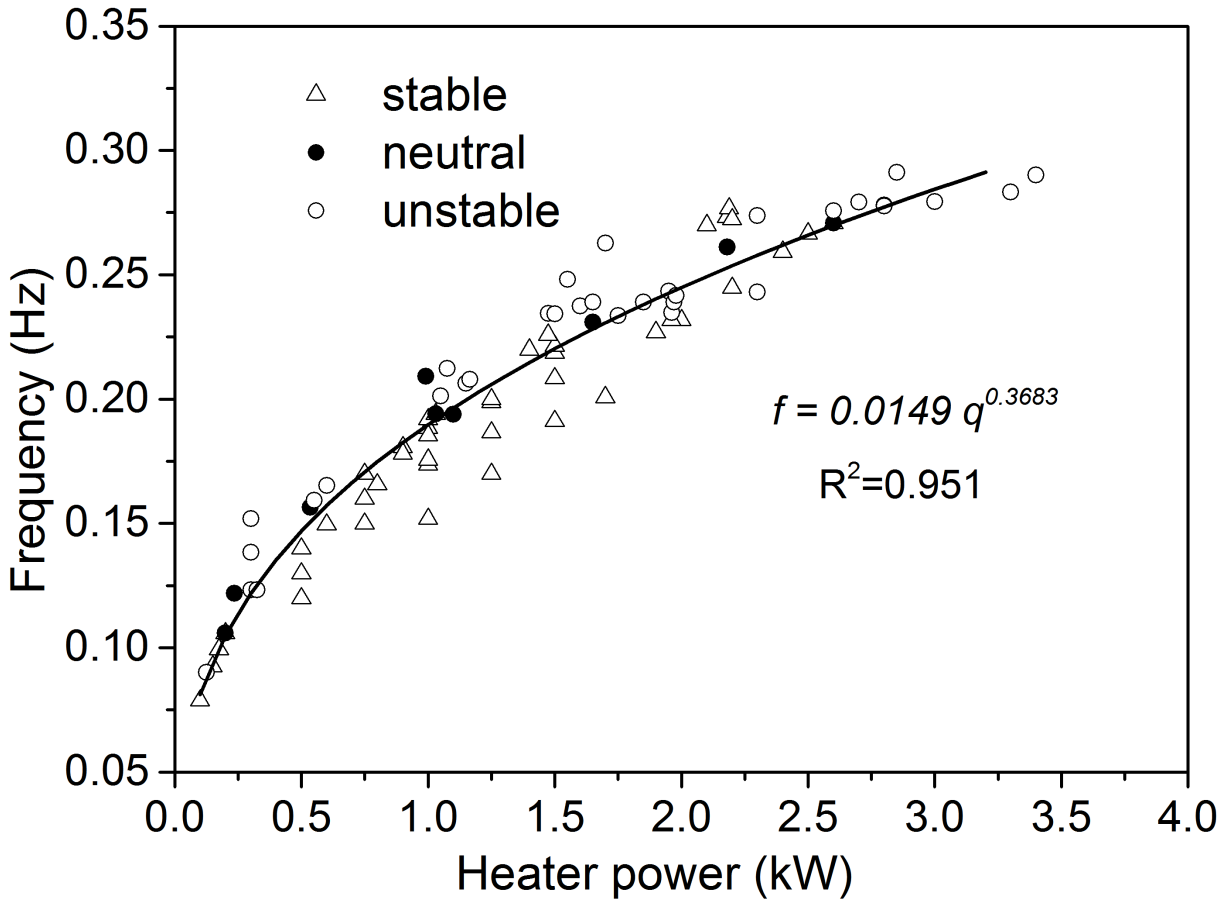

Fig. 3.20: Variation in peak frequency of the discrete dataset evaluated through FFT over a large range of operating parameters; the locus of the neutrally-stable points closely follow a power-law profile

- Static instability is found to be bounded by two limiting powers, both of which can correspond to deterioration in circulation rate. The zone of Ledinegg instability, however, gradually diminishes with rise in sink temperature and vanishes for $T_\infty > T_{pc}$.
- Dynamic instability, characterized by continuous growth in an imposed perturbation, has also been observed for a certain range of power. Both modes of instability are found to disappear beyond the higher power limit of FiHTD.
- The static and dynamic stability maps demonstrate sufficient concordance in terms of the relevant dimensionless variables.
- In loops with larger diameter, the system can continue to retain dynamic instability for very low power levels even when the sink temperature is beyond T_{pc}.

In a nutshell, identification of Ledinegg instability in a closed sNCL is the most significant contribution from the present study. The topic of dynamic instability has also been explored, with systematic discussion about the respective roles of the operating and geometric variables.

Chapter 4

Role of Heat Transfer Regime under Periodic and Non-periodic excitation

4.1 Preamble

Since the system's characteristics are influenced by the interaction of the buoyancy force and the friction force, these two are significantly impacted by any sudden changes in the properties, particularly close to the pseudocritical point. When the flow parameters are disturbed, as we saw in the previous chapter, the stability of the system may change under the steady-state condition. In addition, system dynamics can shift if we observe an abrupt increase in loop temperatures that approaches T_{pc}. Because the operator has no direct control over the heat input condition, such a situation is very likely. A closed NCL, despite being more challenging to model theoretically because of the absence of explicit boundary conditions, is more relevant in practical applications, especially as large-scale cooling options. A real-life loop, such as a reactor core cooling system, is always vulnerable to varied degree of external excitations, leading to transients in the fluid domain. The efficacy of the self-correcting nature of NCL through the internal feedback mechanism is expected to rely on the operating conditions, and hence, it is impractical to anticipate the dynamic trends without any comprehensive analyses. Present study aims at contributing to this specific dearth by assessing the nonlinear response of a rectangular sNCL under the influence of periodic and non-periodic heating power. The horizontal-heater-horizontal-cooler (HHHC) orientation is commonly regarded as the most unstable one [39], and hence the same is considered for the analyses. Temporal variation in important flow variables have been monitored with time, after imposing a time-varying power. Care is taken to relate the observations, as well as

the operating conditions, with the steady-state domains of heat transfer, and therefore, the present study is presupposed to reveal vital inferences on the topic.

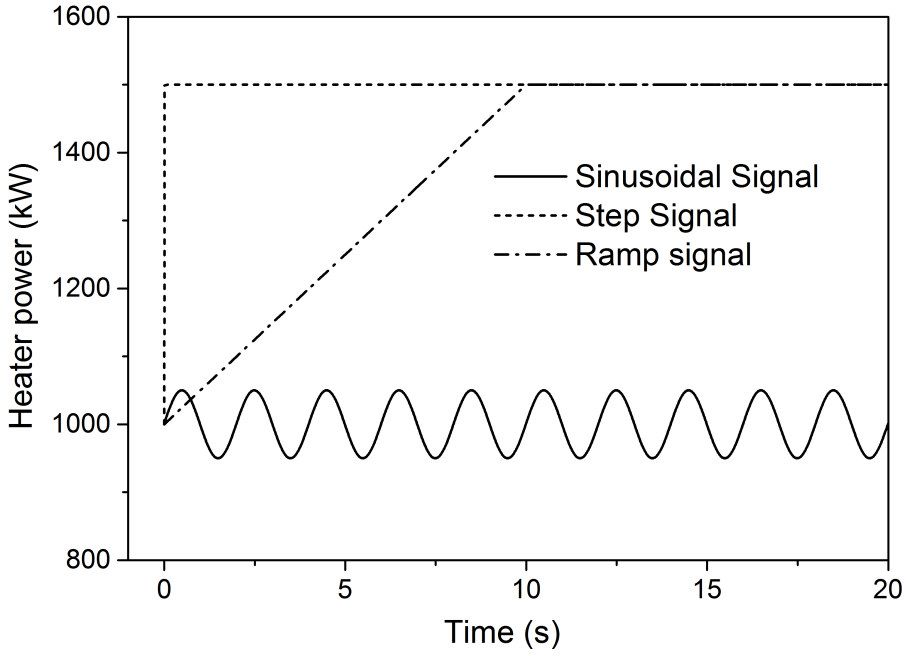

Fig. 4.1: Profile of imposed signal with time

The numerical model, concerned governing equation and methods employed to solve the same are similar to that was used in chapter 3. The difference arose only in the heater power values, equations of each is shown in equations below-

- Step signal

$$\dot{q}\,(t) = \dot{q}_{ss}(1+\phi)$$

- Ramp signal

$$\dot{q}\,(t) = \dot{q}_{ss}\left(1+\phi\frac{t}{t_{trans}}\right)$$

- Sinusoidal signal

$$\dot{q}\,(t) = \dot{q}_{ss}\left\{1+A\,\sin\left(\frac{2\pi}{\tau}\,(t-t_0)\right)\right\}$$

In chapter 2 the multidimensional steady-state appraisal of CO_2-driven sNCL demarcated four distinct regimes of heat transfer, primarily contemplating the fluid temperature levels in the adiabatic sections. The same observations was also reproduced in chapter 3 despite

the use of a completely different numerical structure, with minor changes in the magnitudes of the transition limits. The enhanced and transition heat transfer regimes can be recognized as the most important ones. While the former allows operation with large circulation rate and continually-raising heat transfer coefficient, the other one, commonly associated with a shallow band of heater power, culminates with rapid reduction in both these quantities. Sarkar and Basu[77] coined the term FiHTD to segregate it from the deterioration in forced-flow channels, as the reduction in heat transfer coefficient and consequent rise in wall temperature is induced by the drop in flow rate itself for sNCL. FiHTD can be regarded as a practical limit of operation, to avoid high temperatures and also to insure decent energy transport characteristics. Therefore, the power levels cogitated for the present analyses are also confined to the FiHTD mark, accordingly being affiliated to the enhanced and transition heat transfer regimes. The system pressure and sink temperatures are maintained constant at 8 MPa and 295 K, respectively, and the transformation from the transition regime to the deteriorated heat transfer regime, *i.e.*, FiHTD corresponds to an approximate steady-state power of 1700 W with this combination, consequently consigning an important marker for the present study.

4.2 Effect of Periodic Heating Profile

• Periodic response at low-to-intermediate powers

The focus here being firmly on the dynamics, choice of a uniform initial condition is important, and that is decided to be the steady-state associated to the heater power ($\dot{q}_{ss}$). It can be achieved by solving Eqs. 3.1(a-c), without the temporal terms, and starting with a judicial guess for the circulation rate, while adhering to the convergence limits delineated. Any change in boundary condition can be perceived by the system as a perturbation, activating the self-correcting mechanism. While the system attempts to regain the original steady-state on being subjected to an impulse, if the initial condition is within the stability margin, a continuous input such as a sinusoidal power profile will compel it to catenate the periodic nature. The final outcome, however, should depend on the interaction of the stability threshold with the peak of the sinusoids. For a $\dot{q}_{ss}$ level well below the criterion to reach neutral stability, system never experiences any drastic change, with smooth variations in principal thermophysical properties and consequently in the governing forces. Subsequently, the circulation rate, as well as the CO_2 temperature throughout the loop, starts to follow the periodic pattern after a phase of initial transients, thereby attaining the so-called *dynamic*

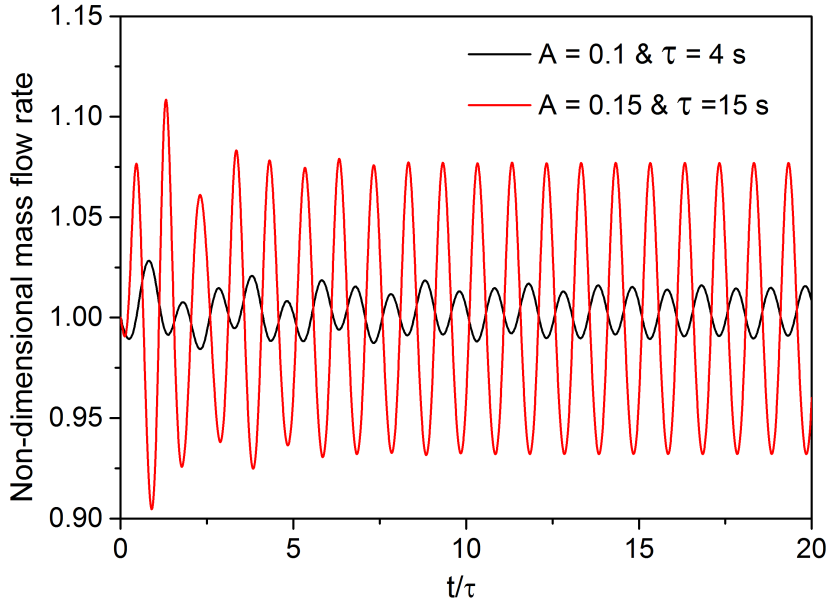

(a) $\dot{q}_{ss}$ = 250 W (low-power regime)

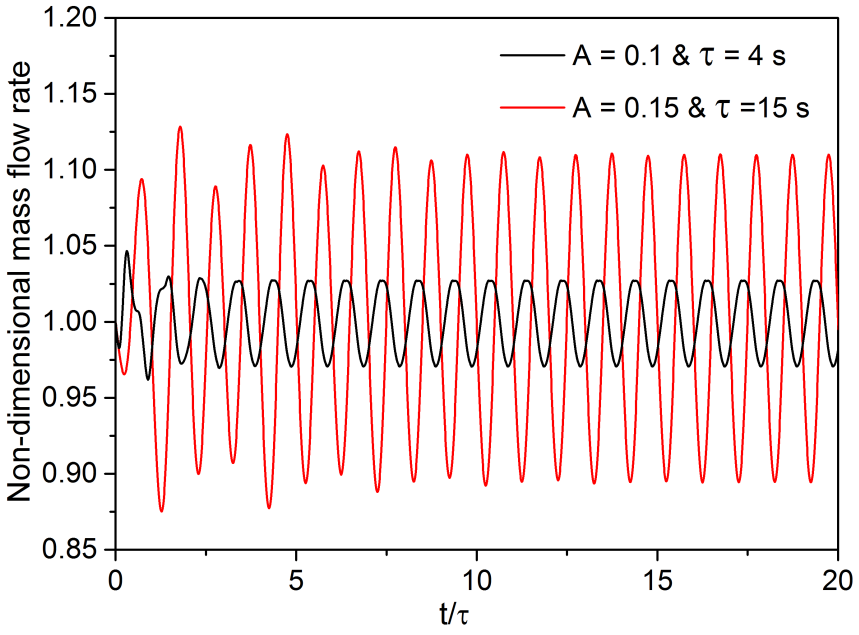

(b) $\dot{q}_{ss}$ = 750 W (enhanced heat transfer regime)

Fig. 4.2: Temporal variations in Normalized mass flow rates ($\dot{m}/\dot{m}_{ss}$) at two different power levels, and under the influence of two different periodic signals; Here p = 8 MPa and T_∞ = 295 K

steady-state. Two such cases are demonstrated in Fig. 4.2 for couple of combinations of amplitude and time period. Here the horizontal axis corresponds to normalized time (= t/τ).

The first of the two selected power levels belongs to the low-power regime, while the other falls into the enhanced heat transfer regime, but is sufficiently way from the transformation to the transition regime. The upper boundary for all the sinusoids remain considerably lower than the stability threshold in each of the studied cases, allowing the loop to achieve the periodic state itself. The time required to realize periodicity, as well as the amplitude of fluctuations, obviously depends on the strength of the imposed signal, without significant contribution from $\dot{q}_{ss}$ on a dimensionless plane. That implies the dominance of the imposed signal in regulating the final characteristics.

A distinct difference can, however, be noted on assessing the characterizing frequencies of the resultant profiles. The discrete dataset obtained through numerical simulation is used to perform fast Fourier transform (FFT) and illustrations are provided in Fig. 4.3 for two representative cases, differing by $\dot{q}_{ss}$. Both of them exhibit explicit peaks around 66.7 mHz, which defines the imposed signal, and therefore, is always expected to be identified. But a second minor peak is also visible for both of them, at different locations. The observation of a second frequency in transient profiles is consistent with Tilak and Basu[144], who ascribed it to the nonlinear dynamics of the system, and drew analogy to natural frequency, without delving into further details. A more meticulous evaluation is available in [152] for single-phase NCLs, where the natural frequency was reported to increase monotonically with heater power till the attainment of stability threshold. Similar conclusions can now be deduced for sNCLs as well, as the characterizing frequency of the present loop is also increasing sharply with the steady-state power, and this trend can be substantiated from table 4.1. In fact, natural frequency of sNCL can be determined simply by imposing a minor momentary perturbation on the steady-state and analyzing the ensuing waveform, which corroborates it as a characteristics of the loop itself.

Table 4.1: Natural frequencies of the present sNCL corresponding to different steady-state heater power ($\dot{q}_{ss}$) at $p = 8$ MPa and $T_\infty = 295$ K

Heater power (W)	**Natural Frequency** (Hz)
250	0.100
750	0.151
1000	0.196
1500	0.233
1600	0.236

No substantial alteration in the qualitative trends can be discerned on increasing the

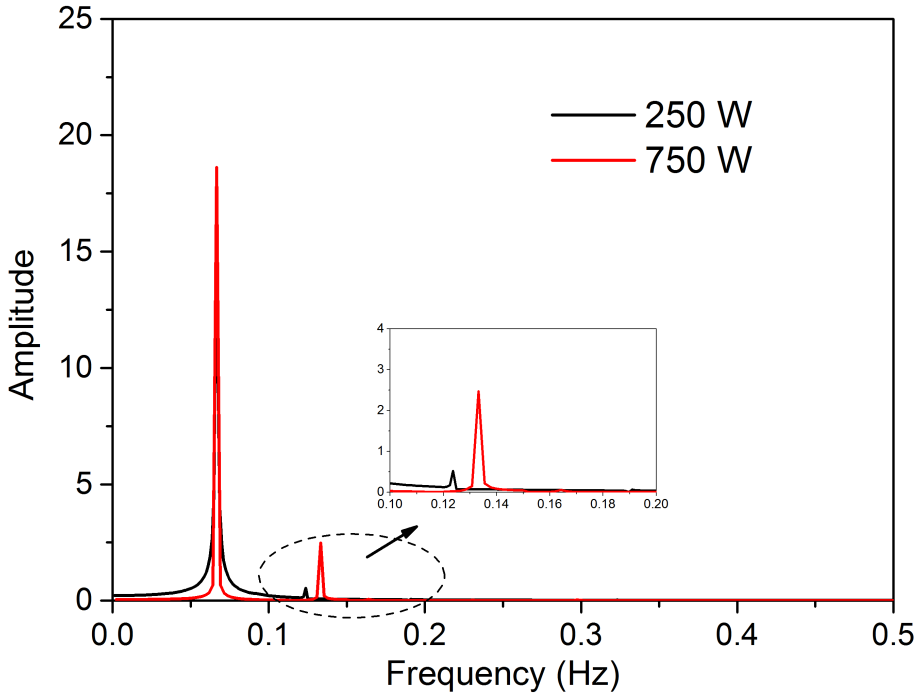

Fig. 4.3: Fast Fourier transform of the transient profiles of circulation rate at two different levels of steady-state heater power; Here $A = 0.15$ and $\tau = 15$ s

steady-state heater power, as long as the peak of the instantaneous power remains comfortably below the stability margin. This is applicable over the entire of the enhanced heat transfer regime even for larger amplitudes such as $A = 0.2$, and also near the lower bound of the transition regime, as long as the amplitude of sinusoid remains small. Three representative situations are displayed in Fig. 4.4 for $\dot{q}_{ss} = 1000$ W. For $\tau = 4$ s, loop promptly reaches the dynamic steady-state for both $A = 0.1$ and 0.2, suggesting no significant role of the amplitude, apart from modulating the extreme levels of circulation rate during transients. Amplitudes in excess of 0.2 have not been attempted within the purview of the present study, considering the practicability.

Increase in time period, or reduction in the imposed frequency, however, is found to introduce certain irregularities in waveform, especially near the peak on the positive slope of the profile. Similar distortion is perceived at all power levels $\dot{q}_{ss} \gtrapprox 1000$ W, and at larger time periods, hinting toward the presence of additional harmonics in the signal. The same can be substantiated from the associated FFTs. While both the loops subjected to sinusoids with $\tau = 4$ s exhibit only the imposed and natural frequencies, multiple additional murmurs are present in the last one, affirming the development of additional influencing factors. Rationale

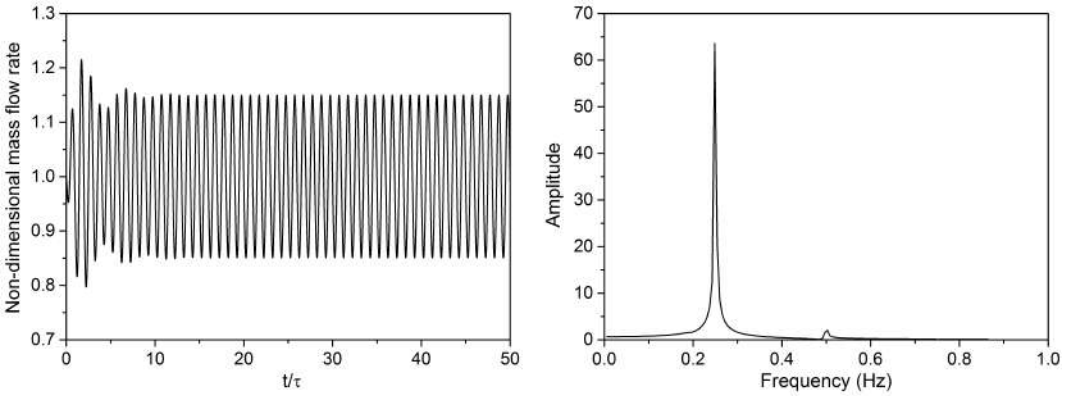

(a) $A = 0.1$ and $\tau = 4$ s

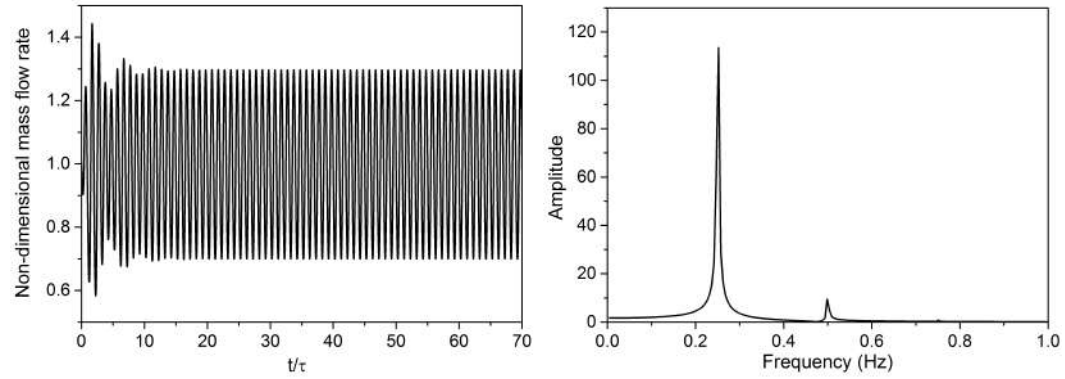

(b) $A = 0.2$ and $\tau = 4$ s

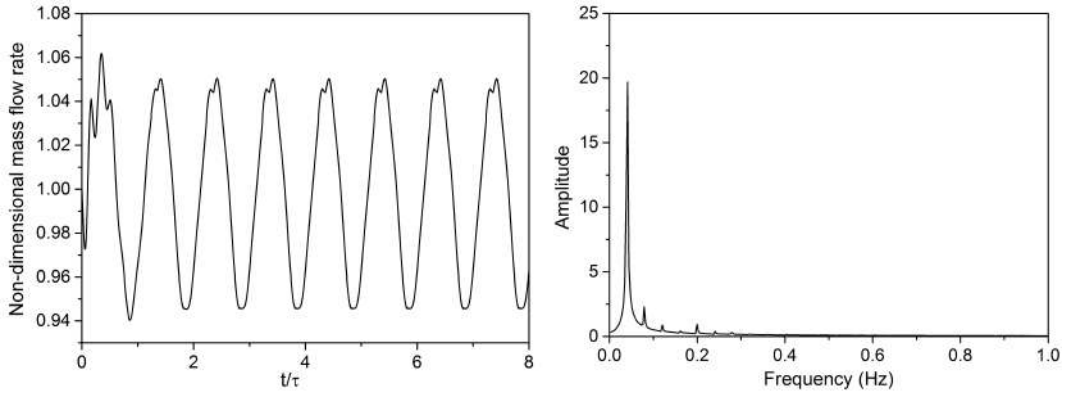

(c) $A = 0.2$ and $\tau = 25$ s

Fig. 4.4: Temporal variations in normalized Mass flow rates and corresponding FFT at $\dot{q}_{ss}$ = 1000 W for three different combinations of amplitudes and time periods

behind such behavior can be gained by monitoring the variations in corresponding thermal fields using Fig. 4.5. For $\dot{q}_{ss} = 750$ W, the highest fluid temperature consistently stays about 0.6 K lower than the pseudocritical limit, while at 1000 W, and also on being subjected to A

$= 0.2$ and $\tau = 25$ s, it is extremely close to T_{pc}. Consequent inequality of about 0.5 K seems a meager one for subcritical fluids and also for supercritical fluids away from the pseudocritical zone. But here it coerces about 13.6% reduction in density and 15.4% decline in dynamic viscosity. The latter degradation weakens the frictional resistances throughout the loop, and the impact of the former can be envisaged from Fig. 4.5(b). Here the density difference corresponds to the disparity in magnitudes associated with the instantaneous temperatures at the middle plane of both the vertical arms, and is, therefore, a reliable estimate of the driving buoyancy field. Both the levels and variations in $\Delta\rho$ are noticeably higher for the second system. Such enhancement of buoyancy, aided by the lowering in friction, attempts to magnify disturbances interior to sNCL, and the minor distortions observed in Fig. 4.4(c) can definitely be imputed to that. However, the intensity of flow resistances is still strong enough, as supercritical CO_2 continues to be within the *liquid-like* regime, accordingly subsiding any major amplification of perturbations. The extent of such disturbances is quite inconsequential from the perspective of the overall system response over the enhanced heat transfer regime, with general inclination toward attains dynamic steady-state for any combination of A and τ.

• Resonance behavior near FiHTD limit

A complete change in dynamics can be noted with admission to the transition regime. On institution of small-amplitude periodic signal, it is possible for the loop to maintain the peak power level below the FiHTD limit (≈ 1700 W at $p = 8$ MPa and $T_\infty = 295$ K), while experiencing fluctuations in maximum CO_2 temperature across T_{pc}. That can induce large alterations in the effective buoyancy and frictional forces, inflicting distortion in the temporal profiles. However, a greater magnitude of A may force a vacillation in state across FiHTD itself, with swift changes in the instantaneous status from enhanced to deteriorated heat transfer regime, passing through the transition one. For example, the upper and lower limits of a periodic signal having $A = 0.15$ for $\dot{q}_{ss} = 1500$ W are contingent to the two contrasting domains, with the steady-state itself being in transition. Very convoluted characteristics are, therefore, expected for such scenarios, demanding careful inspection.

For low- to medium-amplitude signals with $\dot{q}_{ss} = 1500$ W, sNCL displays the distorted profile almost for any time periods, as the peak power persists below the critical limit. Figure 4.6 portrays the response of the system for three different time period, and maintaining identical amplitude. For both $\tau = 2$ s and 10 s, the loop is able to attain periodicity after several cycles, and also with noticeably distorted profiles, hinting toward the presence of multiple

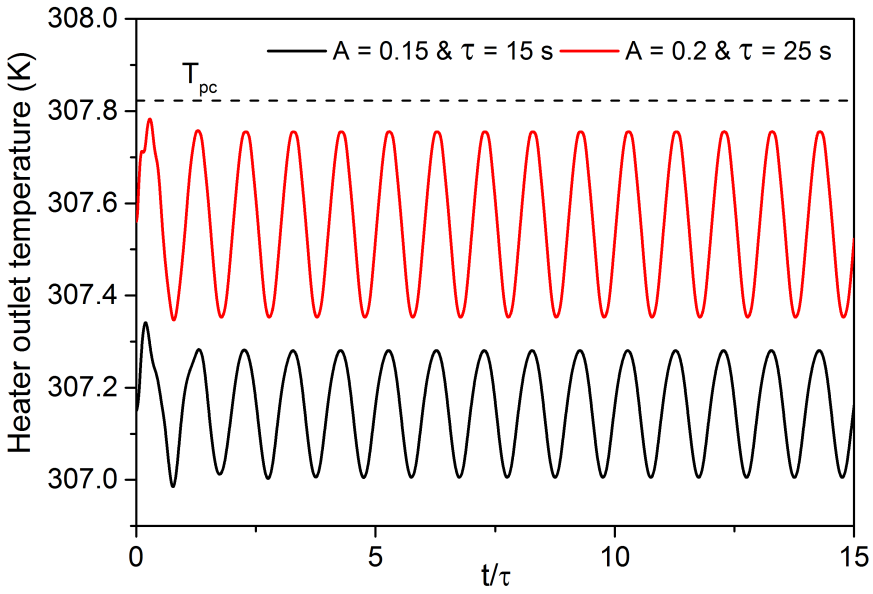

(a) CO_2 temperature at heater outlet

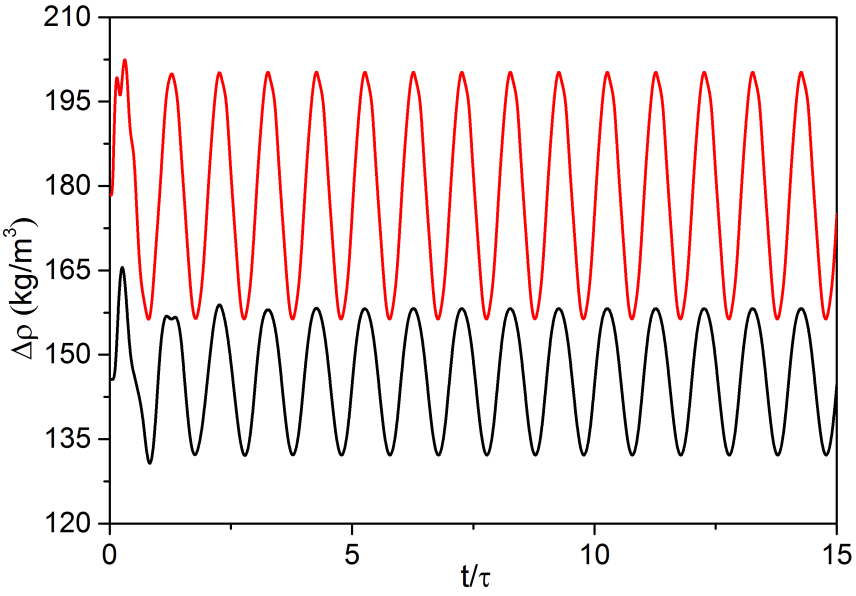

(b) Density difference between the vertical arms

Fig. 4.5: Temporal variations in fluid temperatures at heater outlet and density differences ($\Delta\rho$) between the vertical arms at two different levels of steady-state power and two different periodic profiles; here, $\dot{q}_{ss}$ = 750 W for the black line and $\dot{q}_{ss}$ = 1000 W for the red line

characterizing frequencies and possibly secondary harmonics. Striking difference in response

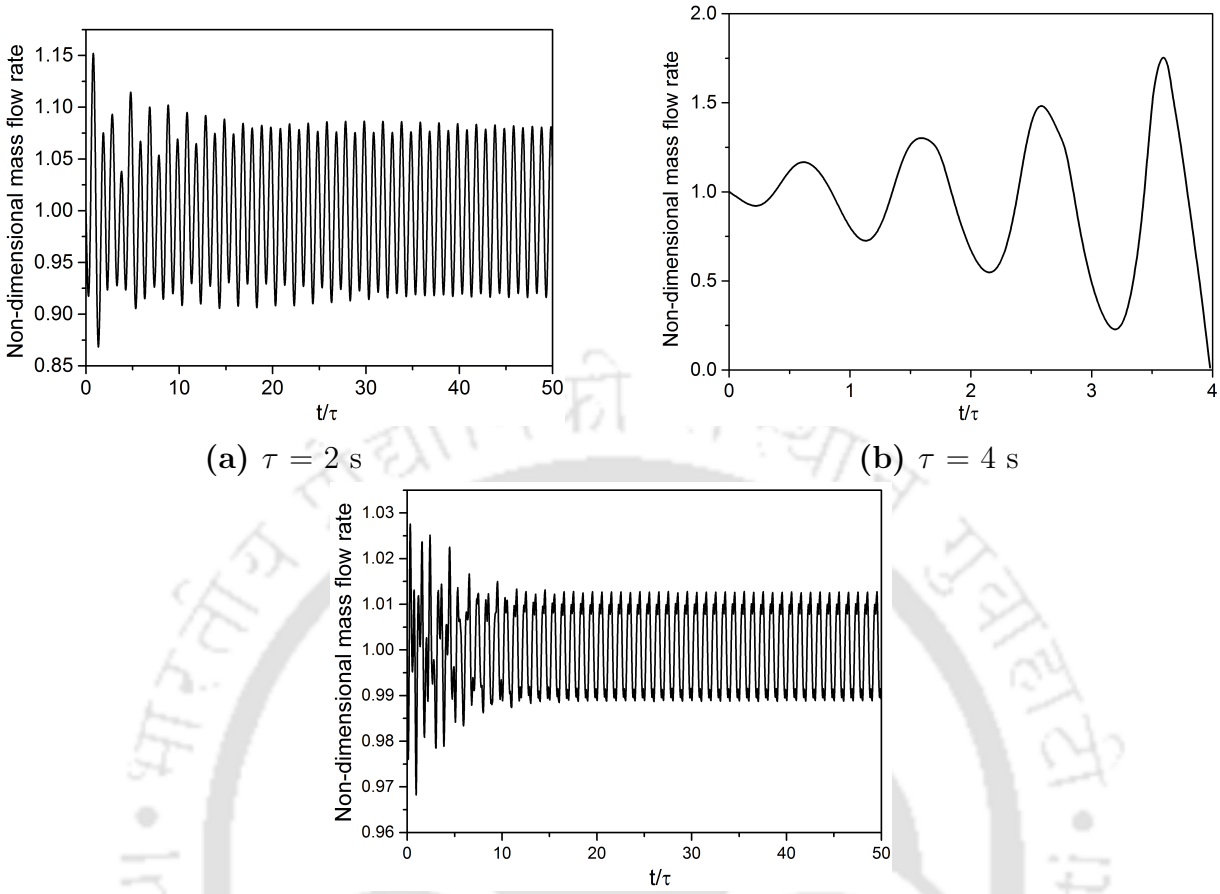

(a) $\tau = 2$ s **(b)** $\tau = 4$ s

(c) $\tau = 10$ s

Fig. 4.6: Temporal variations in normalized mass flow rates at $\dot{q}_{ss} = 1500$ W on being subjected to sinusoidal power profile with $A = 0.1$ and three different time periods

can be note with $\tau = 4$ s. Here, the frequency of the imposed signal is very close to the natural frequency of the loop at 1500 W (refer to table 4.1). The effect of imposing a similar signal at lower powers is generally large-amplitude fluctuations and an early-realization of periodicity, while the resultant waveform logically being defined by a single frequency. For the present case, however, original state of the fluid being very close to T_{pc}, small change in energy content can infuse enormous variation in thermophysical properties, inducing considerable modulation in the associated forces within a small span of time. As presented in Fig. 4.7(a), the increment in CO_2 temperature across the heater abruptly escalates, compelling the driving forces to sway quite substantially. Once the lowest fluid temperature approaches T_{pc}, CO_2 momentarily assumed a *gas-like* representation throughout the flow path, causing a drastic reduction in the driving influence and eventual reversal in the primary flow

direction. Such response has been observed solely on imposing an external signal having the natural frequency of the concerned sNCL, regardless of the amplitude of the sinusoid. That can be substantiated from Fig. 4.7(b). Each selections for the external power profile transpire to flow reversal, with amplitude affecting the physical time and number of cycles necessary to attain that. The variation in the density differential, and hence in the driving buoyancy, is also considerably greater than the levels noted in Fig. 4.5(b). On the contrary, dynamic viscosity of supercritical CO_2 is substantially lower for temperatures greater than T_{pc}. Rise in temperature from 308 K to 330 K at 8 MPa nearly halves the viscosity. Combined impact of augmented buoyancy and diminished friction is an unstable system, typified by oscillation growth, and that is precisely the observation here. The instant of flow reversal corresponds to an instantaneous zero-buoyancy, which is consistent with the turnabout in thermal characteristics experienced by the fluid in the vertical arms. Comparable impact of imposing natural frequency on single-phase NCL was reported by Basu [152] as well, where analogy was drawn with the resonance behavior of transducers. It can be corroborated by using the resultant database to perform FFT (Fig. 4.7(c)) with all the considered cases. Despite the difference in their amplitudes, each of the institute signals yield a single frequency peak. Concerned amplitudes are also substantially greater than the levels observed earlier, authenticating the notion of resonance in a *self-excited oscillator* in the form of sNCL. In fact, administering any periodic signal having frequency near the natural one instigates large-amplitude oscillations in the loop variables and high FFT-peak, regardless of the power level, with the concerned levels being substantially shorter with other signals. Figures 4.4(a-b) can be referred in this contest. Resonance, however, is triggered only for $\dot{q}_{ss}$ values very close to FiHTD limit, and hence, stipulates additional caution during operation.

• Initiation of chaos

Any further increase in time period stimulates chaotic response from the loop at the same power level, specifically on imposing high-amplitude sinusoidal power profiles. With the highest fluid temperature venturing above T_{pc}, inflicting steep instantaneous time rate of changes in the associated forces, the state of the system oscillations around the stability band. However, as the response involves small-amplitude pulses with the imposed frequency being far off the natural one, sNCL has time to employ the self-correcting mechanism through the frictional resistances, which persists to be reasonable over majority of the flow passage. Consequent representations for two situations are available in Fig. 4.8. The qualitative similarity in terms of the continuous cycles of oscillation growth and decay is very evident in both

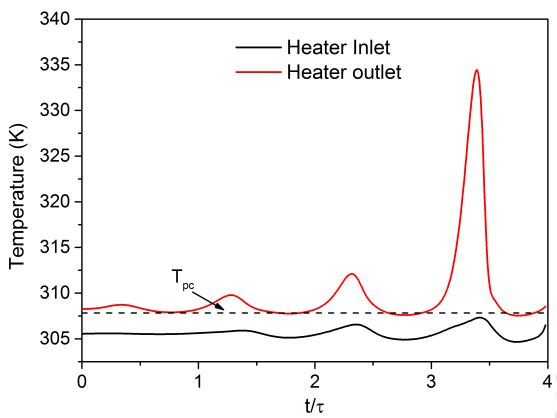

(a) Heater inlet and outlet temperatures

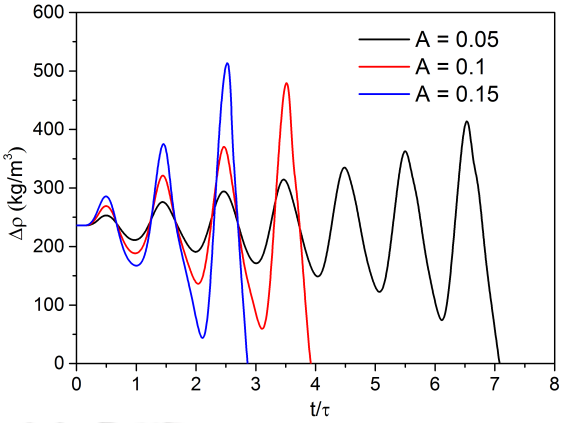

(b) Density difference between the vertical arms

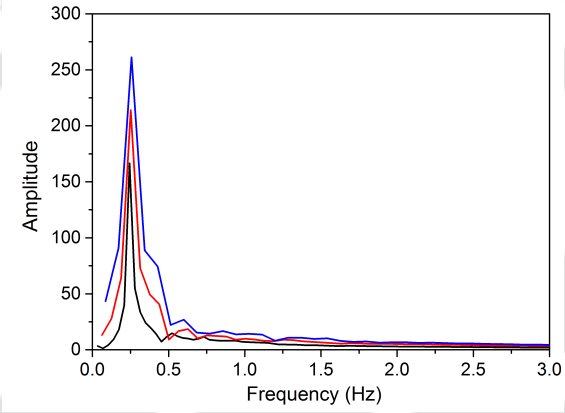

(c) FFT

Fig. 4.7: Temporal variations in (a) fluid temperatures with $A = 0.1$ and (b) density difference ($\Delta\rho$) between the vertical arms with three different amplitudes at $\dot{q}_{ss} = 1500$ W and $\tau = 4$ s; (c) fast Fourier transform of the transient profiles all three different amplitudes

cases, despite the disparity in amplitudes and time periods of the instituted power profiles. Corresponding phase portraits are more revealing, which involves the fluid temperature at the center point of the horizontal heater. The aperiodic nature of the trajectories over a sufficiently long simulation span and sensitivity to the initial conditions, *i.e.*, the definition of the imposed signal, are palpable, which conform perfectly to the definition of chaos [157]. The pattern of projection on the $\dot{m} - T$ plane clearly hints toward the effective dimension of the system being greater than two, serving as a clear indicator of the chaotic response. This is in stark contrast to the limit cycle identified at any of the lower powers (Fig. 4.9), even with the presence of minor distortions.

The amplitude of chaotic oscillations generally is enhanced synchronously with the same

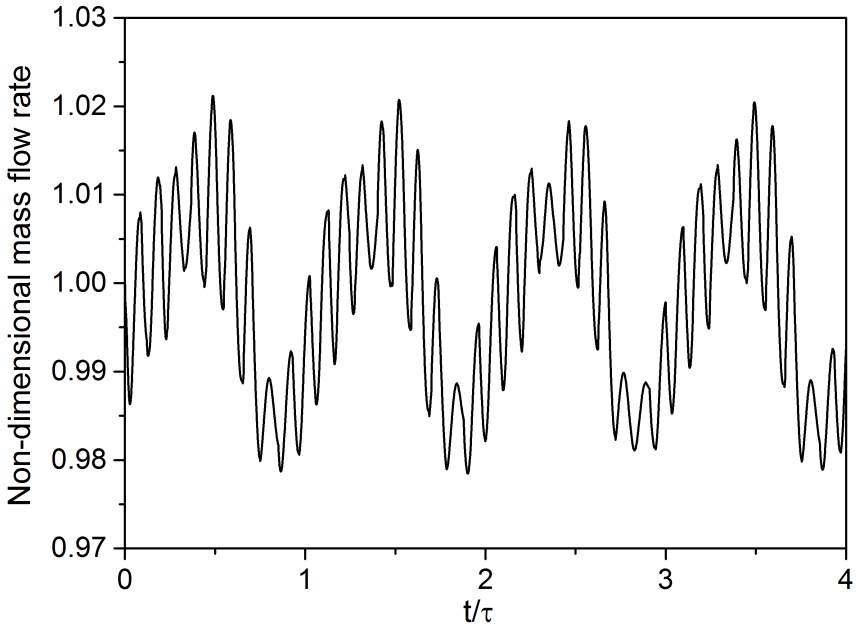

(a) $A = 0.1$ and $\tau = 40$ s

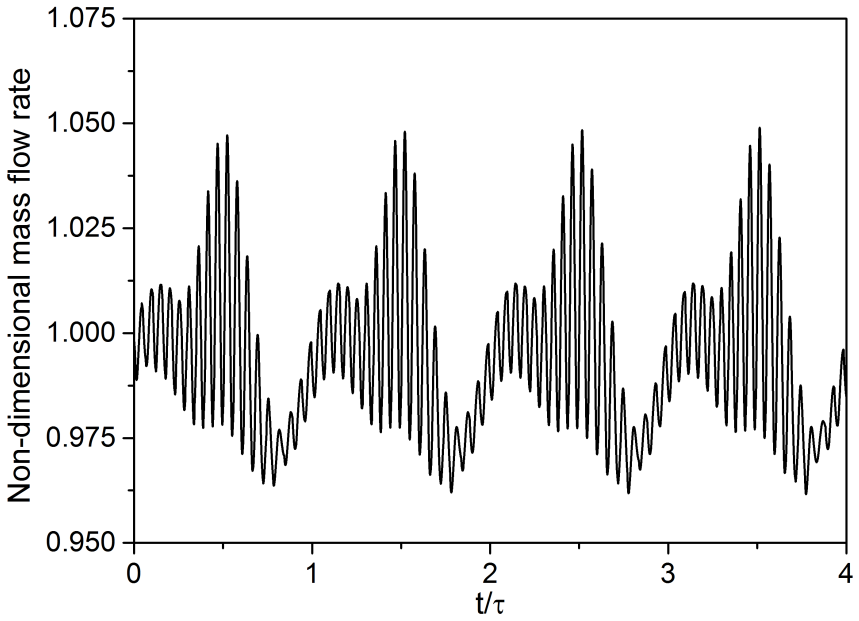

(b) $A = 0.15$ and $\tau = 75$ s

Fig. 4.8: Temporal variations in normalized mass flow rates and phase portraits under the influence of two different signals at $\dot{q}_{ss} = 1500$ W

for the imposed signal, without any visible impact of the time period thereof. The imposed frequency, though, persists to be the determining factor, as the chaotic response can be

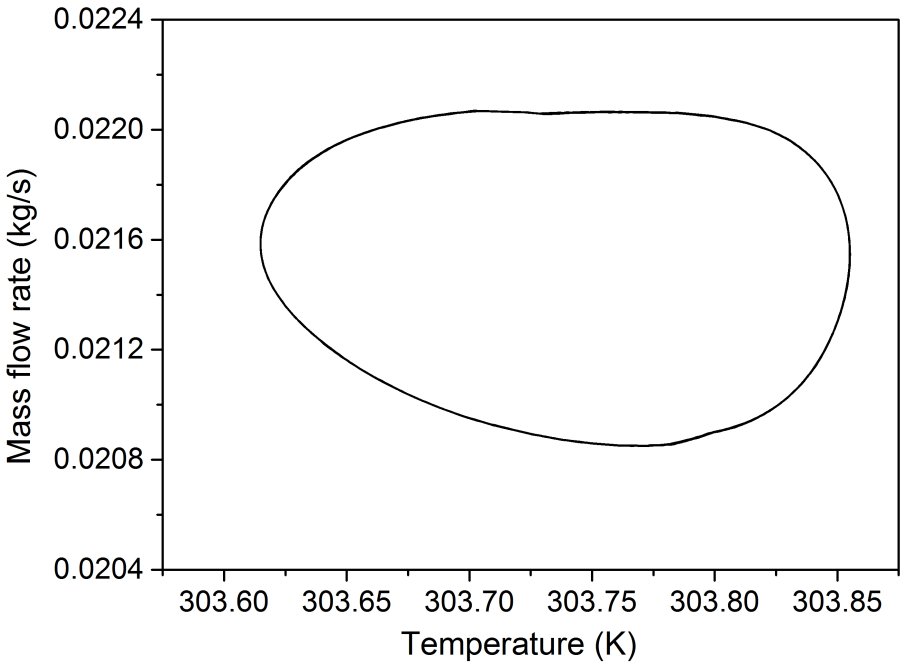

Fig. 4.9: Phase portrait at $\dot{q}_{ss} = 750$ W with $A = 0.1$ and $\tau = 15$ s, demonstrating the appearance of limit cycle and hence periodic behavior

recorded only over a certain range of τ, as is summarized in table 4.2. The expanse of the time period of the imposed signal depends on both the steady-state power ($\dot{q}_{ss}$) and the amplitude of excitation (A). In fact, once the upper limit of instantaneous power breaches the FiHTD barrier, it is possible not to observe any chaotic response. In such situations, and also for very low frequencies of the inflicted power profile, sNCL exhibits bi-periodic transients, and the same can precisely be recognized from Fig. 4.10. Such a trend can be ascribed to the alternating dominance of buoyancy and friction on the instantaneous thermalhydraulics. Indication about the presence of two pertinent frequencies governing the phenomenon can be obtained from the phase plots, which comprise of two closed contours for both the cases. The overall amplitude of fluctuations in the circulation rate, however, is quite small, and continued to diminish parallel to the reduction in the imposed frequency.

It is quite interesting to follow the corresponding frequency responses. As presented in Fig. 4.11, the characterizing frequency of the system continues to retain the original value (~ 0.24 Hz) during the chaotic oscillations, accordingly demonstrating the frequency locking feature. This has been observed consistently at all levels of $\dot{q}_{ss}$, and with any combination of amplitude and time period employed in the transient power profile, where chaotic nature has been diagnosed. There is, however, a complete alteration for scenarios involving bi-

Table 4.2: Range of time period of periodic power profile corresponding to chaotic response at two different power levels

Steady-state power (W)	**Amplitude**	**Minimum power** (W)	**Maximum power** (W)	**Range of** τ (s)
1500	0.05	1425	1575	15
	0.10	1350	1650	25 to 60
	0.15	1275	1725	25 to 50
1600	0.05	1520	1680	15 to 30
	0.10	1440	1760	–
	0.15	1360	1840	–

directional pulsing. While two distinct frequencies can clearly be observed from Fig. 4.12, the characteristic frequency is pushed away from the original position toward the imposed one. The distance between both the final frequencies also reduces with increase in the time period. This phenomenon is defined as frequency pushing.

A quantitative approach dovetails well here to substantiate the chaotic nature of flow observed above over certain ranges of steady-state power, and amplitude and time period of periodic signal. One of the commonly-used tools for analyzing the stability of dynamical systems under such scenarios is the Poincaré map/section, which can be visualized as a plane set across the path of the trajectory, in order to track the propagation of perturbation in each cycle by mapping the state at the beginning of the cycle to that at the end. On working with a discrete dataset as in the present study, a point on the plane can be obtained each time the trajectory returns to intersect the plane, and a series of points for subsequent visits. Here the Poincaré maps are developed by delineating the fluid temperature at the heater center in successive time steps, where the time is selected to be the instant of instantaneous circulation rate crossing a convenient magnitude (set as $\dot{m} = 0.0258$ kg/s in present simulations). When the system is able to attain the dynamic steady-state, concerned phase portrait resembles a closed contour, getting projected as a single point on the Poincaré plane. On the contrary, two distinctive points can be recognized for a loop exhibiting bidirectional pulsing. A chaotic system, however, is expected to yield multiple random points, consistent with the aperiodic nature. Figure 4.13 vividly demonstrates the appearances of all the three categories, based on the imposed time period. Here, both of the selected power level belong to the transition regime, as sNCL is found to always attain the dynamic steady-state when the initial status is outside that. It is also interesting to note the smaller amplitude of oscillation even during chaotic responses, regardless of the amplitude of the imposed profile, which hints toward the

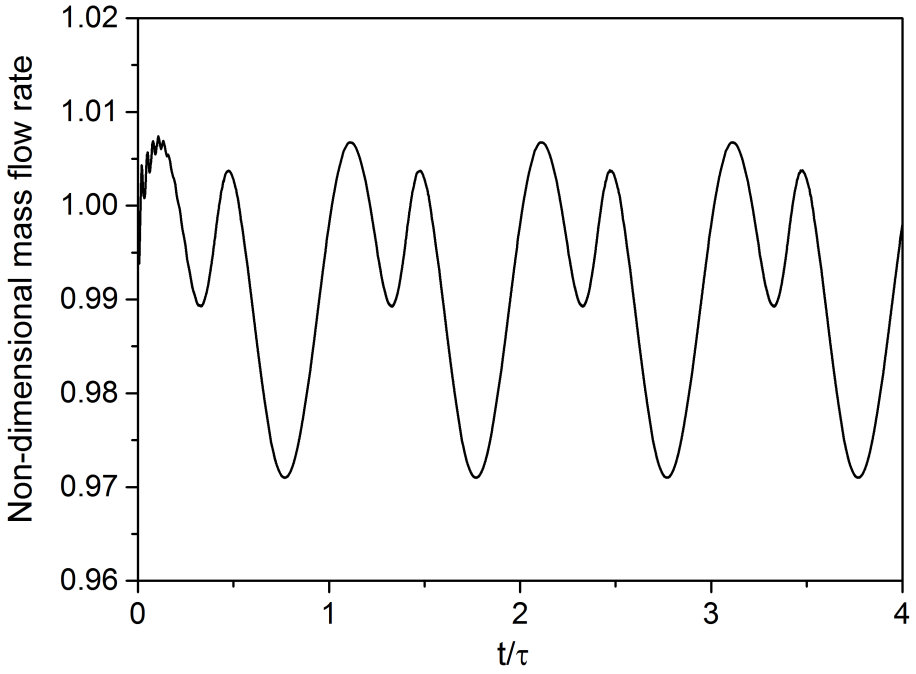

(a) $\dot{q}_{ss} = 1500$ W, $A = 0.15$ and $\tau = 150$ s

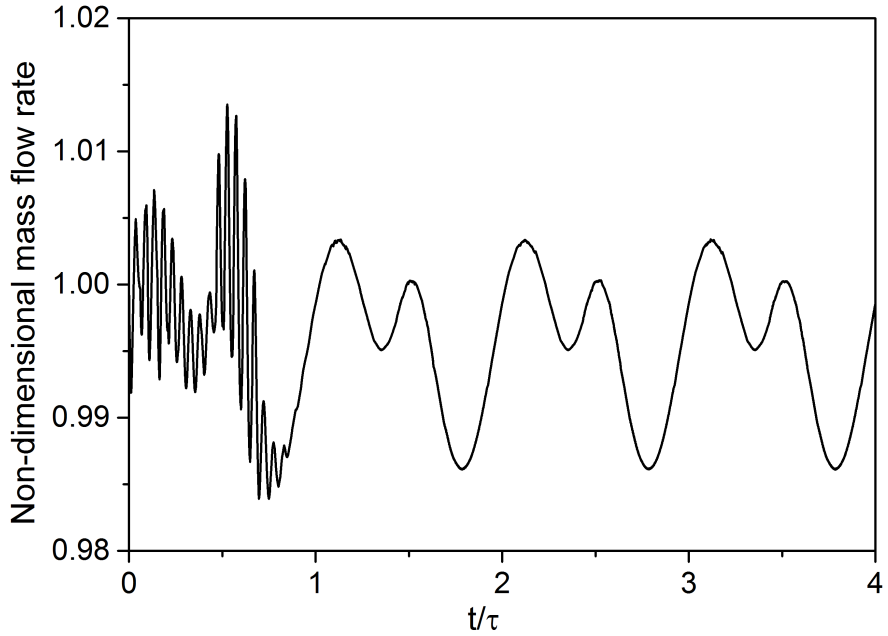

(b) $\dot{q}_{ss} = 1550$ W, $A = 0.1$ and $\tau = 85$ s

Fig. 4.10: Temporal variations in normalized mass flow rates and phase portraits under the influence of two different signals and two different steady-state powers

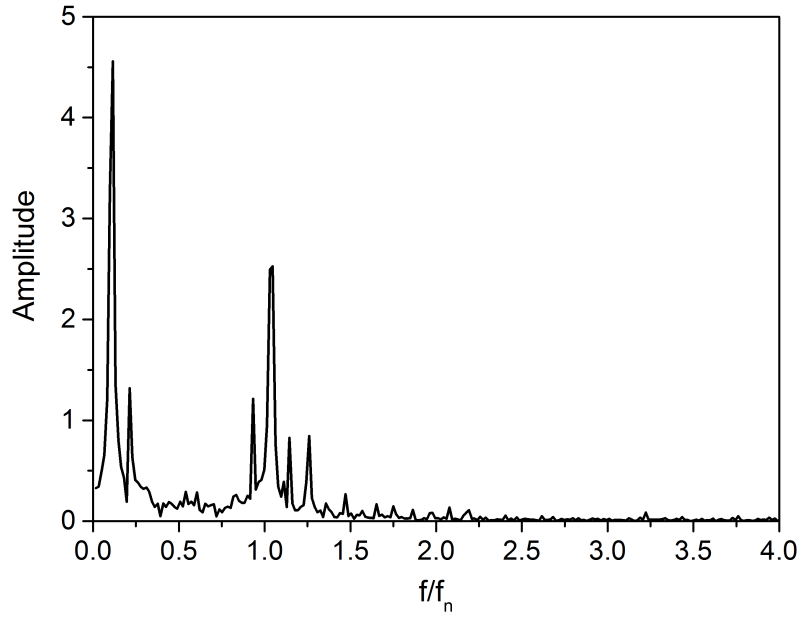

(a) $A = 0.1$ and $\tau = 40$ s

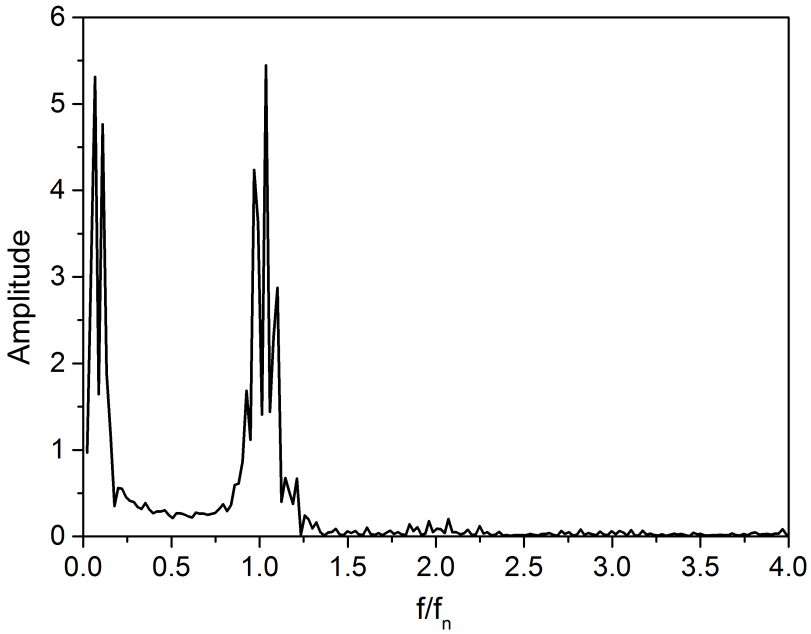

(b) $A = 0.15$ and $\tau = 75$ s

Fig. 4.11: Fast Fourier transform under the influence of two different signals at $\dot{q}_{ss} = 1500$ W, demonstrating frequency locking during chaotic response; here, f_n refers to the natural frequency of the loop

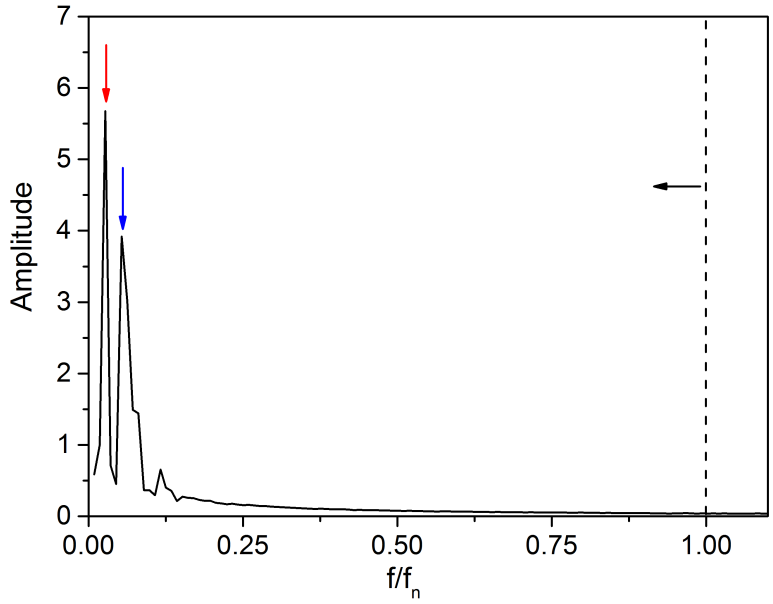

(a) $\dot{q}_{ss} = 1500$ W, $A = 0.15$ and $\tau = 150$ s

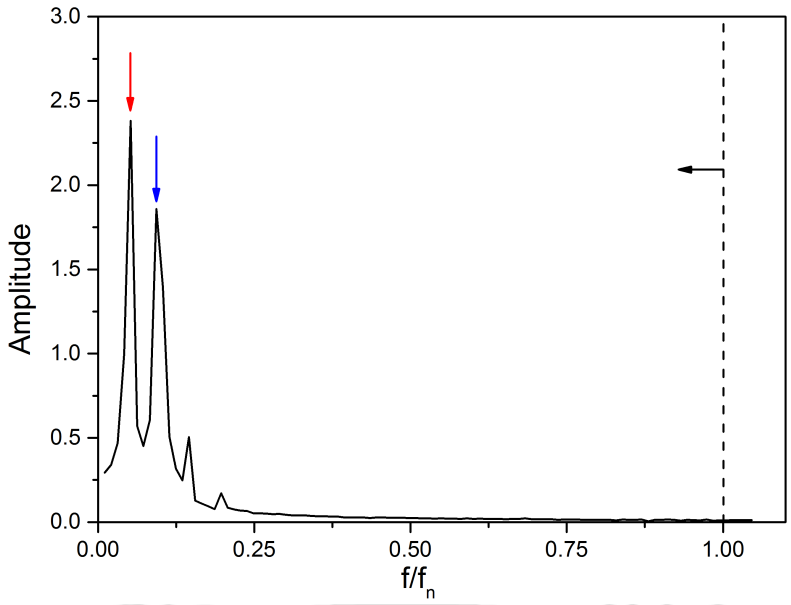

(b) $\dot{q}_{ss} = 1550$ W, $A = 0.1$ and $\tau = 85$ s

Fig. 4.12: Fast Fourier transform under the influence of two different signals and two different steady-state powers, demonstrating frequency pushing, with vertical dashed line ($f = f_n$) representing the natural frequency; here, blue and red arrows indicate the new characteristic frequency and the imposed frequency, respectively

self-correcting nature of sNCL.

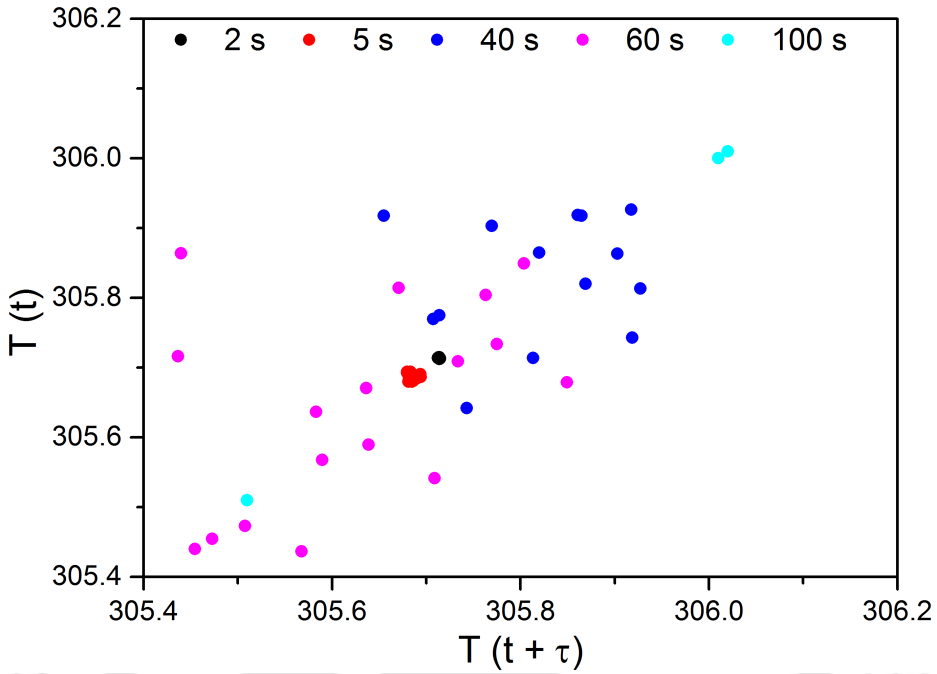

(a) $\dot{q}_{ss} = 1500$ W

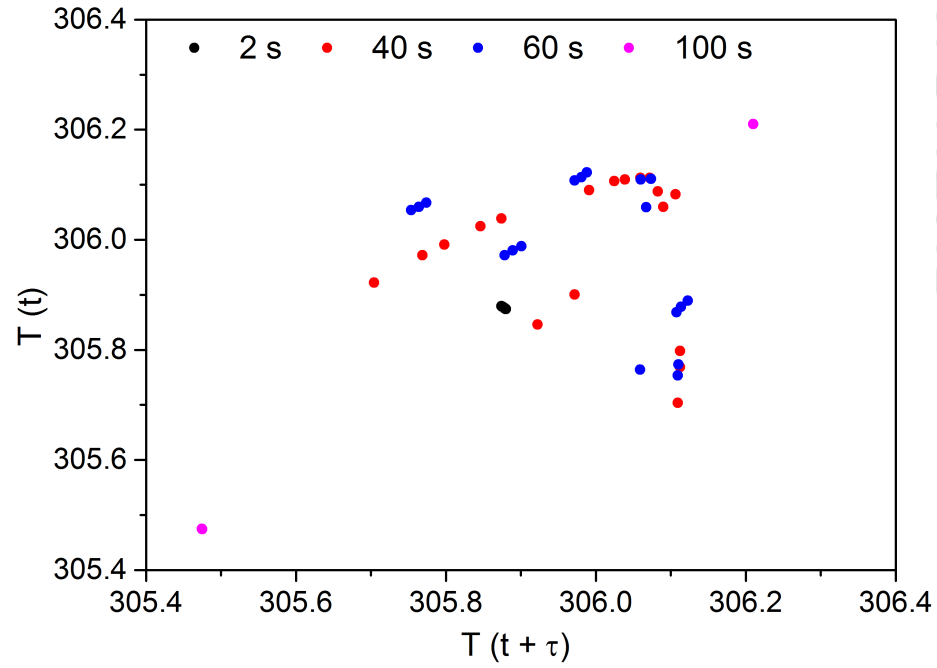

(b) $\dot{q}_{ss} = 1550$ W

Fig. 4.13: Poincaré maps at two different levels of steady-state power and $A = 0.1$

.

• **Response characteristics at high powers (beyond-FiHTD)**

Once sNCL enters into the deteriorated heat transfer regime, temperature throughout the loop is higher than T_{pc}, enforcing the *gas-like* representation. While the dynamic viscosity of the fluid is substantially lower compared the state $T < T_{pc}$, the density variation with temperature also follows a considerably temperate profile. Consequently, friction overshadows the influence of buoyancy in arbitrating both the steady-state thermalhydraulics and dynamics, specifically when the temperature rises above the so-called second pseudocritical point [102]. Consequently, perturbations commonly get suppressed quite easily, and oscillation growth is unlikely. The same is observed here as well, for the representative case of $\dot{q}_{ss}$ = 1750 W, from Fig. 4.14. With each of the imposed signals, system is able to attains the dynamic steady-state, after the initial span of development. There is noticeable reduction in $\Delta\rho$ compared to the levels observed in Fig. 4.7(b), or even in Fig. 4.5(b), despite the latter also achieving the dynamic steady-state. This difference is the definite manifestation of the conversion in the fundamental characteristics of the fluid on either side of T_{pc}. The time period of τ = 4 s closely corresponds to the natural frequency of 0.2596 Hz at this power level, explaining the acute peak in FFT in Fig. 4.14(c). Similar behavior is observed for any power levels over the deteriorated heat transfer regime, regardless of the choice of amplitude or frequency of the imposed excitation, authenticating the dominance of the frictional resistances.

4.3 Effect of Aperiodic Heating Profile

This section discusses the impact of aperiodic heating. Instead of examining each effect separately, a comparison of both inputs has been made using the same targeted power. Input ramp transition times range from 5, 10, and 15 seconds. After reaching a steady-state, the transition from one heat transfer regime to another will be the main focus.

• **Changeover from low power regime to enhanced heat transfer regime**

The base power considered for this case is 250 W. At this power, the initial flow rate is less due to less buoyancy, and temperature levels are substantially lower than the T_{pc}, resulting in a comparatively high offering of friction force against the imposed disturbance. Hence high step rise in the heater power can be imposed as there is a high potential for buoyancy force to grow. As can be seen in the Fig. 4.15a that the system is able to sustain high step rise disturbance of 500 W and 750 W. If the system withstands the rise, it reaches the steady state corresponding to the targeted power, i.e., 750 W and 1000 W. It is vital to

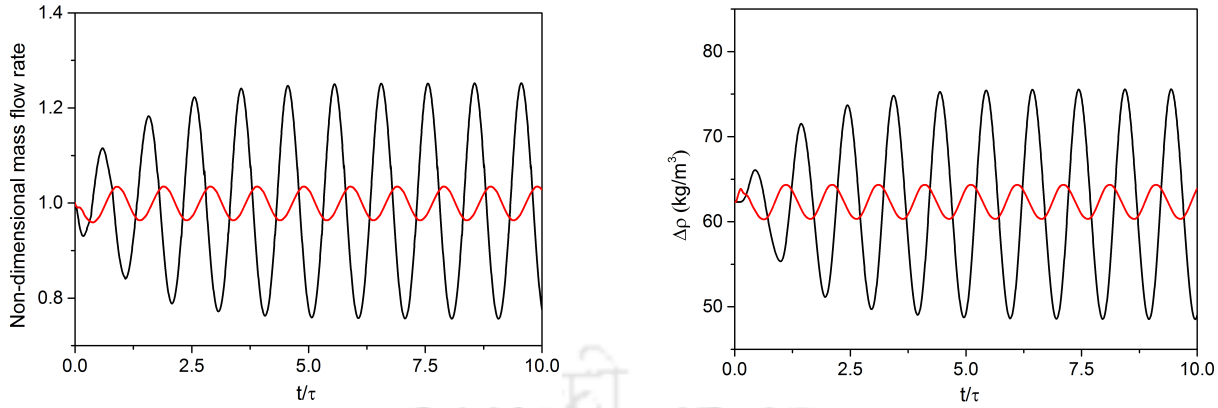

(a) Circulation rate

(b) Density difference between the vertical arms

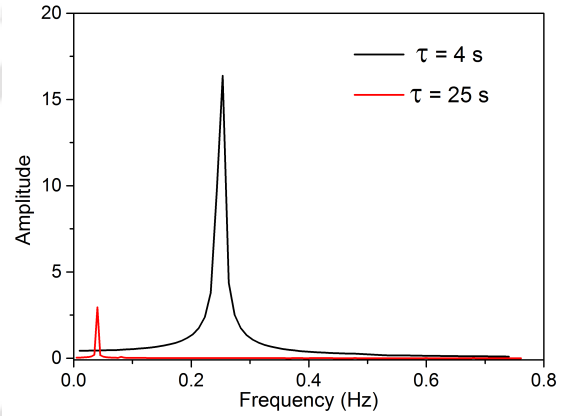

(c) FFT

Fig. 4.14: Temporal variations in (a) normalized mass flow rates and (b) density difference ($\Delta\rho$) between the vertical arms, and (c) fast Fourier transform of the transient profiles with $A = 0.1$ at $\dot{q}_{ss} = 1750$ W

note that if the system is stable, the heater exit temperature is below T_{pc}. Moreover, the corresponding steady-state condition is exactly the same, which corresponds to the targeted heating power. Under the action of a huge power disturbance of 1000 W, the heater exit temperature crosses the pseudocritical limit. This causes the high-density difference between the heater inlet and outlet. The large extent of disturbance does not allow the system to become stable at targeted power, and the system loses its unique sense of direction, causing flow reversal. On the other hand, for the ramp input, the range of power widened for transition, and the system showed stable behavior swiftly. Instead of the sudden jerk, ramp input allows the system to adapt to high changes in the power of more than 1000 W owing to the balancing between buoyancy and friction force, as shown in Fig. 4.15b, the transition

time causes the difference in the extent of initial fluctuations with more fluctuation for t_t = 5s. In spite of the high or the low extent of disturbance, interestingly, the final steady-state mass flow rate condition corresponds to the targeted power, showing the equilibrium of the two forces involved and smooth variation in thermophysical properties. For the step heating case, owing to large buoyancy generation in no time, the system hardly attains a neutral steady-state behavior.

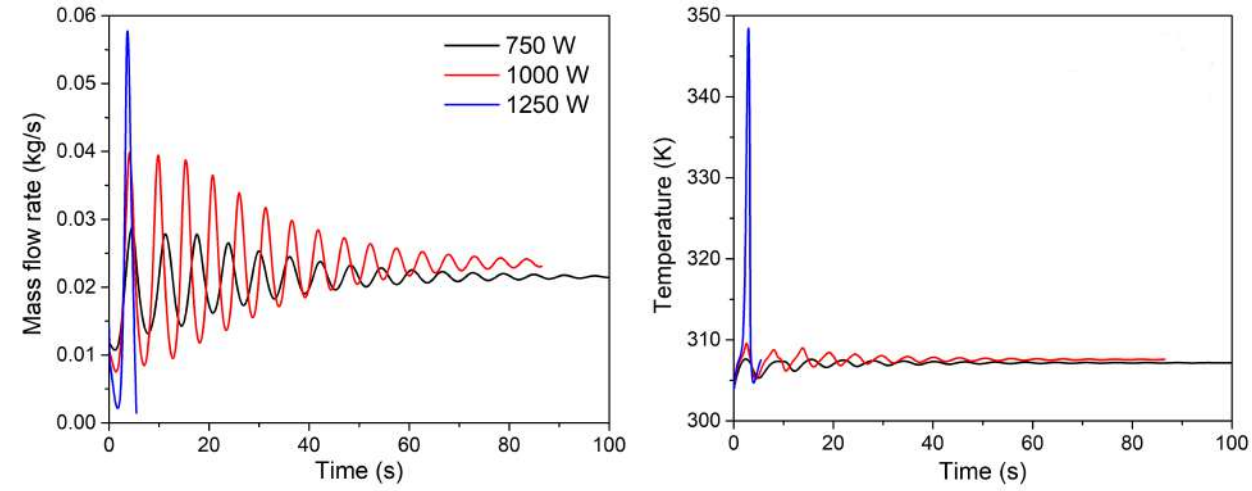

(a) Step input

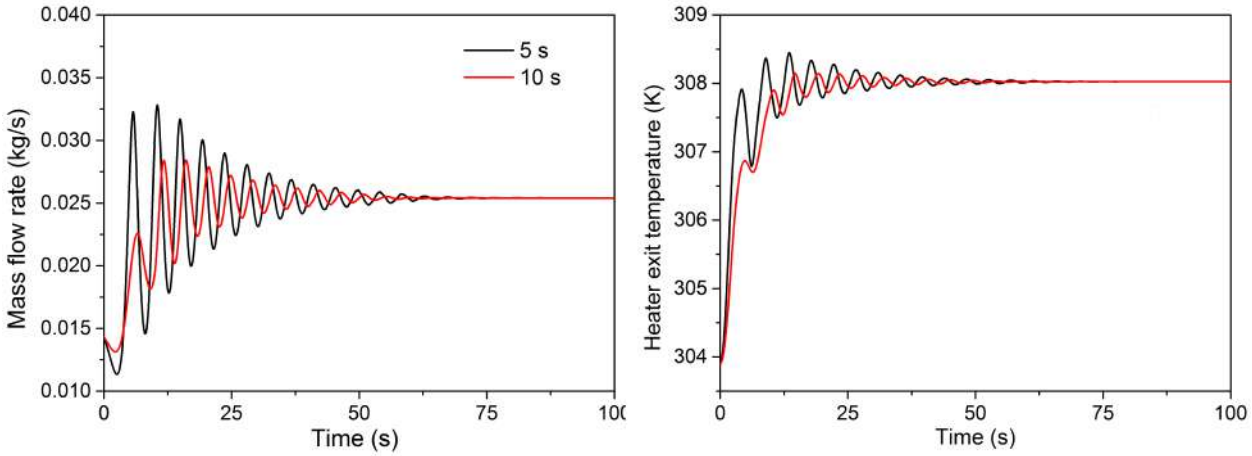

(b) Ramp input

Fig. 4.15: Evolution of mass flow rate and heater exit temperature after (a) step rise (b) ramp-rise from steady-state base power = 250 W

.

However, in the current scenario of flow reversal, where the fluid's condition was extremely close to the T_{pc}, a tiny change in energy content can cause a significant modification in

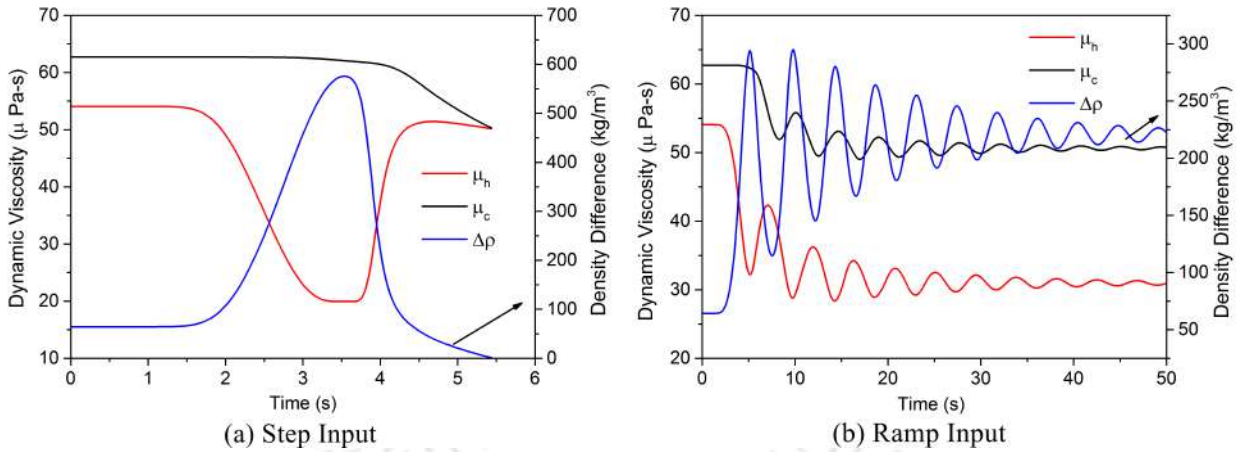

Fig. 4.16: Temporal variation of density differential between the vertical arms and corresponding individual dynamic viscosity for the respective cases of Fig.4.15

thermophysical properties, leading to a rapid shift in the forces involved. The increase in CO2 temperature throughout the heater, suddenly increases, causing the driving forces to fluctuate significantly as shown in the Fig. 4.16(a) of density difference and dynamics viscosity with time. The driving influence of CO2 dramatically decreased as the lowest fluid temperature approached T_{pc}, leading to an eventual reversal. During this brief period of time, CO2 temporarily adopted a gas-like form in the flow path. The same phenomenon is followed by the cases discussed in the subsequent section. Since the change in power is substantially high in this case, the phenomenon can be easily understood. Comparatively, the extent of buoyancy generation and reduction in friction does not happen in the case of ramp heating and hence, does not causes the sudden flow reversal showing the balance of involved forces. Fig.4.16(b) shows the variation of the same properties for the ramp input case, which signifies that even under the high transition in heating power with low t_t.

Though the buoyancy generation is promoted, on the other hand, the viscosity does not drop due to the lowest temperature being significantly below the T_{pc}, which eventually leads to the balancing between the two forces leading to stable condition. This interpretation leads us to conclude the stable nature of the ramp heating profile over the step-up profile.

• **Changeover within enhanced heat transfer regime**

The base (1000 W), as well as the targeted power in this case, lies in the enhanced heat transfer regime. This is the safest operation zone without FiHTD concern and enriched thermal-hydraulics characteristics. Generation of buoyancy is supported as the average-loop temperature approaches T_{pc}. If the base power is close to its entrance zone (i.e., ∼350 W), a large step-rise is possible, similar to the previous case, and the expected stable nature is

viable. But, if we start substantially away from this point with the base power of 1000 W, the window of power transition depletes in comparison. As seen in Fig. 4.17a, we witness the neutral state also, which occurs for the step rise of 450 W from the base power. Any power after this will result in flow reversal after repeated oscillations. The higher the step, the sooner the reversal will be due to the $\dot{q}$ = 1450 W being quite close to the stability threshold ($\sim$ 1500 W), which was obtained by previous work of Srivastava and Basu[153]. Since friction is the limiting factor, it will try to reduce the fluctuations, whereas buoyancy is the driving force and amplifies the vacillation, which leads to instability. Due to being close to the stability threshold, Therefore, if the initial perturbation increases friction more than buoyancy, the overall response will be stable; if not, it will be unstable.

For this particular case, the final state of fluid after the application of increased power was very close to T_{pc}. The enormous variation in thermophysical properties brought about by this change in energy content resulted in a rapid modulation of the associated forces. As shown in Fig. 4.17a, the CO_2 temperature across the heater suddenly increases, allowing the driving forces to alter quite significantly. The driving influence of CO_2 dramatically decreases as the lowest fluid temperature approaches T_{pc}, leading to an eventual reversal in the primary flow direction. During this brief period of time, CO_2 temporarily assumed a gas-like representation throughout the flow path. The same conclusions can be reached by looking at the phase portraits shown in Fig. 4.18. As shown by the trajectory sticking to a succession of circles with continuously decreasing diameters, which is the feature of a stable system [157], the attractor intends to converge to a single point with time for $\dot{q}$ = 1425 W. However, the trajectory for $\dot{q}$ = 1444 W follows a diverging trend, shown by the constant increase in the diameter of the succeeding circles. At $\dot{q}$ = 1450 W, which represents a neutrally stable system and can be seen as the point of transition toward instability, a closed orbit is generated. Here, changes in buoyancy and frictional forces are of the same order, with periodic dominance for each force which causes a prolonged oscillation. Following the variations over time from Fig.4.19, it is possible to estimate the temporal evolution in the corresponding buoyancy fields. While the density differential gradually decreases for $\dot{q}$ = 1400 W, it steadily increases for $\dot{q}$ = 1450, supporting the steadily increasing buoyancy dominance. It is analogous to the phase portrait. With the same analogy as the previous one, the ramp input showed a wide stability zone for the targeted power (1450 W) for all the t_t considered (Fig.4.17b). This signifies the positive impact of the ramp input over the step surge. Since the disturbance rises slowly in the ramp signal till the targeted power, the chances of reaching the neutrally stable state are close to impossible.

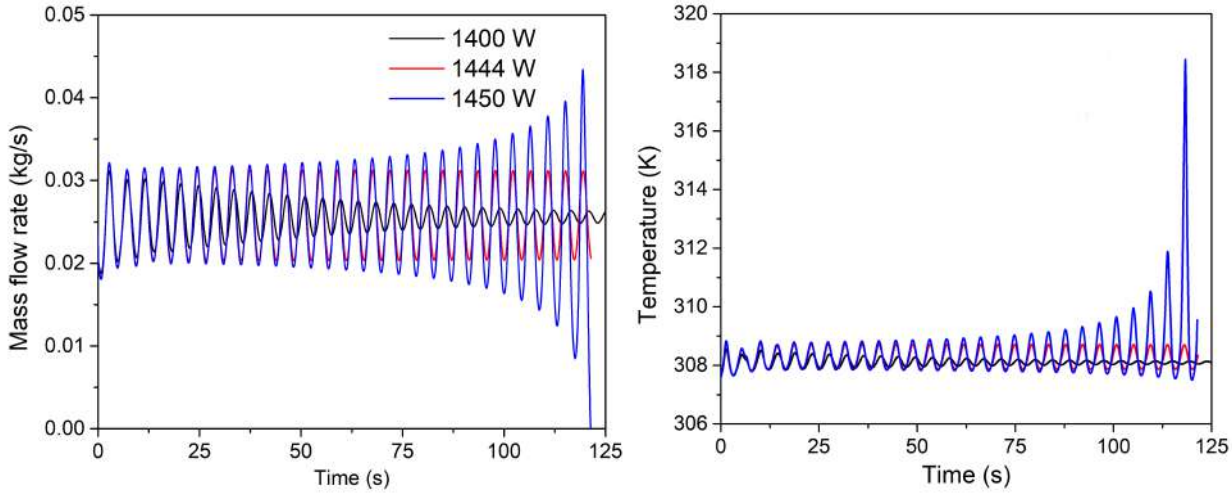

(a) Step input

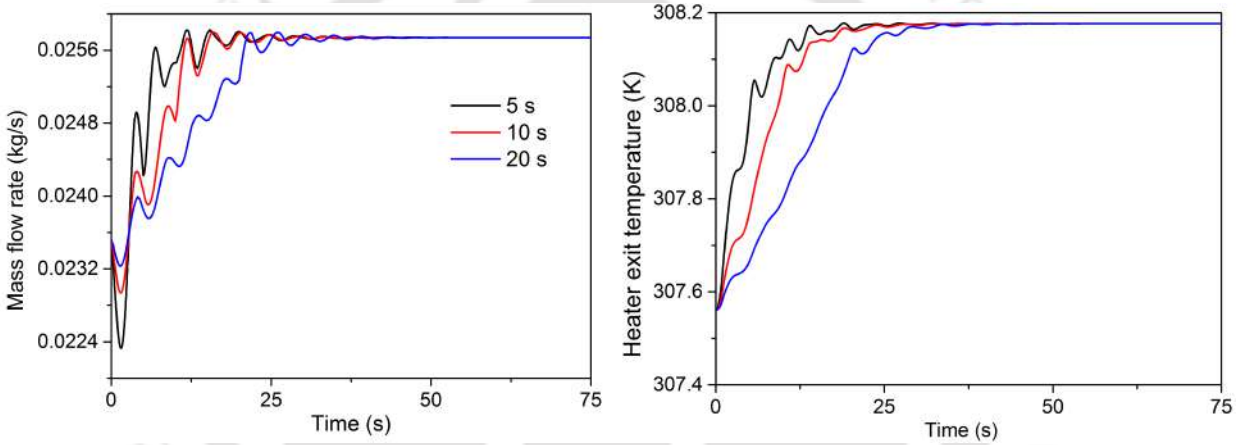

(b) Ramp input

Fig. 4.17: Evolution of mass flow rate and heater exit temperature after (a) step rise (b) ramp-rise from steady-state base power = 1000 W

• **Changeover from enhanced heat transfer regime to transition regime**

The boundary of the transition regime is close to the power level of 1500 W, which is also the stability threshold limit of the present model. Moving from enhanced heat transfer regime to transition, the advent of friction dominance begins, and the flow rate also tends to reach towards the maxima and then slowly starts decreasing till the rapid fall. Starting from 1400 W with the same operating conditions, the unstable zone was obtained for the step of the power greater than 50 W, with the neutral-state appearance at 1450 W as seen in Fig. 4.20a. It should be noted that the window for step rise is now further limited, which was ∼1000 W and ∼450 W in the previous two cases, which depleted further for this case.

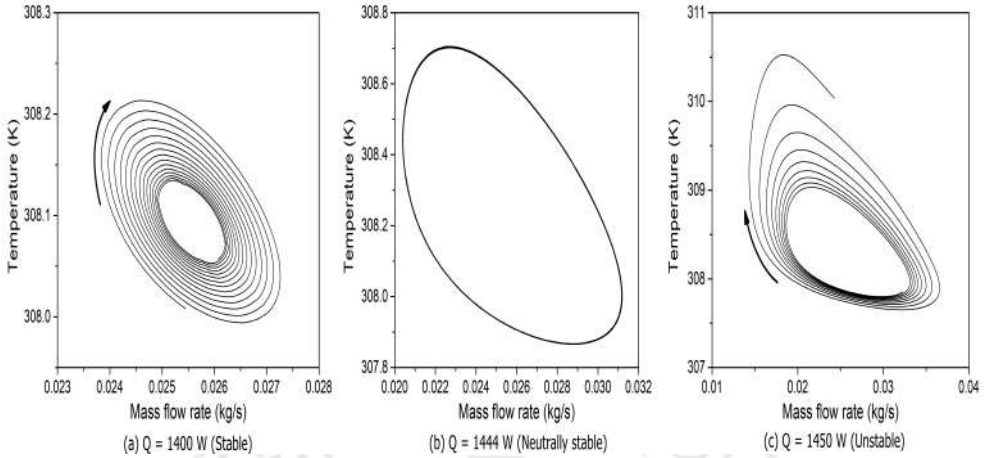

Fig. 4.18: Phase portrait corresponding to the temporal evolution for changeover within transition zone with base power = 1000 W

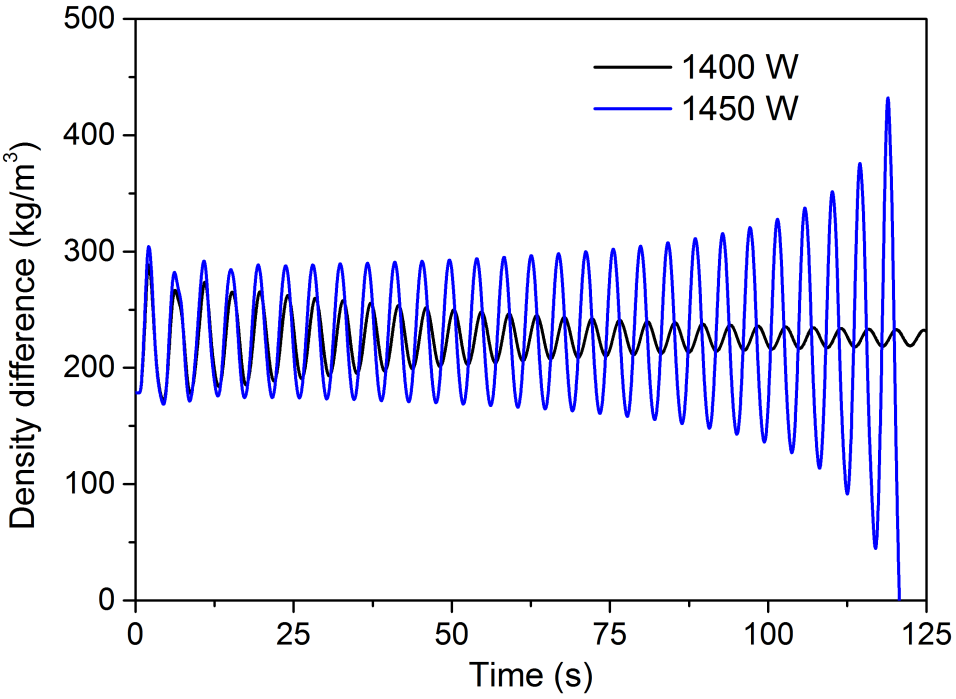

Fig. 4.19: Temporal variations in density differential ($\Delta\rho$) between the vertical arms for two different power levels for step rise from Q = 1000 W

The heater outlet temperature before the flow reversal shoots up to 355 K for a step rise of 150 W. Compared to the previous case, such a high temperature in the small window of the power rise shows the significance of properties variation before and after the T_{pc}.

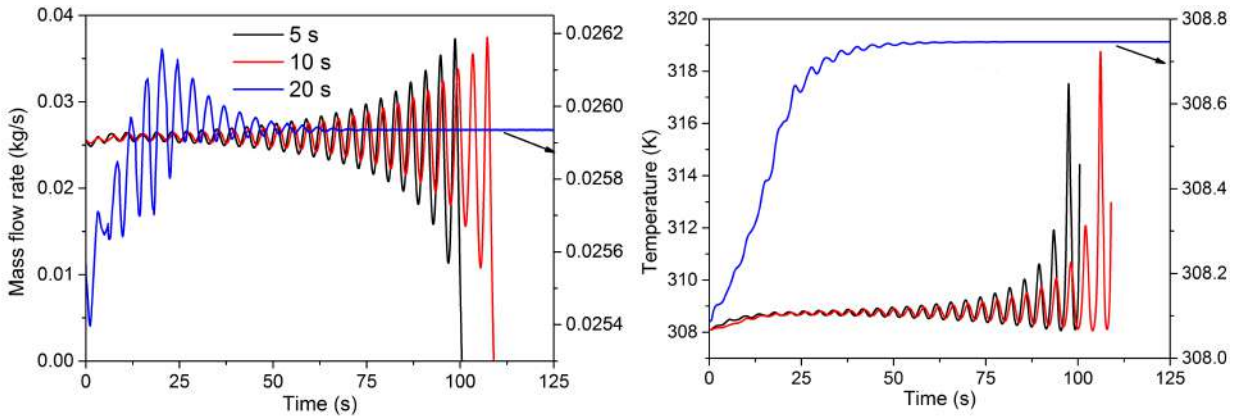

(a) Step input

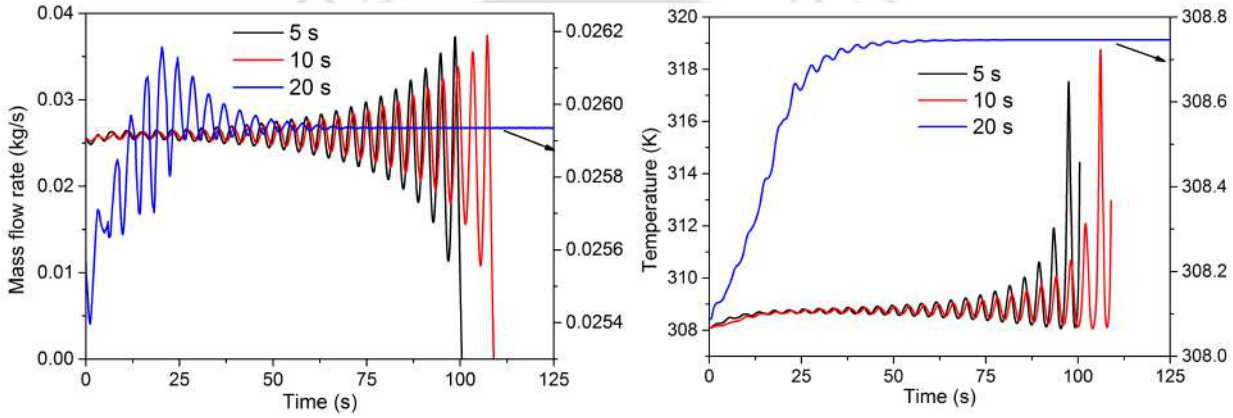

(b) Ramp input

Fig. 4.20: Evolution of mass flow rate and heater exit temperature after (a) step rise (b) ramp-rise from steady-state base power = 1400 W

.

While the ramp input allows some relaxation during the power surge, starting from the same base power of 1000 W to the targeted power (1550 W), a small t_t may bring instability in the system, which can be avoided by a high t_t of 20 s as shown in Fig.4.20b.

• Changeover within transition heat transfer regime

Due to the peak of the thermal expansion coefficient in this zone, buoyancy generation is at its highest because it is close to the pseudocritical temperature. As a result, the mass flow rate reaches its maximum. Moreover, it is inherently unstable at this base power level. From a base power of 1500 W, the system becomes unstable at a step rise of 25 W, as shown in Fig. 4.21a. Operating in this regime has no benefit logically as the stability is compromised in such a small range. Furthermore, the tight zone may contain a neutral stability state,

which is also elusive.

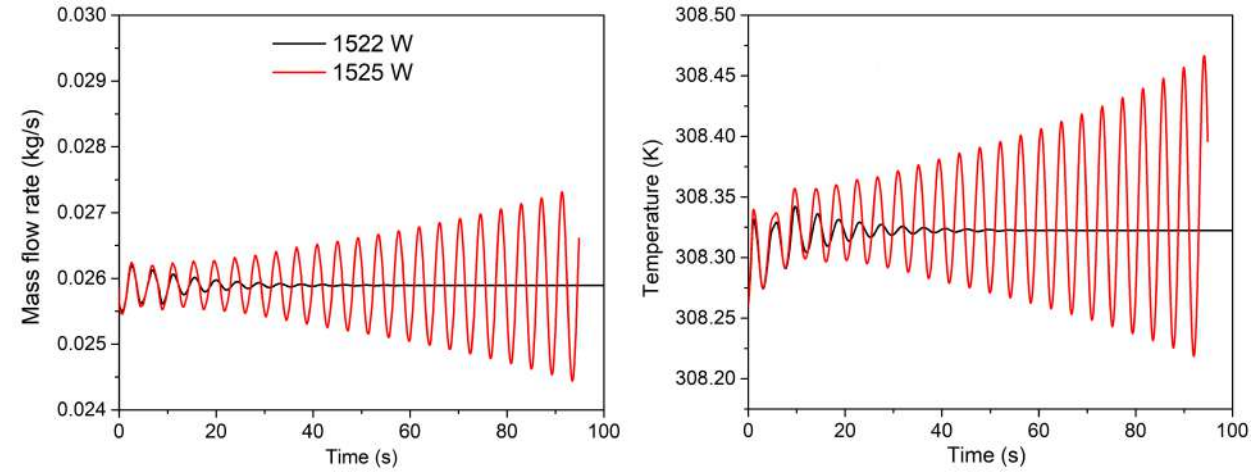

(a) Step input

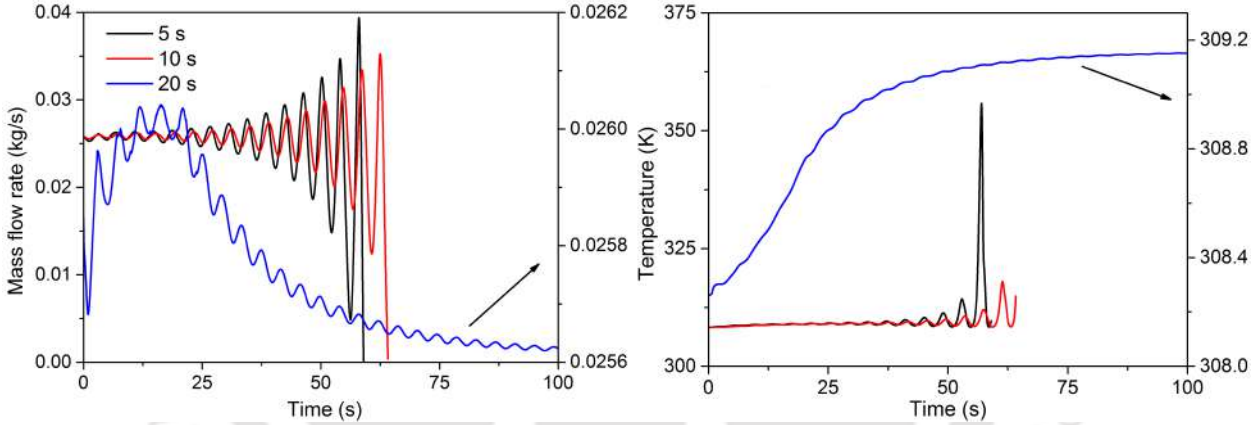

(b) Ramp input

Fig. 4.21: Evolution of mass flow rate and heater exit temperature after (a) step rise (b) ramp-rise from steady-state base power = 1500 W

.

The system displayed instability for the ramp transitions of 5 and 10 s, as shown in Fig.4.21b, while the slow transition of 20 s can make the system stable for the target power Q = 1675. If we contrast 5 and 10 s, the significance of t_t becomes abundantly clear. It is clear that right before flow reversal, the maximum temperature exceeds 350 K for $t_t = 5s$ while remaining below 350 K for $t_t = 10s$ s. The power is on the verge of the FiHTD zone, even in that case, ramp input provides safe operation which signifies the dominance of ramp input over step.

While each of the aforementioned possibilities can offer a qualitative assessment of the

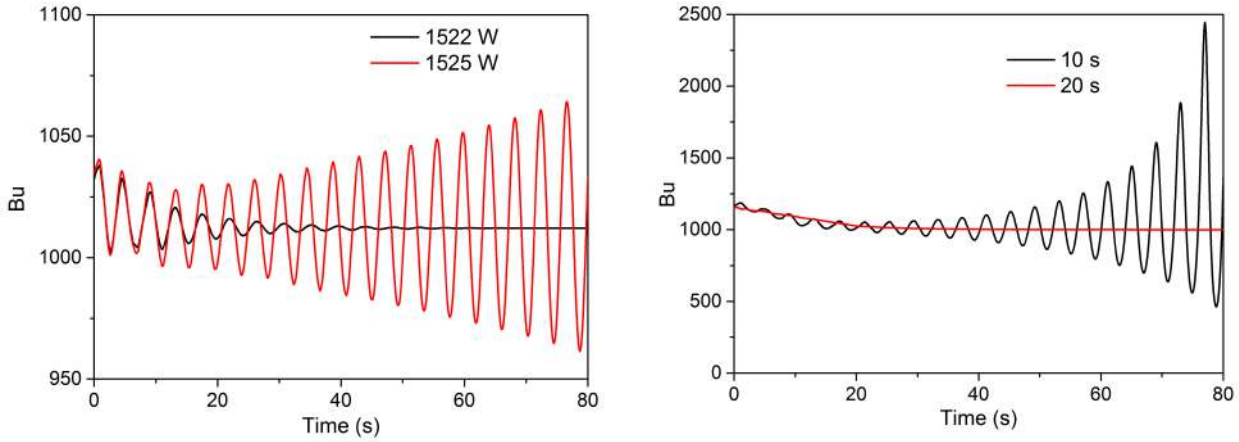

Fig. 4.22: Temporal variation of density differential between the vertical arms and corresponding individual dynamic viscosity for the respective cases of Fig.4.21

nature of flow (improved or worsened), it is not possible to have any quantifiable estimates because this would require a combination of buoyancy and friction. Earlier configurations involving mixed-type flow employed the idea of buoyancy parameters. The same is used here for pure natural convective motion by defining the ratio of the two involved forces as,

$$Bu = \frac{Gr_m}{Re_{ss}^2} \tag{4.1}$$

Exploring the reason for such behavior using Bu gives insight because it is the combination of all the concerned properties. We witnessed that for the rise of 22 W in heating power, the buoyancy rises while, on the other hand, friction pretty much remains the same and does not allow the oscillation to grow, hence stable oscillations. While for the slightly higher step rise of 25 W, friction got much more affected compared to buoyancy force. The buoyancy portrayed the elevated behavior as expected, while the friction could not sustain its stable nature, and diminutive oscillation caused alterations in the flow field that ultimately caused instability.

Moreover, since heating power close to the deteriorated heat transfer zone is on the verge of friction dominance, a slow transition gives enough time for the friction to settle itself down with buoyancy. Due to this, we witness the peak in the mass flow rate because of the sudden peak in buoyancy followed by its suppression by friction. The system remains stable if the target power causes FiHTD in the deteriorated heat transfer regime owing to friction dominance. However, this region of operation is not intended to operate from a safety perspective because the bulk temperature is appreciably high, and the mass flow rate

is too low in the deteriorated regime. This is why it is best to operate in the enhanced zone, where buoyancy force dominates.

4.4 Summary

A thermalhydraulics response of the sNCL has been investigated under time-varying periodic, and a periodic heating profile has been investigated after allowing the system to reach steady-state conditions. The zone of operation has a crucial role in such systems under dynamic loading. The transition zone, especially close to deteriorated heat transfer zone, is very much susceptible to flow reversal. During the transition from one region to another, the interaction of buoyancy and friction force is responsible for the system dynamics. The key findings are as follows-

- The system displayed different types of transient responses depending on how long the imposed sinusoid lasts. While some of them can be quite erratic, others have the propensity to repeat themselves over time. Though if the system is allowed to oscillate for a long enough time, the system may show the double periodic behavior, depending upon the zone of operation and amplitude and time period imposed. Moreover, During the chaos, the natural locking phenomenon, while at a higher time period, the frequency pushing was observed in the double periodic region. Phase portrait and Poincaré map also depict the chaos and two closed cycles for the double period case.

- Mean power very close to the deterioration zone with higher amplitudes that cause deep penetration inside deteriorated heat transfer regime, after the flow reversal for a large range of time period, flow rate drops even at higher time periods, which was termed as FiHTD. Hence, it is interesting to see that FiHTD got delayed in such a condition.

- In the case of ramp or step heating profile, when the transition takes place from low to enhanced heat transfer regime, the change in power of higher magnitude is possible. Sudden buoyancy generation does not hamper the system's stability in such cases. The amplitude of oscillation depends upon the extent of buoyancy generation. The zone of power transition depletes when the transition takes place within enhanced or from enhanced to transition heat transfer regime. Since the step rise is sudden, the neutral stability state was observed, while in the case of a gradual rise, no intermediate state

was witnessed. Higher transition time in the ramp allows the relatively slow properties to shift, making such a system more reliable compared to the step heating profile.

Chapter 5

A Numerical Investigation on the Startup Transients in a Supercritical Natural Circulation Loop

5.1 Preamble

Initiation of motion in natural convective flow systems has traditionally been an intricate and onerous thermofluidic conundrum, owing to the implicit coupling between the buoyancy and viscous forces, and capricious nature of the phenomenon itself. While the development of an unstable density gradient in a body force field is theoretically necessary and sufficient to induce motion in an unbounded or partially-bounded domain, complete depiction of the flow field is a strenuous task. Closed form analytical solutions are possible only for demonstrative cases, recommending numerical appraisal with any deviation from the imposed assumptions. A natural circulation loop (NCL) introduces further complexity by facilitating flow within a closed circuit through the installation of a heat rejection segment, placed at a higher elevation in a gravitational field. It is impossible even to preconceive the direction of motion for a symmetric NCL, with the circulation rate being reliant on thermofluidic properties of the fluid, geometric dimensions, imposed boundary conditions, orientation with respect to gravity, extent of external influence, and numerous other factors. As elucidated by Zvirin [13], the rest state of a simplified thermosyphon is unconditionally stable when the modified Rayleigh number is less than a critical value, suppressing any perturbation. This is consistent with the classical *Rayleigh theory*, which confers about the role of fluid viscosity in stabilizing a layer of fluid subjected to an unstable density gradient. The limiting Rayleigh number was

postulated to be 1708 by Jeffreys [12] for incompressible fluid bounded by two infinite parallel plates. It is, however, implausible to converge on any such limit for a convoluted system like NCL, unraveling a wide domain of sustained investigation.

A significant amount of research effort has, accordingly, been channelized in the previous century to explore the start-up transients and subsequent stability response for both the single- and two-phase versions, with noticeably lesser attention to the mechanism of flow initiation from rest. The first plausible explanation regarding the emergence of instability in a thermosyphon with a point heat source and a point heat sink can be accredited to Welander[26], and his hypothesis was thereupon authenticated by the experiments of Creveling et al. [24] on a toroidal loop. The concept of stability in single-phase NCLs gradually expatiated through the varied contributions from numerous groups over the subsequent decades [36, 158–161], resulting in a rich knowledge base. Observation of unstable oscillations in a two-phase NCL dates back even further to the pioneering study of Wissler et al. [23] and the seminal exercise of Boure et al.[14] in categorizing multiphase instabilities into the static and dynamic modes based on the inherent microdynamics. The dynamic instabilities have received particular attention, as they involve abstruse interactions between multiple field variables [15, 56], resulting in significant runtime influence on real-life appliances and large volume of literature deciphering the same [16, 162].

The physics ingrained in spurring motion in a quiescent NCL, especially the geometrically-symmetric one, however, lacks the requisite deliberation. The simplified analytical approach of Zvirin [13], based on the hypothetical configuration of a pair of insulated vertical branches connecting two reservoirs, derived a critical Rayleigh number of 6. The rest state was always unstable beyond this limit, characterized by the development of local Rayleigh-Bénard cells. He asserted the same limit to be valid for a system with more than two parallel vertical arms [163], whereas postulated it to be a function of the modified Biot number in a toroidal configuration [164]. Bau and Torrance [158], however, found no critical value for an open loop, discerning the rest state to be unconditionally unstable. No concentrated analytical effort can be perceived in literature to resolve this discord. The exhaustive experiments of Vijayan et al.[39], though, noted considerable deadtime prior to flow initiation in a symmetric configuration, which suggests the appeasement of some critical condition, alongside possible hysteresis and strong dependence on the orientation. Similar conclusions were drawn by Misale et al.[38] as well, emphasizing on the role of thermal conduction under the stagnant condition. A pseudo-conductivity model was subsequently developed by Kumar et al.[165, 166], forecasting the enhancement in diffusion through scaled expressions for

local convection currents and claiming successful replication of startup from rest. However, several simplifying assumptions, specifically the adoption of constant fluid properties and Boussinesq approximation, which are not valid for temperature variation in excess of 10^{o} [167], limits the reliability of their model in explaining the true mechanism.

A boiling NCL needs to cogitate several additional factors, owing to the substantial disparity in thermalhydraulic characteristics with change in flow regimes and nonlinear relationship between the mass quality and void fraction. Therefore, as noted by Vijayan et al. [168], analytical or simple numerical approaches generally are futile, emphasizing on experiments and multidimensional system codes. While a two-phase loop can simultaneously experience multiple types of mutually-dependent instabilities during startup [169], it is often difficult to experimentally segregate each because of the dearth of local-level information. Besides, the dominant mode of instability can strongly rely on the prevailing operating conditions [170–172], emanating into periodic oscillations with multiple fundamental frequencies or even chaotic fluctuations, accordingly making it near-impossible to envisage the underlying physical procedure. The adoption of computational tools has, therefore, been a favored approach in comprehending the startup characteristics of two-phase NCLs, often authenticating their methodology with available experimental trends and then expatiating into the fundamentals [173–175]. That has helped in evolution of a more mature knowledge base regarding flow initiation in multiphase loops.

No attempt can, however, be recognized in open literature to envisage the initiation of motion and startup transients in a supercritical NCL. As discussed above, it is not possible to predict the direction of first bulk movement and even the time required to arrive there from the initial stagnant condition in a symmetric orientation. Vijayan et al.[102] noted reduction in startup duration with increase in loop inclination, emphasizing on the role of gravity, but without more focused inspection. Zvirin[13] delineated the initiation of bulk motion as a specific kind of instability for a single-phase loop, while quite a few analytical criteria were also proposed, as elaborated earlier. It may not be theoretically feasible to converge on any such limit for a supercritical system, owing to the strongly nonlinear property variations. But, intriguing flow physics are expected because of the steep property gradients adjacent to both the heater and cooler walls, especially as the flow approaches T_{pc}, and strong local buoyancy effects. The unique approach of Wahidi et al.[176] to explain the emergence of bidirectional pulsing through the transport and diffusion of hot/cold plugs is relatable, but limits the deliberation solely to periodic flow reversals. Chen et al.[97] associated the same concept to the periodical changes in the pressure field and ensuing flow reversals, whereas

the numerically-developed transient traits in [177] were inferred primarily from the heat transfer perspective. Present study focuses on filling the void by exclusively focusing on the initiation of motion in a symmetric rectangular NCL with supercritical CO_2 as the working fluid. The thermal and hydrodynamic fields will be monitored starting from the quiescent condition, and the underlying physics, specifically pertinent to the supercritical fluid, will be unearthed. Effort will be made to define some appropriate criterion to predict the instant of flow initiation.

5.2 Geometry and Mathematical Formulation

5.2.1 Geometric details

As mentioned above, present study concerns a rectangular NCL, and schematic of the same is presented in Fig. 2.1, along with the relevant dimensions. The system receives energy from an external heater, which can be visualized to be mounted on the bottom horizontal arm, resulting in a constant-power-input. Cooling is facilitated along the top horizontal arm through an external heat exchanger installed around it, which simulates an isothermal boundary condition. Remainder of the loop wall is ideally insulated. The configuration, accordingly, is perfectly symmetric with respect to the downward gravity.

5.2.2 Conservation equations

Unsteady versions of the two-dimensional conservation equations are solved here with appropriate initial and boundary conditions. Corresponding equations are summarized below.

$$\frac{\partial \rho}{\partial t} + \frac{\partial}{\partial x_j}\left(\rho u_j\right) = 0 \tag{5.1a}$$

$$\frac{\partial}{\partial t}\left(\rho u_i\right) + \frac{\partial}{\partial x_j}\left(\rho u_j u_i\right) = -\frac{\partial p}{\partial x_i} + \frac{\partial \sigma_{ji}}{\partial x_j} + \rho g_i \tag{5.1b}$$

$$\frac{\partial}{\partial t}\left(\rho h\right) + \frac{\partial}{\partial x_j}\left(\rho u_j h\right) = \frac{\partial}{\partial x_j}\left(\lambda_{eff}\frac{\partial T}{\partial x_j} + u_j \tau_{ji}\right) + \dot{S}_E \tag{5.1c}$$

Here a linear stress-strain relationship is assumed and hence,

$$\sigma_{ji} = \mu_{eff}\left(\frac{\partial u_j}{\partial u_i} + \frac{\partial u_i}{\partial u_j} - \frac{2}{3}\delta_{ij}\frac{\partial u_k}{\partial u_k}\right) \tag{5.2}$$

The energy source terms $\dot{S}_E$ refers to the external interactions. It is positive along the walls of the heater section and is directly proportional to the power catered by the external heater. Similarly, it is associated to the convective energy transferred to the cooler in the upper horizontal arm, and zero elsewhere.

5.2.3 Numerical approach

The finite-volume framework of ANSYS-Fluent is employed for solving the governing equations, starting from the stagnant condition and initializing the fluid over the entire domain with the sink temperature and system pressure. Second-order spatial and first order temporal discretization is adopted. The pressure-velocity coupling at every time step is resolved using the PISO algorithm, where the PRESTO scheme based spatial discretization is followed for the pressure term. The convergence criterion is set as 10^{-3} for each of the field variables, apart from energy, which demands a more stringent yardstick of 10^{-6}.

Precise estimation of each and every thermophysical properties of relevance is critical in any analysis involving supercritical fluid, considering the possibility of encountering steep property gradients in certain segments of the computational domain, especially interior to the thermal boundary layer. The NIST standard reference database [119] is widely regarded as the most comprehensive and reliable one of its kind for industrial fluids, and the same can be invoked in a Fluent session by activating the real gas model. That consequently overrides the inbuilt property relations, and estimates the requisite parameters at every computational node as functions of local instantaneous pressure and temperature with high accuracy even around T_{pc}. Reportedly, the maximum uncertainty in predicting density, dynamic viscosity and thermal conductivity for CO_2 are $\pm 0.05\%$, $\pm 0.3\%$ and $\pm 1.19\%$ respectively, which are adequate for the present study.

5.2.4 Grid spacing and time sensitivity analysis

Precision of any transient numerical treatment relies on the choice of adopted grid and time spacing, both of which are again strongly coupled with each other. Structured non-uniform two-dimensional mesh is developed here over the entire domain, a glimpse of which can be found in Fig. 5.1 for the bottom left corner of the loop. Finer mesh is ensured near both the walls over the entire closed circuit, for accurate resolution of the boundary layers and also to capture steeper gradients of any flow variable. The level of refinement also ensures the recommended y^+ value of thirty or more, accordingly providing a basis for selection of the smallest obligatory mesh size. Identification of the most appropriate time step can

be of even greater importance. As demonstrated in the seminal work of Ambrosini and Ferreri [34], numerical diffusion introduced by incompatible combination of mesh size and time step can result in contradictory prediction about the stability characteristics for NCLs. Debrah et al.[109] suggested a maximum Courant number of 0.9, in order to minimize the numerical diffusion, and the same is secured in the present analyses as well. As a part of the sensitivity appraisal, steady-state simulations are performed for a heater power ($\dot{q}$) of 500 W and sink temperature (T_∞) of 295 K at a system pressure of 8 MPa. After the attainment of the steady-state condition, a perturbation of 10% is imposed on the heater power and the transient simulations are allowed to continue over a sufficiently long period, in order to ascertain the nature of transients. The impact of grid spacing is presented Fig. 5.2(a) for Δt = 0.05 s. No discernible change can be noted for upgrading the mesh structure from model 3 to model 4, despite nearly 66% increase in the resource requirement, and hence model 3 is continued with. It comprises of 143090 number of computational nodes to be exact, with the smallest characteristic dimension of 2.04 mm, and exhibits quite amicable credentials, such as orthogonal quality of 0.998 and skewness of 0.112.

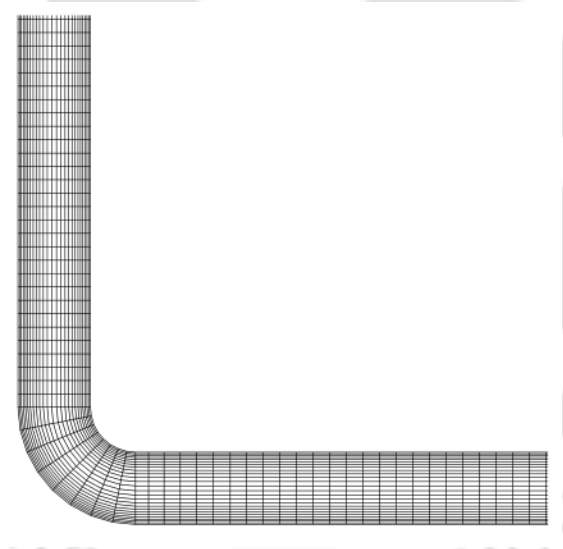

Fig. 5.1: Pictorial view of the grid system selected for the present numerical simulations around the bottom-left bend of the loop

Time step can, however, visibly have a stronger influence on the prediction. A very large value such as 0.25 s dampens the flow fluctuations, under the influence of the artificial viscosity, predicting a stable system, which contravenes the inference with smaller Δt. Reduction in the time step from 0.01 s to 0.0075 s induces only a minor change in the amplitude of the oscillating circulation rate. That, however, does not alter any of the conclusions reported

later in the present study, and hence, a time step of 0.01 s is continued with for the subsequent discussion. Similar exercise has been performed at other power levels as well, and the reported combination of grid and time spacing is found to be adequate for the entire range of operating conditions explored here, while also satisfying the Courant number criterion consistently. Morevover, the implicit scheme has been used in the to for updating the properties in each time step.

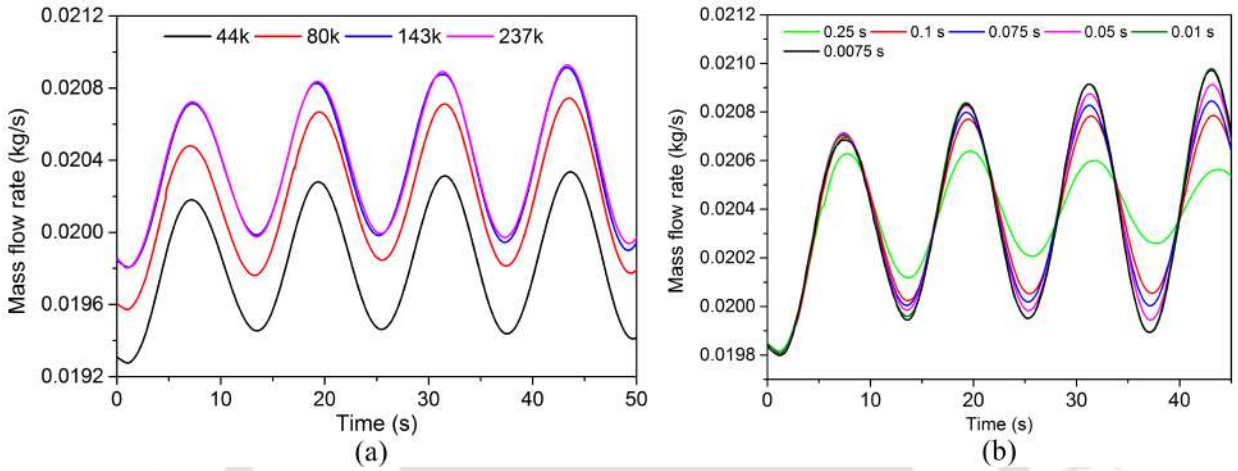

Fig. 5.2: Effect of selection of grid and time spacing on the transient response of the system, after imposing 10% perturbation on the steady-state heater power at $p = 8$ MPa, $\dot{q} = 500$ W and $T_\infty = 295$ K; (a) effect of mesh size at $\Delta t = 0.05$ s and (b) effect of time step for system with approximately 143k nodes

5.2.5 Numerical validation

As a final preparatory step, it is important to engage the developed numerical framework for reproducing crucial interpretations from literature. While the focus here is on transient characterization, the first step of validation is facilitated under the steady-state condition, *i.e.*, by solving equations 5.1(a-c) without the temporal terms. The flow-power relationship amicably adheres to the well-celebrated experimental correlation from Swapnalee et al.[104], which was developed encompassing several supercritical fluids under varied operating conditions and also for several loop orientations. At $p = 8$ MPa and $T_\infty = 295$ K, present set of steady-state data can be reconciled to the form $Re_{ss} = 4.0596 \left(\frac{Gr_m D}{L_t}\right)^{0.406}$, where $Gr_m = \frac{g\beta D^3 \rho^2 \dot{q} H}{A_{cs} \mu^3 c_p}$, and D, H and L_t refer to the pipe diameter, loop height and total circulation length of the loop, respectively. Each of the fluid properties is estimated corresponding to the thermodynamic state at the heater center. The minor deviation observed here can

be attributed to the simple property relations incorporated in the original model, as well as the selection of frictional law thereof, and is consistent with several recent studies, which also perceived similar level of discrepancy [126, 127, 178]. The dimensional flow-power characteristic also complies with the earlier three-dimensional model from the authors [153], as can be evidenced from Fig. 5.3, clearly demonstrating the realization of each of the three major regimes of operation, with minor shift in the concerned transition levels owing to the elimination of the azimuthal variation in a two-dimensional configuration.

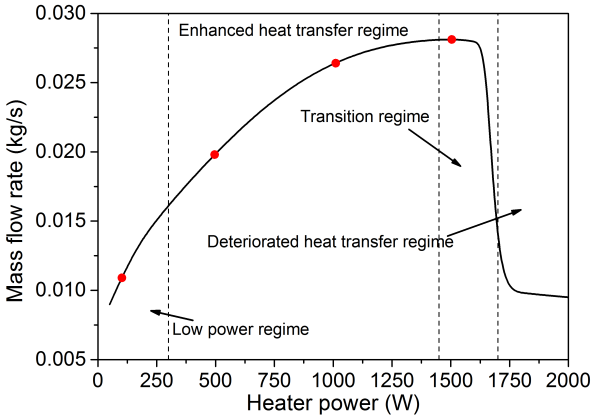

Fig. 5.3: Variation in steady-state circulation rate with heater power ($\dot{q}$) at $p = 8$ MPa and $T_\infty = 295$ K, illustrating different regimes of thermalhydraulic operation and the appearance of deterioration in mass flow rate; power levels selected for subsequent analyses are marked with solid circles

Transient validation is a more convoluted task, considering the reliance of the predicted magnitudes of the instantaneous flow parameters on both initial and boundary conditions, as well as the computational facets, such as the rate and direction of propagation of the numerical errors. Therefore, only qualitative comparisons are realistically feasible and the same is attempted here by simulating the startup transients at three different power levels. Concerned variations in the circulation rate with time, starting from a perfectly stagnant condition, are presented in Fig. 5.4, where $t = 0$ refers to the instant of imposing the thermal boundary conditions. At low power levels represented by $\dot{q} = 100$ W, the loop promptly stabilizes, after a pair of flow reversals, as is manifested by the gradually subsiding circulation rates. Here a positive magnitude of flow rate corresponds to the counterclockwise direction. After a sustained period of apparent inactivity, steep increase in the circulation rate can be observed over the short span of 25 to 32 s, which is immediately followed by flow reversals, with the loop finally settling into steady counterclockwise motion. At intermediate-to-high powers, however, quite complicated fluctuating patterns, with repeated flow reversals, can

be observed. While the highest circulation rate consistently dovetails to the first instant of initiation of bulk motion, substantial variation in the transitional peaks can be noted on either directions. The trends are logically similar to the predictions of Deng et al.[126], despite considerable disparity in terms of both the loop dimensions and the external heat flux. Similar kind of chaotic oscillations with bidirectional pulsing have even been observed for single-phase NCLs as well [167]. It can, therefore, be surmised that the developed computational structure can lead to logical deduction regarding transients in a supercritical NCL, transpiring confidence on its use to reconnoiter the startup transients.

5.3 Results and Discussion

Prevailing nature of flow transients from an initially-stagnant condition can be envisioned from Fig. 5.4 at certain power levels, with each presenting a different perspective. As marked in Fig. 5.3, $\dot{q}$ = 100 W and 500 W belong respectively to the low-power regime and enhanced heat transfer regime, while $\dot{q}$ = 1500 W appears within the transition regime, accordingly being characterized by dissimilar steady-state thermalhydraulics. The same is applicable regarding the startup transients as well, which can amiably be elaborated following the time-dependent characteristics of temperature at the heater center presented in the right column of Fig. 5.4. At $\dot{q}$ = 100 W, temperature of supercritical CO_2 at the concerned location stays well below T_{pc}, accordingly adhering to the liquid-like nature. At 500 W, however, fluid temperature frequently fluctuates across T_{pc}, which can closely be correlated to the repetitive reversals in the direction of circulation. This particular operating condition, therefore, amply represents the alteration between the liquid-like and gas-like characteristics, with the bulk fluid primarily hovering immediately above T_{pc}. On the contrary, fluid temperature is noticeably greater than the pseudocritical limit at $\dot{q}$ = 1500 W, and hence always assumes the low-density behavior. Therefore, the nature of their startup transients and subsequent dynamics are expected to be distinct in terms of the underlying physics and demand separate deliberation. It must, however, be noted that each of the three demonstrations display a span of near-linear rise in fluid temperature, with no discernible bulk motion, to attain a magnitude higher than T_{pc}, which subsequently emanates into the first sign of fluid movement and an immediate flow reversal. The realized magnitude of maximum fluid temperature and time required to reach there, as well as the initial flow direction, though, remain contingent to the imposed heater power, and the same is cogitated below.

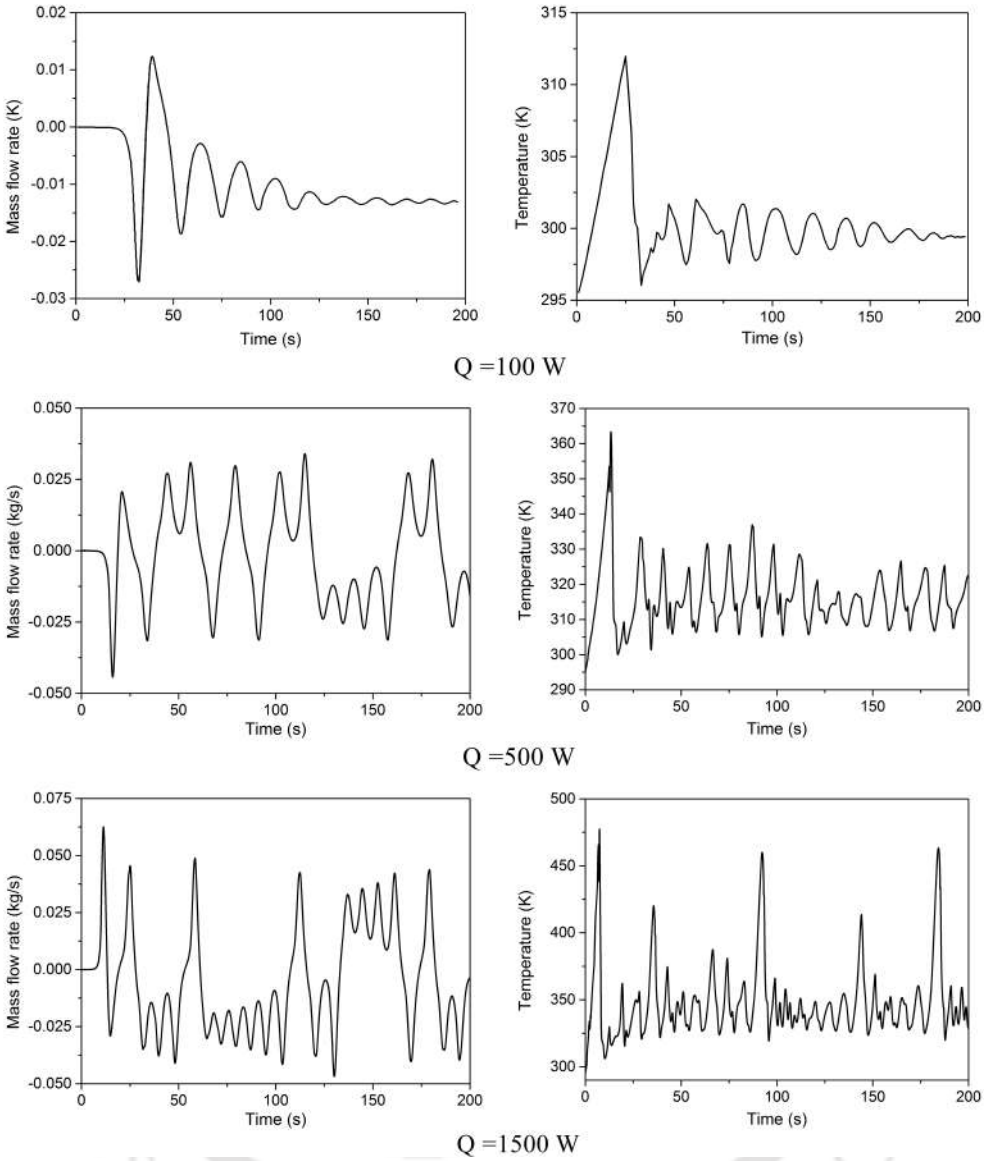

Fig. 5.4: Temporal variation in mass flow rate and temperature at heater center with three different power levels at $p = 8$ MPa and $T_\infty = 295$ K, starting from the quiescent condition; while the system promptly stabilizes at low-powers, complicated fluctuating patterns with repeated flow reversals can be observed at intermediate-to-high levels

5.3.1 Initiation of bulk motion

In order to get an early insight about the mechanism of flow initiation, transient simulation is performed with $\dot{q} = 100$ W, and a series of consequent snapshots at different time instants are presented in Fig. 5.5(a) to facilitate the deliberation. The imposed initial state of zero velocity and isothermal condition, with temperature being equal to $T_\infty = 295$ K, can

be endorsed from the profiles at $t = 0$ s, which exemplifies the complete fluid domain. Owing to the absence of bulk motion, conduction is expected to be the sole mode of heat transfer and, despite being in the high-density region ($T < T_{pc}$), thermal conductivity of supercritical CO_2 is reasonably weak ($\lambda \approx 90.176$ mW/m-K). That initiates the development of slender thermal boundary layers on both the walls of the heater section and raise in fluid temperature adjoining the walls, without any activity away from the heated surface. Increase in temperature lowers the density of the fluid particles ($\beta = 0.012075$ K^{-1} at 8 MPa and 295 K), inspiring an upward motion, primarily localized during the initial instants owing to the absence of any bulk motion. Particles diffusing upward from the bottom wall are expected to dissipate in the bulk, whereas fluid adjacent to the top surface virtually stagnates, allowing more prominent development of the thermal boundary layer there.

While this is true along the length of the entire heating section, the presence of discontinuity in the thermal boundary condition at both ends enforces a crucial intervention. The vertical marker in Fig. 5.5(a) indicates the left extreme of the heater ($x = -400$ mm) and the zone to the left of that has adiabatic walls. Fluid particles to its right and neighboring the upper wall are at a higher energy state relative to the other side, inducing an outward diffusion flux along the upper wall. That is clearly visible from the snapshot corresponding to $t = 1$ s. The fluid near the lower wall, however, is primarily inclined to move upward. So, no such outward potential is available there. The fluid, in fact, experiences a modest inward flux, which is necessary for locally satisfying the conservation of linear momentum, with stationary condition persisting over the entire fluid domain, apart from the heater ends. This hints at the development of local recirculation, and the same is discernible at $t = 2$ s, along with a recognizable boundary layer at the upper wall interior to the heater. The upward migration of the warm fluid from the bottom wall is also very much apparent. Consequently, fluid from the interior of the heater exhibits a propensity to move toward the nearer edge, with identical occurrence at both ends in a symmetric configuration, albeit with near-negligible magnitude for the initial seconds. The symmetrical nature of the flow domain during this span can be substantiated from the velocity vectors presented in Fig. 5.5(b) along both the edges of the heater at $t = 10$ s. The development in the other edge of the heater ($x = 400$ mm) is, therefore, not shown here to avoid repetition. The size of the recirculation vortices and the boundary layer thickness, specifically at the upper wall, as well as the velocity magnitudes, increase with time, and the vortex fronts, therefore, gradually encroach toward the heater center and the bends connecting the vertical arms. Gradual escalation in velocity level can be gauged following the change in the length of the vectors

in Fig. 5.5(a).

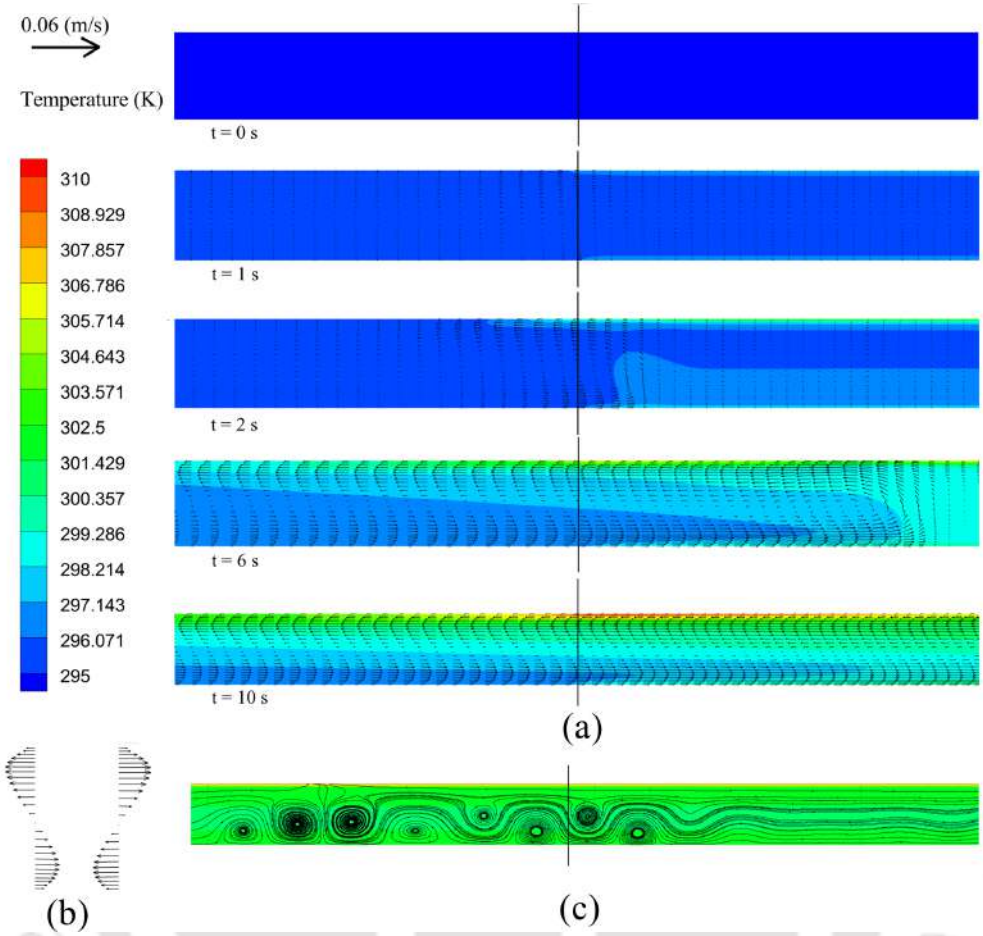

Fig. 5.5: Development of local motion in the bottom horizontal arm for $\dot{q} = 100$ W; (a) temperature contours and velocity vectors around the left edge of the heater ($x = -400$ mm) illustrates the appearance of a local recirculation owing to the disparity in thermal boundary condition at this point, which grows in size with time; (b) Velocity vectors at two ends of the heater at $t = 10$ s, demonstrating near-symmetric nature of the flow domain; (c) Appearance of irregular structures in the streamlines around the heater center at $t = 10$ s, where the vertical line denotes the central plane ($x = 0$)

The nature of streamlines around the heater center, presented in Fig. 5.5(c) at $t = 10$ s, however, is quite counter-intuitive. Considering the consonance in flow initiation at both the edges of the heater, and also absence of any boundary discontinuity around this location, the mid-vertical plane of the heater (marked by the vertical line in Fig. 5.5(c)) is expected to behave like a plane of symmetry, which is not accomplished here. Besides, the temperature distribution is also rather uniform over the entire flow passage under focus, barring a slender boundary layer on the top wall. This is unexpected with a poor conduction like supercritical

CO_2, and hints toward the presence of a second mechanism governing heat transfer in this region. The trend of evolution in temperature at several planes on the left adiabatic leg connecting heater and cooler with time, presented in Fig. 5.6, is also quite noteworthy. No change is expected there till the arrival of the hot fluid front. However, fluid temperature starts increasing uniformly over the entire segment from $t = 0$ s itself, and the homogeneity is maintained till about $t = 8$ s. Beyond this particular instant, the recirculation vortex from the heater enters the vertical arm, and surges upward, as is evidenced by the rapid raise in temperature at the lower bend. It is also interesting to note that the fluid temperature at immediate upstream to cooler begins to reduce gradually, despite absence of bulk motion. Warm fluid is unable to climb even half of the vertical distance till $t = 20$ s, as is substantiated by the considerable difference in temperature of CO_2 at lower bend and middle of vertical arm.

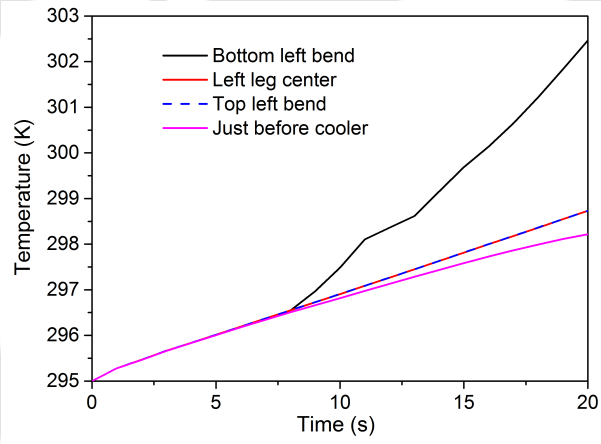

Fig. 5.6: Temporal variation in temperature at the mid-point of four different planes in the left adiabatic segment for $\dot{q} = 100$ W; Temperature increases uniformly over the entire region despite the absence of any bulk motion, indicating the role of adiabatic heating

It needs to be noted that the thermal diffusivity (D) of any supercritical fluid is quite small, and nearly vanishes close to the critical point. For the imposed condition of 8 MPa and 295 K, thermal diffusivity of CO_2 is only about 3.542×10^{-8} m^2/s. Consequently, heat transfer via diffusion is essentially a slow process with supercritical CO_2. However, significantly high level of isothermal compressibility under this condition, which can be four-order greater than any common liquid, allows to draw an analogy with the *piston effect* [179–181], and also provides a logical explanation to the above conundrum. Rapid expansion of near-critical fluid inside the thermal boundary layer and subsequent adiabatic compression of the bulk, resulting in temperature homogenization over a very short time

scale, was first observed under zero-gravity condition. Owing to the thermoacoustic nature of the phenomenon, energy from the hot wall transmits to the bulk nearly at sonic speed, with possible minor difference arising because of the dispersion effects. As demonstrated by Masuda et al. [182], rather than remaining relevant only near T_c, piston effect can be consequential over a wide range of pressure and temperature, if both compressibility and ratio of specific heats ($\gamma = c_p/c_v$) are high. Very important deliberation about the coupling of piston effect and buoyant convection was presented by Zappoli et al.[183, 184], subsequently establishing piston effect as an independent mechanism of heat transfer exclusively for near-critical fluids. While thermal homogenization is attained through the former within a short span, regardless of the level of active gravity, density inhomogeneity is relaxed slowly with the diffusion time scale, allowing the initiation of bulk convection. The difference between both the time scales can be of several orders, even at temperatures away from T_c, as demonstrated by Charlés [185], which perfectly conforms to the present study. Following the simplified thermodynamic approach of Onuki et al.[179], the generalized energy equation at the absence of motion and gravity can be written as,

$$\frac{\partial T}{\partial t} = D\,\nabla^2 T + \frac{\gamma - 1}{\gamma}\,\frac{\partial}{\partial t}\,\langle T \rangle \tag{5.3}$$

where, the spatially-averaged fluid temperature $\langle T \rangle$ involves contribution from both heat transfer and adiabatic compression. While Eq. (5.3) cannot resolve the scales for an intricate configuration like NCL, it sufficiently describes the importance of the second-term on the right-hand side for supercritical CO_2, with a meager value of D.

Rise in temperature of fluid interior to the adiabatic arm during the initial seconds (Fig. 5.6) can be explained now. While most of the seminal works on piston effect concerns fluid bounded in cavities [179, 183, 186], thereby having substantial geometric dissimilarity with the present configuration of a rectangular loop, it still involves near-critical fluid bound in a fixed volume. Hence, any energy interaction is expected to induce pressure and temperature relaxation, with the former being anticipated to adopt the acoustic time scale and maintain near-identical magnitude throughout the flow path at any given instant. That is indeed the observation here, with pressure difference across vertical legs remaining restricted to within mere 200 Pa. As observed above, temperature homogeneity is remarkable over the left leg, exhibiting almost a linear increase till interaction with the propagating front. It is a definite proof of *adiabatic heating* coaxed by the compression of supercritical CO_2 in the adiabatic section by the advancing vortex front. Identical behavior is observed at the right vertical

arm as well, which is illustrated in Fig. 5.7(a). Despite the absence of any bulk motion, CO_2 exhibits consistent rise in temperature, with no distinguishable variation in the radial or axial direction directions, accordingly endorsing the homogeneous nature in conjunction with Fig. 5.6.

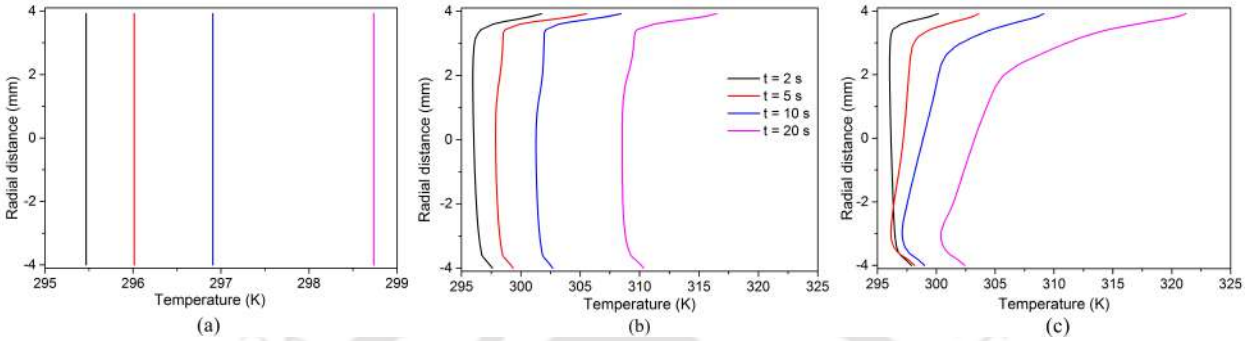

Fig. 5.7: Temperature variation in the radial direction at four different time instants for $\dot{q} = 100$ W at (a) mid-plane of the right vertical arm, (b) mid-plane of the heater, and (c) immediate upstream of the right edge of the heater ($x = 395$ mm); adiabatic heating results in perfect homogeneity in the first one and partial uniformity in the second one

Temperature of the fluid around the heater centerline (Fig. 5.7(b)), which is delimitated by two converging fronts from both ends of the heater, is enhanced via commingling of two different mechanisms. While CO_2 neighboring the heated surface absorbs energy directly from the walls, consequently forming the thermal boundary layer, temperature rise in the bulk is primarily because of the adiabatic compression. As mentioned earlier, boundary layer at the top wall is clearly more prominent compared to the same at the bottom wall owing to the impact of local buoyancy. The fluid outside these layers, however, is reasonably homogenized in terms of the temperature at every instant, with monotonic rise in magnitude. It is not possible to realize such uniformity, coupled with heat transfer, solely by conduction, specifically considering the rapid decline in thermal conductivity of supercritical CO_2 with temperature along an isobar and only moderate rise with pressure. This can be put into perspective by comparing with Fig. 5.7(c), which refers to a location in immediate downstream of the right edge of the heater ($x = 395$ mm), and so directly provides a measure of radial variation within the propagating front. Strong buoyancy and local convective effects are apparent in the temperature profiles, which are strengthened with time, engendering wide boundary layer and steep thermal gradients, particularly around the upper surface. The expanding zone not being under the influence of any compressive effect, thermal homogenization is not achieved, professing a markedly different characteristics. Temperature

rise because of adiabatic compression can, therefore, be earmarked as a crucial heat transfer mechanism for sNCL as well, which helps in augmenting energy content over the entire flow domain right from the instant of imposing external power.

The most notable impact of adiabatic rise in fluid temperature throughout the loop can be identified in the cooler section. It needs to be remembered that the complete domain is initialized with the sink temperature (T_∞), and no heat transfer can be envisaged in the upper horizontal arm till the warm fluid reach there. Subcritical single-phase NCLs experience the same as well. However, as deliberated above, fluid temperature rises uniformly in the adiabatic legs of sNCL, administering a potential for heat transfer at cooler much earlier than anticipated, and the same can be ascertained from Fig. 5.8. Development of slender thermal boundary layer and emergence of minuscule velocity vectors interior to the cooling section can be perceived as early as $t = 2$ s, which flourish into local recirculatory zones around the edges. The discontinuity in thermal boundary condition at two extreme ends of the cooler is pertinent here as well. Boundary layer growth is delayed here in comparison to the heater, which is logical considering the disparity in the mode of energy interaction. Present observation is comparable with the conclusions drawn by Masuda et al.[186] for natural convection involving supercritical water in a differentially-heated cavity. They reported the development of weak convection cells near the cold wall owing to the sudden rise in bulk temperature, leading to a unique two-cell convection pattern. The impact of natural convection, however, was predicted to remain completely decoupled, because of the substantial disparity in the associated time scales, and the same is evident for the present loop as well. This also construes the reduction in CO_2 temperature observed in immediate upstream of the cooler after $t = 8$ s (Fig. 5.6). As the freshly-developed vortex ventures outside the cooler, it absorbs energy from warm fluid in the adiabatic segment, causing a lowering in local temperature.

Temperature, and consequently density, differential can be quite substantial across the face of the propagating fronts inside the heater, specifically as the hot fluid temperature crosses T_{pc}. The relatively heavier fluid confined around the heater center is, therefore, continuously squeezed by the lighter medium from both sides. Such a competition between two piston effects can evoke a gravitational instability in near-critical fluid systems, having characteristics comparable with the Rayleigh-Taylor mechanism [187, 188]. For the imposed initial condition of 8 MPa and 295 K, the Schmidt number is only of the order of 10, owing to the vanishing level of the kinematic viscosity. It can be put into perspective by comparing with the Schmidt number of liquid water under identical thermodynamic state, which is

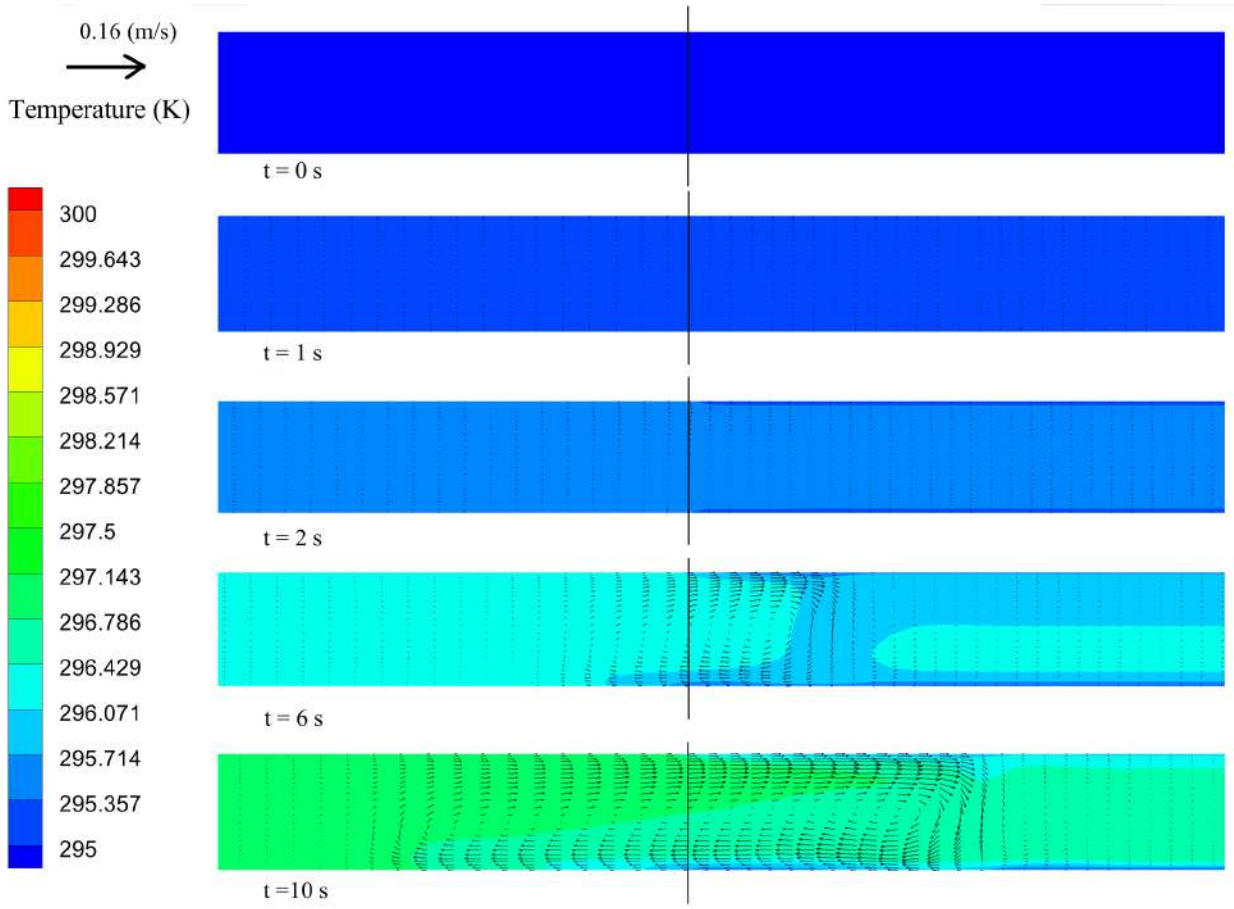

Fig. 5.8: Temperature contours and velocity vectors around the left edge of the cooler ($x = -400$ mm) for $\dot{q} = 100$ W, illustrating the development of local motion in the top horizontal arm without any interaction with the propagating front from heater

of the order of 10^3. Therefore, despite the single-phase-like nature of the flow field, two near-immiscible layers interact with each other at the upstream of both heater-side vortices. The local Rayleigh number is also in excess of 10^6 even for a minute temperature difference across the virtual interface, which leads to the development of irregular structures visible in Fig.5.5(c). Appearance of similar convective structures was also documented by Amiroudine et al.[188] on both the hot and cold walls of a square cavity. It needs to be remembered that both the upper and lower boundaries of the section under focus here have identical thermal condition, and the disparity in corresponding thermal boundary layers appears owing to the local buoyancy effect. Such a geometry is markedly different to the configurations explored in literature in relation with the piston effect till date. It is also unlikely to have similar scenario in a traditional single-phase NCL, as both the momentum and thermal diffusion are much

stronger, and local Rayleigh number can be only of the order of 10^3 with 1 K temperature difference. Therefore, such an evolution is unique to sNCL and is a novel observation as a part of the present study.

Because of the unstable nature of the phenomenon, the structures are often capricious and even chaotic, and oscillates around their position, offering varied degree of resistances to the advancing vortex fronts. Consequently, the extent of advancement of the propagating fronts interior to the heater or rise in the vertical arms can differ, which forces the loop to deviate from symmetry. A clear indication about that can be obtained from Fig. 5.9, which compares the nature of radial variation in velocity magnitudes at both ends of the heater for multiple time instants. Here, a negative magnitude signifies outward motion relative to the concerned ends, and inward movement correspond to a positive value. While both profiles essentially overlap for the initial seconds, minor difference in the upper half of the channel can be noted around $t = 12$ s, which only amplifies with time and escalates across the entire width. As can be discerned from the profiles at $t = 16$ s, CO_2 around the right edge is having a greater tendency to flow out of the heater in comparison with the other end of the heater, which eventually imparts a directional nature on the flow. That is more comprehensively illustrated in Fig. 5.10. The propagating front developing around the right edge of the heater being more prone to flow outward, the vortices don't meet at the heater center, as a direct consequence of the inherent instability. The point of congregation here is ascertained to be $x = 190$ mm, which is considerably toward the right of the heater center. As illustrated in Fig. 5.10(a), both the fronts can clearly be distinguished till around $t = 23$ s, with forward motion in the upper part of the channel, above a recirculatory zone. It is, however, perfectly one-directional motion from $t = 25$ s onward, and hence this juncture can be earmarked as the instant of initiation of bulk motion. Further endorsement can be obtained from Fig. 5.10(b), which traces the height of the vortices in the vertical legs. The propagating front reaches the corresponding bends around $t = 8$ s and rises almost linearly, albeit with a slightly higher level on the right leg, which suggests an early intervention from the instability induced by the piston effect. The deviation is more pronounced after $t = 16$ s. The warm fluid front at the left leg almost stagnates beyond $t = 20$ s and even approaches to descend, which is consistent with the commencement of counterclockwise bulk circulation. No distinguishable vortex fronts or region of recirculation can be identified anywhere within the loop after $t = 24$ s for the same reason. The rise in fluid temperature at the central point of the heater is quite interesting (Fig. 5.10(c)). It monotonously increases till $t = 24$ s, owing to the adiabatic heating and also energy received via diffusion from the neighboring layers.

A drastic reduction, though, can be noted at this instant, as advection starts to govern the rate of heat transfer and consequently the temperature levels. It can, therefore, be concluded that convection evolves into the primary mechanism of heat transfer only after $t = 25$ s for a power supply of 100 W, with phenomena similar to the piston effect and the Rayleigh-Taylor instability dominating the earlier time span, and also determining the first direction of bulk motion. It must also be mentioned that the direction of first movement is equally probable to be clockwise, *i.e.*, toward left, for a separate simulation with identical parameters, as it is affected by the instantaneous status of the unstable zone, and may also by the propagation of numerical errors to some extent. The underlying physics, however, essentially remains consistent to the above discussion for any combination of boundary conditions.

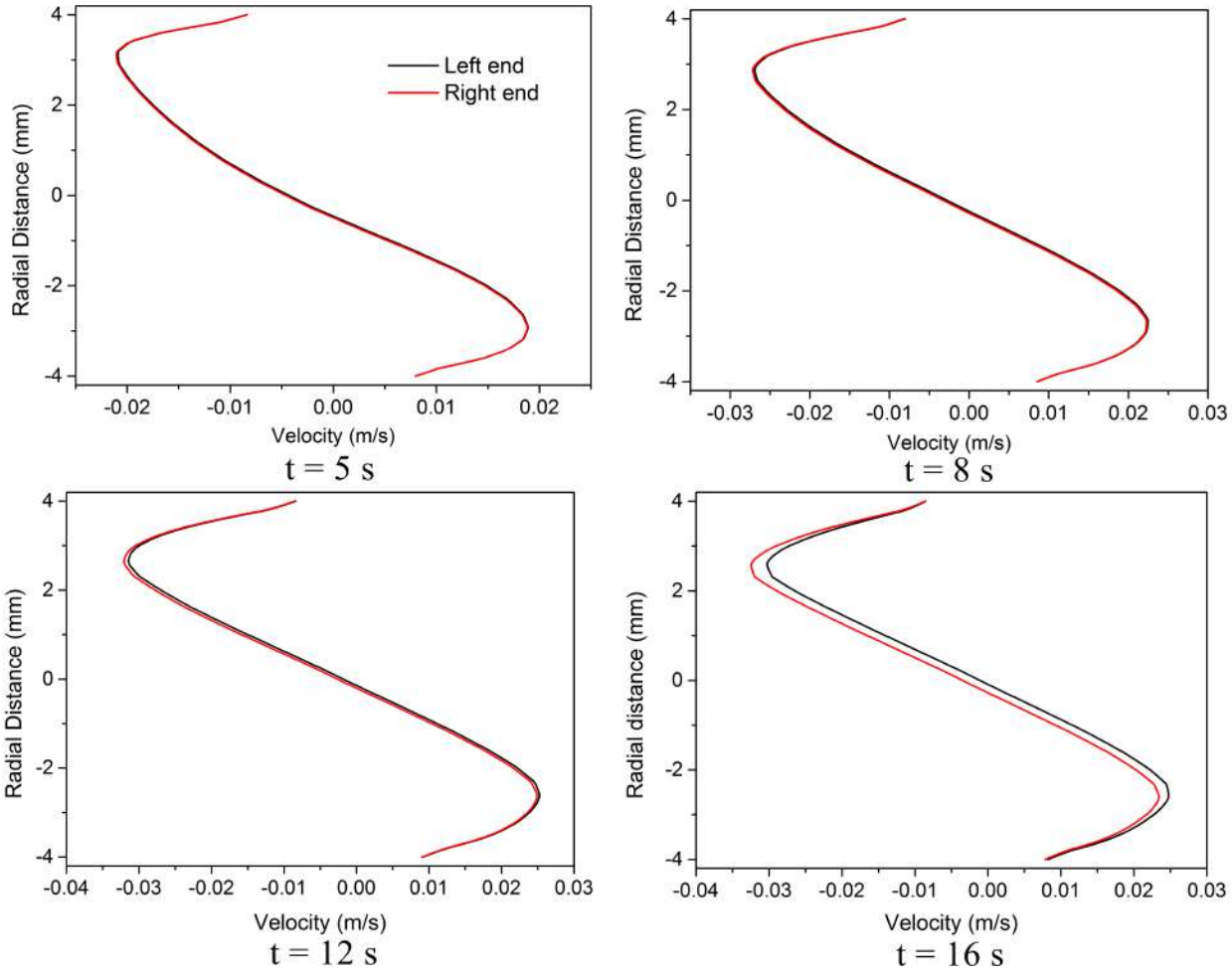

Fig. 5.9: Velocity variation in the radial direction at the two ends of the heater for $\dot{q} =$ 100 W at different time instants, demonstrating the deviation from symmetry with time

Analysing the system with high initial heating power of $\dot{q}$ =1500 W, the mechanism is

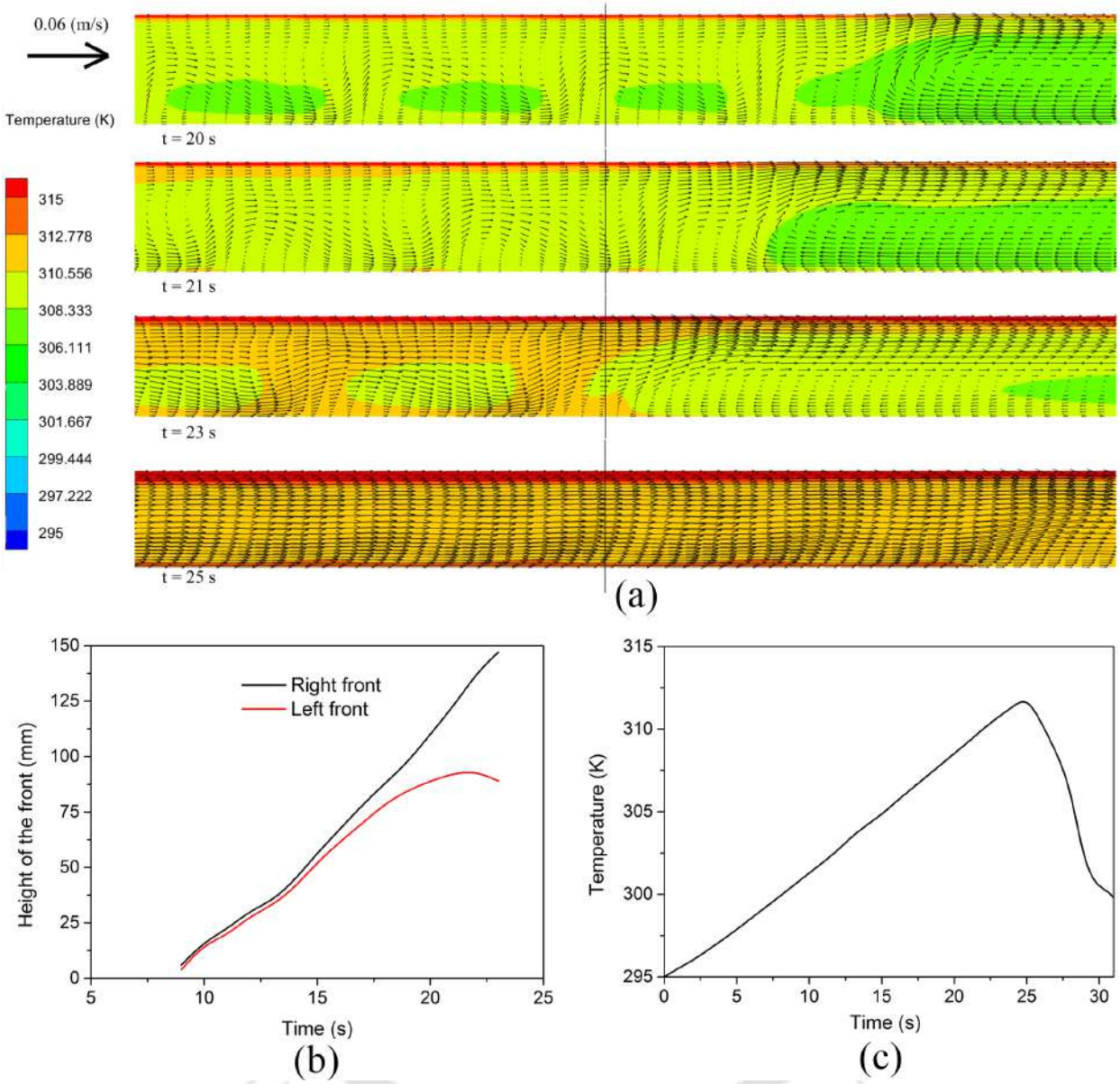

Fig. 5.10: Development of unidirectional motion within the heater for $\dot{q} = 100$ W; (a) temperature contours and velocity vectors show that the recirculation front vanishes around $t = 24$ s at $x = 190$ mm (marked by the vertical line), establishing bulk motion toward left; (b) gradual increase in the height gained by both the fronts in the right and left vertical arms, till they disappear on the commencement of bulk circulation; (c) change in temperature at the heater center with time, exhibiting the initiation of convection

affeced by higher bulk temperature and what we observe in earlier case, might not be visible. Due to high energy input within a short span of time causes the temperature level to rise upto 425 K close to the upper wall region. Due to this the piston effect is not as relevent as

we saw in the lower heating condition due to being substantially away from critical point. But still, the energy from the hot wall transmit to bulk at sonic speed casusing the effect to reach to the whole part of the loop much sooner. Though the initial physics is quite similar for 1500 W, the time taken for the process is significanly less due to faster buoyancy evolution. Boundary layer growth is even faster at the top wall, beacuse of which the local vortices are absent in the core of the heater till the bulk motion initiation. The Fig.5.11 shows the condition at t = 1 s.

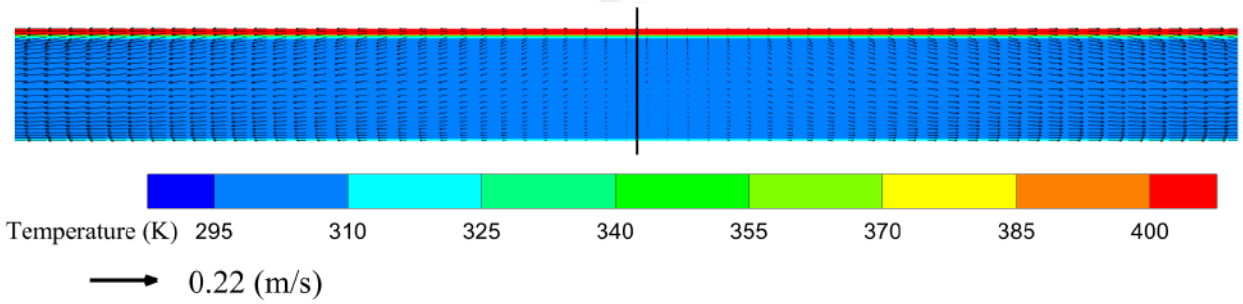

Fig. 5.11: Development of the local motion in the bottom arm near the heater center at t = 1 s at $\dot{q}$ = 100 W where vertical line denotes the central plane

Due to the temperature discontinuity at the heater exit, there is generation of local recirculation in this case as well. The colder fluid in the adiabatic arm tries to push the vortex inward while the fluid in the core pushes the fluid outward creating two vortex front. The vortex generates and moves faster for higher power and tend to reach the core and the adiabatic arms as shown in Fig. 5.12 for different time stamp, showing the escalation in the vorticity level with time.

This leads to the symetrical configuration from both the ends. As the front progresses in the vertical arm, adiabatic heating is pronounced here causing the temperature level surge in less time throughout. Following the similar analogy explained earlier, due to inherent instability, the symmetry breaks earlier for this case which is clearly shown in Fig.5.13.

5.4 Mechanism of Repeated Flow Reversal

Commencement of bulk motion is immediately followed by a pair of flow reversals, disregarding the boundary conditions or initial flow direction, as was observed from Fig. 5.4. The same can also be corroborated from the slump in density differential, and hence in driving buoyancy, after attaining a local maxima in Fig. **??**(b). The near-stagnant situation throughout the loop prior of bulk movement allows the fluid mass present inside the heating

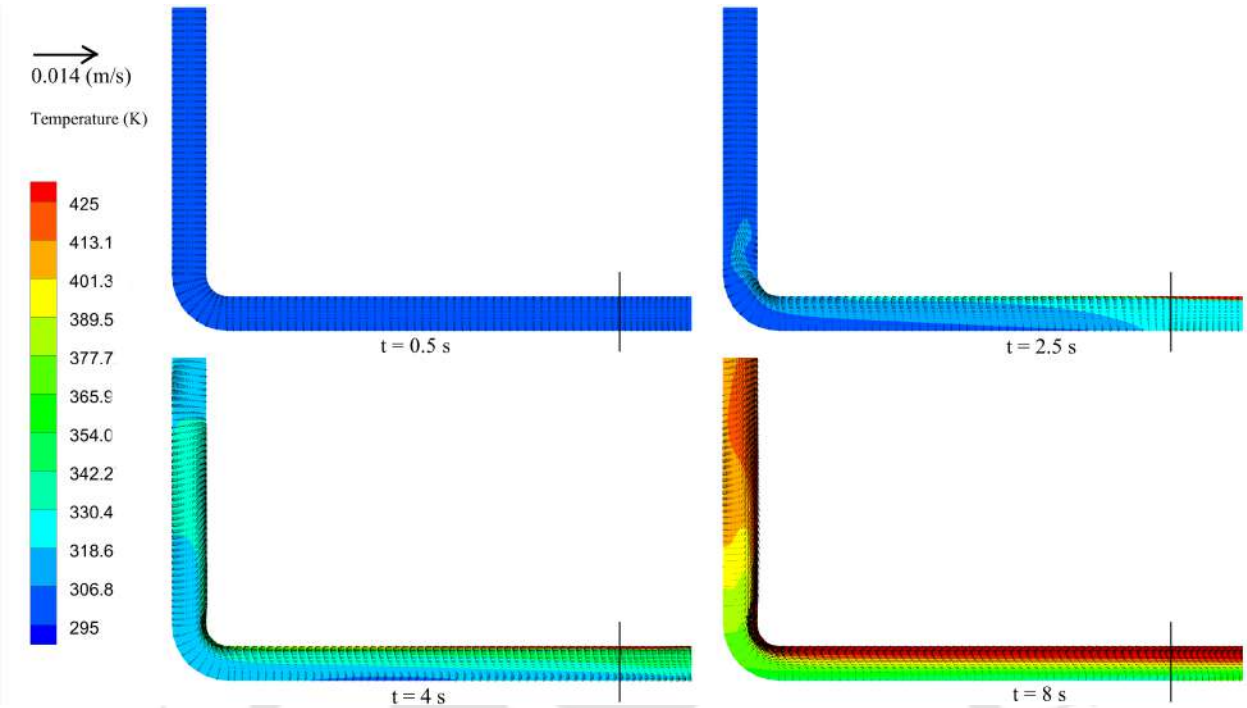

Fig. 5.12: Development of the temperature contours and velocity vector in the bottom arm near the left heater exit for $\dot{q}$ = 1500 W where vertical line denotes the heater exit at different time instances

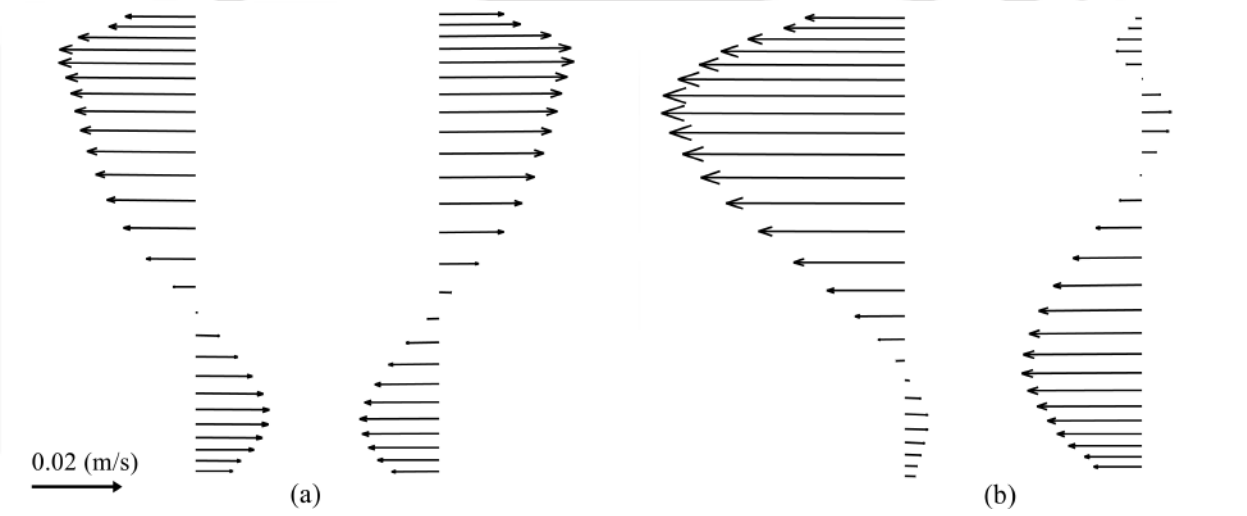

Fig. 5.13: Velocity vector at heater left and right exit for different time instances (a) t = 5 s, and t = 8 s showing symmtrical and unsymmetrical pattern

section to absorb the entire of the supplied energy, with only a small fraction being passed to the other segments, courtesy adiabatic heating and minuscule conduction around the prop-

agating fronts. Accordingly, the first *hot packet of fluid* (adopting the convention from **?**]) can attain very high temperature, the exact magnitude being concomitant to the imposed $\dot{Q}$ and local instantaneous thermophysical properties. Fluid temperature in the remainder of the loop remains reasonably close to T_∞. That culminates into a large buoyancy force on the first sign of circulation, as is indicated by the peak $\Delta\rho$, and subsequently very high instantaneous circulation rate. In fact, both the temperature level and flow rate attained at this instant are the observed to be the highest possible over the entire time span at any power levels (Fig. 5.4), which are synonymous to the strongest buoyancy influence.

Immediate effect of the onset of convection with large rate of fluid movement, however, is a considerable decline in the peak temperature level. At intermediate-to-high powers, highest temperature of CO_2 is well above T_{pc}, accordingly ensuring gas-like behavior and poor thermal conductivity. Therefore, the local heat transfer coefficient along the heater surface is expected to be quite modest. Bulk of the incoming cooler fluid is unlikely to experience any significant raise in energy content, inflicting the lowering in temperature around the heater center, and consequently for the whole warm packet leaving the heater. The scenario can properly be visualized from Fig. 5.14. The hot pocket developed inside the heater enters the left vertical arm around $t = 9$ s, while a cold pocket is also visible to be pushed into the right vertical leg. Temperature of CO_2 in the other segments of the loop is rather uniform, and hovers around T_{pc}, owing to the piston effect. Large density differential is realized around this instant, because of the presence of the hot and cold packets in the vertical arms. There is, however, definite lowering in temperature level interior to the heater following the expulsion of the hot packet, in repercussion to the inadequate rate of heat transfer, coupled with large initial circulation rate. The hot packet partially vanishes after entering the cooler ($t = 12$ s), while the cold packet is not sufficiently energized in the heater, resulting in higher average temperature in the right arm, and hence a reversal in the density differential. That inflicts a prompt change in the direction of motion, which generally is followed by another identical sequence of events, facilitating a second reversal.

At low heater powers, such as $\dot{Q} = 100$ W, temperature of supercritical CO_2 remains consistently below T_{pc} subsequent to the first pair of reversals. Accordingly, the available density differential across the horizontal sections are quite moderate and so is the extent of buoyancy. Besides, owing to the liquid-like nature of the flow domain, viscous stresses are also significant, instituting a stabilizing influence on the flow transients. Therefore, the loop exhibits oscillations with continually diminishing amplitude and no further reversals in flow direction, finally immersing into a steady-state. The startup transient at lower powers,

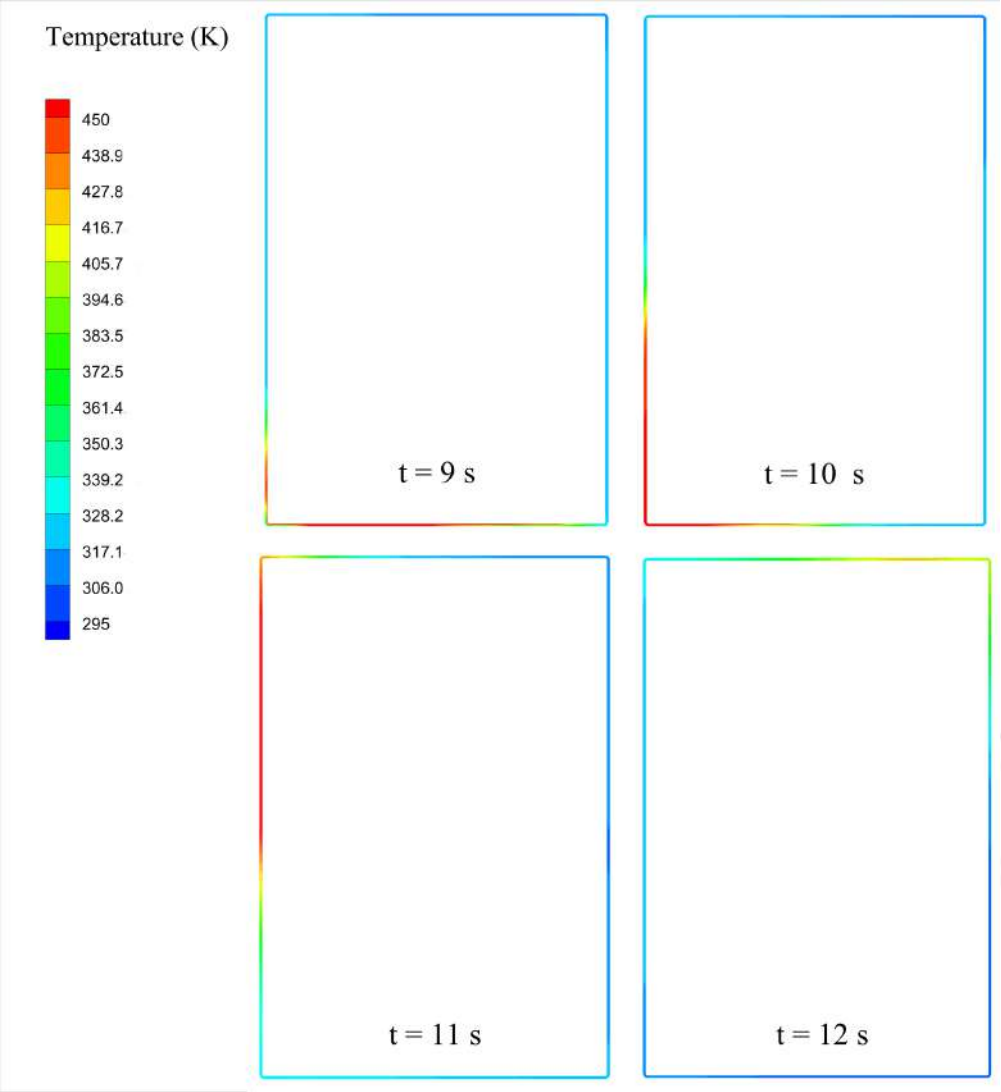

Fig. 5.14: Propagation of the hot packet of fluid through the left vertical arm for $\dot{Q} =$ 1500 W, and reduction in its energy content after entering the cooler, resulting in the pulsatile nature of the flow

therefore, is limited only to the initial reversals, with the final flow direction being identical to the first one. This observation persists over the entire of the low-power regime, as well as the early portions of the enhanced heat transfer regime (Fig. 5.3). With rise in $\dot{Q}$, however, fluid may cross T_{pc} within heater and/or cooler, inflicting a liquid-to-gas-like transformation or vice versa. Consistent to the instantaneous thermodynamic state of CO_2 in the vertical arms, it is possible to have large temporal changes in both driving potential and restraining force, obligating the sNCL to experience large-amplitude oscillations. Multiple flow reversals,

with quite chaotic fluctuations, can be noted at both $\dot{Q} = 500$ W and 1500 W in Fig. 5.4, and similar trend perseveres for majority of the enhanced and transition heat transfer regimes.

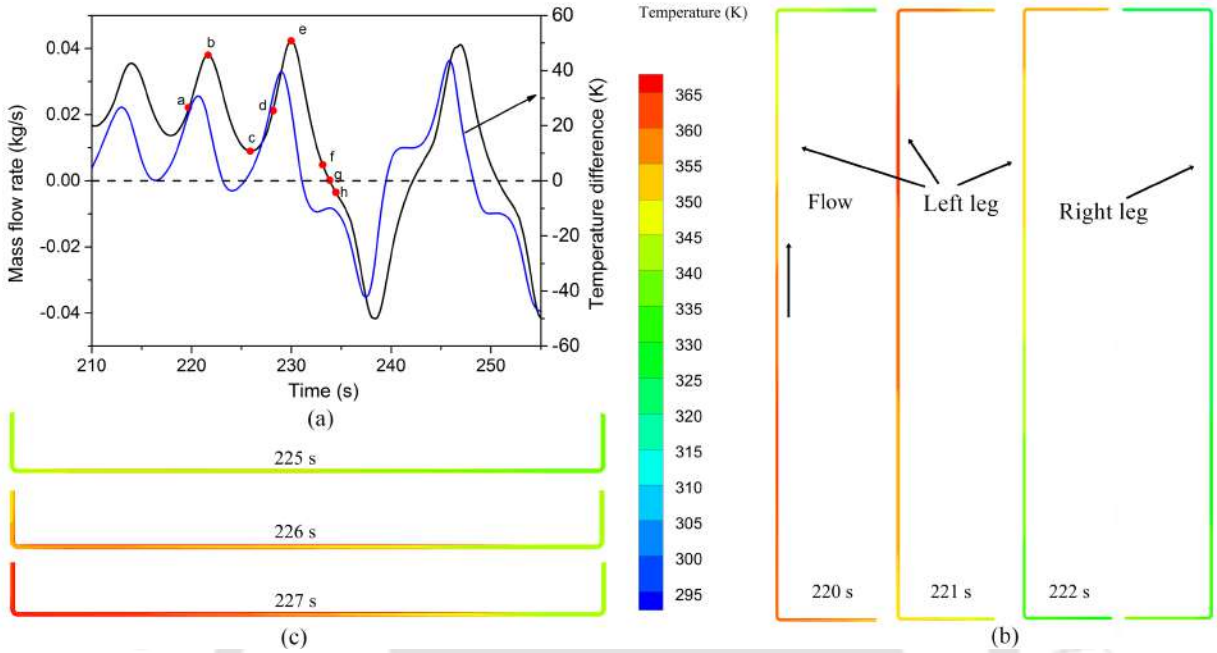

Fig. 5.15: The mechanism of flow reversal illustrated for $\dot{Q} = 1500$ W; (a) Temporal variation in circulation rate and average temperature difference between the mid-plane of the vertical arms, demonstrating the sequential appearance of local maximum and minima of flow rate; (b) Temperature contours at both the vertical arms, demonstrating the rise and fall in buoyancy force during the passage of the hot packet of fluid; (c) Birth of another hot packet inside the heater following the local minima in flow rate

In order to inspect further, a specific window featuring intriguing dynamics is identified with $\dot{Q} = 1500$ W, and concerned transients in circulation rate are illustrated in Fig. 5.15. Several important time instants are also marked on the same profile. As discussed earlier, the temperature of the hot packet of fluid can be really high while leaving the heating section when subjected to such large heater power. Birth of each hot packet is accompanied by the conception of a cold packet in the upper horizontal arm, which is expected to have temperature close to T_∞. During clockwise circulation, as the hot and cold packets enter the left and right vertical legs respectively, the average temperature difference between both the legs start to rise, which can also be perceived from Fig. 5.15. With the extreme temperatures appertaining to the either sides of T_{pc}, large density differential is realized, allowing a steep increase in the circulation rate. Such a situation arrives around $t = 220$ s, and is marked as point 'a'. The hot packet has entered the left riser, creating a non-uniform temperature

distribution thereof. Substantial thermal disparity between the arms can be easily be noted, which helps CO_2 to accelerate throughout the flow passage. A local maxima in flow rate is achieved (marked as point 'b') when $\Delta\rho$ is maxima, which can also be substantiated following the temporal profiles of the temperature difference. The profiles of instantaneous circulation rate and average ΔT between the vertical arms closely follow each other, establishing the dominant role of buoyancy in regulating flow transients. In fact, there is a minute phase shift between the two profiles, which is also logical. It is the change in the temperature level that governs the development of the buoyancy field, and the instantaneous circulation rate is determined by the body force, subsequently affecting the fluid temperature itself.

Once the hot packet leaves the vertical arm, there is a drop in the concerned temperature level, owing to the pulsatile nature of the flow. The substantial variation in the thermodynamic state of the fluid is evident comparing the temperature contours for $t = 220$ s and 222 s in the left arm, while hardly any qualitative deviation can be perceived at the right arm. That forces a degradation in buoyancy, and consequently the flow rate, till the attainment of a local minima at point 'c'. The hot packet loses energy inside the cooler, while the cold packet warms up during its progress through the bottom horizontal arm. No noticeable thermal disparity exist between the vertical legs, as is demonstrated by the near-zero ΔT, justifying the inferior circulation rate. Both flow rate and ΔT rises again with the ejection of another hot packet in the vertical arm, following the sequence of 'c-d-e' points. The generation of the hot packet during $t = 225$ s to 227 s can clearly be identified inside the heater. It is interesting to recognize the gradual increase in the maximum circulation rate and reduction in the minimum value over successive cycles, indicating the progressive upsurge in inertial effect. That leads to pulsations with continually-growing amplitude, and eventually a reversal in the nature of ΔT. The cooler may not be capable to absorb entire amount of energy content in the hot packet, while the cold packet may not receive sufficient energy within the heater. Consequently, the fluid starts to rise along the right arm, which now is at a higher average temperature state. The instant of reversal is marked as point 'g' in Fig. 5.15. The enhanced inertia may force immediate reversals, as can be envisaged from Fig. 5.15, or may allow the system to continue with diverging oscillations over a period prior to another change in flow direction, yielding a quite chaotic characteristics. It can, therefore, be concluded that sNCL may not be able to attain steady-state, enduring sustained period of chaotic fluctuations instead, if subjected to a large heater power directly on the quiescent condition. A different procedure, such as gradual rise in power level or incorporation of active controlling mechanism, may become necessary to assure a steady-state.

5.5 Summary

Initiation of motion in a symmetric NCL always involves convoluted interactions between the associated forces and is commonly associated with some unique thermalhydraulic instabilities. Steep gradients of thermophysical properties around T_{pc} for supercritical fluids contribute further intricacy into the framework, and hence, hardly any concentrated effort can be identified in literature anatomizing the microdynamics of flow initiation in sNCL. Present study employs a 2-D computational model to explore the initiation of bulk motion in a rectangular quiescent loop with horizontal-heater-horizontal-cooler orientation and subsequent transients at multiple power levels, selected carefully to exemplify various regimes of heat transfer.

In general, the system remains apparently inactive over a period of time, during which temperature of CO_2 inside the loop consistently increases to attain a very high level. The concerned time span and maximum temperature both, however, are modulated by the imposed power level, while the inherent physics can also be considerably different. The discontinuity in thermal boundary condition around the heater edges can be earmarked as the first reason for introducing inhomogeneity within the flow domain, resulting in the development of a pair of vortices. The warm fluid front can grow and propagate in both directions, primarily maintaining an apparent symmetry, and the instant of their merger can be proclaimed as the moment of initiation of bulk motion. They, however, don't meet at the heater center, and it is the position of their unification that determines the first direction of circulation. The most fascinating observation is the uniform and near-linear rise in fluid temperature throughout the flow domain before the migration of the vortices. This occurrence is accredited to the thermoacoustic mechanism of adiabatic heating or so-called *piston effect*, which is pronounced for fluids around the critical point, and can be relevant even for temperatures sufficiently away from it. Development of recirculation zone around the ends of the cooler, despite no bulk motion, is the most discernible impact of such adiabatic heating. Confronting fronts interior to the heater leads to Rayleigh-Taylor-type instabilities, which controverts the symmetry and decisively imposes a directional nature. Piston effect, though, is more pertinent at low powers. Much faster rate of rise in temperature at higher powers deviates the system from the critical point, weakening the role of compressibility. Reduced viscous stresses allow faster vortex movement and quicker development of the influence of buoyancy. Accordingly, both the time scale and inherent thermofluidics can be disparate with change in power levels. The sNCL always undergoes a pair of flow reversals immediately after the first sign of bulk motion, to accommodate the substantially-high level of buoyancy and con-

sequent large circulation rate. Subsequent dynamics are governed primarily by the range of fluid temperature. If the highest temperature remains limited below T_{pc}, the loop stabilizes with decaying oscillations, whereas temperature fluctuations across the the pseudocritical level emanates into chaotic oscillations, with repeated change in primary flow directions. In order to realize a steady-state at higher values of heater power starting directly from the quiescent condition, additional measures may be necessary.

Present study, therefore, is able to recognize and decipher important understanding about the microdynamics of the initiation of motion in sNCL. Conception of the role of adiabatic heating and Rayleigh-Taylor-type instabilities to instigate asymmetrical flow structure in sNCL is a novel observation, while the significant difference in flow characteristics with change in power level is also a noteworthy contribution. Further explorations are required to understand the possible logical pattern behind the faster movement of one of the front, which determines the first direction of motion, and hence can formulate the immediate next step of research.

Chapter 6

Experimental Characterization of Rectangular sNCL

6.1 Preamble

This chapter presents an experimental investigation of a CO_2-based NCL with supercritical operating conditions. The extensive literature showed that substantial numerical studies had been conducted with experimental validation support. The preliminary research is focused on the steady-state as well as dynamic response of the system. Understanding the phenomenon of "Flow-induced-Heat transfer deterioration" (FiHTD) will be the investigation's main goal, which occurs when the average loop temperature exceeds the pseudo-critical temperature and friction takes over completely. This results in a decline in overall loop performance. Such occuerrance is only observed in the recent numerical study of Sarkar and Basu [133]. The experimental confirmation i still far from its destination. However, a limited body of knowledge is still far from being fully explored to support numerical studies. The zone of operation is above the critical point, so the system operating pressure is higher than in conventional single- and two-phase systems, which increases the complexity of handling the system.

Liu et al. [81] was the first one to observe such heat transfer deterioration behavior in sNCL locally. But their main focus was on how the system responds when the system pressure, heat flux, and inlet temperature are varied. The experimental study of Archana et al. [72] mainly focused on characterizing the heat transfer zones. Chen et al. [102] investigated the impact of loop inclination from low to high heat flux. In contrast to the current study, their investigation was conducted on a loop with a larger diameter. However,

because there was no arrangement to control the constant pressure in their case, the system pressure was not constant, which is why the pressure increased from 7.5 MPa to 9 MPa despite the low heat flux. This clause has been put into practice. Therefore, the purpose of this investigation is to delve deeper into such behavior from a FiHTD concern. Due to its promising qualities and applicability in numerous engineering fields, as discussed in the first chapter, CO_2 is considered a working fluid. Therefore, more research into this steady-state deterioration phenomenon is required to ensure viability under various operating conditions. The operating conditions are the prime concern to control so as to achieve optimum loop performance. The effects of sink temperature, operating pressure, inclination angle, and input heating power are investigated. For the range of operating conditions that were chosen, there is no evidence of instability. At the end of the study, some experimental results are compared with numerical results, and a decent match is observed.

1. N_2 cylinder 2. DPT 3. Pressurizer 4.Water inlet 5. Cooler 6. Water outlet 7. Heater 8. Variac 9. Vacuum pump 10. CO_2 Cylinder 11. Computer 12. DAS 13. Chiller

Fig. 6.1: Designed experimental structure of natural circulation loop

6.2 Loop Design and Experimental Component

A supercritical natural circulation loop has been designed with a constant diameter standard 3/8" stainless steel pipe, which is selected from the fluid-to-fluid scaling done by Sarkar [133] for their experimental study. The loop's design was done in a way that allows for the investigation of different loop inclinations. A experimental setup with relevant marking of different components is shown in figure 6.1.

• Loop structure

The loop is made of high-quality steel (manufactured by Swagelok), which can easily withstand pressure up to 120 bar. With plywood of a 10 mm thickness acting as support, the entire loop was mounted on a mild steel framework. Using MS support, the entire frame containing the loop was suspended so that it could be rotated about the x-y and y-z axes.

• Heater

Wrapping a heating coil around a pipe is the essential step to making a heater section. However, the issue is that as soon as the heating coil comes into contact with the SS tube, the entire length of the tube will begin conducting electricity. In order to prevent the setup from conducting electricity, it is necessary to choose an electrically insulating material to go between the heating coil and the SS tube on which it is wrapped. Additionally, the insulating material must be thermally conductive in order to allow heat to transfer from the heating coil to the tube surface. A mixture of sodium silicate and aluminum oxide was used as a thermally conductive material and electrical insulation to achieve the aforementioned goal. A paste is created when sodium silicate and aluminum oxide are combined in the right ratio. This paste does not solidify at room temperature, but after a certain amount of heating, it transforms into a very hard substance. The paste is spread over the surface of the tube in accordance with the heater's length, where the heating coil is to be wrapped and heated to harden it. The thermocouple installation location is only revealed by the remaining portion. As a thermal conductor and electrical insulator, this composite material performed admirably.

• Power input circuit

The variac, a multi-function meter, and a nichrome wire constitute the power input circuit. The power input circuit's variac, which controls the input power, is its brain. The input power (measured in W) of the heater is determined directly using the multi-function meter.

• Cooler

A double-pipe heat exchanger will be used in the cooling section of the loop's upper

portion. In addition, water will be used as a side fluid. The internal SS tube (3/8") will be covered by the 38 mm diameter outer pipe. The heat exchanger will be wired so that it can be used in parallel as well as in the opposite direction of flow. Water will be cooled in Julabo-made FL-1701 water-recirculating chiller (Fig. 6.2a). Distilled water temperature can vary from 5 to 40 °C. To go below 5 °C, glycol needs to be mixed in appropriate proportion, and hence up to -20 °C can be attained. The chiller can provide the constant flow rate of 23 l/min. Therefore to control the flow rate bypass system will be provided with using valve. And then, to measure the flow rate, Rota-meter will be used. The metal cap will cover both sides of the heat exchanger to ensure zero leakage. Wherever required, M-seal can be used. Total six thermocouples were used to measure the temperature of the primary loop wall temperature.

(a) Julabo make recirculating chiller

(b) Honeywell make differential pressure transmitter

(c) Keysight make Data Acquisition system

(d) Truvac make vacuum pump

Fig. 6.2: Various instruments used in experiment

To measure the pressure difference, Honeywell make a differential pressure transducer (Fig. 6.2b) will be used. To monitor the output values of these components, Key sight make Data Acquisition system (Fig. 6.2c) will be used, which can monitor the data with time. To

maintain the constant operating pressure inside the loop, a pressurizer will be installed in the inverted position, which will be filled by nitrogen gas (which is non-reactive and lighter compared to CO_2). The vacuum pump (Fig. 6.2d) will be required to create a vacuum inside the loop to ensure no air is trapped inside before filling the loop with working fluid. 50 mm of thermal conductivity 0.12 W/m-K ceramic insulation will be installed to stop heat from escaping into the surroundings.

6.3 Calibration of Thermocouple

As intrusive thermocouples will cause an additional pressure drop, a total of 18 thermocouples were installed on the wall. However, two thermocouples were installed at the heater's inlet and outlet in order to measure the heat transfer coefficient by taking the temperature along the heater's length. A thermocouple must be calibrated to ensure accuracy before being used. Numerous thermocouples were submerged in thermal baths for thermocouple calibration. The recirculation cooler temperature is initially set at 15 °C. When the cooler temperature reaches 15 °C, both temperatures, i.e., cooler temperature and thermocouple temperature, are recorded. Once a reading has been taken, allow the cooler temperature to rise by 10 °C before repeating the process up to 95 °C. In Fig. 6.3, the temperature readings obtained by thermocouple and recirculation thermal bath are compared and they are found to be in excellent concensus.

6.4 Data Reduction

It can be assumed that q_w is uniformly distributed because there is little variation in the tube's resistivity over the experimental temperature range. The heat flux of the test section is determined by

$$\dot{q}_w'' = \frac{\dot{q}}{\pi d_i L} \tag{6.1}$$

where $\dot{q}$ is the heating power, L and d_i are the effective length and inner diameter of the test section, respectively. The inner wall temperature $T_{w,i}$ is determined by the following equation:

$$T_{w,i} = T_{w,o} - \frac{\dot{q}_w'' r_i}{2\lambda}\left(\frac{a^2 - 2lna - 1}{1 - a^2}\right) \tag{6.2}$$

where $T_{w,o}$ is the outer wall temperature, a is the ratio of inner tube radius to outer tube

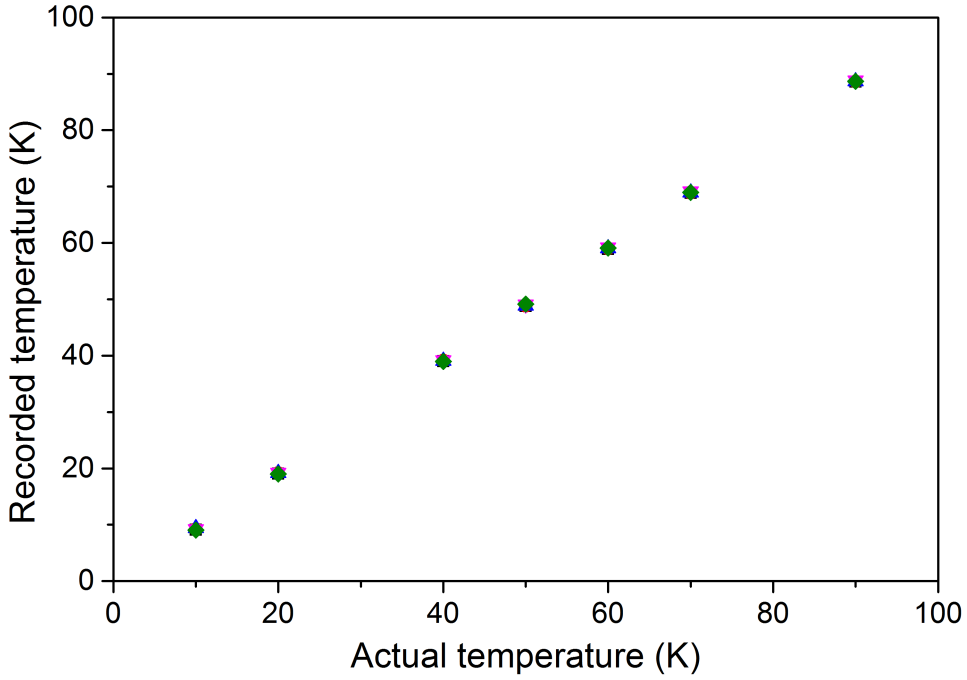

Fig. 6.3: Calibration chart of thermocouple

radius, $a = r_i/r_o$. Where r_i is the inner radius of the test section, and λ is the thermal conductivity of the tube.

The mass flow rate estimation is done using the energy balance equation, which is given by the following equation.

$$\dot{m} = \frac{\dot{q}}{\Delta h} \tag{6.3}$$

The heat transfer coefficient h is obtained by the following equation:

$$U = \frac{q_w}{T_{w,i} - T_b} \tag{6.4}$$

where T_b is the bulk fluid temperature, which is obtained using bulk enthalpy and the pressure. Whereas, h_b is decided based on the inlet and outlet enthalpy of the heater, given by the following equation:

$$h_b = h_i + \frac{(h_o - h_i)L_b}{L_h} \tag{6.5}$$

6.5 Uncertainty Analysis

System parameters that are crucial for flow measurement and whose accuracy may hamper the final values are -

- Voltage
- Current
- Enthalpy

The parameters measured by instruments and their uncertainties are shown in Table 6.1.

Table 6.1: Parameters and their uncertainty

Parameter	Uncertainity
Voltage	1.2% of the reading
Current	2.5% of the reading
Temperature	0.75% of the reading

The uncertainty measured in mass flow rate is defined by the following equation-

$$\Delta\dot{m} = \left|\frac{\partial\dot{m}}{\partial V}\right| |\Delta V| + \left|\frac{\partial\dot{m}}{\partial I}\right| |\Delta I| + \left|\frac{\partial\dot{m}}{\partial \Delta h}\right| \left|\frac{dh}{dT}\Delta T\right| \tag{6.6}$$

The above calculation gives the uncertainty of 0.5 % in the calculation of mass flow rate.

6.6 Experimental Procedure

• Leakage testing

Initially, it is necessary to vent out the air present inside the loop. For this, the vacuum pump is turned on, keeping all the valves closed. The vacuum pump used has a cfm rating of 4.6. The loop is then pressurized at a pressure of 120 bar with Nitrogen and maintained at this pressure for a sufficiently long time. The pressure drop was observed to be less than 1 bar when kept for more than 24 hrs.

• Filling of loop

For filling of CO_2, the loop was again vented, which was filled by N_2 for pressure testing, and CO_2 was filled at a pressure of 65 bar (which is the rated pressure of CO_2 cylinder). Then both horizontal and vertical coolers were turned on at a temperature of 10°C. Due to

condensation of CO_2, the pressure of the system dropped, which allows more and more CO_2 to get inside the system. Repeating the same process many a time, there came a condition when the pressure of the system stopped changing, which means no more CO_2 can be filled.

• **Pressurization**

Till this step, there was only CO_2 inside the loop and supply of N_2 was disconnected. To increase the pressure to desired level, the valve of N_2 (which is at the higher pressure) was opened whose line is connected from the bottom of the loop. Since the N_2 is lighter, it remains above the CO_2 causing the formation of the interface at some level and the level is ensured is such that it does not enter the main loop. Once the desired pressure was achieved,the nitrogen cylinder was isolated from the system. Sufficient time was allowed to reach thesteady state before the heating process began.

The range of operating conditions is mentioned in table 6.2-

Table 6.2: Range of operating parameter

Parameter	Range
Operating pressure	7.5 to 9 MPa
Cooler temperature	5 - 25°C
Tilt in Y-Z plane	0 - 45°
Heater power	0 - 1200 W

6.7 Comparison With Literature

Before proceeding to the final experiments, the reliability of the results is crucial. For this purpose, validation is necessary with the previous literature. Non-dimensional numbers Re and Gr are famous in the field of supercritical natural circulation loops steady-state validation. The same has been adopted in the current study. Following the two-dimensional group, the range of operating conditions chosen is mentioned in the table 6.2. As can be seen in Fig. 6.4 that there is good conformity between the present study and the literature. The results also adhere to the 3-D model developed earlier and also wander around the experimental study of Swapnalee et al.[104].

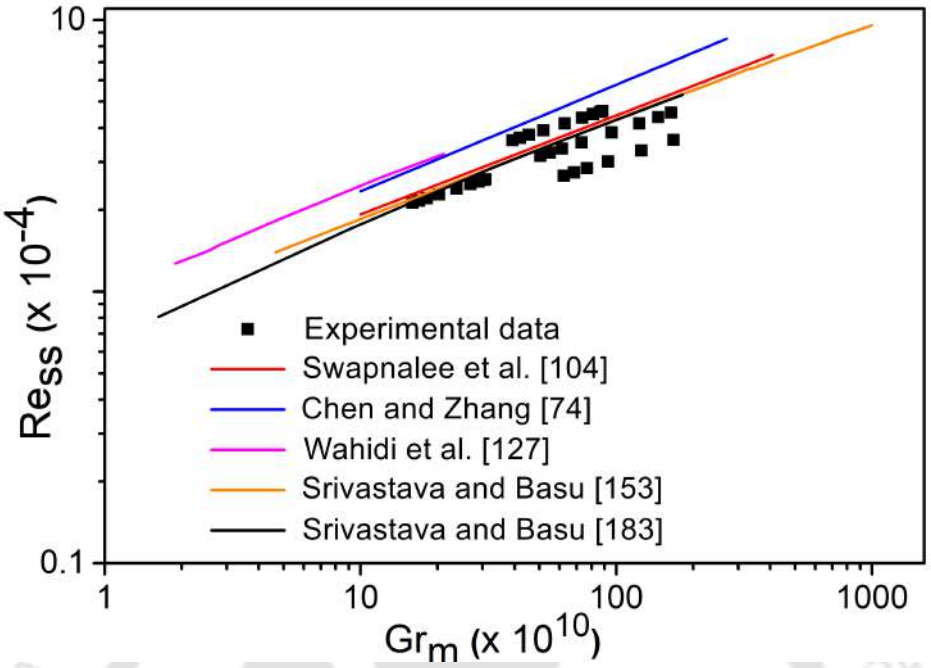

Fig. 6.4: Validation of the steady-state results with previous literature

6.8 Results and Discussion

The motivation of the present study is to investigate the steady-state thermal hydraulics of the sNCL from the FiHTD point of view, which has not been explored in recent times. Though, in the case of forced flow conditions, HTD is a well-explored phenomenon and needs attention in natural circulation systems. In the present, the investigation of system pressure, sink temperature and loop inclination effect has been taken care of. Due to the limitation of the tube length sizes, the maximum inclination that could have been investigated was limited to 45°. In the present case, the steady-state analysis is of major focus due to the fact of the targeted aim of analyzing FiHTD. Moreover, looking at the various parameters, the system was found to be stable throughout the boundary conditions considered.

6.8.1 Variation of mass flow rate

Natural circulation is the interplay between buoyancy force and friction force. In the beginning, when the heat is supplied to the heater, the disturbance leads to the generation of buoyancy by overcoming the friction force. Hence, it is called a buoyancy-dominant region. As the heater power increases, the generation of buoyancy is promoted, and the mass flow rate increases. The same has been depicted in Fig. 6.5 for the four boundary conditions and

loop orientations. The same has also been compared with the results of the 1D model as well as the 3D model. Due to being imposed by many limitations in the 1D model, there is certainly a substantial difference in the comparison, but in comparison, the 3D model showed good consensus. As per the definition of FiHTD given by Sarkar and Basu [77], when the loop average temperature crosses the pseudocritical temperature, there is a sharp drop in the thermalhydraulic behavior of the system. As observed, for 8 MPa and 280.5 K sink temperature, the mass flow rate increases rapidly at low heater power and rises suddenly as it enters the enhanced heat transfer regime. It is interesting to see there is a good degree of conformity in numerical and the present experimental data in the enhanced heat transfer regime. Soon after the beginning of the transition regime, where the mass flow rate attains the peak, the flow starts decreasing suddenly after that, and that is the condition of heat transfer deterioration. The same phenomenon is observed in all the cases considered.

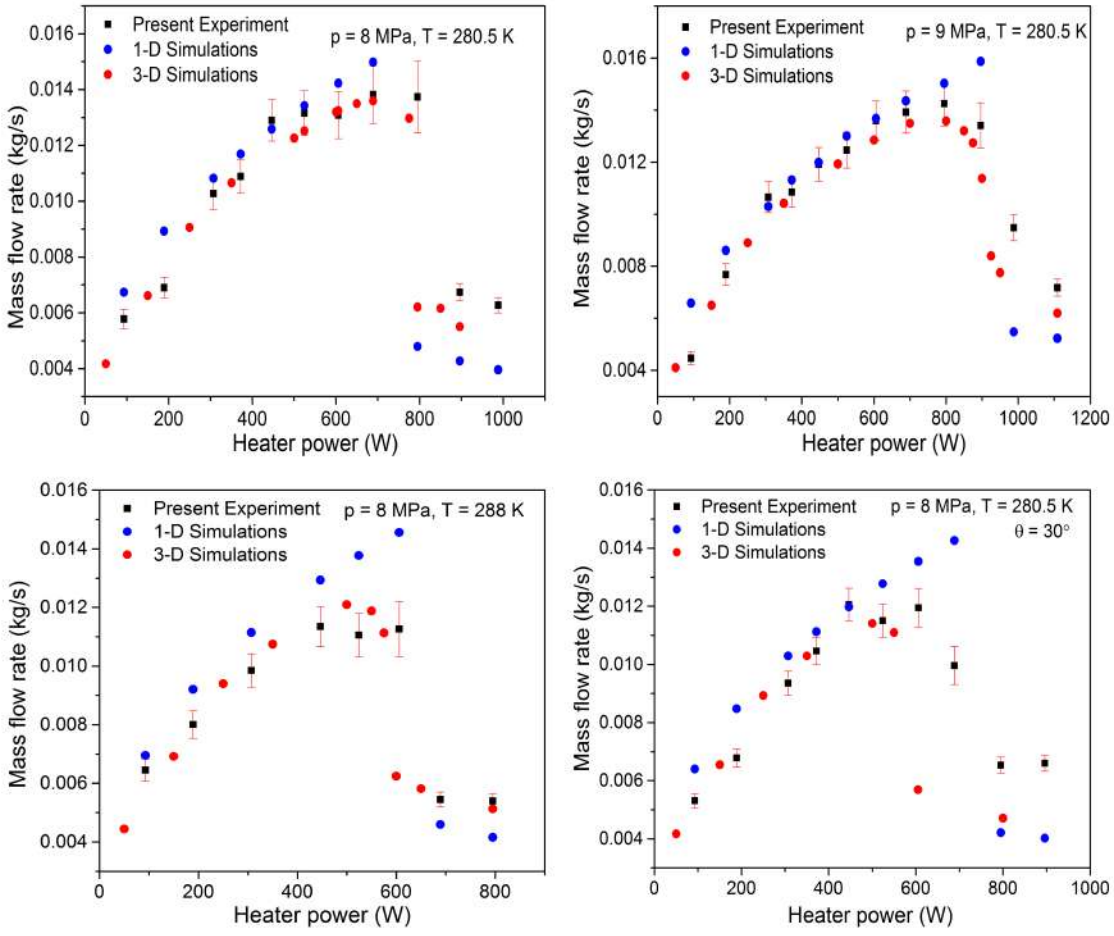

Fig. 6.5: Trend of mass flow rate at four different boundary conditions and loop orientation

It was observed that in the case of the 1D model, due to Ledinegg instability, the flow also started decreasing at around 750 W heater power, while the same was observed at 896 W heater power, which is a good degree of correctness owing to the limitations of 1-D model. Under the Ledinegg instability, there is a case of multiple flow rate value, which was obtained in the 1-D model. While the same was not observed in the present experimental study. The possible reason is the inventory of CO_2 inside the loop. If the amount of injected CO_2 is increased, then there is a possibility of getting a higher mass flow rate, and consequently, the power corresponding to the FiHTD can also be enhanced. Table 6.3 shows the heater power for the 1D model and the present experimental study, indicating the boundary of Ledinegg instability for different cases considered. It is crucial to point it out that the experimental values of heating power mentioned in the table 6.3 are coarse date and hence we can expect the value may differ by some percentage. But the overall idea we can extract is that the presence of Ledinegg instability but, since it is the first experimental outcome, more rigorous experiments should be done.

Table 6.3: Heater power corresponding to the low flow rate (static stability)

	8 MPa 280.5 K	**9 MPa 280.5 K**	**8 MPa 288 K**	**8 MPa 288 K θ =45°**
Experiment	795 W	896 W	605.8 W	605.8
1-D model	896 W	950 W	688.8 W	700 W

The main similarity between the experimental study's findings and earlier research on FiHTD is a sharp decline in flow rate and heat transfer characteristics. The same has been seen here as well. The bulk temperature inside the loop, however, rises sharply, as shown by Sarkar and Basu [77]; this phenomenon was not present here.

For 9 MPa, the T_{pc} is higher, leading to a delay in the FiHTD. Due to the inclination of the loop, the effective height decreases and leads to relatively poor performance and early appearance of the FiHTD. The same has been observed here also, characteristics of which are clearly visible in Fig. 6.5 and 6.6. To delay the limit of the zone of FiHTD, the possible way is to inject more and more CO_2 inside the loop.

6.8.2 Effect on wall and bulk temperature

With the increment in the heater power, the bulk temperature also increases. Once the loop average temperature crosses the pseudocritical limit, the flow rate drops. Such a phenomenon

occurs when the thermal expansion coefficient and specific heat attain the maxima, leading to the highest flow rate region. Till this region arrives, the inlet and outlet temperature monotonically increase, and just after that, there is no such jump in the inlet temperature, but the outlet temperature suddenly rises. This, in turn, leads to the sudden rise in the enthalpy, as can be seen in Fig. 6.6. The sudden rise in the outlet enthalpy is due to the fact that bulk temperature reached way beyond the pseudocritical limit. Because of this, the temperature is the hot leg is high, creating a small density difference between the cold and hot leg, leading to a drop in flow rate.

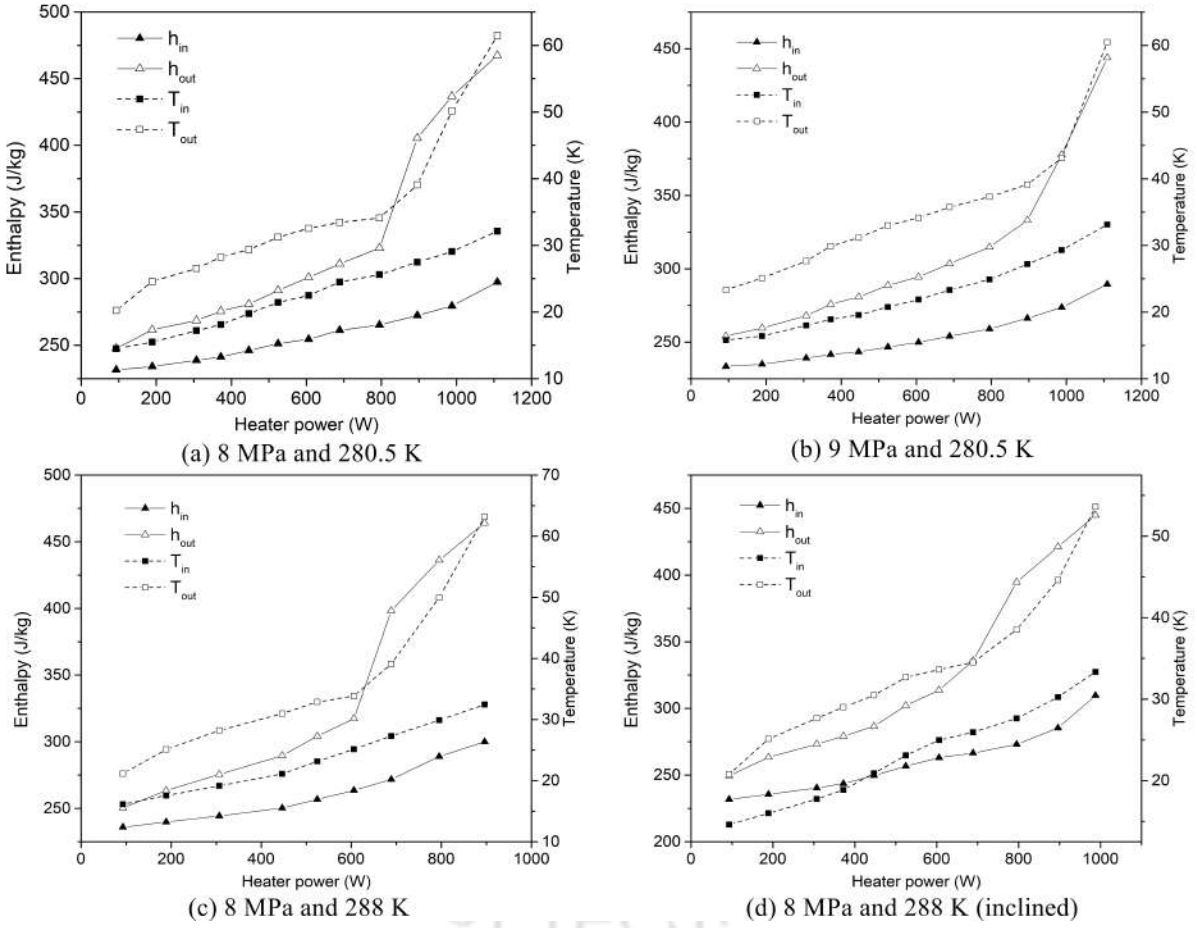

Fig. 6.6: Variation of inlet & outlet temperature and enthalpy at various boundary condition with respect to heater power

The Fig. 6.7 shows the variation of bulk temperature at heater inlet and outlet and the wall temperature at heater center with time (raw data) for the two cases of Fig. 6.6(a) and (b). For other cases as well, the same could have been presented but since it is not representing any valuable information except showing the stable loop nature, two might be

sufficient to give clear picture. Though there are number of thermocouples were installed along the length of the heater, yet only one is presented for clarity.

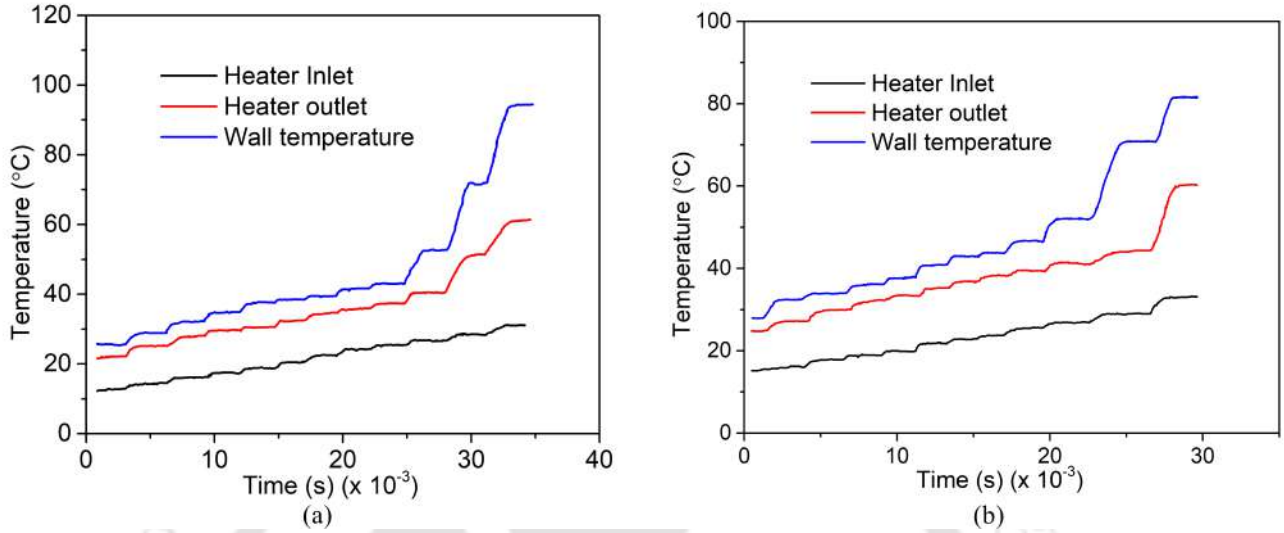

Fig. 6.7: Raw data of variation of inlet & outlet temperature and the wall temperature (at heater center) with time for the cases presented in Fig.6.6(a and b)

6.8.3 Heat transfer characteristics

There were a total of 10 thermocouples installed initially on the heater surface. But, due to uneven heating in the heater section from the Nichrome heating wire, some thermocouples showed absurd readings due to direct contact with the heater coil. So a total of 5 were discarded. Fig.6.8 shows the trend of inner wall temperature (computed from eq.6.2) & bulk temperature (computed from eq.6.5) along with the concerned heat transfer coefficient along the length of the heater for all the cases. Heat transfer coefficient is a function of the two above-mentioned quantities as well as the heat flux as mentioned in equation 6.4.

The wall temperature rises in conjunction with the wall temperature for a zone with low heating power. The difference grows as well, which causes the heat transfer coefficient to fall. The wall temperature decreases as the heating power rises as a result of CO_2's increased capacity to absorb heat, which raises the heat transfer coefficient. The enhanced heat transfer zone is what this area is commonly referred to as. The heat transfer coefficient reaches its maximum in this area and decreases as we move downstream along the heater. Once the heater power enters the FiHTD, there is a significant drop in the heat transfer coefficient, which leads to an upsurge in the wall temperature and bulk temperature. In the enhanced

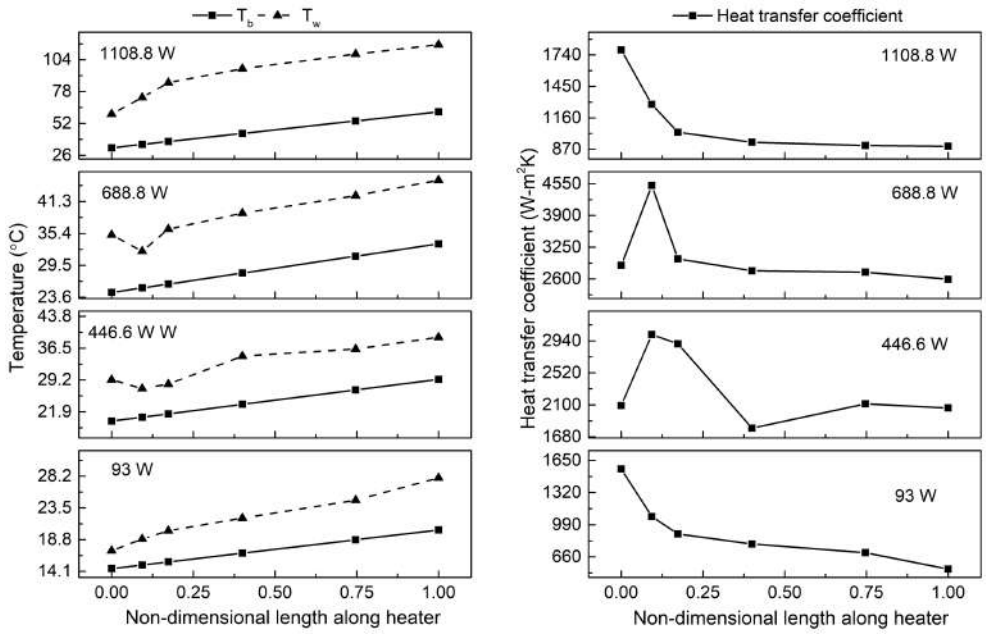

(a) 8 MPa and 280.5 K

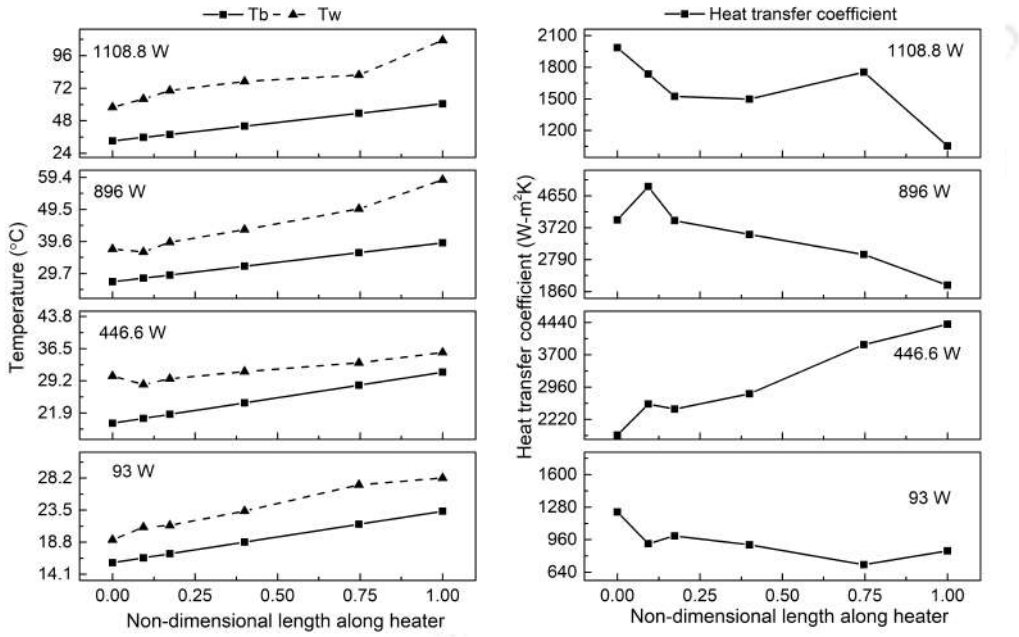

(b) 9 MPa and 280.5 K

Fig. 6.8: Variation of inner wall temperature and bulk temperature (left column) and corresponding heat transfer coefficient (right column)

and transition regime, there is an appearance of a peak of heat transfer coefficient, which

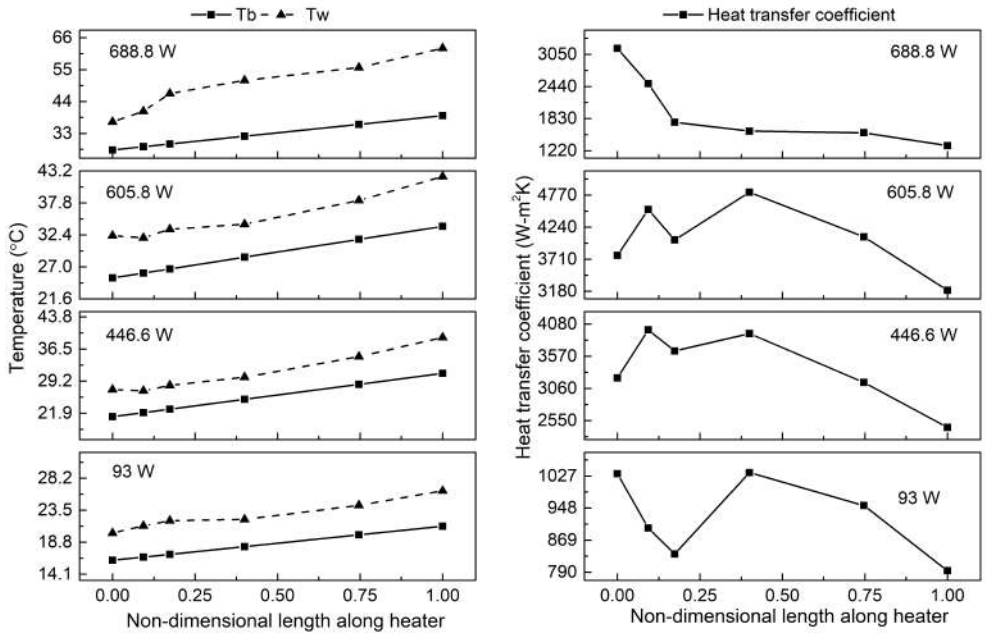

(c) 8 MPa and 288 K

Fig. 6.8: (cont.) Variation of inner wall temperature and bulk temperature (left column) and corresponding heat transfer coefficient (right column)

disappears in FiHTD with relatively low heat transfer values, termed as deteriorated heat transfer. The loop condition under FiHTD, as defined by Sarkar and Basu [68], is not found to be similar here. Rather, local behavior with a low heat transfer nature is similar. Other cases also showed the same behavior with different magnitudes of heat transfer coefficient and mostly adhering to the different heat transfer regimes.

6.9 Summary

To anticipate the occurrence of FiHTD, the current experimental investigation using a rectangular natural circulation loop was conducted. The steady-state aspect of the study was the main focus. At cooler side sink temperatures of 280.5 K and 288 K, the experiments were conducted at 8 MPa and 9 MPa. To study the impact of effective height, the loop was also inclined 45 degrees. The following are the findings-

- The flow rate increases with the heater power due to the generation of buoyancy force. The flow rate drops sharply after a specified heater power where the friction dominates.

- The drop in flow rate was observed at the heater power corresponding power where the static instability was occurred in 1-D model.
- The drop can be termed as deterioration of heat transfer because the drop in the heat transfer coefficient was observed with significantly low in magnitude.
- This deterioration is similar to the observation claimed by sarkar which the called FiHTD. But, the difference lies in the overall loop behaviour. As a consequence of deterioration, there is not much surge in the bulk temperature throughout the loop.
- Going for higher heating may increase the bulk temperature at each location which was indicated by variation of bulk temperature.
- The system was found to be stable due to the implication of small diameter of the rectangular loop.

Chapter 7

Conclusion and Scope for Further Work

7.1 Summary

The present work deal with the numerical and experimental investigation of the supercritical natural circulation loop with CO_2 as the working fluid. The work comprehends both steady-state (employing a 3D model) as well as stability investigation (employing a 1D model). Dirichlet boundary condition has been applied as a constant heat flux on the heater surface. With a fixed diameter and height, the computational model remains the same throughout the chapters. The main goal of the thesis is to examine the insight of FiHTD, which is observed when the average loop temperature exceeds the pseudo-critical temperature and causes safety concerns for the loop due to a spike in bulk temperature. The high-dimensional simulations were performed in ANSYS Fluent, while the 1D simulations were executed in Python language.

The first study is of the 3D computational model. Based on the temperature levels and heating power corresponding to imposed pressure and sink temperature, different heat transfer regimes were identified, namely, a) Low power regime, b) enhanced heat transfer regime, c) transition regime, and d) deteriorated heat transfer regime. The inclined loop offers less generation of buoyancy compared to the vertical loop, and hence the location of the respective regime may alter even under the same boundary condition. Temperature contours at the heater center under the same power depicted the higher bulk temperature and hence the early arrival of FiHTD. It was observed that till the region of buoyancy dominance, the friction factor inside the heater varies with the negative slope, while the

same under the complete friction-dominated regime, the slope changes its sense to negative, which is an indication of the onset of deteriorated heat transfer regime. A non-dimensional parameter called the Buoyancy parameter (Bu) was also defined and plotted against the heater power. The maximum value of Bu qualitatively gives the idea of the occurrence of FiHTD. When plotted against the friction factor, the region below the curve was considered safe to operate in.

The next part of the study is the 1D model that explores the stability characteristics of sNCL, and the appearance of static instability is the most significant outcome of the present study. Dynamic instability, which is characterized by an imposed perturbation that keeps growing over time, was found near the vicinity of the transition regime. While static instability was found for a range of heating power and mostly covers the enhanced heat transfer regime. The range of heating power of its existence depletes with the increment of the sink temperature. On the non-dimensional plane, there was a coherence of both the instability between two instabilities.

This part is the continuation of the previous one, where the dynamical response of the sNCL has been investigated under periodic as well as non-periodic heating profiles. It is interesting to see that response of the system adheres heat transfer regime's effect. For a range of time periods, chaos, and for even higher time periods, double periodic nature was witnessed along with the occurrence of frequency locking in the former, and frequency pushing phenomenon was observed in the latter one. Flow reversal was observed when mean heater power was in the transition regime under the imposed frequency of 0.25 Hz as well as when the maximum power reached close/just crossed the boundary of the deteriorated regime. When the maximum power is deep inside the deteriorated heat transfer regime, the condition of FiHTD occurs under the action of high amplitudes. In the case of the step and ramp heating profile, change in the power, the zone of initial base power plays a crucial role. So, in simple words, if the staring base power is close to the boundary of deteriorated heat transfer regime, the smaller increment in heating power in step manner is possible and higher step rise is possible if the base power is significantly away from this zone boundary. The sudden generation of buoyancy makes the system more vulnerable to instabilities in step change rather than the slow transition to targeted power in the case of the ramp input. Moreover, the intermediate limit cycle was also witnessed in the step rise case.

The next part of the thesis gives insight of the start-up transient of fluid motion initiation of the sNCL, which is the much explored topic in single and two-phase NCL. Since the supercritical fluid is highly susceptible to change of properties near the pseudocritical point,

thereby, the initiation of flow is very much expected to be different than that in other simple systems. For this purpose, 2D numerical simulations were performed in ANSYS Fluent. It was observed that the due to the low thermal diffusivity and high isothermal compressibility of the sCO_2 for the selected boundary condition, the heat transfer through the diffusion is anticipated to be slow while analogy via piston effect is very much viable and provides a logical explanation. Because of the coupling between the piston effect and buoyant convection, the thermal homogeneity is attained through the former one, while the density inhomogeneity is relaxed with the diffusion time scale allowing the initiation of bulk convection. Moreover, the piston effect is likely to embrace with acoustic time scale, maintaining the near identical pressure throughout the flow path at any given time instant. The rise in the temperature of the fluid in the adiabatic arm is because of the propagating fronts (propagating in both the legs) which is an indication of adiabatic heating. While the temperature rise in the core of the heater is due to the compression via two converging fronts. Such a squeezing of the fluid from both ends evokes the gravitational instability, having characteristics similar to the Rayleigh-Taylor mechanism. Owing to the strong local buoyancy despite the identical thermal condition on both the walls, disparity in the thermal boundary layer was clearly visible. Due to this inherent instability, the two propagating fronts do not meet at the heater centre and the symmetric nature eventually breaks and the corresponding time for occurrence of such is solely dependent on the imposed heating power. At the time when the circulatory zone of the front is in motion, primarily in one direction, that instant is the time of the initiation of the bulk motion and the convection evolves as the primary mechanism of heat transfer. It must also be mentioned that the direction of first movement is equally probable to be clockwise, i.e., toward left, for a separate simulation with identical parameters, as it is affected by the instantaneous status of the unstable zone, and may also by the propagation of numerical errors to some extent. The underlying physics, however, essentially remains consistent to the above discussion for any combination of boundary conditions. It is unlikely to have similar scenario in traditional single-phase NCL in relation to the piston effect as both the momentum and the thermal diffusion are much stronger and local Rayleigh number can be only of the order of 10^3 with 1 K temperature difference and hence, such a evolution is unique to sNCL.

The last chapter discuss about the experimental aspect of sNCL from the point of view of FiHTD. The rectangular NCL is of the same geometrical configuration as that of numerical one. Outcome of the experiments under various condition revealed that the nature of the system is same as we found in the numerical simulations of 3D and 1D models with a good

degree of consensus. The drop in the mass flow rate was is quite visible similar to the FiHTD. While the difference lies in the bulk temperature along the heater which are not quite significantly huge as expected. On the other hand, validation with the literature and uncertaininty in the results consolidates about the correctness of the results. Peak in the heat transfer coefficient showing the significance of enhanced heat transfer regime.

In the nut shell, the major outcomes of the present thesis is listed below

- Based primarily on the temperatures in the adiabatic arms, four distinct regimes have been identified. Operating under the enhanced heat transfer regime is preferred since it provides high HTC with low temperature levels and high circulation rates.
- Recognition of the maxima in buoyancy parameter as the most feasible option of identifying the initiation of FiHTD in any sNCL. This can serve as an important design basis by concentrating on expanding the upper limit of Bu at the stage of conceptualization itself.
- The system exhibits Ledinegg instability over an intermediate range of heater power, demonstrated by the onset of a number of steady-state solutions and the negative slope of the pressure drop profile. The static and dynamic stability maps show enough agreement with regard to the pertinent dimensionless variables.
- Irrespective of the type of time varying heating profile, the zone of operation of heat transfer regime play a crucial role in dynamical response of the system. Under certain amplitudes (A) and time period (τ), system also exhibit chaotic nature. On the other hand, small step rise in the power with base power in transition regime, flow reversal occured, while under the same condition ramp input showed stable nature.
- Initial flow transient in sNCL is governed by the several mechanism namely piston effect and adiabatic heating. Moreover till the bulk inititiation of motion, the instability associated is similar to Rayleigh-Taylor mechanism.

7.2 Future Scope

Based on the study done for the sNCL from the point of view of FiHTD and the stability aspect of it, following are the recommendations for the future investigation-

- In the 3D simulations, non-dimensional criterion Bu_{max} for the safer operation has been defined. Since the FiHTD phenomenon is relatively new and needs more attention.

Investigation of Bu_{max} in conjunction with the stability aspect need to be incorporated numerically and experimentally as well during the design phase of such systems.

- In 1D model, the disturbance in steady-state solution was imposed to be 5%, but behaviour under severe condition may lead to higher order perturbation. The dynamic stability can be further explored under such condition.
- The Static instability is found for the 1^{st} time for sNCL using sCO_2. Its validation on higher dimensional system as well as the experimental support is required.
- Experimental characteristics depends upon the inventory of the CO_2. Higher charge may lead to delay in FiHTD. For that high level of cooling will be required, the present investigation may be extended to explore this behaviour.

References

[1] D. Kim, M. H. Kim, J. E. Cha, S. O. Kim, Numerical investigation on thermal-hydraulic performance of new printed circuit heat exchanger model, Nuclear Engineering and Design 238 (12) (2008) 3269–3276.

[2] D. J. Close, The performance of solar water heaters with natural circulation, Solar Energy 6 (1) (1962) 33–40.

[3] P. M. Koffi, H. Y. Andoh, P. Gbaha, S. Touré, G. Ado, Theoretical and experimental study of solar water heater with internal exchanger using thermosiphon system, Energy Conversion and Management 49 (8) (2008) 2279–2290.

[4] A. Zerrouki, A. Boumédien, K. Bouhadef, The natural circulation solar water heater model with linear temperature distribution, Renewable Energy 26 (4) (2002) 549–559.

[5] K. Nidhul, A. K. Yadav, S. Anish, U. Arunachala, Thermo-hydraulic and exergetic performance of a cost-effective solar air heater: Cfd and experimental study, Renewable Energy 184 (2022) 627–641.

[6] A. D. Atrens, H. Gurgenci, V. Rudolph, Electricity generation using a carbon-dioxide thermosiphon, Geothermics 39 (2) (2010) 161–169.

[7] D. B. Kreitlow, G. M. Reistad, C. R. Miles, G. G. Culver, Thermosyphon models for downhole heat exchanger applications in shallow geothermal systems, Journal of Heat Transfer 100 (4) (1978) 713–719.

[8] K. E. Torrance, Open-loop thermosyphons with geological applications, Journal of Heat Transfer 101 (4) (2010) 677–683.

[9] J. H. Choi, Passive safety systems in advanced water cooled reactors, Vol. 3, 2012.

[10] G. R. Dimmick, V. Chatoorgoon, H. F. Khartabil, R. B. Duffey, Natural-convection studies for advanced CANDU reactor concepts, Nuclear Engineering and Design 215 (1-2) (2002) 27–38.

[11] J. Madejski, J. Mikielewicz, Liquid fin—A new device for heat-transfer equipment, International Journal of Heat and Mass Transfer 14 (3) (1971) 357–363.

[12] H. Jeffreys, The stability of a layer of fluid heated below, The London, Edinburgh, and Dublin Philosophical Magazine and Journal of Science 2 (10) (1926) 833–844.

[13] Y. Zvirin, The instability associated with the onset of motion in a thermosyphon, International Journal of Heat and Mass Transfer 28 (11) (1985) 2105–2111.

[14] J. Boure, A. Bergles, L. Tong, Review of two-phase flow instability, Nuclear Engineering and Design 25 (2) (1973) 165–192.

[15] K. Fukuda, T. Kobori, Classification of two-phase flow instability by density wave oscillation model, Journal of Nuclear Science and Technology 16 (2) (1979) 95–108.

[16] A. Nayak, P. Vijayan, Flow instabilities in boiling two-phase natural circulation systems: A review, Science and Technology of Nuclear Installations 2008 (2008) 573192.

[17] L. E. O'Neill, I. Mudawar, Review of two-phase flow instabilities in macro-and micro-channel systems, International Journal of Heat and Mass Transfer 157 (2020) 119738.

[18] L. Belblidia, C. Bratianu, Density-wave oscillations, Annals of Nuclear Energy 6 (7-8) (1979) 425–444.

[19] D. N. Basu, S. Bhattacharyya, P. Das, A review of modern advances in analyses and applications of single-phase natural circulation loop in nuclear thermal hydraulics, Nuclear Eengineering and Design 280 (2014) 326–348.

[20] Y. Zvirin, A. Shitzer, A. Bartal-Bornstein, On the stability of the natural circulation solar heater, in: International Heat Transfer Conference Digital Library, Begel House Inc., 1978.

[21] S. A., K. D., Z. Y., G. G., Experiments With a Flat Plate Solar Water Heating System in Thermosyphonic Flow, Solar Energy 22 (1979) (1978) 27–35.

[22] H. Cohen, F. Bayley, Heat-transfer problems of liquid-cooled gas-turbine blades, Proceedings of the Institution of Mechanical Engineers 169 (1) (1955) 1063–1080.

[23] E. H. Wissler, H. Isbin, N. Amundson, Oscillatory behavior of a two-phase natural-circulation loop, AIChE Journal 2 (2) (1956) 157–162.

[24] H. F. Creveling, J. F. de Paz, J. Y. Baladi, R. J. Schoenhals, Stability characteristics of a single-phase free convection loop, Journal of Fluid Mechanics 67 (1) (1975) 65–84.

[25] J. B. Keller, Periodic oscillations in a model of thermal convection, Journal of Fluid Mechanics 26 (3) (1966) 599–606.

[26] P. Welander, On the oscillatory behaviour of a differentially heated fluid loop, J. Fluid Mechanic 29 (1967) (1967) 17–30.

[27] M. Sen, C. Treviño, Dynamic analysis of a one-dimensional thermosyphon model, Journal of Thermal Engineering 3 (1982) 15–20.

[28] D. Pilkhwal, W. Ambrosini, N. Forgione, P. Vijayan, D. Saha, J. Ferreri, Analysis of the unstable behaviour of a single-phase natural circulation loop with one-dimensional and computational fluid-dynamic models, Annals of Nuclear Energy 34 (5) (2007) 339–355.

[29] M. Misale, Overview on single-phase natural circulation loops, in: Proceeding of the International Conference on Aadvances in Mechanical and Automation Engineering–MAE, 2014.

[30] P. Vijayan, A. Date, Experimental and theoretical investigations on the steady-state and transient behaviour of a thermosyphon with throughflow in a figure-of-eight loop, International Journal of Heat and Mass Transfer 33 (11) (1990) 2479–2489.

[31] P. Vijayan, A. Date, The limits of conditional stability for single-phase natural circulation with throughflow in a figure-of-eight loop, Nuclear Engineering and Design 136 (3) (1992) 361–380.

[32] M. Gartia, D. Pilkhwal, P. Vijayan, D. Saha, Metastable regimes: a parametric study in reference to single-phase parallel channel natural circulation systems, in: International Conference on Nuclear Engineering, Vol. 42436, 2006, pp. 63–74.

[33] W. Ambrosini, J. Ferreri, The effect of truncation error on the numerical prediction of linear stability boundaries in a natural circulation single-phase loop, Nuclear Engineering and Design 183 (1-2) (1998) 53–76.

[34] W. Ambrosini, J. C. Ferreri, Stability analysis of single-phase thermosyphon loops by finite-difference numerical methods, Nuclear Engineering and Design 201 (1) (2000) 11–23.

[35] W. Ambrosini, J. C. Ferreri, Prediction of stability of one-dimensional natural circulation with a low diffusion numerical scheme, Annals of Nuclear Energy 30 (15) (2003) 1505–1537.

[36] Y. Jiang, M. Shoji, Flow stability in a natural circulation loop: influences of wall thermal conductivity, Nuclear Engineering and design 222 (1) (2003) 16–28.

[37] M. Misale, F. Devia, P. Garibaldi, Experiments in a single-phase natural circulation loops: effects of interaction between the wall tube and fluids properties, in: 6th International Symposium on Heat Transfer, Beijing, China, June, 2004, pp. 15–19.

[38] M. Misale, P. Garibaldi, J. C. Passos, G. G. de Bitencourt, Experiments in a single-phase natural circulation mini-loop, Experimental Thermal and Fluid Science 31 (8) (2007) 1111–1120.

[39] P. K. Vijayan, M. Sharma, D. Saha, Steady state and stability characteristics of single-phase natural circulation in a rectangular loop with different heater and cooler orientations, Experimental Thermal and Fluid Science 31 (8) (2007) 925–945.

[40] M. Misale, M. Frogheri, Stabilization of a single-phase natural circulation loop by pressure drops, in: Thermal Sciences 2000. Proceedings of the International Thermal Science Seminar. Volume 1, Begel House Inc., 2000.

[41] Y. Lee, U. Mital, A two-phase closed thermosyphon, International Journal of Heat and Mass Transfer 15 (9) (1972) 1695–1707.

[42] K. Chen, Y. Chen, S. Shiao, P. Wang, An experimental study of steady-state behavior of a two-phase natural circulation loop, Energy conversion and management 31 (6) (1991) 553–559.

[43] R. Duffey, J. Sursock, Natural circulation phenomena relevant to small breaks and transients, Nuclear Engineering and Design 102 (2) (1987) 115–128.

[44] F. D'Auria, G. Galassi, Methodology for the evaluation of the reliability of passive systems (2000).

[45] A. Nayak, M. Gartia, A. Antony, G. Vinod, R. Sinha, Passive system reliability analysis using the apsra methodology, Nuclear Engineering and Design 238 (6) (2008) 1430–1440.

[46] A. Garg, P. Sastry, M. Pandey, U. Dixit, S. Gupta, Numerical simulation and artificial neural network modeling of natural circulation boiling water reactor, Nuclear Engineering and Design 237 (3) (2007) 230–239.

[47] J. E. Matsson, An Introduction to ANSYS Fluent 2022, SDC Publications, 2022.

[48] I. Babelli, S. Nair, M. Ishii, Two-phase flow instabilities in a vertical annular channel, Tech. rep., US Nuclear Regulatory Commission (NRC), Washington, DC (United States) (1995).

[49] S. Jiang, Y. Zhang, X. Wu, J. Bo, H. Jia, Flow excursion phenomenon and its mechanism in natural circulation, Nuclear Engineering and Design 202 (1) (2000) 17–26.

[50] X. Yang, S. Jiang, Y. Zhang, Mechanism analysis on flow excursion of a natural circulation with low steam quality, Nuclear Engineering and Design 235 (22) (2005) 2391–2406.

[51] A. Bergles, S. Kandlikar, On the nature of critical heat flux in microchannels, Journal of Heat Transfer 127 (1) (2005) 101–107.

[52] L. Jiang, M. Wong, Y. Zohar, Phase change in microchannel heat sinks with integrated temperature sensors, Journal of Microelectromechanical Systems 8 (4) (1999) 358–365.

[53] L. Zhang, E. N. Wang, K. E. Goodson, T. W. Kenny, Phase change phenomena in silicon microchannels, International Journal of Heat and Mass Transfer 48 (8) (2005) 1572–1582.

[54] A. Koşar, C.-J. Kuo, Y. Peles, Boiling heat transfer in rectangular microchannels with reentrant cavities, International Journal of Heat and Mass Transfer 48 (23-24) (2005) 4867–4886.

[55] M. E. Steinke, S. G. Kandlikar, An experimental investigation of flow boiling characteristics of water in parallel microchannels, Journal of Heat Transfer 126 (4) (2004) 518–526.

[56] A. Clausse, R. T. Lahey Jr, The analysis of periodic and strange attractors during density-wave oscillations in boiling flows, Chaos, Solitons & Fractals 1 (2) (1991) 167–178.

[57] Y. Lin, C. Pan, Non-linear analysis for a natural circulation boiling channel, Nuclear Engineering and Design 152 (1-3) (1994) 349–360.

[58] J. Lee, C. Pan, Dynamics of multiple parallel boiling channel systems with forced flows, Nuclear Engineering and Design 192 (1) (1999) 31–44.

[59] J. Der Lee, C. Pan, Nonlinear analysis for a nuclear-coupled two-phase natural circulation loop, Nuclear engineering and design 235 (5) (2005) 613–626.

[60] IPCC, Climate Change Synthesis Report 2014. Contribution of Working Groups I, II and III to the Fifth Assessment Report of the Intergovernmental Panel on Climate Change [Core Writing Team, R.K. Pachauri and L.A. Meyer (eds.)], Tech. rep. (2014).

[61] J. M. Blackburn, D. P. Long, A. Cabañas, J. J. Watkins, Deposition of conformal copper and nickel films from supercritical carbon dioxide, Science 294 (5540) (2001) 141–145.

[62] H. Yamaguchi, X.-R. Zhang, K. Fujima, Basic study on new cryogenic refrigeration using CO_2 solid–gas two phase flow, International Journal of Refrigeration 31 (3) (2008) 404–410.

[63] P. Nekså, H. Rekstad, G. R. Zakeri, P. A. Schiefloe, CO_2-heat pump water heater: characteristics, system design and experimental results, International Journal of refrigeration 21 (3) (1998) 172–179.

[64] P. Bondioli, C. Mariani, A. Lanzani, E. Fedeli, A. Mossa, A. Muller, Lampante olive oil refining with supercritical carbon dioxide, Journal of the American Oil Chemists' Society 69 (5) (1992) 477–480.

[65] V. Dostal, P. Hejzlar, M. J. Driscoll, The supercritical carbon dioxide power cycle: comparison to other advanced power cycles, Nuclear technology 154 (3) (2006) 283–301.

[66] V. Silin, V. Voznesensky, A. Afrov, The light water integral reactor with natural circulation of the coolant at supercritical pressure B-500 SKDI, Nuclear Engineering and Design 144 (2) (1993) 327–336.

[67] S. J. Bushby, G. Dimmick, R. Duffey, N. Spinks, K. Burrill, P. S. Chan, Conceptual designs for advanced, high-temperature candu reactors (2000).

[68] M. K. S. Sarkar, D. N. Basu, Numerical appraisal on the suitability of supercritical condition in natural circulation loop with isothermal boundary conditions, International Journal of Thermal Sciences 111 (2017) 30–40.

[69] P. Garibaldi, M. Misale, Experiments in single-phase natural circulation miniloops with different working fluids and geometries, Journal of Heat Transfer 130 (10) (2008).

[70] K. Kiran Kumar, M. Ram Gopal, Experimental studies on CO_2 based single and two-phase natural circulation loops, Applied Thermal Engineering 31 (16) (2011) 3437–3443.

[71] S. K. Mousavian, M. Misale, F. D'Auria, M. A. Salehi, Transient and stability analysis in single-phase natural circulation, Annals of Nuclear Energy 31 (10) (2004) 1177–1198.

[72] V. Archana, A. Vaidya, P. Vijayan, Numerical modeling of supercritical CO_2 natural circulation loop, Nuclear Engineering and Design 293 (2015) 330–345.

[73] Y. Cao, X.-R. Zhang, Flow and heat transfer characteristics of supercritical CO_2 in a natural circulation loop, International Journal of Thermal Sciences 58 (2012) 52–60.

[74] L. Chen, X. R. Zhang, Simulation of heat transfer and system behavior in a supercritical CO_2 based thermosyphon: Effect of pipe diameter, Journal of Heat Transfer 133 (12) (2011) 1–8.

[75] L. Chen, X.-R. Zhang, S. Cao, H. Bai, Study of trans-critical CO_2 natural convective flow with unsteady heat input and its implications on system control, International journal of heat and mass transfer 55 (23-24) (2012) 7119–7132.

[76] G. Liu, Y. Huang, J. Wang, F. Lv, L. K. H. Leung, Experiments on the basic behavior of supercritical CO_2 natural circulation, Nuclear Engineering and Design 300 (2016) 376–383.

[77] M. K. Sarkar, D. N. Basu, Influence of geometric parameters on thermalhydraulic characteristics of supercritical CO_2 in natural circulation loop, Nuclear Engineering and Design 324 (5) (2017) 402–415.

[78] A. K. Yadav, M. Ram Gopal, S. Bhattacharyya, CFD analysis of a CO_2 based natural circulation loop with end heat exchangers, Applied Thermal Engineering 36 (1) (2012) 288–295.

[79] L. Chen, X.-R. Zhang, B.-L. Deng, Near-critical natural circulation flows inside an experimental loop: Stability map and heat transfer, Heat Transfer Engineering 37 (3-4) (2016) 302–313.

[80] A. K. Yadav, M. Ram Gopal, S. Bhattacharyya, Computational fluid dynamic analysis of a supercritical CO_2 based natural circulation loop with end heat exchangers, International Journal of Advances in Engineering Sciences and Applied Mathematics 4 (3) (2012) 119–126.

[81] G. Liu, Y. Huang, J. Wang, L. H. Leung, Heat transfer of supercritical carbon dioxide flowing in a rectangular circulation loop, Applied Thermal Engineering 98 (2016) 39–48.

[82] V. Archana, A. M. Vaidya, P. K. Vijayan, Effect of Pressure on Steady State and Heat Transfer Characteristics in Supercritical CO_2 Natural Circulation Loop, Procedia Engineering 127 (2015) 636–644.

[83] V. Chatoorgoon, Stability of supercritical fluid flow in a single-channel natural-convection loop, International Journal of Heat and Mass Transfer 44 (10) (2001) 1963–1972.

[84] V. Chatoorgoon, SPORTS - A simple non-linear thermalhydraulic stability code, Nuclear Engineering and Design 93 (1) (1986) 51–67.

[85] A. H. Harvey, E. W. Lemmon, NIST / ASME Steam Properties — STEAM-Version 3.0, 2013.

[86] P. K. Vijayan, H. Austregesilo, Scaling laws for single-phase natural circulation loops, Nuclear Engineering and Design 152 (1-3) (1994) 331–347.

[87] P. K. Vijayan, Experimental observations on the general trends of the steady state and stability behaviour of single-phase natural circulation loops, Nuclear Engineering and Design 215 (1-2) (2002) 139–152.

[88] M. A. Bernier, B. R. Baliga, A 1-D/2-D model and experimental results for a closed-loop thermosyphon with vertical heat transfer sections, International Journal of Heat and Mass Transfer 35 (11) (1992) 2969–2982.

[89] B. J. Huang, R. Zelaya, Heat transfer behavior of a rectangular thermosyphon loop, Journal of Heat Transfer 110 (2) (1988) 487–493.

[90] H. H. Bau, K. E. Torrance, On the stability and flow reversal of pressure-driven flow in an asymmetrically heated U-shaped tube, Journal of Heat Transfer 107 (1) (1985) 112–117.

[91] M. Sharma, D. S. Pilkhwal, P. K. Vijayan, D. Saha, R. K. Sinha, Steady state and linear stability analysis of a supercritical water natural circulation loop, Nuclear Engineering and Design 240 (2010) (2010) 588–597.

[92] M. Sharma, D. S. Pilkhwal, P. K. Vijayan, D. Saha, R. K. Sinha, Steady-state behavior of natural circulation loops operating with supercritical fluids for open and closed loop boundary conditions, Heat Transfer Engineering 33 (9) (2012) 809–820.

[93] S. Sadhu, M. Ramgopal, S. Bhattacharyya, Steady-State Analysis of a High-Temperature Natural Circulation Loop Based on Water-Cooled Supercritical CO_2, Journal of Heat Transfer 140 (6) (2018).

[94] Y. Cao, X. R. Zhang, Flow and heat transfer characteristics of supercritical CO_2 in a natural circulation loop, International Journal of Thermal Sciences 58 (2012) 52–60.

[95] X. R. Zhang, H. Yamaguchi, Y. Cao, Hydrogen production from solar energy powered supercritical cycle using carbon dioxide, International Journal of Hydrogen Energy 35 (10) (2010) 4925–4932.

[96] P. Vijayan, M. Sharma, D. Pilkhwal, D. Saha, R. Sinha, A comparative study of single-phase, two-phase, and supercritical natural circulation in a rectangular loop, Journal of Engineering for Gas Turbines and Power 132 (10) (2010).

[97] L. Chen, X. R. Zhang, H. Yamaguchi, Z. S. Liu, Effect of heat transfer on the instabilities and transitions of supercritical CO_2 flow in a natural circulation loop, International Journal of Heat and Mass Transfer 53 (19-20) (2010) 4101–4111.

[98] L. Chen, B.-l. Deng, X.-R. Zhang, Experimental study of trans-critical and supercritical CO_2 natural circulation fl ow in a closed loop, Applied Thermal Engineering 59 (1-2) (2013) 1–13.

[99] L. Chen, B. L. Deng, X. R. Zhang, Experimental investigation of CO_2 thermosyphon flow and heat transfer in the supercritical region, International Journal of Heat and Mass Transfer 64 (2013) 202–211.

[100] A. K. Yadav, S. Bhattacharyya, M. R. Gopal, Optimum operating conditions for subcritical/supercritical fluid-based natural circulation loops, Journal of Heat Transfer 138 (11) (2016) 1–13.

[101] M. K. Sarkar, D. N. Basu, Working regime identification for natural circulation loops by comparative thermalhydraulic analyses with three fluids under identical operating conditions, Nuclear Engineering and Design 293 (2015) 187–195.

[102] L. Chen, X. R. Zhang, B. L. Deng, B. Jiang, Effects of inclination angle and operation parameters on supercritical CO_2 natural circulation loop, Nuclear Engineering and Design 265 (2013) 895–908.

[103] A. K. Yadav, M. R. Gopal, S. Bhattacharyya, Effect of tilt angle on subcritical/supercritical carbon dioxide-based natural circulation loop with isothermal source and sink, Journal of Thermal Science and Engineering Applications 8 (1) (2016).

[104] B. T. Swapnalee, P. K. Vijayan, M. Sharma, D. S. Pilkhwal, Steady state flow and static instability of supercritical natural circulation loops, Nuclear Engineering and Design 245 (2012) 99–112.

[105] L. Chen, B. L. Deng, B. Jiang, X. R. Zhang, Thermal and hydrodynamic characteristics of supercritical CO_2 natural circulation in closed loops, Nuclear Engineering and Design 257 (2013) 21–30.

[106] G. Liu, Y. Huang, J. Wang, F. Lv, Effect of buoyancy and flow acceleration on heat transfer of supercritical CO_2 in natural circulation loop, International Journal of Heat and Mass Transfer 91 (2015) 640–646.

[107] Y. Li, G. Xin, B. Yuan, S. Zhang, W. Du, Experimental investigation on natural circulation heat

transfer of supercritical CO_2 in a closed loop, International Journal of Heat and Mass Transfer 200 (2023) 123503.

[108] L. Chen, X. R. Zhang, B. Jiang, Effects of heater orientations on the natural circulation and heat transfer in a supercritical CO_2 rectangular loop, Journal of Heat Transfer 136 (5) (2014) 1–13.

[109] S. K. Debrah, W. Ambrosini, Y. Chen, Discussion on the stability of natural circulation loops with supercritical pressure fluids, Annals of Nuclear Energy 54 (2013) 47–57.

[110] P. K. Jain, Rizwan-uddin, Numerical analysis of supercritical flow instabilities in a natural circulation loop, Nuclear Engineering and Design 238 (8) (2008) 1947–1957.

[111] M. Sharma, P. K. Vijayan, D. S. Pilkhwal, Y. Asako, Steady state and stability characteristics of natural circulation loops operating with carbon dioxide at supercritical pressures for open and closed loop boundary conditions, Nuclear Engineering and Design 265 (2013) 737–754.

[112] K. Chen, On the oscillatory instability of closed-loop thermosyphons, Journal of Heat Transfer 107 (1985) 826–832.

[113] L. Cammarata, A. Fichera, A. Pagano, Stability maps for rectangular circulation loops, Applied Thermal Engineering 23 (8) (2003) 965–977.

[114] V. Chatoorgoon, A. Voodi, D. Fraser, The stability boundary for supercritical flow in natural convection loops: Part I: H_2O studies, Nuclear Engineering and Design 235 (24) (2005) 2570–2580.

[115] V. Chatoorgoon, A. Voodi, P. Upadhye, The stability boundary for supercritical flow in natural convection loops: Part I: CO_2 and H_2, Nuclear engineering and design 235 (24) (2005) 2581–2593.

[116] J. Zhao, P. Saha, M. Kazimi, Stability of supercritical water-cooled reactor during steady-state and sliding pressure start-up conditions, in: International Topical Meeting on Nuclear Reactor Thermal Hydraulics (Nureth 11); Avignon (France); 2-6 Oct 2005, France, 2005.

[117] W. Ambrosini, M. Sharabi, Dimensionless parameters in stability analysis of heated channels with fluids at supercritical pressures, Nuclear Engineering and Design 238 (8) (2008) 1917–1929.

[118] W. Ambrosini, J. Ferreri, The effect of truncation error on the numerical prediction of linear stability boundaries in a natural circulation single-phase loop, Nuclear Engineering and Design 183 (1-2) (1998) 53–76.

[119] E. Lemmon, M. O. McLinden, M. L. Huber, NIST Standard Reference Database 23: Reference Fluid Thermodynamic and Transport Properties, version 9.0, National Institute of Standards and Technology, Gaithersburg (2002).

[120] R. Jain, M. L. Corradini, A linear stability analysis for natural-circulation loops under supercritical conditions, Nuclear Technology 155 (3) (2017) 312–323.

[121] M. Sharma, P. Vijayan, D. Pilkhwal, D. Saha, R. Sinha, Linear and nonlinear stability analysis of a supercritical natural circulation loop, Journal of Engineering for Gas turbines and Power 132 (10) (2010) 102904.

[122] X. R. Zhang, H. Yamaguchi, An experimental study on evacuated tube solar collector using supercritical CO_2, Applied Thermal Engineering 28 (10) (2008) 1225–1233.

[123] P. Vijayan, H. Austregesilo, V. Teschendorff, Simulation of the unstable oscillatory behavior of single-phase natural circulation with repetitive flow reversals in a rectangular loop using the computer code athlet, Nuclear Engineering and Design 155 (3) (1995) 623–641.

[124] S. K. Rai, G. Dutta, T. Sheorey, Stability analysis of supercritical water natural circulation loop with vertical heater and cooler, in: Proceeding of Proceedings of the 24th National and 2nd International ISHMT-ASTFE Heat and Mass Transfer Conference (IHMTC-2017), no. December, Begellhouse, Connecticut, 2018, pp. 607–611.

[125] A. K. Tilak, D. N. Basu, Computational investigation of the dynamic response of a supercritical natural circulation loop to aperiodic and periodic excitations, Nuclear Engineering and Design 284 (2015) 251–263.

[126] B. Deng, L. Chen, X. Zhang, L. Jin, The flow transition characteristics of supercritical CO_2 based closed natural circulation loop (NCL) system, Annals of Nuclear Energy 132 (2019) 134–148.

[127] T. Wahidi, R. A. Chandavar, A. K. Yadav, Supercritical CO_2 flow instability in natural circulation loop: CFD analysis, Annals of Nuclear Energy 160 (2021) 108374.

[128] S. Thimmaiah, T. Wahidi, A. K. Yadav, A. Mahalingam, Comparative computational appraisal of supercritical CO_2-based natural circulation loop: effect of heat-exchanger and isothermal wall, Journal of Thermal Analysis and Calorimetry 141 (6) (2020) 2219–2229.

[129] W. Ambrosini, On the analogies in the dynamic behaviour of heated channels with boiling and supercritical fluids, Nuclear Engineering and Design 237 (11) (2007) 1164–1174.

[130] S. Lomperski, D. Cho, R. Jain, M. L. Corrandini, Stability of a natural circulation loop with a fluid heated through the thermodynamic pseudocritical point, in: Proceedings of ICAPP '04 Pittsburgh, PA USA, June 13-17, 2004 Paper ID 4268, Pittsburgh, PA USA, 2004, pp. 1–6.

[131] L. Chen, X.-R. Zhang, Experimental analysis on a novel solar collector system achieved by supercritical CO_2 natural convection, Energy Conversion and Management 77 (2014) 173–182.

[132] J. Yu, S. Che, R. Li, B. Qi, Analysis of Ledinegg flow instability in natural circulation at supercritical pressure, Progress in Nuclear Energy 53 (6) (2011) 775–779.

[133] M. K. S. Sarkar, Computational and experimental assessment of supercritical natural circulation loop: Steady-state thermalhydraulics and stability aspects, Ph.D. thesis (2019).

[134] M. K. S. Sarkar, D. N. Basu, Numerical comparison of thermalhydraulic aspects of supercritical carbon dioxide and subcritical water-based natural circulation loop, Nuclear Engineering and Technology 49 (1) (2017) 103–112.

[135] S. Koshizuka, N. Takano, Y. Oka, Numerical analysis of deterioration phenomena in heat transfer to supercritical water, International Journal of Heat and Mass Transfer 38 (16) (1995) 3077–3084.

[136] S. E.-D. El-Morshedy, S. M. Ibrahim, A. Alyan, A. Abdelmaksoud, Heat transfer deterioration mechanism for water at supercritical pressure, International Journal of Thermofluids 7 (2020) 100020.

[137] X. R. Zhang, H. Yamaguchi, Forced convection heat transfer of supercritical CO_2 in a horizontal circular tube, The Journal of supercritical fluids 41 (3) (2007) 412–420.

[138] S. Zhang, X. Xu, C. Liu, X. Li, C. Wu, C. Dang, Experimental investigation and theoretical analysis on the heat transfer deterioration of supercritical CO_2 in mixed and forced convection in vertical-straight tube with downward flow, International Journal of Heat and Mass Transfer 187 (2022) 122510.

[139] R. Span, W. Wagner, A new equation of state for carbon dioxide covering the fluid region from the triple-point temperature to 1100 K at pressures up to 800 MPa, Journal of physical and chemical reference data 25 (6) (1996) 1509–1596.

[140] G. Scalabrin, P. Marchi, F. Finezzo, R. Span, A reference multiparameter thermal conductivity equation for carbon dioxide with an optimized functional form, Journal of physical and chemical reference data 35 (4) (2006) 1549–1575.

[141] A. Fenghour, W. A. Wakeham, V. Vesovic, The viscosity of carbon dioxide, Journal of Physical and Chemical Reference Data 27 (1) (1998) 31–44.

[142] G. Filonenko, Hydraulic resistance in pipes, Teploenergetika 1 (1954) 40–44.

[143] A. Kiss, M. Balaskó, L. Horváth, Z. Kis, A. Aszódi, Experimental investigation of the thermal hydraulics of supercritical water under natural circulation in a closed loop, Annals of Nuclear Energy 100 (2017) 178–203.

[144] A. K. Tilak, D. N. Basu, Computational investigation of the dynamic response of a supercritical natural circulation loop to aperiodic and periodic excitations, Nuclear Engineering and Design 284 (2015) 251–263.

[145] G. Batchelor, Heat transfer by free convection across a closed cavity between vertical boundaries at different temperatures, Quarterly of Applied Mathematics 12 (3) (1954) 209–233.

[146] A. Gallagher, A. M. Mercer, On the behaviour of small disturbances in plane Couette flow with a temperature gradient, Proceedings of the Royal Society of London. Series A. Mathematical and Physical Sciences 286 (1404) (1965) 117–128.

[147] D. Harden, J. Boggs, Transient flow characteristics of a natural circulation loop operated in the critical region, Proc. Heat transf. Fluid mech. Inst 38 (1964).

[148] M. Adelt, J. Mikielewicz, Heat transfer in a channel at supercritical pressure, International Journal of Heat and Mass transfer 24 (10) (1981) 1667–1674.

[149] M. Sharma, P. Vijayan, D. Pilkhwal, Y. Asako, Natural convective flow and heat transfer studies for supercritical water in a rectangular circulation loop, Nuclear Engineering and Design 273 (2014) 304–320.

[150] A. K. Yadav, M. R. Gopal, S. Bhattacharyya, CO_2 based natural circulation loops: new correlations for friction and heat transfer, International Journal of Heat and Mass Transfer 55 (17-18) (2012) 4621–4630.

[151] G. vanRossum, Python reference manual, Department of Computer Science [CS] (R 9525) (1995).

[152] D. N. Basu, Dynamic frequency response of a single-phase natural circulation loop under an imposed sinusoidal excitation, Annals of Nuclear Energy 132 (2019) 603–614.

[153] T. Srivastava, D. N. Basu, Numerical characterization of heat transfer deterioration in supercritical natural circulation loop and role of loop inclination, Nuclear Engineering and Design 390 (2022) 111704.

[154] M. Ledinegg, Instability of flow during natural and forced circulation, Die Wärme 61 (1938).

[155] G. V. D. Prasad, M. Pandey, M. S. Kalra, Review of research on flow instabilities in natural circulation boiling systems, Progress in Nuclear Energy 49 (6) (2007) 429–451.

[156] S. K. Rai, P. Kumar, V. Panwar, Numerical analysis of influence of geometry and operating parameters on Ledinegg and dynamic instability on supercritical water natural circulation loop, Nuclear Engineering and Design 369 (2020) 110830.

[157] S. H. Strogatz, Nonlinear dynamics and chaos: with applications to Physics, Biology, Chemistry and Engineering, 2nd Edition, CRC press, 2018.

[158] H. H. Bau, K. Torrance, Transient and steady behavior of an open, symmetrically-heated, free convection loop, International Journal of Heat and Mass Transfer 24 (4) (1981) 597–609.

[159] A. Nayak, P. Vijayan, D. Saha, V. V. Raj, Mathematical modelling of the stability characteristics of a natural circulation loop, Mathematical and Computer Modelling 22 (9) (1995) 77–87.

[160] A. Pacheco-Vega, W. Franco, H.-C. Chang, M. Sen, Nonlinear analysis of tilted toroidal thermosyphon models, International Journal of Heat and Mass Transfer 45 (7) (2002) 1379–1391.

[161] D. N. Basu, S. Bhattacharyya, P. Das, Influence of geometry and operating parameters on the stability response of single-phase natural circulation loop, International Journal of Heat and Mass Transfer 58 (1-2) (2013) 322–334.

[162] S. Bhattacharyya, D. N. Basu, P. K. Das, Two-phase natural circulation loops: A review of the recent advances, Heat Transfer Engineering 33 (2011) 461–482.

[163] Y. Zvirin, The onset of flows and instabilities in a thermosyphon with parallel loops, Nuclear Engineering and Design 92 (2) (1986) 217–226.

[164] Y. Zvirin, The onset of motion in a toroidal thermosyphon, Journal of Engineering Mathematics 20 (1986) 3–20.

[165] N. Kumar, J. Doshi, P. Vijayan, Investigations on the role of mixed convection and wall friction factor in single-phase natural circulation loop dynamics, Annals of Nuclear Energy 38 (10) (2011) 2247–2270.

[166] N. Kumar, K. N. Iyer, J. Doshi, P. Vijayan, Investigations on single-phase natural circulation loop dynamics part 1: Model for simulating start-up from rest, Progress in Nuclear Energy 76 (2014) 148–159.

[167] M. Krishnani, D. N. Basu, On the validity of Boussinesq approximation in transient simulation of single-phase natural circulation loops, International Journal of Thermal Sciences 105 (2016) 224–232.

[168] A. Knaani, Y. Zvirin, Bifurcation phenomena in two-phase natural circulation, International Journal of Multiphase Flow 19 (6) (1993) 1129–1151.

[169] S. Jiang, X. Wu, Y. Zhang, Experimental study of two-phase flow oscillation in natural circulation, Nuclear Science and Engineering 135 (2) (2000) 177–189.

[170] C. Wu, S. Wang, C. Pan, Chaotic oscillations in a low pressure two-phase natural circulation loop under low power and high inlet subcooling conditions, Nuclear Engineering and Design 162 (2-3) (1996) 223–232.

[171] S. Jiang, M. Yao, J. Bo, S. Wu, Experimental simulation study on start-up of the 5 MW nuclear heating reactor, Nuclear Engineering and Design 158 (1) (1995) 111–123.

[172] L. Zhu, J. Yu, Experimental investigation on startup performances of a separator assisted two-phase loop thermosyphon, International Journal of Heat and Mass Transfer 148 (2020) 119141.

[173] J. Paniagua, U. Rohatgi, V. Prasad, Modeling of thermal hydraulic instabilities in single heated channel loop during startup transients, Nuclear Engineering and Design 193 (1-2) (1999) 207–226.

[174] S. Lakshmanan, M. Pandey, Analysis of startup oscillations in natural circulation boiling systems, Nuclear Engineering and Design 239 (11) (2009) 2391–2398.

[175] K. Saikia, D. N. Basu, M. Pandey, Parametric studies on startup transients in multiple parallel channels of a natural circulation boiling system, Annals of Nuclear Energy 138 (2020) 107211.

[176] T. Wahidi, R. A. Chandavar, A. K. Yadav, Stability enhancement of supercritical CO_2 based natural circulation loop using a modified Tesla valve, The Journal of Supercritical Fluids 166 (2020) 105020.

[177] L. Chen, B. L. Deng, B. Jiang, X. R. Zhang, Thermal and hydrodynamic characteristics of supercritical CO_2 natural circulation in closed loops, Nuclear Engineering and Design 257 (2013) 21–30.

[178] T. Srivastava, D. N. Basu, Numerical evaluation of static and dynamic stability characteristics of a supercritical CO_2-driven natural circulation loop, The Journal of Supercritical Fluids 191 (2022) 105782.

[179] A. Onuki, H. Hao, R. A. Ferrell, Fast adiabatic equilibration in a single-component fluid near the liquid-vapor critical point, Physical Review A 41 (4) (1990) 2256.

[180] B. Zappoli, D. Bailly, Y. Garrabos, B. Le Neindre, P. Guenoun, D. Beysens, Anomalous heat transport by the piston effect in supercritical fluids under zero gravity, Physical Review A 41 (4) (1990) 2264.

[181] J. Straub, L. Eicher, A. Haupt, Dynamic temperature propagation in a pure fluid near its critical point observed under microgravity during the German Spacelab Mission D-2, Physical Review E 51 (6) (1995) 5556.

[182] Y. Masuda, T. Aizawa, M. Kanakubo, N. Saito, Y. Ikushima, One dimensional heat transfer on the thermal diffusion and piston effect of supercritical water, International Journal of Heat and Mass Transfer 45 (17) (2002) 3673–3677.

[183] B. Zappoli, S. Amiroudine, P. Carles, J. Ouazzani, Thermoacoustic and buoyancy-driven transport in a square side-heated cavity filled with a near-critical fluid, Journal of Fluid Mechanics 316 (1996) 53–72.

[184] B. Zappoli, A. Jounet, S. Amiroudine, A. Mojtabi, Thermoacoustic heating and cooling in near-critical fluids in the presence of a thermal plume, Journal of Fluid Mechanics 388 (1999) 389–409.

[185] P. Carlès, A brief review of the thermophysical properties of supercritical fluids, The Journal of Supercritical Fluids 53 (1-3) (2010) 2–11.

[186] Y. Masuda, T. Aizawa, M. Kanakubo, N. Saito, Y. Ikushima, Numerical simulation of two-dimensional piston effect and natural convection in a square cavity heated from one side, International Communications in Heat and Mass Transfer 31 (2) (2004) 151–160.

[187] B. Zappoli, S. Amiroudine, S. Gauthier, Rayleigh–Taylor-like instability in near-critical pure fluids, International Journal of Thermophysics 20 (1999) 257–265.

[188] S. Amiroudine, P. Bontoux, P. Larroudé, B. Gilly, B. Zappoli, Direct numerical simulation of instabilities in a two-dimensional near-critical fluid layer heated from below, Journal of Fluid Mechanics 442 (2001) 119–140.

Publications

International Journal

1. **T. Srivastava**, D. N. Basu, Numerical characterization of heat transfer deterioration in supercritical natural circulation loop and role of loop inclination, Nuclear Engineering and Design 390 (2022) 111704.
2. **T. Srivastava**, D. N. Basu, Numerical evaluation of static and dynamic stability characteristics of a supercritical CO_2-driven natural circulation loop, The Journal of Supercritical Fluids 191 (2022) 105782.
3. **T. Srivastava**, D. N. Basu, Dynamic Characterization of Supercritical Natural Circulation Loop under Periodic Excitation, International Journal of Thermal Sciences 197 (2024) 108835.
4. **T. Srivastava**, D. N. Basu, Numerical investigation of the microdynamics of the initiation of motion and startup transients in a supercritical natural circulation loop, International Journal of Heat and Mass Transfer 224 (2024) 125289 .
5. **T. Srivastava**, Ashok K Gond, D. N. Basu, Numerical appraisal of the role of heat transfer regimes on transient response of carbon dioxide based supercritical natural circulation loop during power upsurge, Nuclear Engineering and Design 429 (2024) 113601.
6. **T. Srivastava**, Ashok K Gond, D. N. Basu, Naturally Circulated System Under Low to Moderate Heating Condition with Supercritical Fluid: A Comprehensive Investigation of Loop Orientation and Ledinegg Instability (In **Applied Thermal Engineering**).
7. Experimental Identification of the Heat Transfer Regimes in a Suoercritical Natural Circulation Loop (Under Preperation)
8. Comparitive Analysis on the Mechanism of Flow Initiation in Single-Phase and Supercritical Natural Circulation Loops (Under Preperation)

Book chapter

1. **T. Srivastava**, P. Sutradhar, D. N. Basu, and L. Chen. An overview of the dynamics of supercritical natural circulation loops. In Dynamics and Control of Energy Systems, pages 85–110. Springer, 2020.
2. **T. Srivastava**, P. Sutradhar, M. K. S. Sarkar, and D. N. Basu. Supercritical natural circulation loop: A technology for future reactor. In Handbook of Research on Advancements in Supercritical Fluids Applications for Sustainable Energy Systems, pages 338–369. IGI Global.

International conference

1. **T. Srivastava**, D.N. Basu, Fluid-to-fluid scaling of supercritical natural circulation loop under steady-state condition, Proceedings of the 8^{th} International and 47^{th} National Conference on Fluid Mechanics

and Fluid Power 9^{th} - 11^{th} December 2020 Indian Institute of Technology Guwahati, India, Paper no - 256

2. P. Sutradhar, **T. Srivastava**, D. N. Basu, Numerical study of supercritical natural circulation loop under condition of different inclination and diameter, in: Proceedings of the 26thNational and 4th International ISHMT-ASTFE Heat and Mass Transfer Conference December 17-20, 2021, IIT Madras, Chennai-600036, Tamil Nadu, India, Begel House Inc., 2021.

3. **T. Srivastava**, D.N. Basu, Steady-state thermal-hydraulic response of supercritical natural circulation loop under different loop orientations, The 1st World Conference on Multiphase, Transportation, Conversion & Utilization of Energy (MTCUE-2022), 27^{th} - 31^{th} July 2022,Xi'an China, Article number-220118.